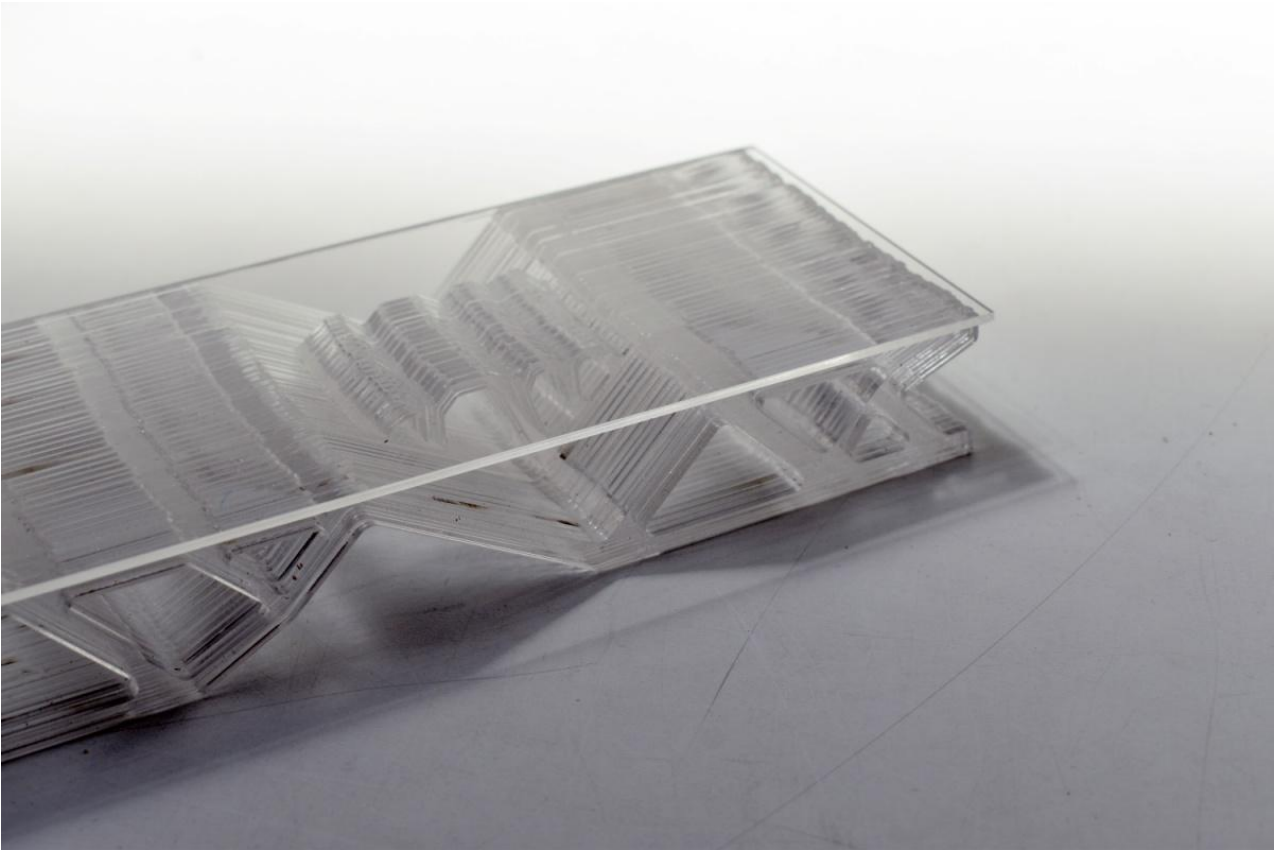# Just Glass.

Development of a Topology Optimization Algorithm
for a Mass-Optimized Cast Glass Component.

Anna Maria Koniari
June 2022

Student: Anna Maria Koniari | 5374480

First mentor: Dr. Faidra Oikonomopoulou
Chair of Structural Design & Mechanics

Second mentor: Dr. Charalampos Andriotis
Chair of Structural Design & Mechanics

TUDelft

Abstract

This thesis continues the investigation in the direction of exploring the potential regarding the use of Topology Optimization techniques for the design of cast glass structures. Previous theses in TU Delft have underlined the large potential for the design of these megaliths, but at the same time they have also underlined the strong limitations that derive from the use of commercial software as the tool for it.

The limitations are directly related to the brittle nature of glass which results in significantly different behavior regarding its maximum tensile and compressive allowable limits. This renders fundamental to be able to evaluate both of these criteria during the optimization process. If this is not possible, as it was the case in the previous theses, a secondary (post-processing) phase should be integrated in the process in order to alleviate the peak stresses that may occur in the structure. This increases significantly the time and effort needed for the design and, therefore, it was underlined as an issue to be tackled in further exploration.

This thesis aspires to address this problem with the creation of a customized optimization tool that takes all the structural constraints into consideration and, additionally, integrates the criteria specifically related to the glass manufacturing process, such as the overall annealing time needed. The tool is created in Matlab with the use of Finite Element Method equations in order to develop the structural model. The results of the structural analysis were validated through comparison with results obtained through ANSYS.

The literature review covers a wide scope of topics. Firstly, the glass properties and the casting process are investigated in order to properly indicate the criteria and constraints that arise in every phase. The second part refers to topology optimization. A comparative review of the different algorithmic methodologies is realized and SIMP is selected as the most appropriate for the project. Additionally, the different categories of formulation for the optimization problem – stress, compliance and volume based – are discussed in order to select the appropriate objective and constraints. At the same time, a review of the previous theses is realized in order to indicate which method was used in every case and how the constraints were integrated in the process every time.

In the end two different algorithms are developed based on two different problem formulations; one with compliance objective and a second one with volume objective. The aim is to investigate if the volume objective optimization can be a robust alternative to the classical compliance approach leading to more lightweight structures which at the same time fulfill the criteria regarding their feasibility to be manufactured.

Firstly, the performance of the algorithm in relation to each objective and constraint individually is evaluated though application in a smaller scale benchmark problem. The results showed that all the setups work and, therefore, they can be used for the final design experiments. However, it also indicated that some constraints, such as stress, cannot be applied individually but they always have to be combined with another constraint that guides the optimization in order to lead in a reasonable result. Afterwards, a combination of objective and constraints for each of the two aforementioned formulations – compliance and volume - is tested and applied in the case study example which refers to a slab that serves as a small pedestrian bridge inside the British Museum.

The results validate the estimation that a volume-based problem formulation can offer a robust result which resembles the result obtained from the traditional compliance-based formulation. Moreover, the result in the volume-based case is clearer and sharper and for this reason it was selected in the end for implementation in the final design. The formulation is then used in combination with different glass types, boundary conditions and design domain in order to conclude to the final shape of the slab.

Acknowledgements

The end of this thesis marks the end of some really crazy months which broadened my knowledge in a lot of aspects but, most importantly, got to redefine from scratch my boundaries and my perception of what I can now consider as possible to achieve. It also marks the end of a larger 2-year journey which was equally crazy and revealing and I would like to sincerely thank everybody that has been part of it.

Additionally, I would like to particularly thank all the people that helped me for the realization of this project. In this regard, I would like to thank Hans Hoogenboom for kindly offering me one of the computers in the VR lab in order to run my simulations. Given that my laptop has limited memory and processing capacities, this thesis would not have been possible to realize to that extent in another case. Moreover, I would like to thank Telesilla Bristogianni and Jackson Lee Jewett for offering me constructive feedback regarding the glass behavior and topology optimization respectively. Their comments were always to the point and helped me light up the dark spots in my research while their enthusiasm about their fields of expertise was always inspiring.

Furthermore, I would like to deeply thank my family and all my friends in Delft, Greece and all over the different places. Thank you for being there for me and supporting me in this path. Particularly, I want to give a special thanks to Vasilis for reminding me that when something feels scary and difficult, all it takes is to just remember why you started and why you love what you do.

Lastly, my biggest thanks go to my mentors, Faidra Oikonomopoulou and Charalampos Andriotis. Thank you for all the effort you put, as well as your feedback, patience and motivation. But most importantly, I sincerely thank you for being truly my partners in this journey, believing in me and showing so much enthusiasm about the project. You always motivated me to be more confident, take more risks and put the maximum effort in order to finally make it happen.

Table of contents

1. Research framework

This chapter sets the research framework that serves as the basis for the development of the thesis in general. The posed problems as well as the main research goal that derives based on it are determined. Additionally, the strategy in order to achieve the research goal is discussed and the research question, as well as the methodology which will be followed in order to answer it, are defined.

1.1 Introduction

In recent years, the vast shaping potential of cast glass has been unveiled. The possibility for creation of any type of shape and cross section (Oikonomopoulou et al., 2020) has been proven through experiments that refer not only to works of art (Figure 1a), but also to components which can efficiently be used for structural implementations. Regarding the latter ones, the kiln-casting technique has been used in order to form elements of complex shape (Figure 1c) which can, additionally, be designed in order to interlock between them(Figure 1b).

(a)   (b)   (c)
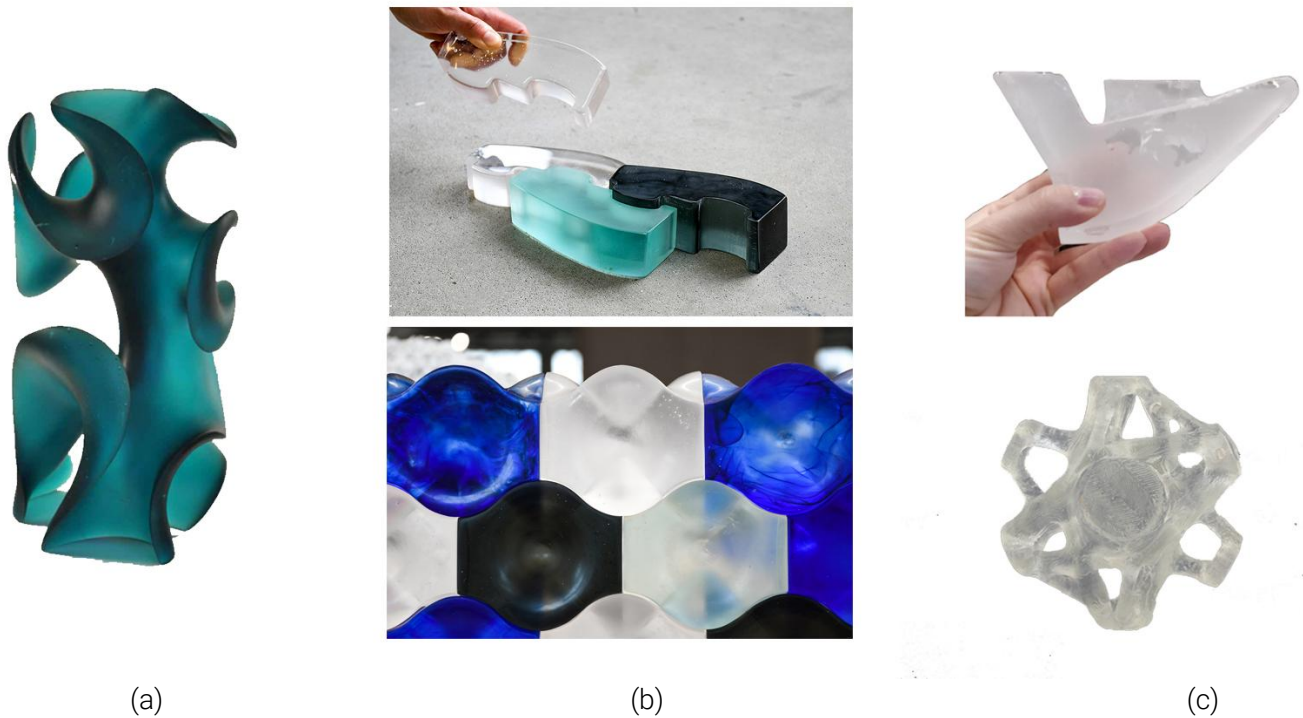
Figure 1 Experiments with cast glass and kiln-casting technique (a) Glass sculpture. (b) Interlocking glass components. (c) Glass components with customized shape made from previous theses at TU Delft.[1]

The large shaping potential of cast glass in combination with its high compressive strength, which surpasses the strength of traditional structural materials such as concrete or structural steel, as well as its added benefits regarding transparency, durability and recyclability (Oikonomopoulou, 2019) highlight the importance of glass for use as a building material. However, there are major issues arising mainly from its annealing process that render it difficult to be used for manufacturing. Particularly, the large time period along with the great amount of energy needed for the meticulous annealing process of the elements make it time and cost inefficient for the industry.

Several factors influence the annealing time of the glass components. These are, mainly, their mass and the overall form of the geometry but also the chemical composition of the glass type and the thermal expansion coefficient which is related to it (Oikonomopoulou, 2019).

Till now, the applications of cast glass in the construction industry are limited only to components which are composed from small glass bricks (Figure 2) since, due to their small size, these bricks are feasible to be

---

[1] The images sources are mentioned in total at the end of this report.

annealed in a reasonable time. Moreover, when combined with a glass composition that has a low thermal expansion coefficient, the annealing time needed can be further reduced as shown in (Figure 3) which illustrates that cast glass bricks made from borosilicate glass have reduced annealing time for approximately same sizes.
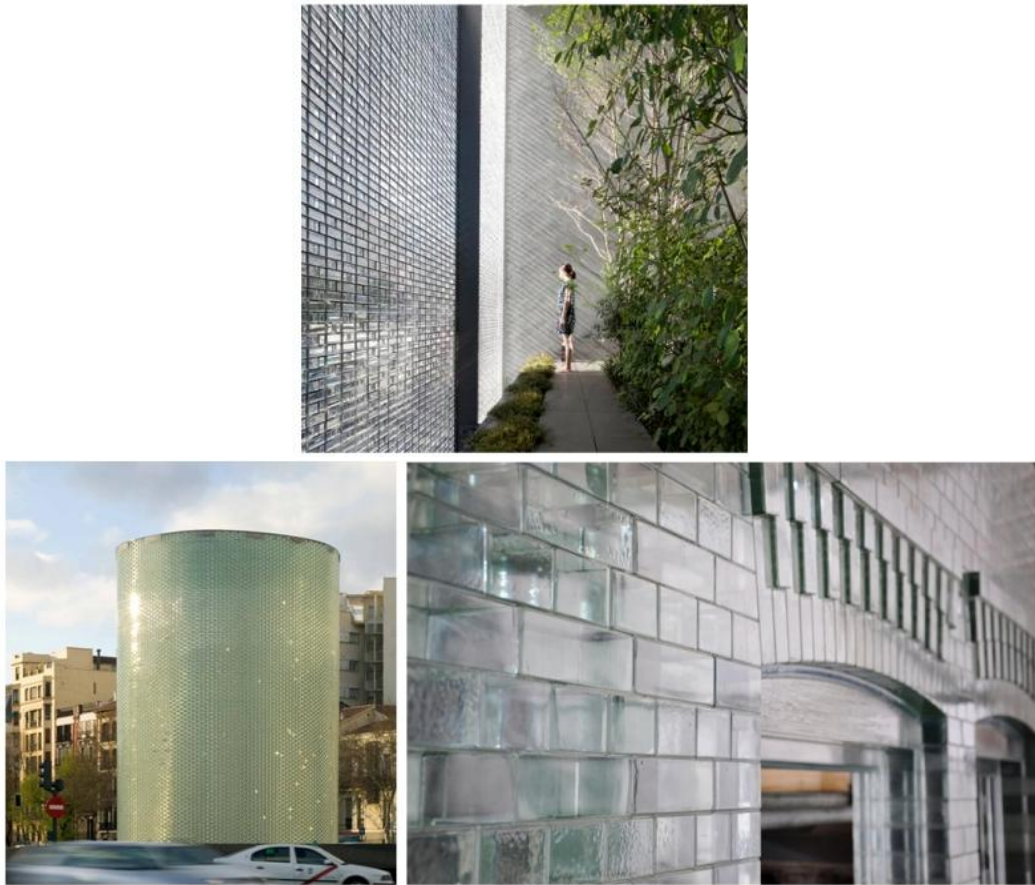
Figure 2 Glass brick structures with metal substructure at Optical House (top) or adhesively bonded at (bottom left) Atocha Memorial and (bottom right) Crystal Houses Façade.

Crystal Houses	Atocha Memorial	Optical House
Soda-lime, low-iron glass	Borosilicate glass	Borosilicate glass
(105 mm – 210 mm) x 210 mm x 65 mm to	200 mm x 300 mm x 70 mm	50 mm x 50 mm x 235 mm
3.6 kg – 7.2 kg (based on size)	8.4 kg	2.2 kg
8 h – 38 h annealing (based on size)	20 h annealing	unknown

Figure 3 Size and annealing time for glass bricks of different glass compositions.

However, there are also experiments in the direction of creating cast glass structures of larger sizes. These can serve to highlight, firstly, the large effect that the size has on the overall annealing time needed, and, secondly, the large potential that mass optimization can have on making the structure more time efficient.

Particularly, in the state of the art, the large cast glass sculptures (height: 50,8cm, diameter: 142cm) made from Roni Horn for Opposites of white (Figure 4) needed four months in order to be successfully cooled down. The pieces were compact and had no inner voids in their mass. On the other hand, the realized structures that incorporate honeycomb structures into the glass elements, such as the giant telescope lens (Figure 5) have demonstrated that an optimized geometry and mass distribution can not only reduce significantly the length of the annealing process, but also increase drastically the size of monolithic cast class components which can be achieved (Oikonomopoulou et al., 2020). Particularly, in the case of the Giant Magellan telescope lens, a large monolithic piece of diameter 8.4m needed only 3 months to be successfully cooled down (Hill et al., 1998).

Figure 4 'Opposites of white' by Roni Horn displayed in Kroller Moller museum.

Telescope	Hooker blank	Hale-1 blank	Giant Magellan blank
glass type	Wine bottle glass (St Gobain)	Pyrex Glass (Corning)	E6 Borosilicate Glass (Ohara Inc)
therm. exp. coefficient (α)	$9*10^{-6}$ $*1/C$	$3.25*10^{-6}$ $*1/C$	$2.8*10^{-6}$ $*1/C$
diameter Ø	2.5 m	5 m	8.4 m
max. thickness	325 mm	660 mm	894 mm
weight	4 tn	20 tn	16 tn
annealing time	12 months	10 months	3 months
	solid disc	reduce weight: honeycomb structure	further reduce weight: thinner ribs reduce post-processing: spin-casting
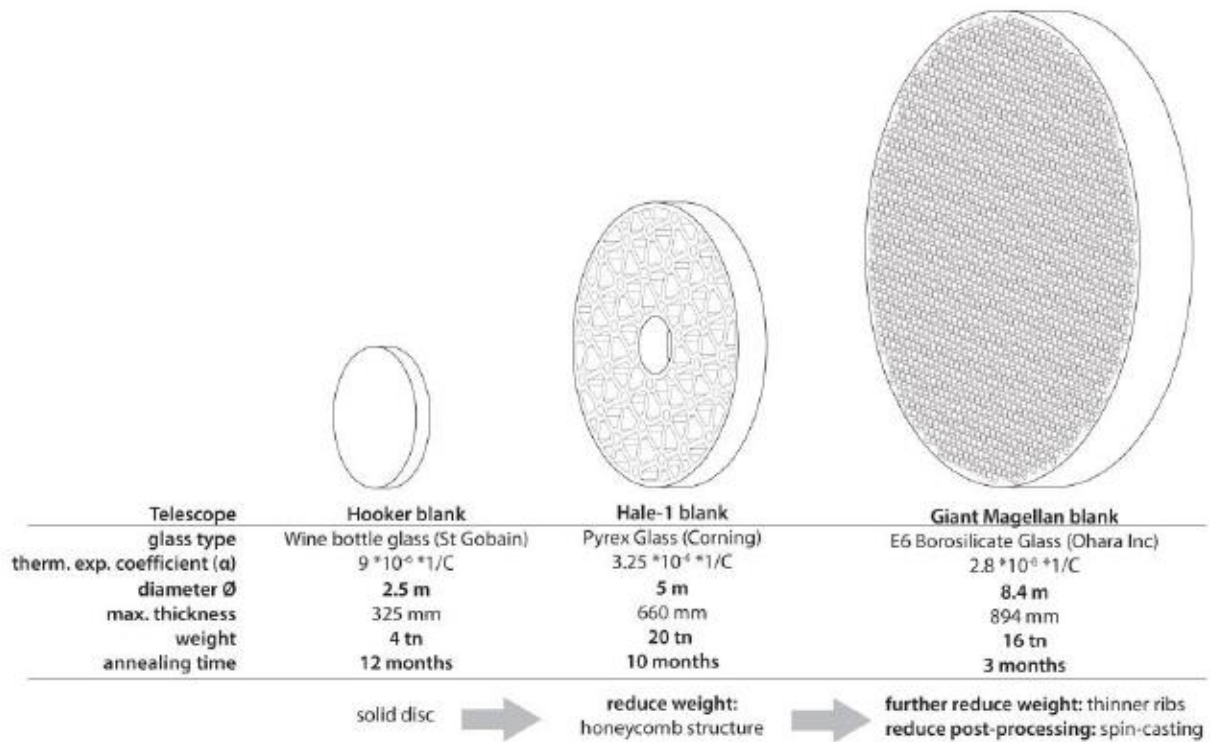
Figure 5 Size and annealing time for different telescope lens (Oikonomopoulou et al., 2020).

Nevertheless, despite the significant developments, there is still a lot to be investigated in the direction of creating efficient massive cast glass components, Particularly, although the annealing process has been considerably shorter in the telescope applications, it still needs a lot of time to be completed, fact that works as an impediment for the time and cost efficiency of the structures and subsequently for their integration in the construction industry. However, it showcases the large shaping potential and it raises the question that with further optimization of the form and control over the cross section, larger and more complex components would be feasible. In recent years, Master students of TU Delft have been experimenting in this direction, taking advantage of Topology Optimization tools for the form exploration of monolithic cast glass structures.

1.2 Research framework

The large potential of this research direction has already proven through the applied case study examples of all the previous theses. However, it still remains as a drawback that the existing commercial software is largely oriented towards ductile materials and, thus, it does not offer different criteria in terms of stress constraints. This has led the previous projects to optimizing only according to tension and evaluating compression values in a secondary level, leading to a considerably more time-consuming process.

This thesis intends to contribute in this research direction by creating a custom algorithm that will take into consideration the specific needs in terms of glass structural properties and will incorporate the relevant manufacturing and annealing criteria in order to finally create a complete tool for the design of cast glass components.

1.2.1 Research goal

Taking the aforementioned into consideration, the main research goal of the project is defined as:
- To investigate the potential of applying Topology Optimization methods in an algorithm for the design of technically and economically feasible cast glass elements

Secondary goals, which will help to further highlight the potential of the method, are:
- To try to estimate the annealing time for the designed structure
- To compare the properties of the final outcome with similar experiments designed through available commercial TO software

1.2.2 Research question

In this regard, the main research question is defined as followed:

- What are the main aspects and inherent limitations of composing a Topology Optimization algorithm for the design of massive cast glass structures which are time and cost efficient?

To be able to reach this outcome, the thesis is divided into two main parts. The first one consists of the literature review which will set the necessary foundation in terms of both glass structures and topology optimization techniques. The second part will focus on the composition of the algorithm and the application on the case study design. In order to have a well-founded result, the following sub-questions need to be answered:

- Which are the structural, annealing and manufacturing criteria for the design of glass structures that will be taken into consideration for the algorithm?
- Which are the main design principles that will be taken into account for the design of the slab?
- Which algorithmic methodology or combination of algorithmic methodologies will be used during the Topology Optimization process?
- Which are the objectives and constraints which are going to be posed and how the optimization problem will be formulated?
- Which will be the approximated annealing time for the construction of the slab?
- How the structural and design properties as well as the time and cost efficiency of the outcome are comparable to similar experiments using TO commercial software?
- How can the customized tool be used from a designer and which is the reflection on the final shape architecturally?

1.2.3 Methodology

The project is divided to different phases, which lead to specific outcomes in order to conclude, in the end, to the final result (Figure 6).

The research starts with the literature review concerning both scientific studies that had already been developed and theses which are developed lately in TU Delft regarding similar topics. It focuses on three main themes; the features related to the glass material, the Topology Optimization methods and the characteristics related to the case study application. The different outcomes, which derive from each theme, are going to be used in the next phase for the formulation of the optimization problem.

Particularly, the studies on glass features will give information regarding the structural, manufacturing and annealing criteria, whereas the review of Topology Optimization methods will result in selecting the method and formulation which is going to be applied to the project and defining the principles regarding the problem statement respectively. Lastly, the design principles and the restrictions based on the location will be derived from the case study analysis.

The next steps refer to the research by design process, through formulation of the optimization problem and implementation into the respective code. The code is going to be applied in the design domain as defined by the case study and the result will be evaluated. Errors and deviations from the desired outcome will lead to updates and modifications in the problem formulation and the code respectively.

After the design of the slab is determined, it will be post-processed in order to conclude to the final shape which is going to be applied for the final structural validation. The performance of the algorithm will be critically assessed through evaluation of the properties of the final outcome in comparison to projects developed through the use of commercial software.
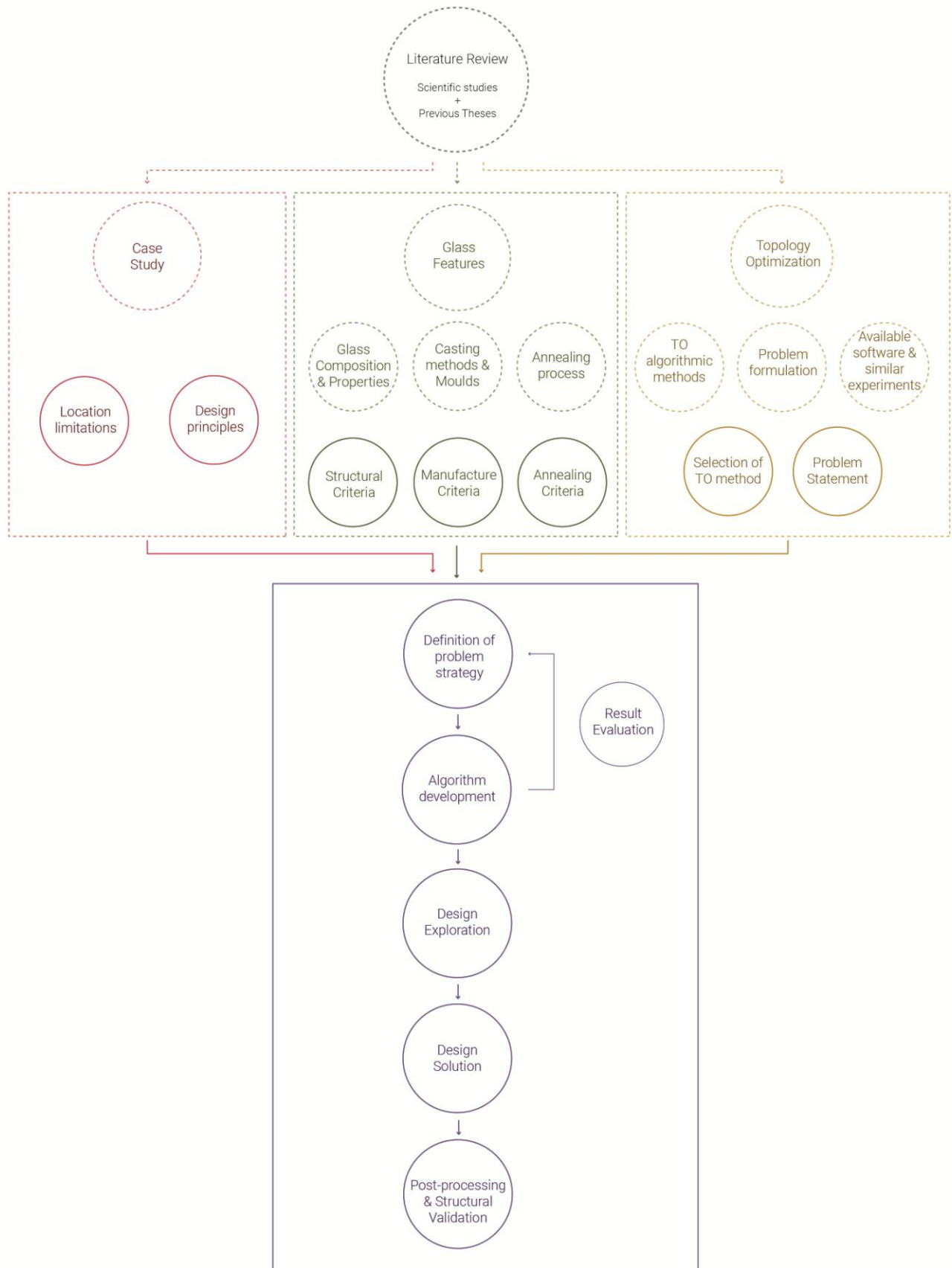
Figure 6 Diagram of the research methodology as followed in the project.

2. Case Study - Description

The efficiency of the Topology Optimization algorithm will be proved through an application on a case study example. This chapter will describe the main characteristics of the example selected, as well as the main reasons that led to its selection.

2.1 Example description

The case study example is located inside the Great Court of the British Museum in London. It refers to an existing small slab that functions as a pedestrian bridge connecting the big volume of the Reading Room to the rest of the exhibition spaces (Figure 7). The intervention was held by Foster + Partners architecture studio in 2000 and it also involved the creation of the big glass roof that covers the inner court.
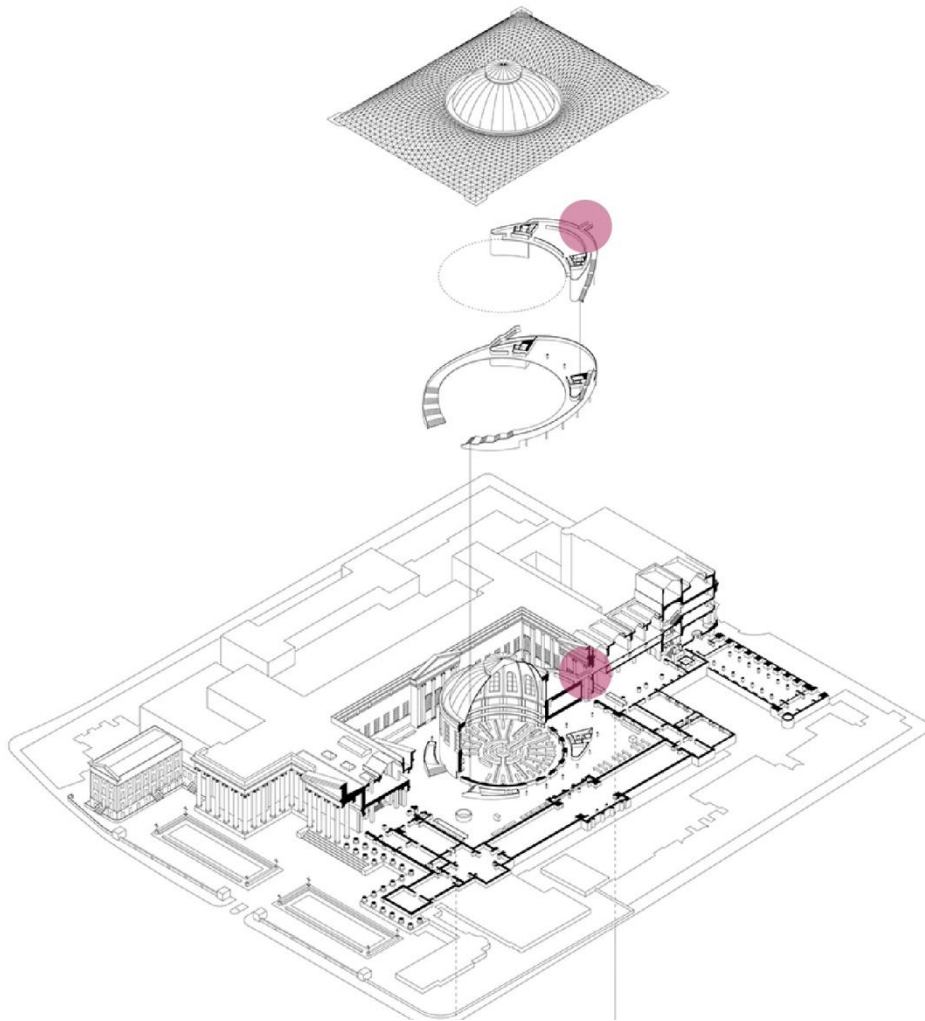

Figure 7 Axonometric of the intervention & location of glass slab.

Selecting a slab element as the case study application is a key point for this thesis, since it adds to the challenge already posed and it can further showcase the potential of cast glass structures. The reason is that the demands of these components in terms of tensile strength –which is the most critical factor for glass - are considerably higher than the respective components which are exposed mainly to compressive loads, such as the columns and, therefore, they are considered as the most challenging ones to be examined.

Specifically, the case study slab has relatively small dimensions (~2.30m*4.20m*0.20m) and is a typical example of the conventional glass structures, made from sheets of float glass and supported from a metal substructure which is fixed on the neighboring walls. The railing is fixed on top of the slab and it also consists of

laminated glass sheets supported by metal frame. Overall, it serves perfectly the purpose of, showing how this new architectural vocabulary can be applied in existing shells and change the qualities of the space. If constructed, it would be able to be seen from all sides – top, side & bottom – so the complex forms which are expected to be created, could serve both for structural but also for an aesthetic point of view.
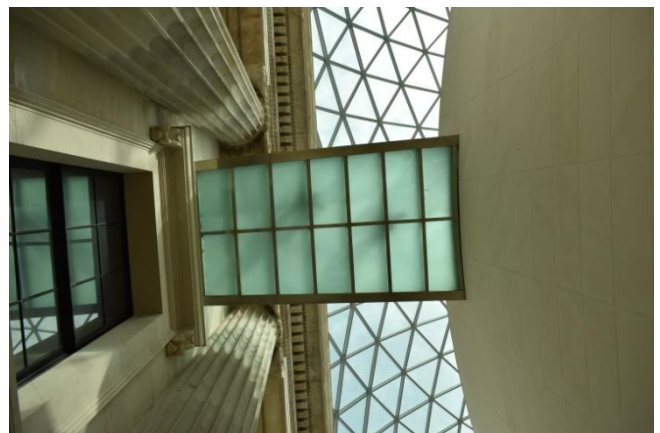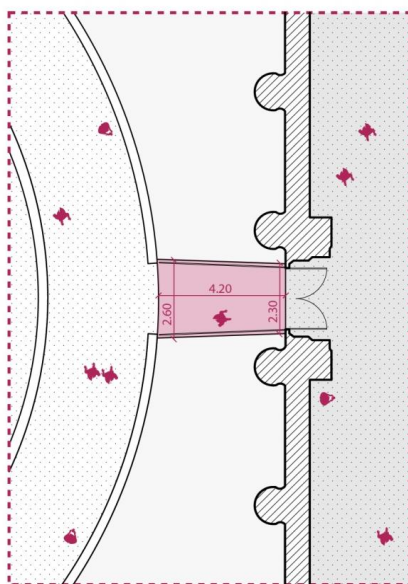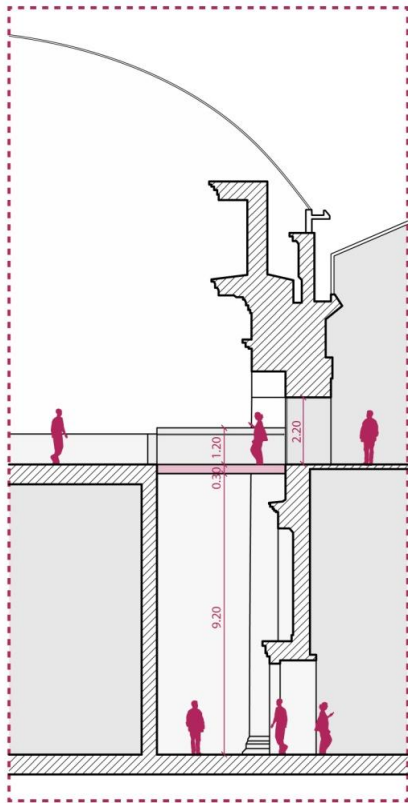
Figure 8 Drawings & photos of the existing glass slab.

3. Glass

In this chapter the characteristic properties of glass, as well the casting and annealing process will be discussed. The potential of the different glass compositions and molding methods will be highlighted in order to select the more suitable options for this object. Moreover, the most critical aspects in each step will be pinpointed in order to define the respective structural, annealing and manufacturing criteria which will be later posed to the algorithm.

3.1 Glass Composition

There are different types of glass based on the composition of its ingredients. Their characteristic structural and thermal properties vary according to them.

Firstly, the types that include a large percentage of silica – aluminosilicate, fused silica and 96%silica -, have a high annealing point (Figure 9), which results in a lengthy and meticulous annealing process and, therefore, in a rather high manufacturing cost. For this reason they are not favored for use in the creation of structural components.

The lead silicate glass has a relatively low viscosity in comparison to the other types, which makes it softer and, thus, easier, firstly, to be formed into the different shapes and, secondly, to be processed through grinding or polishing. Nevertheless, it has insufficient thermal properties, while the increased percentage of PbO in the melt leads to more fragile and heavier[2] components (Shelby, 2005). Moreover, its vulnerability to scratching renders it finally only feasible for use in art installations (Oikonomopoulou, 2019).

Glass type	Mean melting Point at 10 Pa.s*	Softening Point	Annealing Point	Strain Point	Density	Coefficient of Expansion 0°C – 300°C	Young's Modulus
	[°C]	[°C]	[°C]	[°C]	Kg/m³	10⁻⁴/°C	GPa
Soda-lime (window glass)	1350-1400	730	548	505	2460	8.5	69
Borosilicate	1450-1550	780	525	480	2230	3.4	63
Lead silicate	1200-1300	626	435	395	2850	9.1	62
Aluminosilicate	1500-1600	915	715	670	2530	4.2	87
Fused-silica	>>2000	1667	1140	1070	2200	0.55	69
96% silica	>>2000	1500	910	820	2180	0.8	67

*These values are only given as a guideline of the differences between the various glass types. In practice, for each glass type there are numerous of different recipes resulting into different properties.

Figure 9 Properties based on the different glass composition (Oikonomopoulou, 2019).

In this regard, the most appropriate options to be used as a building material are soda-lime and borosilicate glass. Soda-lime glass is the most widely used type of glass. It is cost efficient and durable, although it is not sufficiently resistant to large and quick temperature oscillations. Borosilicate glass offers better mechanical and thermal properties than soda-lime. Particularly, due to its lower thermal expansion coefficient, it renders it possible to reduce the annealing time even in half. Other advantages are related to its durability and the good shaping behavior, due to large working range.

Taking the aforementioned into consideration, it is decided that, although it is relatively more expensive, borosilicate glass will be selected for the needs of this project. However, given that soda-lime glass has comparable structural properties to borosilicate glass and overall is a more recorded material[3], its properties will also be used as reference points throughout the project. A comparative review of the properties of soda-lime and borosilicate glass can be found on Table 1.

---

[2] The increased weight derives from the relatively higher density of lead silicate glass comparing to the rest of the glass types (Fig. 9).
[3] This derives from the fact that soda-lime has been the predominant recipe used in applications in the built environment, such as architectural glass or insulated glass units.

	Symbol	Units	Soda-lime	Borosilicate
Young's modulus	E	GPa	60-70	70
Poisson's ratio	ν	-	0.22 − 0.24	0.2
Density	ρ	Kg/m^3	2500	2200-2500
Thermal expansion coefficient	$α_T$	10^{-6}/K	9	Class 1: 3.1-4 Class 2: 4.1-5 Class 3: 5.1-6
Thermal conductivity	k	W/(m*K)	1.06	1.15
Specific heat capacity	c_p	J/(kg*K)	870	800

Table 1 Comparative review of properties between soda-lime and borosilicate glass.

3.2 Material Properties

Glass is an isotropic material and its characteristic properties vary slightly based on the composition of its ingredients. Overall it possesses properties comparable to those of other typical building materials, such as values for Young's modulus and compressive strength similar to aluminum and stainless steel respectively (Oikonomopoulou, 2019). However, it differs from them in the sense that it cannot yield (O'Regan, 2014) and therefore brittle failure is caused at normal temperature. Consequently, its behavior can be described as almost perfectly elastic (Oikonomopoulou, 2019) and can only be compared to the behavior of other brittle materials, such as unreinforced concrete.

As a result of its brittle behavior, one of the most characteristic features of glass is the large differentiation on the allowable values between tensile and compressive stresses. This is because, although glass has a significantly high compressive strength[4], it shows considerably low resistance under tension since it cannot withstand plastic deformation and, consequently, tensile stresses will finally lead to fracture of the components.

	Symbol	Units	Values

---

[4] According to (Oikonomopoulou, 2019), the values regarding the compressive stress of strength may differ significantly based on the literature which is consulted each time. For this project, the values extracted from the experiments of (Oikonomopoulou et al., 2017b) are going to be used.

Flexural strength[5]	f_{fl}	MPa	69
Tensile strength	f_t	MPa	45
Compressive strength	f_c	MPa	500

Table 2 Characteristic values of flexural, tensile and compressive strength for borosilicate glass in the form of float glass sheets, data from (Oikonomopoulou, 2019).

In Table 2, the characteristic values of tensile and compressive strength for borosilicate glass in the case of float glass sheets are demonstrated. However, it needs to be underlined that the values related to the strength of cast glass elements and particularly the values for flexural and tensile strength, although comparable to the ones related to float glass, they are slightly compromised in the first case. This derives from the fact that a larger amount of flaws exist in the cast glass components because of their increased volume and the non-automated control of flaws during the manufacturing process.

The flaws and defects in glass are mainly caused during the casting process and belong to the following categories (Oikonomopoulou, 2019):

- **Inclusions**, such as bubbles, stones or cords (Figure 10a). Each category can be generated due to different factors. However, they share the same characteristic of acting as local stress concentrations inside the glass structure– caused by their different mechanical and thermal expansion properties – and may lead to failure. They can be removed right after the pouring of the glass melt through auxiliary paths on the mold that allow them to rise in the upper surface.

- **Edge & Surface flaws** (Figure 10b). They have the larger impact on the strength of glass and are usually caused by problems during the machining procedure. Possible ways to responding to these type defects are either to remove part of the surface material through mechanical polishing, in order to reduce the length of flaws, or to apply an additional safety factor on the allowable limits for glass strength.
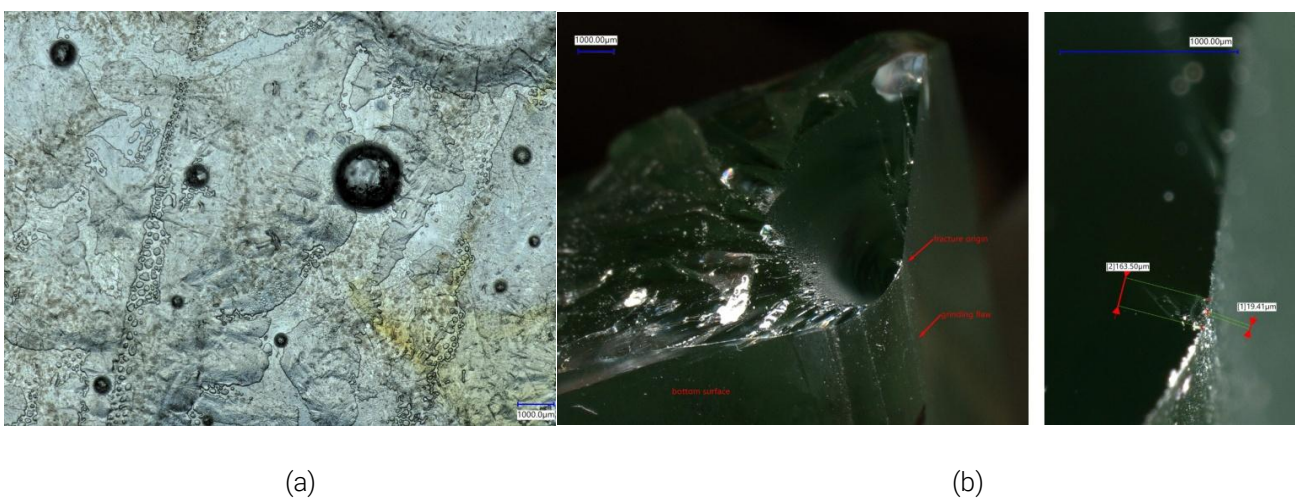

(a)   (b)

Figure 10 Casting defects as seen in the microscope. (a) Inclusions, (b) Edge Crack (from Telesilla Bristogianni).

---

[5] It refers to the stiffness of the material in bending, as mentioned in Granta EduPack 2020.

The existence of flaws is important because they affect the resistance of glass under tension, which is the most critical factor in the case of glass design. They tend to act as stress concentrators increasing locally the tensile stress values and, therefore, leading faster to an exceedance of the allowable limits and ultimately causing fracture (Oikonomopoulou, 2019). In contrast, compressive strength remains unaffected by the geometric defects, since these do not expand in a compressive stress field (Figure 11).
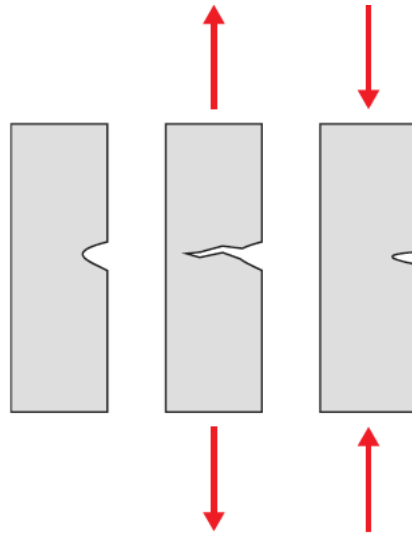

Figure 11 Diagram illustrating how the crack propagates under tension but closes/remains unaffected during compression (Damen, 2019).

Nevertheless, the effect of flaws in the absolute value of flexural strength is expected to be slight and not significant, since the majority of flaws appear on the meso-structure and the number of critical surface flaws remains limited (Oikonomopoulou, 2019). Thus, the values for the flexural strength of cast glass are only slightly compromised in comparison to float glass. Particularly, experiments from (Bristogianni et al., 2020) showcase that the flexural strength of borosilicate cast glass is 44 MPa (Table 3). This value is used as a reference point in order to extract an approximate value for the tensile strength of cast glass. Assuming that the flexural and tensile strength are proportional, we can calculate the tensile strength of cast glass as::

$$f_{t,cast} = \frac{f_{t,float}}{f_{fl,float}} \times f_{fl,cast} = \frac{45}{69} \times 44 = 28,7 \sim 29 \; MPa$$

	Symbol	Units	Float glass	Cast glass
Flexural strength	f_{fl}	MPa	69	44
Tensile strength	f_t	MPa	45	29

Table 3 Characteristic values of flexural and tensile strength for borosilicate glass in the case of float glass and cast glass elements.

Given that currently there are no guidelines specialized to the design of cast glass structures, the regulations for float glass structures are going to be used as a reference. Therefore, the formula from the German structural design standard is going to be adapted in order to derive a conservative yet safe value for the tensile

strength of cast glass. According to the German standard, the design tensile strength is significantly smaller from the characteristic tensile strength (Table 4) and should be calculated as followed (DIN 18008):

$$R_{d \, float} = \frac{k_{mod} * k_c * f_t}{\gamma_m}$$

where:
k_{mod} : Coefficient for consideration of the load duration of annealed float glass (0.4 for medium loads)
k_c : Coefficient for consideration of the type of construction (1.0 for float glass horizontal construction)
γ_m : Partial safety factor of resistance of the material (1.8 for float glass)

The load scenario which is assumed is the one related to loads of medium duration, since these are expected in the case of the case study interior bridge. The resulting values are going to be applied as the limits for the respective stresses in the algorithm (Table 4). It needs to be underlined that, given that the behavior of glass under compression remains unaffected by flaws and defects, the total value of compressive strength is used as the respective design limit (Table 4).

	Symbol	Units	Values for medium loads
Design tensile strength	$f_{t,des}$	MPa	6,4
Design compressive strength	f_c	MPa	500

Table 4 Design values for tensile and compressive strength of glass after calculations according to DIN 18008.

Regarding the allowable deformation in the case of glass elements, there are two different characteristic values. The first one is a stricter limit and is related to the deflection of the component during the construction and placement phase, whereas the second one is related to the serviceability of the structure after it is successfully placed and therefore is more relaxed (Table 5). In this project, the limit related to the serviceability of the structure is going to be considered.

	Symbol	Units	Values
Deflection during construction phase	d_c	m	$\frac{l}{250}$
Deflection for serviceability	d_s	m	$\frac{l}{500}$

Table 5 Design values for deflection in glass components.

3.3 Casting Methods

The methods of casting glass can be distinguished into two main categories:

- **Primary casting.** In this case, the glass melt is created directly from the raw materials that compose it according to the glass recipe. In this case, the main process is hot-forming and involves, firstly, creating the glass melt in a furnace and, secondly, pouring it inside a mould (Figure 11a). Afterwards, the melt is passed onto a second furnace in order to cool down.

- **Secondary casting.** In this case, the glass melt is created from melting already formed glass batch components (Shelby, 2005). The main process in this case is kiln-casting. Particularly, after re-heating the batch components up to the necessary temperature, the glass melt which is created falls inside the mould, forms the desired shape (Figure 11b) and it then remains inside the same furnace until it is efficiently cooled down. Consequently, secondary casting need less operating temperatures than primary casting.

It is evident that the two main differences among the casting methods are the initial state of the materials and the equipment needed for it. In the first case, the material used is in its raw phase and two different furnaces are needed; whereas in the second case only one furnace is needed in total and the glass melt is created from glass batch components. Overall, primary casting is favored in the case of industrial scale production, while secondary casting is the preferred method in the case of customized components.
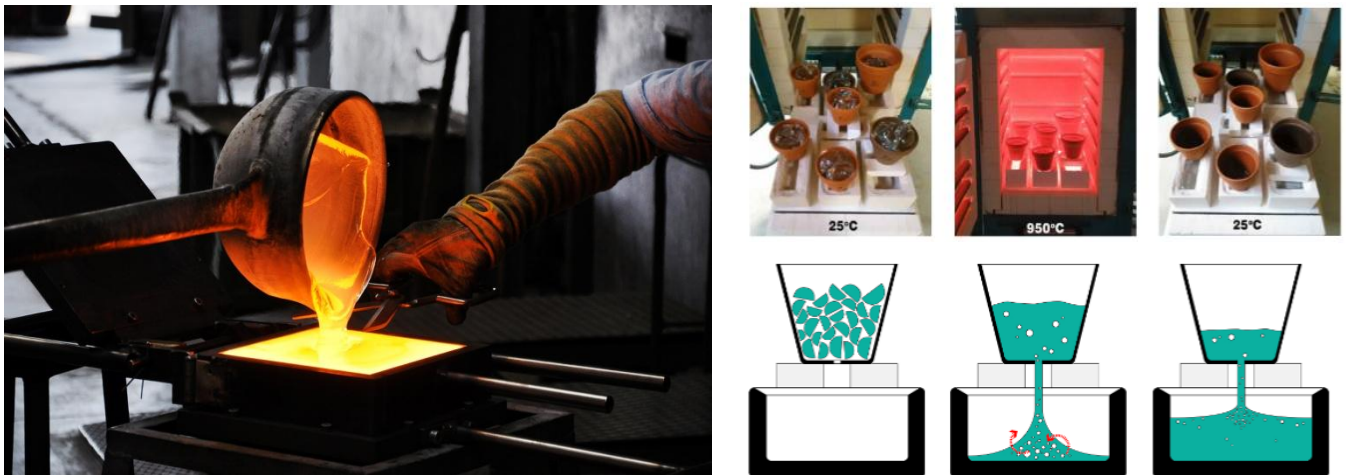

Figure 12 (a) Primary and (b) secondary casting glass process

3.4 Annealing process

Independently of the method followed for the casting of the glass elements (primary or secondary), the same process needs to be followed in order to be efficiently cooled down. This includes passing from different characteristic points (temperatures) defined based on the composition of the glass recipe. Each of these points serves a different role in the forming of the final product and the cooling rate for passing from the one characteristic point to the other is strongly related to it. The most characteristic temperature points are[6] (Figure 12):

---

[6] The information related to the characteristic temperature points is extracted from (Shelby,2005).

- **Melting Temperature:** It refers to the point where the viscosity of the melt is such (<10^3 Pa) that homogeneity and fining can be obtained in a reasonable time.
- **Working Point:** It refers to the viscosity of the melt when it is delivered at a processing device (10^3 Pa). The melt must be able to flow under reasonable stresses, but have a sufficient viscosity so that it maintains its shape after forming.
- **Softening Point:** At this point the glass melt has sufficient viscosity ($10^{6.6}$ Pa) in order to be able to resist any deformation under its own weight.
- **Annealing Point & Strain Point:** These two points define the annealing temperature range, which is very critical for the final quality of the cast glass product. The annealing process starts after the temperature falls below the softening point and serves to eradicate any existing strains. In order to achieve that, the cast glass product is retained at the annealing point for sufficient time and then is cooled down with a slow rate so that no other internal residual stresses are generated during the cooling. Sufficiently below the strain point the stress cannot be released and is considered permanent. Afterwards, the product can be cooled at a faster rate but still slow enough in order to avoid breakage.
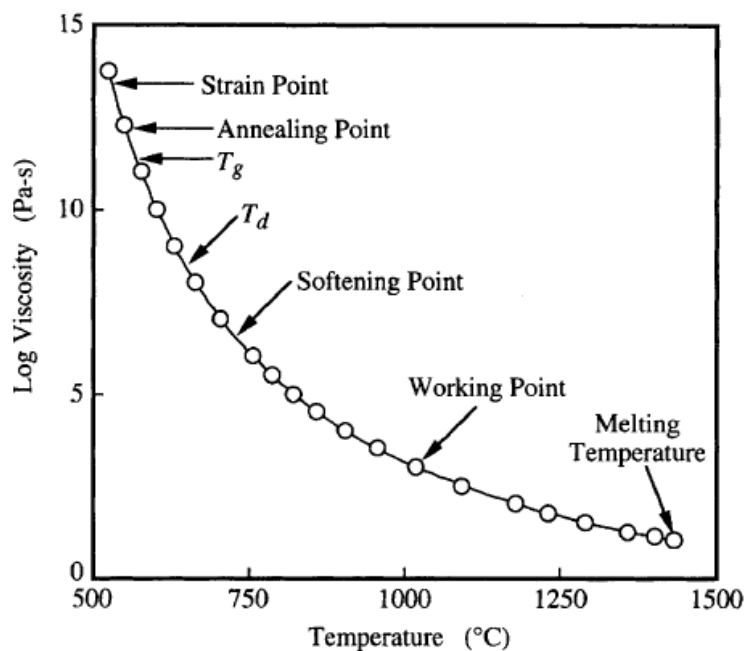

Figure 13 Diagram of viscosity as a function of temperature for a soda-lime melt.

It is evident that the part of the cooling process which is more time-consuming and, therefore, has the largest effect on the overall long length of the process is the one related to the annealing phase. At this step, the process needs to be delayed significantly in order to have sufficient time for the release of strains and preventing the generation of residual stresses. Characteristically, the duration of this process may last from several days to several months or years and, therefore, it should be significantly reduced in order for a structure to be considered as feasible to be manufactured.

Consequently, only this time range is going to be considered for the creation of the algorithm constraint and the reduction of the overall time needed. Particularly, the time range that is going to be calculated is the one mentioned as Phase B (initial cooling) in (Oikonomopoulou, 2019). It includes a relaxed version of the temperature range between annealing and strain point in order to ensure that the whole process is covered (Figure 13). For borosilicate glass, the range starts 5 $^{\circ}$C before the annealing point and is completed α=20 $^{\circ}$C below the strain point (Table 6).
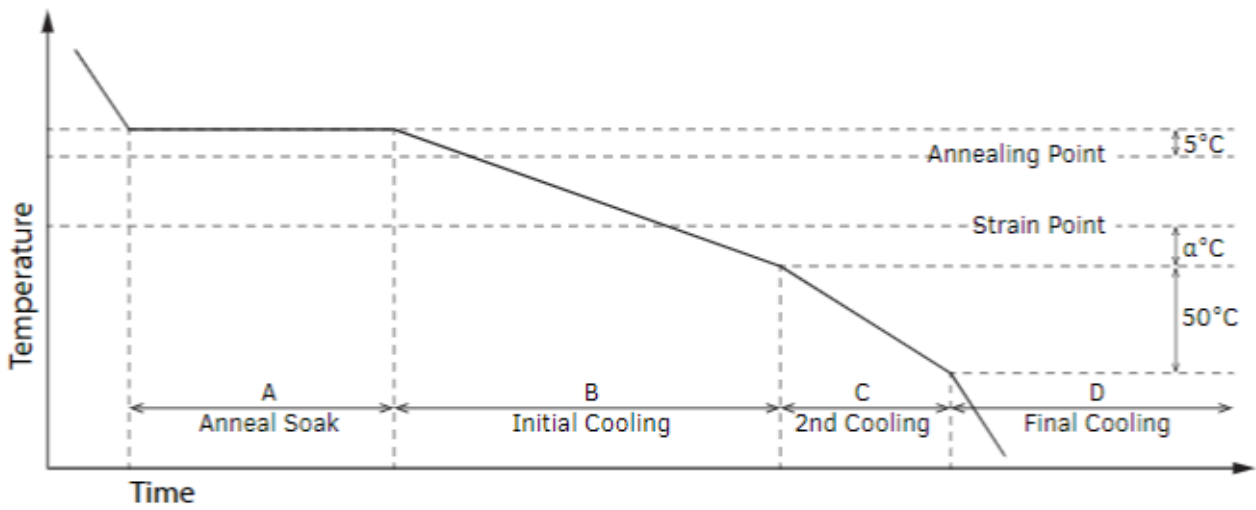
Figure 14 Typical annealing scheme for soda-lime glass.

	Metric Units	Borosilicate glass
Annealing point	°C	525
Strain point	°C	480
Initial Cooling range (total)	°C	530-460

Table 6 Characteristic temperature points for borosilicate glass.

The amount of time needed to delay in order to efficiently cool down the cast glass product until its strain point is strongly related to the size of the maximum cross section. This is why, as mentioned in Chapter 1, larger elements that incorporate a honeycomb structure to their design tend to have relatively smaller annealing times. It derives from the fact that the time needed is defined based on the dimension of the cross section of each smaller part and not on the size of the whole element in total (in the case that this is not made from full material).

There are several formulas that intend to approximate the annealing time needed. They take into consideration both the element size but also a wide range of other factors that play a role on cooling such as the material thermal properties[7] or the geometric characteristics and the total shape of the component[8]. Nevertheless, it needs to be underlined that, although these formulas provide a good approximation, there are also other aspects which cannot be directly integrated to them, such as the number of sides exposed to cooling, the existence or not of other thermal masses in the furnace or even the geometry of the furnace itself (Oikonomopoulou, 2019).

---

[7]The glass composition affects the thermal expansion coefficient which has an impact on the time needed for the annealing. In general, glass components with lower thermal expansion coefficient will need shorter annealing time.
[8] Reducing the mass along with introducing inner voids and ribs in the design will facilitate the heat flow and, thus, the annealing process (Stefanaki, 2020).

In (Koopman, 2021) the total annealing time is calculated as a function of the thickness of the cross section using the following formula:

$$T = 0{,}0156 \times t^2 + 0{,}139 \times t + 0{,}7266$$

where t is the thickness of a flat slab in mm

The formula describes the minimum time needed for the annealing process of a flat slab created by soda-lime glass when exposed only on its two large sides. As a result, further modifications needed to be done in the formula in order to approximate better the different conditions that were assumed on the project, such as the use of a different glass composition or the amount of sides exposed to cooling[9].

Because of the large dependence of this formula in the specific characteristics of the example it refers to, in this project another equation for the calculation of the cooling rate h is considered as most suitable due to its adaptability into different glass compositions and shapes. Specifically, it refers to annealing with the use of an annealing lehr, where the glass article is cooled from the top part, although the faces on the sides are also not completely blocked. The formula derives as a variation of the formula mentioned in (Shand & Armistead, 1958) and is defined by (Hubert, 2015) as followed:

$$h = \frac{\sigma}{M d^2 b}$$

$$h = \frac{\sigma}{\dfrac{E\, \alpha_{ex}\, \rho\, c_p}{(1-\mu)\, \lambda} \times d^2 \times b}$$

where σ is the maximum allowable permanent stress in the glass article (normally 1 MPa), d is the characteristic dimension (in case of a glass sphere it refers to the radius), b is the shape factor (0.066 for spheres) and the parameter M is defined according to the following equation:

$$M = \frac{E\, \alpha_{ex}\, \rho\, c_p}{(1-\mu)\, \lambda}$$

where:
E is the Young's modulus of the material (MPa)
α_{ex} is the thermal expansion coefficient (K^{-1})
ρ is the density (kg/m^3)
c_p is the specific heat (J/(kg*K))
μ is the Poisson's ratio
λ is the thermal conductivity (W/(m*K))

Through these calculations the cooling rate h in K/s can be extracted. The temperature range in K refers to the initial cooling range as defined earlier.

Apart from the overall time needed, there are also other critical aspects regarding the annealing process that need to be taken into consideration in order to efficiently reduce the creation of internal residual stresses. The distribution of the mass in the component should be approximately equal and, thus, the size of the cross

---

[9] (Koopman,2021) suggests that for components made from borosilicate glass the annealing time should be halved, whereas when less sides are exposed to cooling, the annealing time should be increased – in this example doubled.

section in all the parts should lie between a limited range so that there are not significantly different – larger or smaller – areas. This derives from the fact that a big difference in the distribution of the mass would result in significantly different cooling times and, therefore in local stress concentrations which could even cause fracture. In this regard, attention should also be paid to the corners of the shape, since sharp and thin edges will cool much faster than the rest of the component increasing the possibility for cracks in the component. Therefore, thin elements or sharp edges should be avoided and they should be replaced by elements of a minimum dimension and round edges respectively.
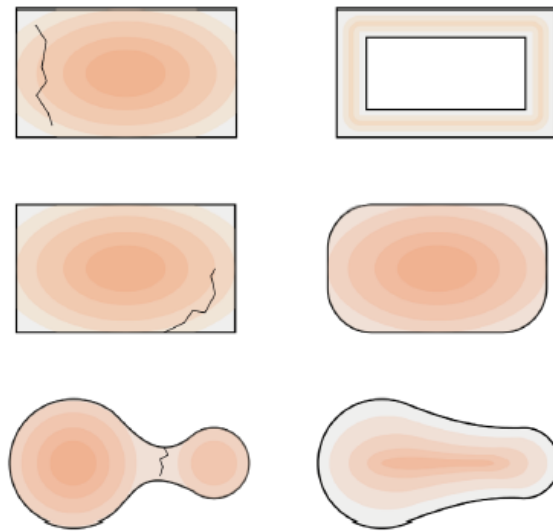
Figure 15 Different scenarios that can help in avoiding cracking because of thermal shock (from top to bottom: weight reduction, sharp edges, unequal mass distribution), (Damen, 2019).

3.5 Moulds

In general, the glass moulds are divided into two large categories based on their durability under exposition into high temperatures and, therefore, their capability to be used for multiple castings:

- **Disposable moulds**: They are made from brittle materials and they can only withstand a small number of operations. Therefore, they are beneficial for use in small batch quantities and only when kiln-casting process is applied. Additionally it needs to be mentioned that, in the case of casting with disposable moulds, the glass product needs post – processing due to the roughness of the result (Oikonomopoulou et al., 2020). The level of accuracy as well as the manufacturing cost of the disposable moulds is highly dependent on the material from which they are made each time. Silica-plaster offers a low level of accuracy, whereas alumina-silica fiber moulds provide a good level of accuracy, but with a high manufacturing cost. On the contrary, recent experiments referring to the use of 3d-printed sand moulds show that they can achieve a high level of accuracy for complex shapes including undercuts in a relatively quick and cost-efficient way.

- **Permanent moulds**: They are made mainly from stainless steel and they are strongly resistant when exposed to high temperatures. For this reason they can also be used in primary casting processes. They offer a high level of accuracy as well as a glossy outcome by the end of the casting which does not need any further post-processing. However, the high manufacturing cost – which increases even more in the case of complex geometries – renders it unsuitable for the casting of topology optimized geometries (Oikonomopoulou et al., 2020).

Through comparing the different mould types along and their characteristic properties (Table 7) it is concluded that 3d-printed sand moulds are the best option for casting of the TO optimized cast components. They offer high precision for complex forms along with a relatively small cost, while they are also better in terms of sustainability since they can easily be dissolved into sand and reused as a 3d printing material multiple times (Bhatia, 2019).

In practice, the 3d-printed sand moulds have already been used for casting of concrete and steel elements (Figure 16). However, it should be highlighted that the maximum size of 3d-printed sand mould that can currently be achieved by the Voxeljetprinter VX4000 is 4m*2m*1m (Oikonomopoulou et al., 2020), so, in the case of large slabs, the total mould should be divided into smaller parts. In terms of casting of glass products, the suitability of 3d-printed sand moulds has already been proven through the experiments of (Bhatia, 2019) and (Damen, 2019), shown in Figure 16.

Through these experiments, additional manufacturing constraints regarding the use of moulds have been defined. As already mentioned, a major constraint is the maximum size of the 3d-printed sand moulds. Additionally, auxiliary paths needed to be designed in the mould in order for bubbles to be efficiently removed during the casting process. The space for the screw holes that will serve the connection of the different mould parts should also be taken into account, and it should be ensured that every part of the formwork can be accessed in order to be efficiently removed afterwards. Lastly, the minimum size of void in the TO structure should be defined, so that the formwork has always a sufficient thickness and is able to withstand the pressure which will be developed during the pouring of the glass melt.

Characteristics | Mould type

Reusability	Disposable			Permanent				
Material	Silica plaster	Alumina silica	Sand	Steel/Stainless steel			Graphite	
Adjustability	-	-	-	Adjustable	Fixed	Pressed	Adjustable	Fixed
Production method	Investment casting/ lost wax technique	Milling	3d printing	Milling/cutting and welding			Milling/grinding	
Manufacturing costs	Low	High	Low	Moderate to high			High	
Top temperature	900-1000 ^{o}C	~1650 ^{o}C	unknown	~ 1200°C/1260°C			unknown	unknown
Glass annealing method	Mould not removed for annealing			Mould usually removed for annealing/only maintained if high accuracy is required			Mould not removed for annealing	
Release method	Immerse in water	Water pressure	unknown	Release coating necessary			Release coating necessary	

Level of precision	Low/ moderate	High	High	Moderate/High	High	Very high	Moderate/ High	High
Finishing surface	Translucent/rough			Glossy			Glossy with surface chills	
Post-processing requirements	Grinding and polishing required to restore transparency			Minimum or none post-processing			Minimum or moderate post-processing	
Applicability	Single component/low volume production			High volume production			High volume production	

Table 7 Different types of moulds and respective properties (edited from (Oikonomopoulou, 2019)).

Figure 16 3d-printed sand moulds used for the casting of (top left & middle) concrete slab, (top right) steel node, (bottom left & middle) cast glass node and (bottom right) cast glass prototype.

3.6 Discussion

To conclude, the large shaping potential of glass as well as the high values of Young's modulus and compressive strength, which are comparable or even higher than the respective values of other conventional structural materials, support the argument that massive cast glass components can have large potential for structural applications. The main drawback that impedes the development in this direction is the large annealing time needed. This is affected both by geometric parameters, such as the mass of the component, and material thermal properties, such as the thermal expansion coefficient, which differ based on the glass composition that is used every time. In the first case, it has already been demonstrated that TO methods can be a useful tool for the design of cast glass structures which are feasible to be manufactured, since the reduction of the mass results in reducing considerably the total annealing time needed. However, the brittle behavior of glass, which results in considerably different allowable limits for tension and compression, renders it unsuitable to use available commercial software, which is mainly oriented towards ductile materials.

Regarding the glass composition, borosilicate glass has proven to be the most adequate for these applications, since it combines good structural properties with low thermal expansion coefficient as well as workable melting temperature. However, because there are not a lot of available data for borosilicate glass, through this project, the values regarding the structural limits of soda-lime glass will also be used as reference.

In order to create an algorithm that will simulate better the physical conditions, the criteria which derive from the several casting phases have to also be identified and incorporated to it.

In terms of the casting of the component, attention should be paid in order to avoid flaws, such as inclusions, that can act as local stress concentrators in the structure. For this reason, vent paths should be added to the mould in order to eliminate the inclusions by letting them rise to the surface. Edge and surface flaws can also act as stress concentrators. In order to be removed, the upper level of material is removed through machining. However, since they can never be completely removed, a safety factor should be added to the glass calculations. Overall, given that the existence of flaws in the casting process can significantly deteriorate the structural integrity of the glass structure by activating faster the fracture mechanisms and, thus, resulting to brittle failure, several safety factors were considered when evaluating the tensile strength of cast glass in order to be able to provide a sufficient estimation.

In terms of annealing, the time needed can be calculated as a function of the size of the cross section, so its thickness should not exceed a maximum value. Additionally, it is very important to set a minimum allowable glass thickness that could be manufactured as well as ensure that there is homogeneous mass distribution in the structure. In this regard, the minimum and maximum size of cross section should always lie inside a specific range in order not to have large differences that would result in considerably different annealing times and could even cause failure. Additionally, sharp edges should be avoided because they can also lead to large residual stresses and break.

Lastly, it is concluded that the most suitable type of mould for the casting of complex glass geometries is 3d-printed sand mould. The criteria which derive in this part have to do mainly with the maximum size of sand mould that can currently be 3d printed as well as the minimum thickness of the formwork in each part in order to be able to withstand the hydrostatic pressure developed when pouring the glass melt.

3.7 Input values & hard criteria

Taking the aforementioned into consideration, the tables with the specific input values selected regarding the material properties as well the allowable limits and the respective hard criteria are defined. These are going to later be used as input for the algorithm optimization.

	Symbol	Units	Input values (Borosilicate glass)
Young's modulus	E	GPa	70
Poisson's ratio	v	-	0.2
Density	ρ	Kg/m^3	2500
Initial cooling range (annealing process)	ΔT	$^{\circ}$C	530-460 (=70)
Thermal expansion coefficient	$α_T$	1/K	3.25×10^{-6}
Thermal conductivity	k	W/(m*K)	1.15
Specific heat capacity	c_p	J/(kg*K)	800

Table 8 Input values.

	Symbol	Units	Input values (Borosilicate glass)
Design tensile strength	$f_{t,des}$	MPa	6,4
Design compressive strength	f_c	MPa	500
Deflection	d	m	$\dfrac{l}{500}$
Maximum annealing time	$t_{ann,max}$	s	432000 (5 days)
Minimum element dimension	d_{min}	m	0.06
Ratio of maximum to minimum element dimension	r_{ann}	-	2
Maximum permanent residual stress (after annealing)	$σ_{res,max}$	MPa	1

Table 9 Hard criteria.

4. Structural Design Optimization

In this chapter the different categories of Structural Design Optimization will be described. The emphasis will be placed mainly on Topology Optimization methods, which will be analyzed and critically compared between them in order to finally select the most adequate option for this project. Additionally, methods will be discussed regarding how the criteria set in the previous chapters can be integrated into the algorithm as well as which problem formulation is the most adequate for implementation in this case. The final problem statement will be formulated taking also into consideration the methods used by available commercial software, as well as the strategies used in previous experiments regarding glass and other brittle materials, such as unreinforced concrete.

Structural Design Optimization refers to the use of numerical techniques in order to define the optimal material distribution of a structure for a given set of objective and constraints. In recent years, it has been proven to be of significant importance especially for the construction industry, since it serves for the design of material and cost efficient structures, which, at the same time, fulfill the demands in terms of structural performance. The development of these innovative solutions has been strongly related to the synchronous advances in digital manufacturing technologies that have made it possible for these structures to be realized.

4.1 Optimization problem

A typical optimization problem is formulated as (Boyd & Vandenberghe, 2004) :

$$\min_{x} \ f(x)$$

$$subject \ to \ \ g_i(x) \leq 0, \qquad i = 1,2,\dots,m$$
$$h_i(x) = \ 0, \qquad i = 1,2,\dots,p$$
$$x \in \Omega_{mat} \subseteq \Omega \ \in \ R^n, \qquad n = 2,3$$
$$f_0(x) \colon R^n \ \rightarrow \ R$$

It describes the process of finding the value x (design variable), which belongs to the domain Ω^{mat} and minimizes the function $f(x)$, which refers to the objective of the problem. This domain Ω^{mat} needs to be specified in order to apply the respective loads and boundary conditions for the structure and is part of the reference domain Ω in R^2 or R^3, referring to two-dimensional or three-dimensional shapes respectively (Bendsoe & Sigmund, 2004).

Lastly, the functions $g_i(x)$ and $h_i(x)$ describe the state variables, referring to the constraints that must be fulfilled in order for a design to be considered as admissible. These are mostly related to the structural performance of the design and the limitations in terms of the manufacturing process.

4.2 Categories

Based on the parameters that are changeable each time, structural design optimization can be classified in the following categories:
- Sizing Optimization (Figure 17 - left). In these problems, the variables are mostly related to geometrical parameters and the problem seeks to optimize a specific numeric value, e.g. the optimal thickness of a specific member. The design domain and the state variables remain unchanged during the optimization process (Bendsoe & Sigmund, 2004).
- Shape Optimization (Figure 17 - middle). Here all the admissible designs result from an initial design guess as variations of its boundary shape. However, the topology[10] remains fixed throughout the optimization and, therefore, no new boundaries can be generated −e.g. by creating new holes (Allaire et al, 2019).
- Topology Optimization (Figure 17 - right). In this type of optimization problems, not only the shape, but also the topology can change, meaning that new holes can also be added to the design and an initial guess is not needed.

---

[10] Topology refers to the branch of geometry describing the properties of a figure that remain unaffected by continuous distortion, such as stretching or knotting (Collins Dictionary). It defines the characteristics of a geometric object, such as the number of its inner holes and, in general, the connectivity of its domain (Bendsoe & Sigmund, 2004, p.1).
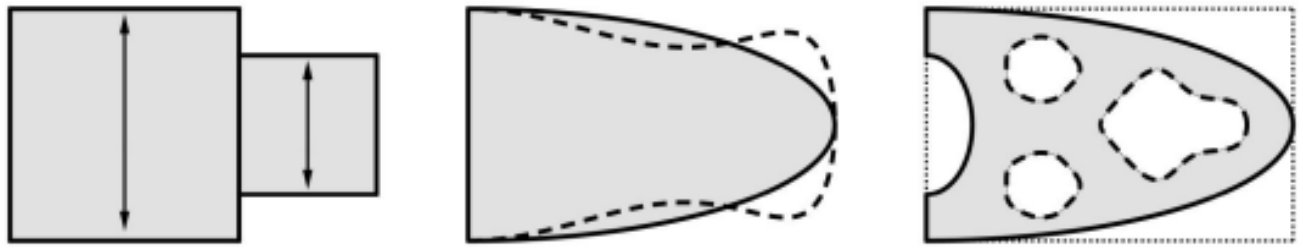
Figure 17 Diagrams for (left) Size, (middle) Shape and (right)Topology Optimization problems (Allaire et al, 2019).
.

4.3 Algorithmic methodologies

It can easily be concluded that TO offers the larger potential in terms of design exploration and, therefore, this thesis is going to emphasize on methods and approaches referring to this optimization category. Overall, the methods that have already been developed can be distinguished between Gradient-based, which use functions and their derivatives for the optimization, and Gradient-free methodologies.

4.3.1 Gradient-based methodologies

There are two main subdivisions in this category. The first one refers to Density-Based methodologies, which convert the TO problem into an equivalent sizing problem in order to solve it, and combined Shape and Topology methodologies.

4.3.1.1 Density-based methodologies

The characteristic of the approaches that belong to this category is that the geometric object is described as a distribution of pseudo densities throughout the design domain, which reflect the existence or not of material in each specific position. Homogenization method and Solid Isotropic Material with Penalization are the most popular approaches in this category and, along with their variations, are of the most widely used TO methodologies in general.

A. Homogenization method

It is the first TO method introduced (Bendsoe & Kikuchi, 1988) and it is making use of the properties of composite materials in order to describe the spatial material distribution as an interpolation of void and full material (Bendsoe & Sigmund, 2004). Particularly, the homogenization method consists in discretizing the design domain in infinitely small rectangular elements with inner voids, reflecting the structure of a porous medium (Figure 18)[11]. In this regard, the TO problem is formulated as a sizing problem, aiming to define the optimum dimensions of each void and, therefore, the optimum porosity of the element in total (Xie & Steven, 1992).

---

[11] Each element contains a rectangular void with dimensions μ_α, μ_β ranging from $\mu_\alpha = \mu_\beta = 1$, which corresponds to totally void, to $\mu_\alpha = \mu_\beta = 0$, which corresponds to totally full (Kumar, 2016).
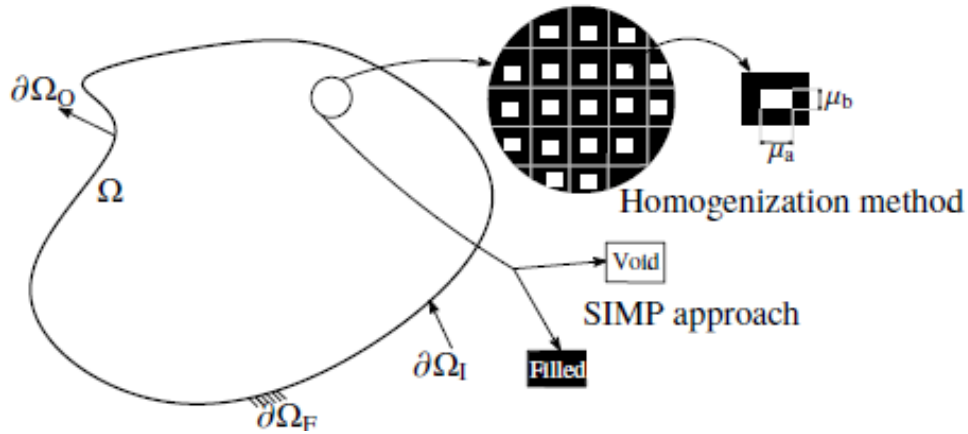
Figure 18 Inner structures in Homogenization method & SIMP approach (Kumar, 2016).

Although the structure of the methodology refers to a sizing problem, it is still considered as a Topology Optimization method in the sense that in the fractions of the material domain which have only void elements, inner holes will be created (Querin et al., 2017).

B. Solid Isotropic Material with Penalization (SIMP)

It is a simplified version of the homogenization method that resembles a black and white raster image, in the sense that no inner voids are taken into account and each rectangular element is assigned only one value ranging from 0 to 1. Similarly to the homogenization method, SIMP is structuring the optimization problem as a sizing problem on a fixed domain (Bendsoe & Sigmund, 2004), but, throughout the process, the topology of the element is also being altered.

The values assigned to each element are directly related to a pseudo density function ρ(x), where ρ(x)= 0 stands for void and ρ(x)=1 stands for full material (Nathan et al., 2020). In most of the cases, these variables are continuous allowing also for intermediary densities that create not only 'black' and 'white', but also 'grey' areas in the element (Bendsoe & Sigmund, 2004).

The SIMP method refers to isotropic materials and it is important that each time the optimization process takes into account the characteristic material properties of the physical model. For this reason, in the problem formulation, the pseudo density function ρ(x) is combined with the stiffness tensor in the $E_{ijkl}(x)$ function and, thus, in the end the values in each element range from 0 to E^0_{ijkl}. However, it is important to avoid a lot of intermediary densities that, although they will add to the volume, they will not contribute a lot to the stiffness of the structure. In this regard, a penalization value p is introduced in the pseudo density function ρ(x), which when p>3 ensures that the values obtained will be leaning towards the boundaries 0-1(Bendsoe & Sigmund, 2004). In this regard, the basic formulation of the SIMP problem is Bendsoe & Sigmund, 2004):

$$E_{ijkl}(x) = \rho(x)^p E^0_{ijkl}, \qquad p > 1$$

$$\int_\Omega \rho(x)d\Omega \leq V, \qquad 0 \leq \rho(x) \leq 1, \qquad x \in \Omega$$

$$E_{ijkl}(\rho = 0) = 0, \; E_{ijkl}(\rho = 1) = E^0_{ijkl}$$

The density-based optimization approaches result in problems that can efficiently be solved and can easily incorporate the global constraints posed (Sigmund & Maute, 2013). However, in spite of the large potential of the SIMP approach in terms of design experimentation, different issues arise through the optimization processes which need to be overcome in order to have more accurate and feasible solutions.

Firstly, it has been questioned how the intermediary values of the pseudo density function can be translated in reality, since, if the resulting values have not completely converged to 0 and 1, the properties described in the solution can only be achieved with composite materials(Bendsoe & Sigmund, 2004). Additionally, it happens that the optimization outcome is not fixed, but changes based on the number of elements obtained through the mesh discretization and, therefore, there is not an optimum solution achieved (Bendsoe & Sigmund, 2004). The mesh dependence of the optimization outcome derives from the fact that, in principle, introducing a larger number of inner cavities leads to more efficient use of material and, thus, it is favored in the optimization. In this regard, if a finer discretization is applied and it is feasible to further analyze the inner cavities, more holes will appear in the structure (Figure 19).
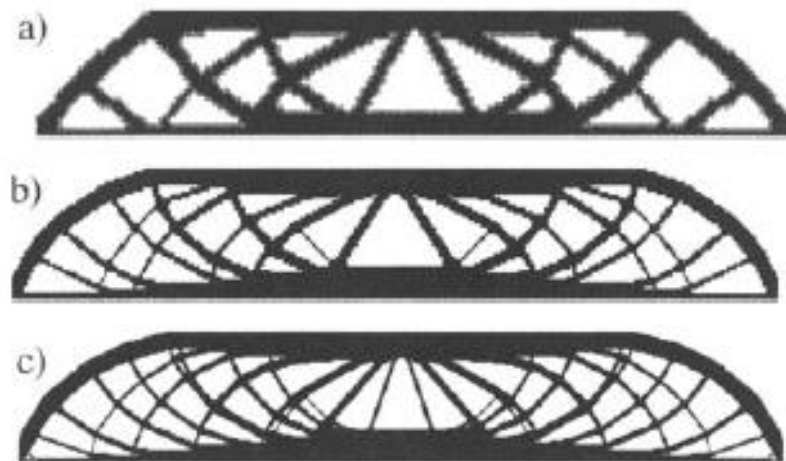
Figure 19 Mesh dependence in optimization of MBB-beam example with SIMP approach. Solution for discretization with a) 2700, b) 4800 and c) 17200 elements (Bendsoe & Sigmund, 2004).

Moreover, geometric singularities are common issues that arise through using rectangular cells for the TO process. They should be avoided, since they result in false estimations regarding the performance of the element designed. The main categories which are detected are:

- Checkerboards (Figure 20a). It is often the case that the element obtained through TO do not have a solid surface, but, on the contrary, it is filled with patches of checkerboard pattern[12]. This derives from the fact that the checkerboard structures falsely appear to perform better in terms of stiffness during the finite element analysis and, thus, they are favored from the software (Bendsoe & Sigmund, 2004).

- Point flexures (Figure 20b). This refers to connections that resemble the function of revolute joints and happen when two large elements are connected in a single point[13]. Although these connections may indeed perform

---

[12] A checkerboard pattern resembles the pattern of a draught board with alternating black and white rectangular cells.

[13] The connection may consist of more than one rectangular cell, but its surface in total is so small in comparison to the element surface, that it is considered as a single point.

well in terms of compliance[14], they result in increased localized stresses and they are not feasible to be manufactured. (Yin & Ananthasuresh, 2003)

- Layering & Islanding (Figure 20c). This refers to parts of the structure that are totally disconnected from all sides of the main elements and, therefore, cannot have any physical translation (Saxena, 2011).
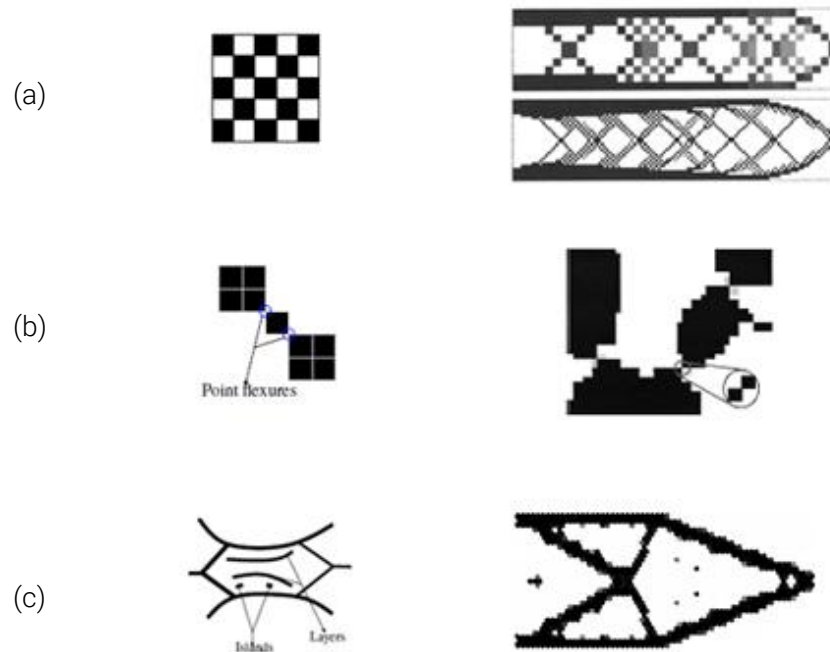

Figure 20 Geometric singularities. (a) Checkerboard pattern (b) Point Flexures (c) Layering & Islanding. Adapted from (Kumar, 2016) &(Bendsoe & Sigmund, 2004) & (Yin & Ananthasuresh, 2003) & (Saxena, 2011).

Lastly, another common issue, which results in inaccuracies regarding the estimation of the structural performance of the element, is related to the boundaries of the element obtained. These are often blurred and not completely discrete, with angles that prevent from the creation of one continuous boundary line (Figure 21). This has an effect not only in the precision of the shape, but may also lead to larger compliance during the structural analysis (Nathan et al., 2020).

---

[14] They allow for large deformations without increasing a lot the strain energy in the structure (Yin & Ananthasuresh, 2003).
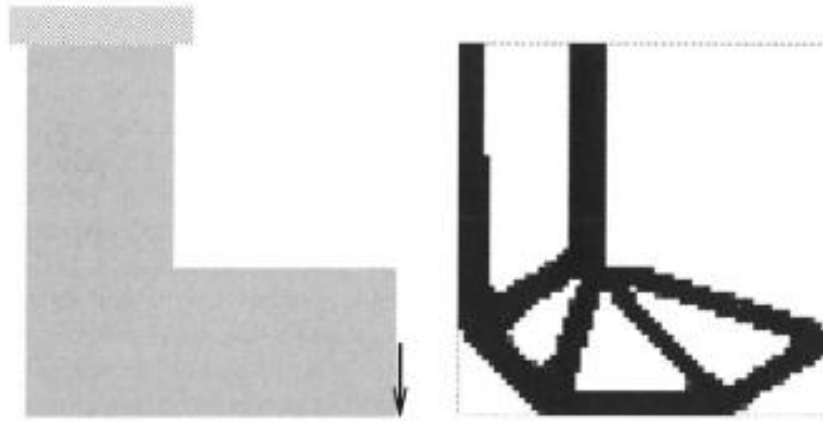
Figure 21 Jagged boundary after the optimization of a loaded knee-structure (Bendsoe & Sigmund, 2004).

.

Throughout the years, there are several ways developed in order to overcome the aforementioned problems. They are related to adaptations in the shape of the elements (e.g. honeycomb tessellation from (Saxena, 2008)), filtering according to the neighboring densities ((Poulsen, 2002) and (Bendsoe & Sigmund, 2004)), applying constraints in terms of the minimum size of the design cross section (Guest, 2009) or gradient and perimeter constraints (Sigmund & Maute, 2013).

4.3.1.2 Combined Shape and Topology Methods

Unlike the density-based methodologies, where the TO problem is converted into a sizing problem, the combined shape and topology methods analyze the TO problem in a set of shape optimization steps which in total alter also the topology of the design. The characteristic in this category is that the mesh is not discretized into smaller elements and the geometry is taken into consideration as a whole with a discrete boundary.

A. Bubble method

It is one of the first TO methods developed already by (Eschenauer et al., 1994). The notion of this method is that it starts with an initial guess regarding the design and performs a shape optimization for its boundary considering the relevant objective and constraints. Afterwards, holes are inserted inside the shape in positions defined analytically based on the criteria which have already been posed. Lastly, the shape of the holes, as well as the overall shape of the design boundary is being optimized in order to find the optimal relation between them (Figure 22). For the shape definition, the formulas related to the NURBS curves are used.
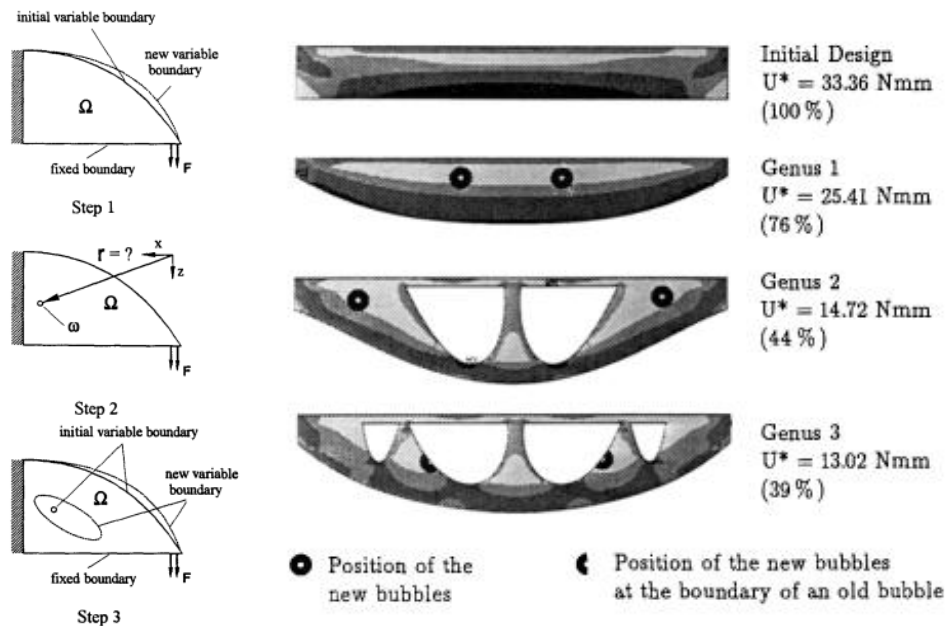
Figure 22 Process followed in the bubble method approach (Eschenauer et al., 1994).

Nevertheless, due to the quick developments in the other TO methods and the advanced intricacy of the shape optimization approaches, the bubble method was not considerably developed through the years (Sigmund & Maute, 2013).

One important approach based on this method is the Topological Derivatives method, which suggests a combination of the bubble method as described by (Eschenauer et al., 1994) with the homogenization method as described by (Bendsoe & Kikuchi, 1988). Particularly, it is stated that the sensitivity for the creation of inner holes in the structure can be extracted through the investigation of a porous composite with infinitesimal circular holes, when its density bound goes toward 0. In this regard, topological derivatives can be considered as a special version of the homogenization approach. It can be combined with the SIMP and the Level Set approach – discussed afterwards – for the placement of small holes, but its numerical accuracy is questionable (Sigmund & Maute, 2013).

B. Level Set Method

Unlike the bubble method, where the design boundaries are described explicitly, in Level-Set approaches an implicit definition of boundaries is being used. Therefore, these methods allow not only for shape optimization, but also for topological changes.

In Level Set Methods the boundaries of the design derive as iso-contours of a Level-Set function φ (van Dijk et al., 2013). Particularly, a cut-off level is translated in the vertical direction and alters its shape based on the point that it intersects with the LSF graph. The rate of the vertical translation is usually defined by a velocity function according to the principles of the Hamilton-Jacobi equation[15].

For a given constant c – which is normally set to c = 0 – and a point x of the design domain, the following domains are specified based on the LSF φ (Figure 23):

$$
\begin{cases}
\varphi(x) > c \ \Leftrightarrow\ x \ \in \Omega \ (material) \\
\varphi(x) = c \ \Leftrightarrow\ x \ \in \Gamma \ (interface) \\
\varphi(x) < c \ \Leftrightarrow\ x \ \in (D \backslash \Omega) \ (void)
\end{cases}
$$

The material domain Ω and the interface Γ are only considered for the topology optimized design and, afterwards, for the estimation of the structural performance. Nevertheless, the domain D\Ω is not considered as completely void, but is assumed to be filled with a very compliant material with low value εE (ε << 1) in order to avoid singularities in the calculations (de Ruiter & van Keulen, 2004).
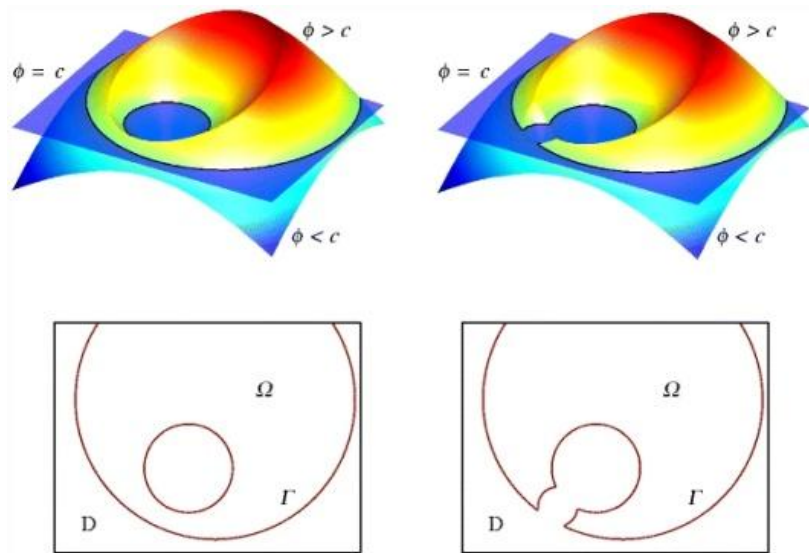
Figure 23 A Level Set Function (LSF) graph along with the corresponding material domains for different vertical positions of the cut-off level (van Dijk et al., 2013).

---

[15] As described in Wikipedia, Hamilton-Jakobi equation is "a necessary condition describing extremal geometry in generalizations of problems from the calculus of variations", which is " the field of mathematical analysis that uses variations, which are small changes in functions and functionals, to find maxima and minima of functionals.

The shape of the LSF φ is defined based on the design variables posed on the problem formulation. Different variations have also been developed, where the basis function derives as the superposition of different basis functions φ$_i$ *(de Ruiter & van Keulen, 2004)*, which are related to the separate design variables s$_i$ respectively (Figure 24).

In this case the basis function φ is defined as follows:

$$\varphi(x,s) = \sum_{i}^{n} \varphi_i(x, s_i)$$

The superposition of the basis functions may also vary depending on the level of detail which is demanded in the different areas of the design. In this regard, the distribution can be denser in the areas that demand an increased level of detail and sparser in the areas which do not (de Ruiter & van Keulen, 2004).

The LSF may be subsequent to further modifications. It can be parametrized according to auxiliary fields related to the design variables. In this case, the discretization due to parametrization should be dissociated from the discretization of the mesh regarding the structural evaluation, in order the preserve the necessary accuracy and efficiency in both terms.
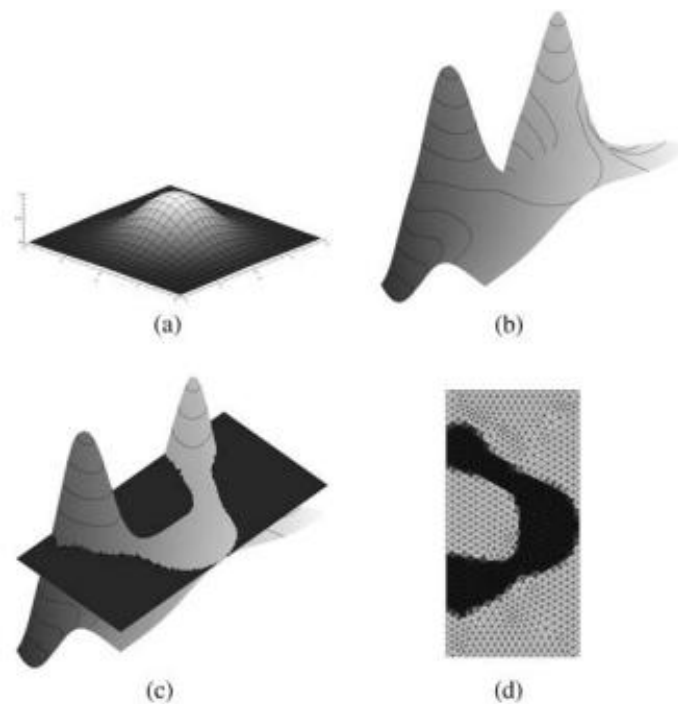
Figure 24 Notion of Topology Description Function. (a)Basis function (b) Superposition of basis functions according to design variables (c) Cut-off level (d) Surface obtained from the intersection with the LSF (de Ruiter & van Keulen, 2004).

The surface obtained through this process should be discretized in smaller elements in order to be used for the structural evaluation of the design. In this regard, there are different approaches, which vary based on the shape of FE elements obtained and the level of precision −crispness- of the surface boundaries.

Conforming discretization refers to analyzing only the material domain Ω and, therefore, the mesh discretization changes according to the alterations in the overall shape (Figure 25a). Although the simulation benefits from a very good approximation of the outer boundaries, additional computational time will be needed for changing the mesh division in each iteration, whereas the different types of FE may also create noise in the structure.

The drawbacks that derive from the restructuring of the mesh in each iteration are avoided in the case of the Immersed Boundary Techniques (IBTs). In this regard, the mesh discretization for the structural analysis remains unchanged and modifications are applied specifically on the elements that are placed on the interface between material and void, resulting in a good approximation of the outer boundaries (Figure 25b). Particularly, the approaches that have been developed, like the eXtended Finite Element Method (X-FEM), allow for local variations of the FE used according to the interface line (domain Γ) defined by the iso-contour of the LSF in each iteration.

The advantage in both the aforementioned approaches is that there are no ambiguities related to the existence or not of material, since there are no 'grey' areas as described in the density-based methodologies. However, it is important to avoid confusions of the geometric model in terms of stress analysis caused by small intersections or non-smooth boundaries. In this regard, filtering schemes for the smoothness of the boundary should also be applied in this case.

The last approach in terms of geometry mapping resembles the density-based methodologies as discussed in Chapter 4.3.1.1. In this case, the mesh discretization remains the same through the optimization and only the material domain Ω is changed each time according to the alterations in the design (Figure 25c). The material is described according to the pseudo density function ρ(x), which can again be multiplied with the stiffness tensor in order to reflect additionally the properties of the material used. Regarding the elements of the boundary interface, the percentage of material to void is calculated and the material properties are scaled based on it (Figure 25d). However, this type of intermediate values is not directly comparable to the 'grey' values as described in SIMP method.

In total, it is important to highlight that the mesh used for the FE discretization is decoupled from the surface used during the optimization process. This avoids the creation of mesh-dependent solutions as already described in the SIMP method.

| (a) | (b) | (c) | (d) |
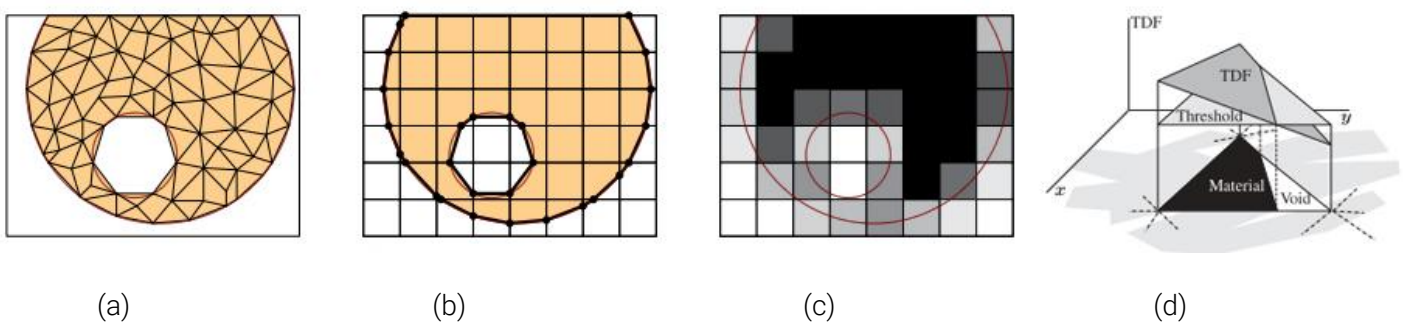
Figure 25 Geometry mapping. (a)Conforming discretization (b) Immersed Boundary Technique (c) Density-based discretization (d) Scaling of boundary element properties based on material proportion Adapted from (van Dijk et al., 2013) and (de Ruiter & van Keulen, 2004).

Shape sensitivities can also be used along with Level-Set Methods in order to update the LSF throughout the optimization process. It is important to mention that shape sensitivities are not meant to update the LSF in terms of topological changes -e.g. adding new holes-, but only regarding the overall shape of the gradient. In this

regard, the topological alterations of the shape obtained are incidental and rely only on the vertical translation of the cut-off level.

To be able to create inner cavities, the topological sensitivities and information should be exploited. In this regard, different approaches can be used, such as the bubble method - mentioned before-, the topological derivatives and the natural extended velocity fields. Nevertheless, the LSM are still more close to shape optimization techniques and, thus, they strongly depend on the initial design guess. Consequently, it is usually the case that they end up to local and not global minima.

Different approaches have been developed in the direction of improving the convergence behavior and avoiding local minima. They are related either to regularization techniques applied during the definition of the basis functions according to the design variables, or techniques aiming to manage the slope and smoothness of the Level-Set Function[16]. These affect the convexity and nonlinearity respectively, aspects that influence directly the level of convergence. However, attention should be paid in order to avoid numerical inconsistencies while applying these techniques (van Dijk et al., 2013).

4.3.2 Gradient-free approaches

They were first introduced by (Xie & Steven, 1992) and the main characteristic that distinguishes them from the aforementioned methodologies is that there is no mathematic function that works as the basis for the creation of the design. In contrast, the algorithm begins from a starting material domain and progressively removes (ESO) or adds (BESO) material to the volume based on the results of the stress analysis.

A. Evolutionary Structural Optimization (ESO) method

It was the first type of evolutionary approach introduced and includes only gradual removal of material from the volume. In this method, the starting domain is discretized into smaller elements in order to be able to run a FE analysis, which helps to identify the design areas which are low-stressed. Particularly, this is achieved through comparing the stress in every point with the maximum stress allowed for the structure based on a rejection ratio RR (Xie & Steven, 1997):

$$\frac{\sigma_e}{\sigma_{max}} < RR_i$$

Subsequently, material is removed from the areas that do not fulfill this criterion and the iterations continue till all the points are into the desired stress levels (Figure 26).
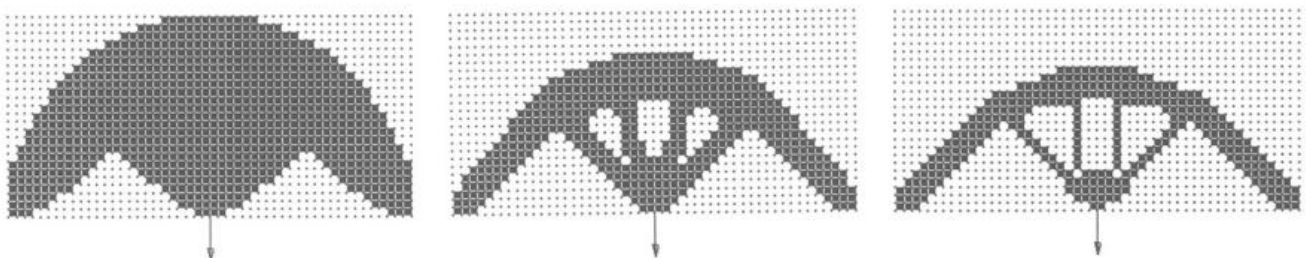
Figure 26 ESO optimization for a Michell-type structure. Adapted from (Xie & Steven, 1997).

---

[16] In general, steeper slopes lead to better convergence due to smaller boundary displacements.

It is suggested that ESO can be used along with shape optimization techniques to find the optimal shape of a boundary (Figure 27). In this case, no inner cavities are being considered and any holes should be firstly positioned in the design in order to have their shape optimized (Xie & Steven, 1997).
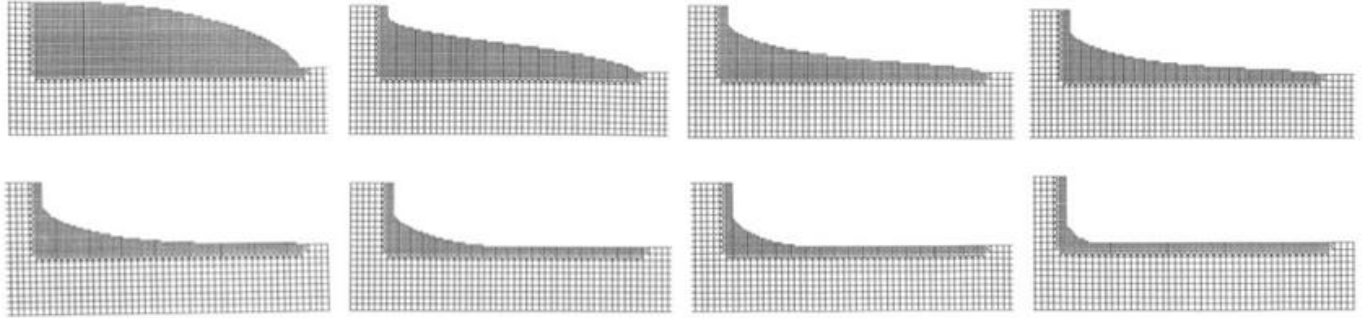
Figure 27 ESO for shape optimization. Adapted from (Xie & Steven, 1997).

B. Bi-directional Evolutionary Structural Optimization (BESO) method

It was first introduced by (Young et al., 1999) as an extension of the ESO method. The basic difference lies on the fact that the algorithm is enabled to remove material from the low-stressed areas, but also to add material in the areas that have high-stresses in order to alleviate them. In this regard, the optimization process does not start from a maximum, but from a minimum design domain.

Similarly to ESO, BESO performs a finite element analysis in order to find the stresses in all the points of the structure. Afterwards, an inclusion ratio IR is used along with the rejection ratio RR for the comparison of the stresses in every point with the maximum stress allowed for the structure (Xia et al., 2016):

$$\frac{\sigma_e}{\sigma_{max}} < RR_i$$

$$\frac{\sigma_e}{\sigma_{max}} > IR_i$$

Consequently, material is removed from the areas that do not fulfill the first criterion, whereas material is added when the second criterion is not met (Figure 28). The iterations continue until the algorithm meets the desired stress levels.
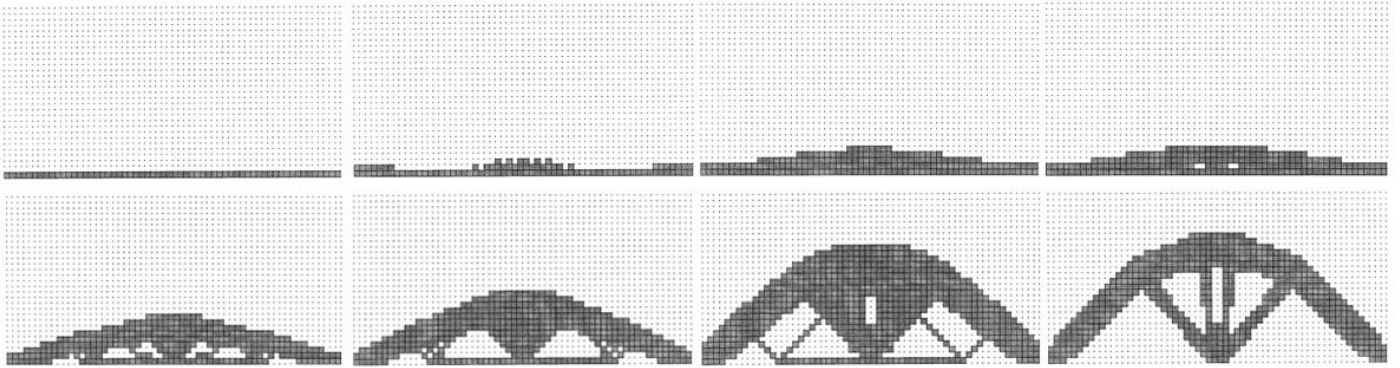
Figure 28 BESO optimization for a Michell-type structure. Adapted from (Querin & Steven, 1998).

It can be noticed that BESO results in a similar shape to that achieved through the ESO optimization (Figure 28). However, it needs to be highlighted that the optimization with BESO is considerably faster than the respective process with the ESO method and is considered to result in more robust solutions (Young et al., 1999).

Nevertheless, all the evolutionary approaches are still criticized for having insufficient algorithmic convergence. This also concerns the criteria which are applied in order to put an end to the iterations. These are questionable, since they are mostly related either to degeneration of the structure or stagnation of the algorithm – when it is chosen as an optimal solution the one having the best performance of all the experiments (Sigmund & Maute, 2013). Alternatively, the algorithm may stop when it reaches the desired volume fraction, without investigating if there are more efficient solutions inside this range. In all the cases, it is doubtful if the process can reach a global minimum. Additionally, the mathematical model used is considered to not be able to adapt non-linear limitations systematically.

Similarly to the SIMP method, both ESO and BESO suffer from geometric singularities, such as the checkerboard pattern, while the results show again a dependency on the mesh which is posed as the initial situation (Xia et al., 2016).

4.3.3 Comparison of methods

There have been several papers developed for each of the aforementioned methods that try to solve specific inaccuracies related and test their performance through applications in characteristic case studies.

Regarding the density-based methods, SIMP is the most widely popular solution since the use of the homogenization method is mostly restricted to applications with composite materials. In general, SIMP optimization problems have a simple structure and lead to fast and robust simulations with good convergence. However, the main problems lie in the geometric defects that may derive, the dependency of the result on the penalization value and the mesh refinement as well as the definition of boundaries, which is not direct because of the 'grey' areas related to the elements with intermediate densities. Other drawbacks are related to the jagged boundaries that are created through the operation, which have been proven to result in slightly higher compliance outcome (Figure 29) than the respective operation with LSM (Nathan et al., 2020) and need more post-processing in order to create the final shape. Lastly, although, homogenization method – and therefore also SIMP – is not dependent in any starting shape and it is possible to result in a global minimum, it seems that the design is highly dependent to the objective and constraints as posed in the problem formulation (Allaire, 2005). Similar problems have been mentioned in (Damen, 2019) where the design of a TO shell node changed

drastically when different wind loads were applied to it. On the other hand, LSM can process broader objective functions and mechanical models (Allaire, 2005).

Topology Representation	5 iterations		50 iterations		300 iterations	
Solid Isotropic Material with Penalization (SIMP)		0.8209		0.5793		0.5781
Level-Set Function (LSF)		0.4627		0.5482		0.5512

Figure 29 Bridge optimization results with the respective compliance values (Nathan et al., 2020).

Regarding the Level-Set Methods, the main advantage is the clear definition of boundaries. Given that this time there are no intermediate densities and the FEs are cut into the respective shapes using the xFEM method, there is no need for post-processing of the final shape. However, attention should be paid in filtering the cut FEs in order to remove very small parts that will result in false stiffness values. In total, the main drawbacks are, firstly, that - as with all the shape optimization techniques - the final result, although independent from the mesh refinement, it is strongly influenced by the initial guess and, therefore, will not result necessarily to global minima (Allaire, 2005). Additionally, it is highlighted that it is more time-consuming computationally and for this reason using a code written in a lower level language, such as C++ or Fortran is suggested (Andreasen et al., 2020).

Despite their large differences, (Allaire, 2005) suggests that a combination of the homogenization and level-set method can be achieved. Particularly, it is mentioned that LSM can be used as a secondary step, having as initial shape the outcome of the density-based TO operation.

The last category discussed refers to the evolutionary algorithms. Although they can result in fast solutions, they are strongly criticized for the fact that they usually result to local minima. In this regard, it is difficult to set an appropriate stopping criterion for the operation that will be able to efficiently monitor convergence. The criteria may relate to the degeneration of the structure, the difference in the outcome between subsequent steps or the achievement of the posed objective, but none of them can assure that a global minimum is achieved (Sigmund & Maute, 2013).

4.4 Manufacturing Criteria

Topology Optimization methods have already been used in various projects. This led to the creation of solutions that would enable to incorporate some characteristic manufacturing criteria in the optimization process.

4.4.1 Minimum & Maximum member size

There are different ways to control the size of the cross section based on the characteristics of each method separately.

Regarding density-based approaches, it is suggested that the minimum width of the different members can be manipulated through introducing a nodal weighted function (Guest et al., 2004), whose projection corresponds to a circle, in the case of two-dimensional elements, or a cone, in the case of three-dimensional elements, with radius r_{min} (Figure 30). The function takes into account the proximity of solid FE each time and expresses each fraction of element e as the weighted average $\overline{x}^e$ of the volume fractions of all the nodes which are inside a circle of radius r_{min} as described before. The value r_{min} is independent of the refinement of the mesh. In this regard, the weighted function is defined as (according to (Guest et al., 2004) :

$$w\left(x - \overline{x}^e\right) = \begin{cases} \dfrac{r_{min} - r}{rmin}, & if\ x\ \in\ \Omega_w^e \\ \\ 0 \end{cases}$$

where $x\ \in\ \Omega_w^e\ \ if\ \ r\ \equiv\ \left\|x - \overline{x}^e\right\|\ \leq\ r_{min}$

If S_e is the set of the nodes in proximity, then the element fraction in each element e is calculated as:

$$\rho_e = \frac{\sum_{j\in S_e}\rho_j\,w\left(x - \overline{x}^e\right)}{\sum_{j\in S_e} w\left(x - \overline{x}^e\right)}$$

(a) (b) (c)
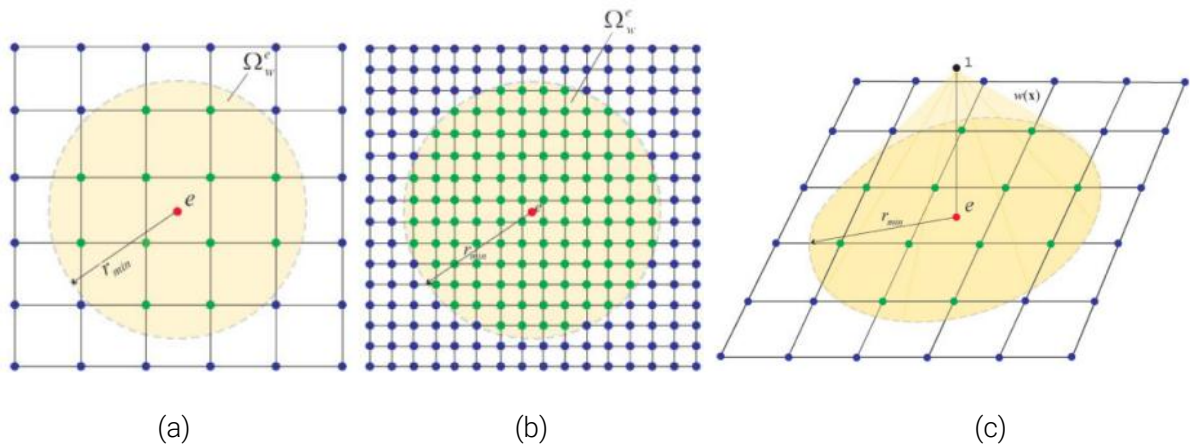
Figure 30 Projection of the weighted function in the case of (a) 2D mesh, (b) 2D mesh with bigger refinement, (c) 3D mesh (Guest et al., 2014).
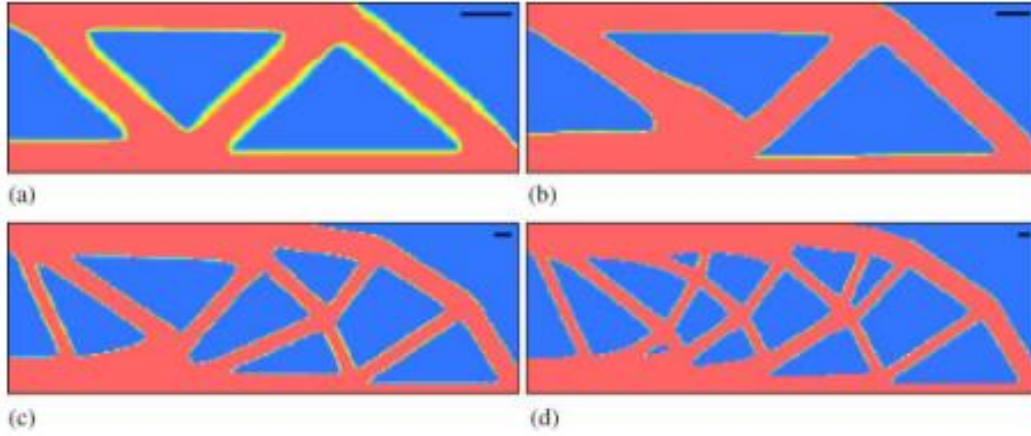
Figure 31 Optimization result for different min lengths (shown with black bars), (Guest et al., 2014).

In terms of manipulation regarding the maximum size of the cross section, a similar method has been suggested from (Guest, 2009). In this, a circular area related to the max size r of cross section is introduced and the sum of the densities of the elements belonging to this region is calculated each time. The criterion is much simpler than the one mentioned before –in the sense that it only checks that not all the elements inside this region are solid - and is formed as followed:

$$\int_{\Omega_r(y)} \rho(x)\, d\Omega \; < \; \int_{\Omega_r(y)} d\Omega \quad \forall\, y \in \Omega$$

where Ω_r is the domain of the circular area related to the max cross section

A similar method can be used in order to check for the minimum size of voids in the structure. The total volume of voids inside the circular region is calculated by using the formula:

$$V_v^e(\rho_e) = \sum_{i \in R^e} v^i (1 - \rho^i + \rho^e_{\min})^n$$

where v_i the volume of element i, $\rho_{\min}$ the limit as set in the problem formulation and n a value that determines how much the intermediate densities will be taken into consideration.

The minimum void size is checked by comparing with the minimum allowable void volume using the inequality:

$$V_V^e(\rho^e) \geq V_{min}^e$$

Regarding the LSM methods, there are different approaches developed. Regarding the maximum thickness of each member, the method introduced uses the maximum size of a sphere inscribed in the Level Set Function, whereas regarding the minimum length of the components it is suggested that dimensional variables can be used (Jihong et al., 2020).

4.4.2 Void continuity

As it is already mentioned, it is highly important for glass structures to be able to create single-connected structures, i.e. to avoid enclosed voids in the topology optimized geometry. They are not feasible to be constructed, since they would leave no space for the removal of the formwork.

In this regard, (Liu et al., 2015) suggest the Virtual Temperature Method as a way to evaluate the connectivity while maintaining a simple structure of the optimization problem. This is achieved through converting the connectivity problem to a temperature problem and performing a heat flow analysis.

In specific, it is assumed that void areas are occupied by a heat conductive material, whereas solid areas are occupied by a thermal insulator respectively. When conducting a heat analysis, the voids which are totally enclosed will, therefore, show a significantly high temperature, whereas, otherwise, the heat will be exported in the outer area and, thus, a lower temperature will be maintained inside the cavity (Figure 32).
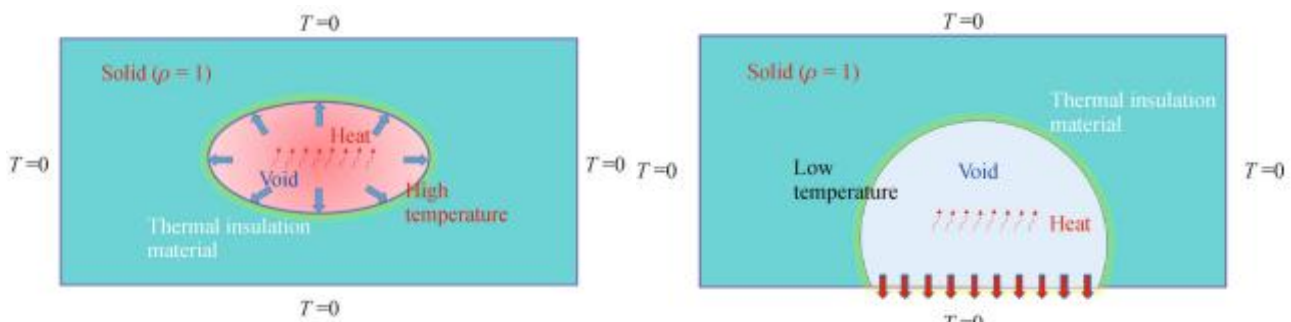
Figure 32 Virtual Temperature Method in the case of enclosed and open voids (Liu et al., 2015).

Setting an appropriate temperature threshold will therefore evaluate the connectivity between the voids and can be considered as an equivalent to the easiness of removal of the formwork.

4.5 Available commercial TO software

Several TO software applications have been developed till now, following the principles of the algorithmic methodologies as discussed in the previous chapters. As it can be seen in Table 10, to this day the majority of the available TO software has incorporated the SIMP methodology. This clearly reflects the efficiency of the density-based methodologies, and especially SIMP, in terms of computational time and robustness of solutions, as already discussed in chapter 4.3. Regarding homogenization, the plug-ins which are developed based on this approach (e.g. Millipede) have been proven to take more time in comparison to the respective SIMP plug-ins (e.g. TOPOS).

It can also be noticed that there are several software which, besides the TO with SIMP, offer also the option to use Level-Set Methods. However, it needs to be highlighted that, in most of the cases, it is followed by limitations in its application. For example, Autodesk Fusion 360 offers the possibility to use it only for Generative Design, while in Altair OptiStruct and ANSYS only a very small number of the manufacturing criteria available for SIMP can also be applied in Level-Set.

A common characteristic in all the software, independently of the method they are using, is that they also have an integrated FEM solver in order to design structures which will be also structurally efficient. However, the lack of possibility to differentiate the values for the two principal stress constraints renders them unsuitable to be

accurately used for the optimization of a glass structure. This derives from the fact that – as discussed in chapter 3- glass has significantly different allowable values for tension and compression and, therefore, they cannot be simultaneously evaluated with the same criterion. This supports the argument that a new algorithm tool should be created in order to be able to efficiently optimize a glass structure.

	Homogenization	SIMP	Level Set	ESO / BESO
ANSYS		✓	✓	
AUTODESK FUSION 360		✓	✓	
Altair HyperWorks		✓	✓	
Millipede	✓			
TOPOS		✓		
DS SIMULIA		✓		
Ameba				✓
Karamba 3D parametric engineering				✓
3D TopOpt App		✓		
COMSOL MULTIPHYSICS	✓	✓	✓	

Table 10 Overview of TO software and respective algorithmic methodologies.

4.6 Problem Formulation

As discussed in Chapter 4.1, the optimization problem is formulated mathematically according to the following standard formula (Boyd & Vandenberghe, 2004):

$$\min_{x} \ f(x)$$

$$subject \ to \ \ g_i(x) \leq 0, \qquad i = 1,2,\ldots,m$$
$$h_i(x) = \ 0, \qquad i = 1,2,\ldots,p$$
$$x \in \Omega_{mat} \subseteq \Omega \in R^n, \qquad n = 2,3$$
$$f_0(x): R^n \rightarrow R$$

In this regard, the problem consists of one objective function which sets the goal for the optimization and several functions that reflect the equality and inequality constraints posed to the optimization. The problem formulation affects considerably the computational time needed for the operation, the convergence of the algorithm and the final outcome of the optimization. While the constraints may refer to a wide range of aspects, such as structural performance or manufacturing criteria, the objective functions are mainly divided into three categories[17].

4.6.1 Compliance-based

In topology optimization, compliance-based is the most classical approach for the formulation of the problem and has been proven to provide fast and robust solutions. In general, minimizing the compliance equals maximizing the overall stiffness and is usually accompanied by a constraint referring to the volume fraction of the final structure. The standard formulation is (Sigmund, 2001):

$$\min_{x} \ C(x) = \ U^T K U$$

$$subject \ to: \ \frac{V(x)}{V} \leq f$$

$$KU = F$$

$$0 < x_{min} \leq x \leq 1$$

where $c(x)$ is the compliance function, $v(x)$ is the volume function, v is the total volume of the virgin material and f is the percentage of the volume fraction which is acceptable. K, U and F are the assembly, displacement and load matrix of the structure respectively.

Although it is a well mastered approach and has been proven to result in robust solutions, there are some drawbacks that limit its use. Firstly, the limit regarding the volume fraction, which affects largely the final outcome, is highly dependent on the experience of the end user (Hailu Shimels et al, 2017). In this regard, it cannot be ensured that the algorithm is going to find the optimal result in terms of mass at all times, meaning that a more lightweight and stiff structure could possibly be achieved. Secondly, given that compliance-based problems, in their general form, do not take into consideration the stress requirements that could lead in a

---

[17] The formulations presented are following the SIMP approach. In this regard, the objective functions are expressed according to the density variables x which are assigned to each element.

failure of the structure, they cannot fully ensure that the structures which derive as outcome will be feasible to be manufactured (Collet et al., 2017). This is based on the fact that, although a stiff structure can be ensured, peak stresses may arise locally resulting to failure.

4.6.2 Stress-based

As already mentioned, minimizing the compliance – and therefore maximizing the structural stiffness – does not ensure that the structure is going to also perform well in terms of stresses. In this regard, another way to formulate the optimization problem arose. It aims to minimize the stresses in the structure while also applying a constraint for the volume fraction. It is formulated according to the following standard formula (Yang & Chen, 1996):

$$\min_{x} \ G(x)$$

$$subject\ to: \int_{\Omega} x\, d\Omega \le M_0$$

where $G(x)$ is the global stress function for the Von Mises stresses and M_0 is the volume that can be maintained.

Results from (Yang & Chen, 1996) show that the minimum stress optimization converges in an outcome which is significantly different from the minimizing compliance one. Particularly, the outcome showcases that minimizing the peak stresses is possible but it considerably deteriorates the overall stiffness of the structure when a respective constraint is not posed. This further underlines the necessity to have both of these aspects – stress and compliance - taken into consideration in one uniform operation.

One of the major issues that need to be taken into consideration in a stress-based approach is the local nature of the stresses, meaning that the stress constraints need to be evaluated in every element individually in order to efficiently control the peak stresses. This affects considerably the convergence of the problem and the computational time needed for completing the operation, since it increases significantly the number of constraints in the problem. An alternative approach is to integrate the local stress constraints into one uniform stress constraint which approximates the maximum stress value. Although this method succeeds in increasing the computational efficiency of the problem, it cannot efficiently indicate local peak stresses that may exist in the structure (Le et al., 2010).

Apart from it, there are also two other major issues that also need to be taken into account. The first one is related to the so-called 'singularity' problem which refers to the fact that elements with quasi-zero densities falsely appear to have non-zero stress values during the optimization (Bruggi & Duysinx, 2012). This problem is addressed with mathematical perturbations that serve to improve the convergence of the optimization algorithms, such as the ε-relaxation parameter (Cheng & Guo, 1997) or the qp-approach (Bruggi, 2008).

Secondly, problems may arise due to the highly non linear dependence of stress to the design. Particularly, given that stresses are largely affected by the changes in their neighboring elements, they may provoke problems in the numerical consistency and convergence of the algorithm when it comes to large spatial gradients. (Le at al., 2010)

4.6.3 Volume - based

The last problem formulation category that has been explored in the literature refers to minimizing the volume of the structure while at the same time applying constraints regarding the structural performance of the component. The constraints usually refer to both the stiffness - through checking the compliance - but also the material strength – through evaluating the stresses.[18] In this regard, the compliance constraint serves to guide the optimization process towards a stiff structure, whereas at the same time the stress constraints ensure the feasibility of the final result. (Bruggi & Duysinx, 2012). A typical way of formulating the problem is:

$$\min_{x} \ V(x) = \sum_{N} x_e V_e$$

$$subject\ to:\ KU = F$$

$$\frac{c}{c_L} \leq 1$$

$$x_e^{(p-q)} \frac{\sigma_e}{\sigma_{Lt}} \leq 1, \qquad e = 1, \dots, N$$

$$0 < x_{min} \leq x \leq 1$$

The aforementioned formulation entails that the stresses are evaluated with local constraints in each finite element. This method is considered robust, but, as already discussed in Chapter 4.6.2, it demands a lot of computational time and power, both for the optimization algorithm and for the sensitivity analysis, in order to be executed (Bruggi & Duysinx, 2012). Alternatively, a global constraint can be posed but it cannot efficiently ensure that all the local peak stresses will be avoided.

Another variation regarding the application of the strength constraint in the structure proposes the use of a material failure criterion instead of evaluating the absolute values of stresses each time. Von Mises criterion is the most frequently used because of its simplicity. It serves efficiently for the evaluation of the strength performance of materials that behave similarly in tension and compression. Alternatively, the Drucker-Prager failure criterion can be applied in the case of materials that have unequal properties in tension and compression (Bruggi & Duysinx, 2012), so it can efficiently be used in the case of brittle materials, such as concrete or glass.

4.6.4 Comparison

There have been several studies that aspire to evaluate the performance of the different problem formulations. Overall, it has been shown that volume-based optimization with compliance and stress constraints can improve the result obtained from the classical compliance approach. Additionally, it is mentioned as a robust alternative to the respective compliance-based optimization with volume and strength constraints (Bruggi & Duysinx, 2012).

(Bruggi & Duysinx, 2012) compare the results obtained through applying the volume-based approach with compliance and stress constraints individually but also with the two constraints are combined together. Overall, it is shown that the results are almost identical (Figure 33) and, additionally, have similar characteristics with the ones obtained by applying a pure compliance based approach. In terms of computational time, it is mentioned that the approach with combined compliance and stress constraints was twice as fast as the approach with

---

[18] As already mentioned by (Yang & Chen, 1996), taking into account both the compliance and stress can result in a better outcome, while at the same time ensure numerical stability and faster convergence.

only stress constraint applied, but it resulted in a slightly heavier outcome which, however, performed better both in stiffness and stresses. The improved speed is related to the fact that the compliance constraint serves for concentrating the material faster around the optimal layout in the beginning of the process, whereas after the first convergence the two algorithms perform similarly in order to conclude to the final shape.
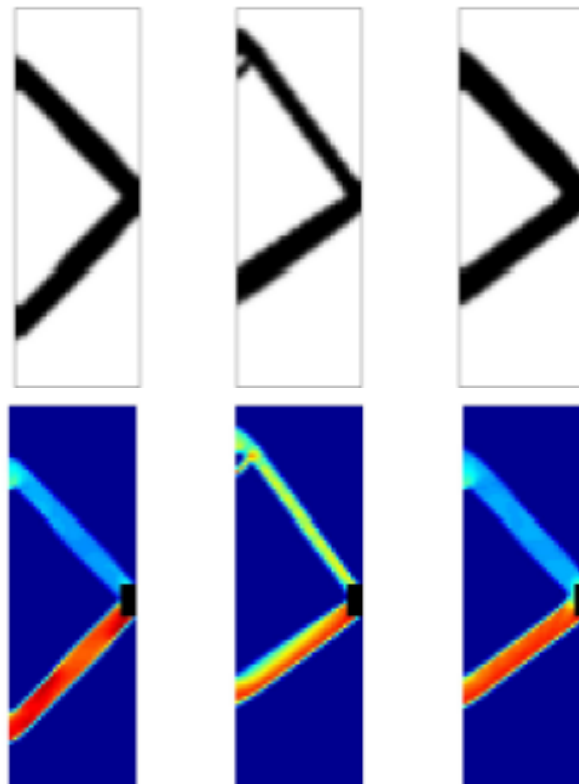
Figure 33 Outcomes and respective stress analysis after optimization with (left) volume objective & compliance constraint, (middle) volume objective & stress constraint, (right) volume objective & both compliance and stress constraint (Bruggi & Duysinx, 2012)..

Additionally, (Lee et al., 2012) compare the results obtained through a problem formulated as compliance-based with volume constraint and a problem with volume minimization objective and stress constraint (Figure 34). In general, it is observed that the results from the compliance minimization may include regions with local peak stresses that violate the admissible stress limit, whereas when minimizing the mass with stress constraint, this is avoided and a fully stressed design is achieved. However, it is underlined that mass minimization with stress constraint is more likely to result in local minima.
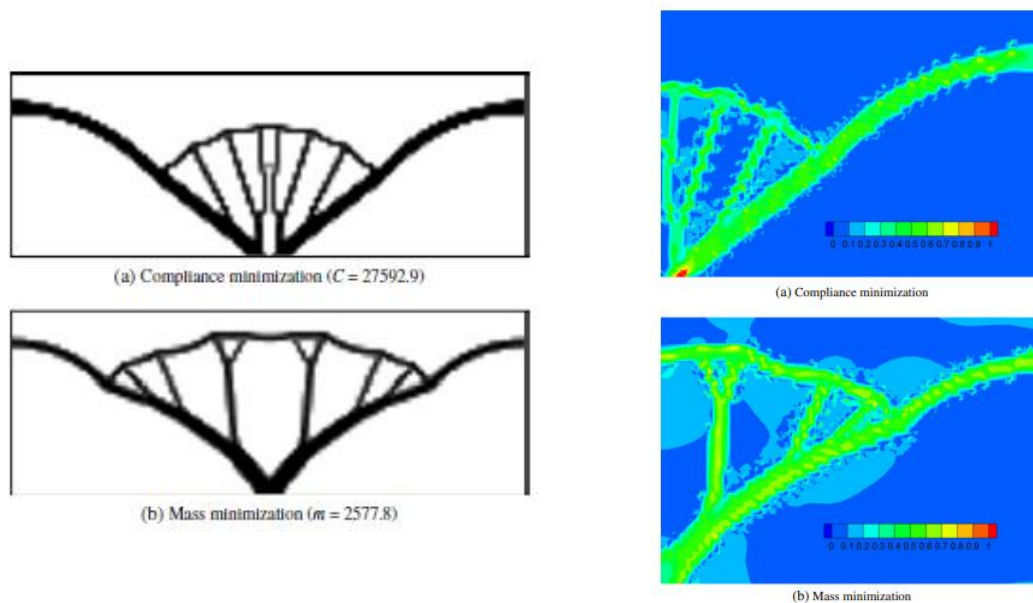
Figure 34 Outcomes and respective stress analysis after optimization with (a) compliance objective & volume constraint, (b) volume objective & stress constraint (Lee et al., 2012).

4.7 Related projects with other materials

The available software has already been applied in several projects, most of which have already been fabricated and tested in real conditions. The material which is mostly used till now is concrete, both reinforced and unreinforced.

Homogenization method through Millipede plug-in was used for the design of Prototype A (Figure 35a) in ETH Zurich. The TO plug-in was used in order to create a two-dimensional design, which was later vectorized in order to produce the 3d geometry. The final design for the production was created by smoothness of the mesh outcome through Catmull-Clark and loop subdivision algorithms (Jipa et al., 2016). The prototype was mainly constructed with the use of a 3d-printed sand formwork which was not removed afterwards and, thus, allowed for the creation of relatively thin member cross sections.

In contrast, SIMP method via the Simulia Abaqus plug-in was used for the design of Prototype B. It refers to the design of a slab with four fixed supports, optimized for minimum stress concentration and with application of a volume constraint (18%). The fabrication constraints which were posed were not directly applied in the TO process, but were used for the filtering of the design in a post-processing phase (Jipa et al. , 2016). Similarly to Prototype A, the construction was made with the use of 3d-printed sand formwork, which was removed after the casting of the concrete in this case (Figure 35b).

(a)   (b)

Figure 35 (a) Prototype A (b) Prototype B.

A prototype referring to a TO post-tensioned concrete slab was realized in Concre3DLab (University of Ghent). A SIMP algorithm was used for the TO optimization of the longitudinal cross-section in two-dimensions with minimum compliance as objective and volume constraint. Afterwards, the three-dimensional shape of the slab was created using Autodesk fusion software (Vantyghem et al., 2020). The resulting geometry was evaluated for its structural performance with FEM analysis in a next stage. The construction (Figure 36a) was realized with 3d-printed concrete components which, therefore, have hollow sections where the post-tensioned elements were integrated.

Another example of TO beams made from plain concrete is the one related to the work of (Jewett & Carstensen, 2019). A density-based approach is used for the development of three different designs; one with minimum compliance objective and two with minimum volume objective but with high and low stress constraints respectively. It is highlighted that, although several stress-based optimizations use the Van Mises criterion, in this study the Drucker-Prager criterion[19] – adapted for the concrete design - is used in order to be able to evaluate different values regarding tension and compression. All the prototypes were made from cast unreinforced concrete (Figure 36b) and were tested for their structural performance.
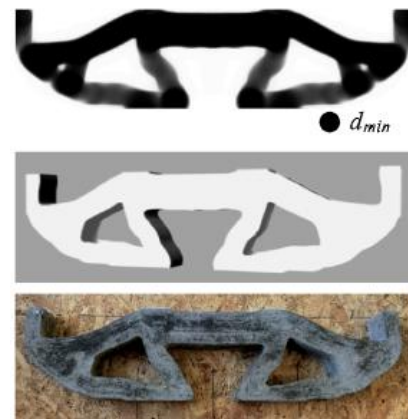
(a)   (b)

Figure 36 (a) Post-tensioned concrete slab. (b) Concrete prototypes.

---

[19] "The Drucker−Prager failure criterion is a three-dimensional pressure-dependent model to estimate the stress state at which the rock reaches its ultimate strength. […]The Drucker−Prager failure criterion was established as a generalization of the Mohr−Coulomb criterion for soils". From (Alejano & Bobet, 2012).

Several other projects have also been realized with the aim of creating structures with more efficient material use (Figure 37). However, they are out of the scope of this literature review, since they either use form-finding techniques for the shape exploration (Figure 37a), or they are not composed of cast components (Figure 37b). Nevertheless, they further underline the potential and the importance of the continuous research in that direction.

(a)   (b)

Figure 37 (a) Smart slab developed in ETH Zurich. (b) The Glass Swing developed in TU Delft using the BESO method.

4.8 Related projects regarding TO cast glass structures

In this chapter, a critical evaluation of the projects related specifically to TO cast glass structures will be held in order to identify further areas for improvement. The projects are mostly referring to research which has been held from students of the MSc Building Technology in TU Delft during the last years. The research covers different stages of the design, from optimizing the overall shape to more specific experiments regarding the moulds and the manufacturing process of the complex shapes.

Glass Vaults (van der Weijst, 2019)

This thesis refers to the design of a cast glass vault. It is mentioned that because of the annealing time limitation and the need for a vast oven, the option to create it monolithically was eliminated. In this regard, the vault was analyzed into smaller interlocking cast glass voussoirs, which would facilitate its construction. The overall funicular form of the shell (Figure 38-right) was designed with a form-finding process and structural validation with FEM using the Karamba plugin. Manufacturing constraints such as the maximum angle between the voussoirs were applied with a Grasshopper script.

Prototypes of the voussoirs were also created. Because of the large number of voussoir shapes in the shell, an adjustable mould was intended for the glass casting. The mould was made from 3d printed PLA which, because of its incapacity to withstand the high temperatures that occur during glass casting, made it necessary to introduce an intermediate phase of creating cast wax components which were later used for the kiln casting process (Figure 38-left). Despite their relevant smaller size, it was highlighted that the voussoirs with the larger mass needed long annealing time and it was suggested that in further research inner cavities could be introduced in the mould.
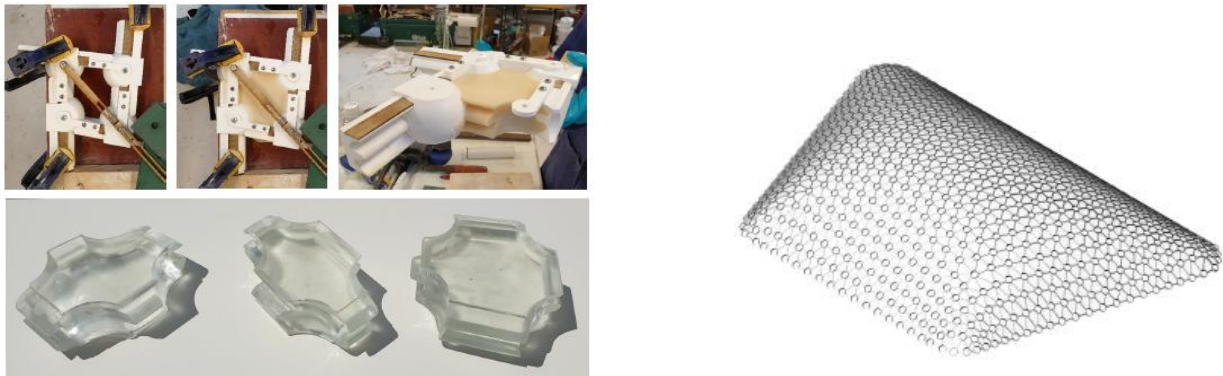
Figure 38 (left) Adjustable mould from 3d-printed PLA & Final glass voussoir prototypes, (right) Final shell geometry.

Topology Optimized Cast Glass Grid Shell Nodes (Damen, 2019)

Similarly to the thesis of (van der Weijst, 2019), the overall form of the shell was defined through form-finding and validated structurally with the Karamba plug-in. However, in this case, TO was applied for the design of a node with decreased mass and, therefore, smaller annealing time. TO was applied through commercial software, and particularly ANSYS, using the SIMP methodology. However, it was highlighted that because commercial software is adapted in the characteristics of ductile materials, such as steel, several approximations needed to be made in order to reflect the glass features.

The most important difference lies in the use of the stress criteria for the optimization. Van mises stresses are mostly used but, given that they can only apply one criterion for the stress evaluation, they cannot be directly used for glass which needs two differentiated constraints for tension and compression values. Optimization with principal stresses is mentioned as more complicated and not directly incorporated in the software. In this regard, compliance is used as the most suitable option, which, however, is likely to lead to peak stresses and therefore a structural validation should be held afterwards.

In this regard, the optimization problem is formulated with minimum compliance as objective and constraints referring to the mass reduction, the tensile stress – which was chosen as the main stress limiting factor – and the minimum member size. The shape was post-processed in order to eliminate extreme stress values, have a smoother boundary and remove sharp edges that would increase the residual stresses during annealing.

One of the most important findings in this thesis was the fact that one prevailing loadcase should exist in the optimization at all times in order to have a final result that can efficiently resist multiple loading scenarios. This effect is further intensified in this project due to the small size of the node, which makes it highly susceptible to the loads which are applied to it. For this reason, although different load cases were applied, one load case, i.e. the self weight, had to always be maintained as the prevailing one. This can be achieved either by enlarging the main load case (e.g. by having an overall heavier structure) or by designing the shell in a way that is protected from direct climate effects so that the values of the variable load cases remain overall small.

The node was made into a prototype using two different mould types for the casting. Firstly, the conventional technique was used with 3d printing the wax initial element because of the complicated shape (Figure 39b). Secondly, a 3d printed sand mould was tested (Figure 39c). Overall, it was concluded that 3d –printed sand

moulds have more potential, because of the large amount of manual work needed for the kiln-casting. The process finally proved that the annealing time was successfully reduced[20].

(a)	(b)	(c)	(d)
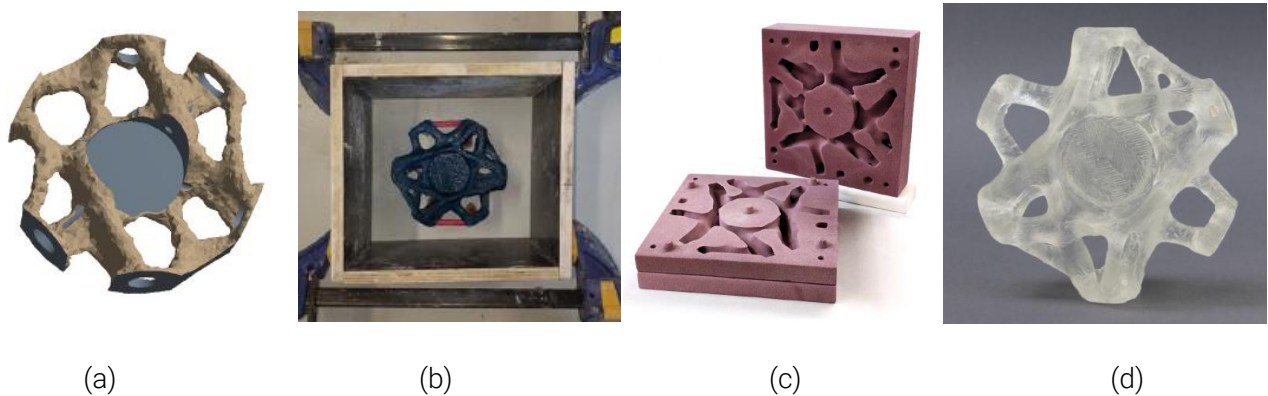
Figure 39 (a) TO design of the node (b) 3d printed wax element for kiln casting (c) 3d printed sand mould (d) Final glass prototype.

Topologically Optimized cast glass column (Bhatia, 2019)

Unlike the previous projects, this thesis does not refer to the optimization of a small element, but of a large monolithic column, which would be placed in an archaeological space. In this regard, additionally to the manufacturing criteria as already posed in the other theses, the transportation limitations are taken into account and, therefore, the column is split in different parts. Moreover, visual parameters were added in order to ensure that the column will not block the view of the archaeological area in the eye level. In this regard, the structure should be as solid as possible in the areas aligned with the human perspective in order to avoid visual distortion.

The method followed was similar to that of (Damen, 2019). TO following the SIMP methodology was held through ANSYS software. Compliance was set as the objective and constraints regarding the mass and the manufacturing process were posed. The outcome was structurally validated and post-processed in order to result to the final shape. A drawback regarding the process was that a series of subsequent iterations was needed in order to conclude to the final result. This is because the ANSYS educational license can only process a specific numbers of nodes. In order to achieve a sufficiently accurate and not bulky result, the mesh was optimized in various steps having every time as starting point the outcome of the previous iteration.

Similarly to before, a small prototype was made with 3d printed sand moulds. The result validated that it is possible to create complex forms using this technique (Figure 40).

---

[20] The estimated annealing time for the node was 4 hours, instead for 48 for a non-optimized node of the same size (Damen, 2019).
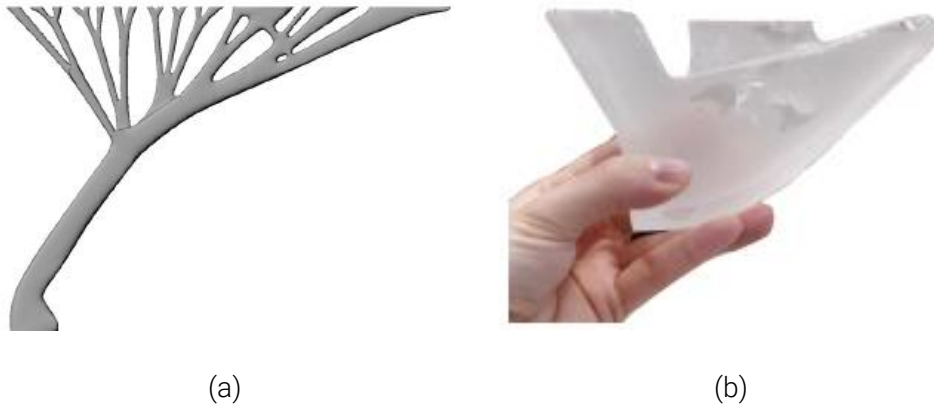
Figure 40 (a) Design of the Topologically Optimized Column (b) Prototype of part of the column in a smaller scale.

Topologically Optimized Cast Glass Shell (Naous, 2020)

An approach similar to those of (Damen, 2019) and (Bhatia, 2019) was applied. The ANSYS commercial software with SIMP methodology was used and the objective referred to the minimum compliance. Additionally to the constraints already posed in the previous theses, (Naous, 2020) suggested that the minimum mould size should also be taken into consideration. This is very important, since this mould sections will not be able to resist to the pressure while pouring the glass melt. Lastly, it was highlighted that, in order to achieve the homogeneous mass distribution, both the minimum and maximum member size should be checked in order to ensure that they fall inside an allowable range.

The initial form of the shell was defined using form - finding techniques which were also verified structurally. The shape was applied as the starting form for the TO in ANSYS ad different operations were performed regarding different shell thicknesses. The designs were verified structurally afterwards and post- processed. The final shape was defined as a combination of the results of the different operations (Figure 41). Suggestions for further exploration referred to the integration of the Drucker - Prager criterion for brittle materials in the operation, as well as the creation of a custom algorithm that will take all the specific characteristics of glass into consideration.

(a)   (b)
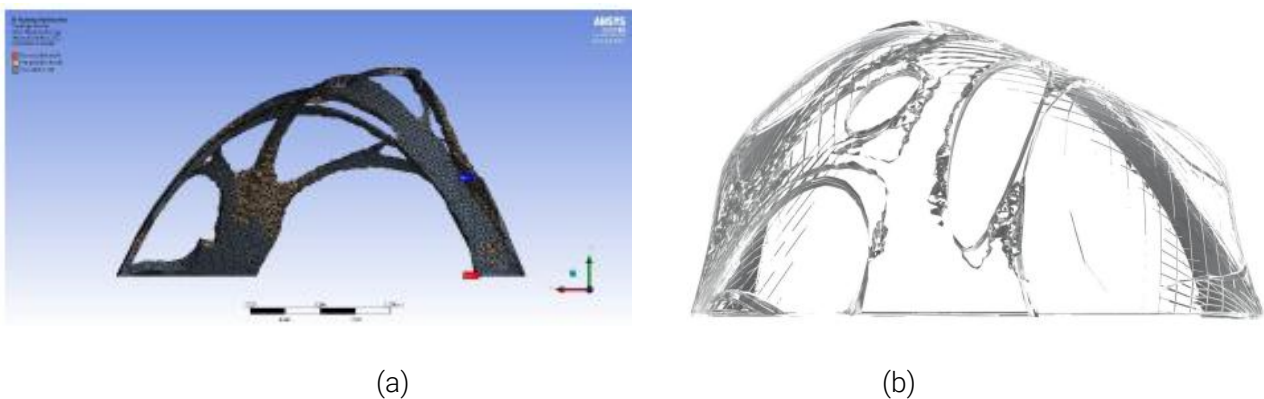
Figure 41 (a) Design of the Topologically Optimized Shell (b)Final shape after post-processing.

Glass Giants. Mass-optimized Massive Cast Glass Slab (Stefanaki, 2020)

Following the aforementioned experiments, this project refers to the TO of a cast glass slab. The approach is again similar, applying a compliance optimization with SIMP methodology through ANSYS and implementing all the manufacturing, transportation and annealing criteria already mentioned. The structural validation and the post-processing in order to ensure a form able to be manufactured are applied in a later stage. Some additional design principles are applied related to the case study, such as the need for a flat and solid surface in the top part so that people are able to walk on it.

Similarly to before, it was mentioned that a principal based optimization would be more adequate given the brittle behavior of glass. However, it is considered as more complicated since the principal stresses are related to the reference plane which, in the case of a TO complex shape, is constantly changing.

Moreover, there are the same limitations in terms of the mesh discretization that can be processed each time and, therefore, the project uses the same strategy of applying multiple optimization iterations, which are time consuming in the sense that the mesh should also be processed before every structural validation. in this project, it is also mentioned that a way of improving the tensile stresses would be to introduce an arched bottom part, which, however, was not applied and a cross section with a shallow vault on the bottom part was intended.

Following the previous theses, here it is also suggested that 3d printed sand moulds are used for the fabrication of the optimized slab. In order to address the problem of the maximum mould size that can be 3d-printed with sand, a novel interlocking system of moulds is developed. In that, the overall mould is split into different parts which have extensions, undercuts and frequent nodes in order to avoid leakages in the parts where the two pieces are connected together.

(a)   (b)
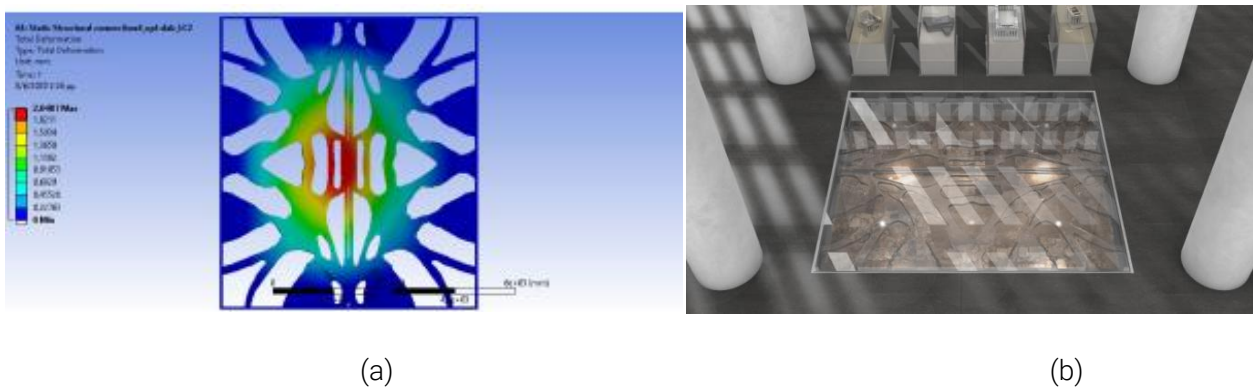
Figure 42 (a) Structural validation of the TO design (b) Final slab design.

Topology Optimized Cast Glass Bridge (Koopman, 2021)

The project of (Koopman, 2021) refers to the TO of a monolithic cast glass bridge. The structure of the optimization problem is again the same. A compliance based optimization through ANSYS with constraints regarding to the structural, manufacturing, annealing criteria and a second turn of structural validation with FEM in order to check the stresses both regarding tension and compression. If all the parts are not fully stressed, then another optimization is being held in order to further reduce the mass.

However, there are some major differences this time. Instead of using ANSYS with SIMP methodology, the Level Set option was selected. This ensured that a clearer boundary could be extracted after the optimization and not

a lot of post-processing was needed. Regarding the criteria, in this project some added aspects were considered. These refer to the maximum cross section size, the maximum feasible dimension of each 3d printed sand mould component as well as the space needed in the mould for screw holes, vent pipes and risers.

The optimization process was first held for the two-dimensional longitudinal section of the bridge and then for the whole three-dimensional geometry. In this project, both a linear - referring only to the float glass elements - and non-linear analysis - including also the polyurethane layers placed in the connections of the different parts of the bridge – were held (Figure 43). The non-linear analysis is mentioned to give better results for deformation and stresses comparing to the linear one.

Similarly to the aforementioned theses, the need for a custom algorithm which will integrate the evaluation of both the principal stresses in the optimization process is highlighted, even though it is mentioned that this may lead to results strongly dependent on the load cases set each time. Lastly, it was pinpointed that investigation of the 3d printed sand mould in terms of its behavior along with the glass shrinkage is a research direction worth exploring.

(a)   (b)
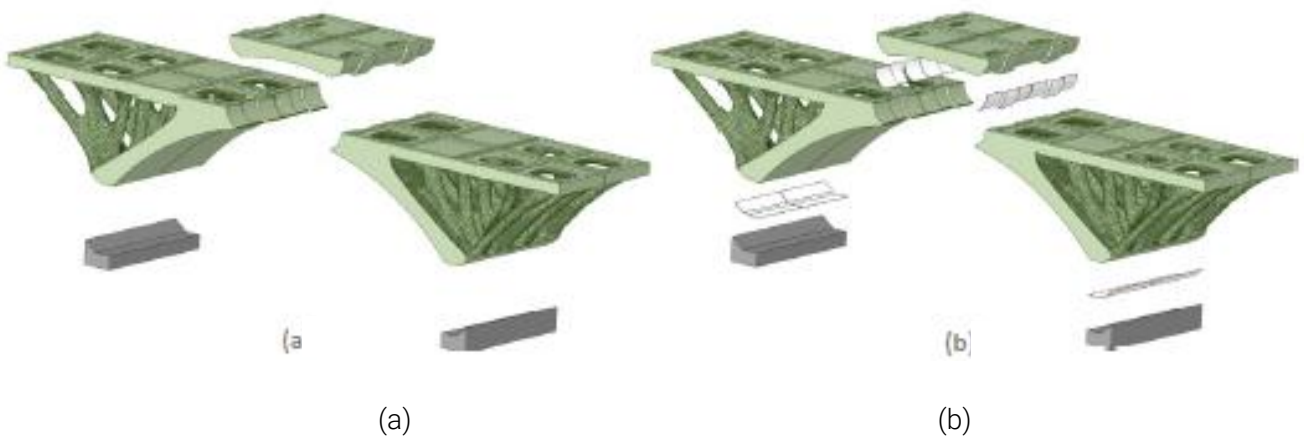
Figure 43 (a) TO model for linear analysis (b) TO model for nonlinear analysis.

4.9 Discussion

As already discussed in chapter 4.3.3, each of the different Topology Optimization algorithmic methodologies has different advantages and drawbacks. In total, Gradient-Based methodologies have better convergence than the Gradient-Free ones because of the mathematic model they are using in order to solve the optimization problem. However, there are also differences in terms of solution robustness inside the different types of Gradient-Based methods. Density-based methods lean in total to faster and more robust solutions, although there is the need to make specific adaptations in order to avoid potential geometric defects and they do not result in a clear shape boundary. On the other hand, Level Set methods lead to a specific and smoother boundary, but there is big likelihood that they end up in local minima because of the dependence of the final outcome to the initial guess.

Regarding the different problem formulations, although compliance-based optimization is the most widely used in the literature, studies have shown that volume-based optimization can also be a robust alternative to it. Stresses have also been proven to be an essential part of the problem that ensures the feasibility of the final outcome, although when implemented alone the overall stiffness of the structure is deteriorated. In general, the importance of considering both compliance and stresses in the optimization problem is highlighted, but specific attention needs to be paid in the method of applying the stress constraint, since it can increase significantly the overall computational time needed for the operation.

Currently, the available commercial TO software uses mainly the SIMP methodology techniques, but there are programs that have also incorporated Level-Set Methods along with SIMP. The BESO method is offered through separate plug ins. There are projects which have already been developed and built using all the different options. In the case of cast structural components, the built examples refer mainly to concrete, both reinforced and unreinforced. The latter one shows a similar behavior to glass because of its brittle behavior. Despite the different techniques that they are using, all the developed projects can be considered as successful since they managed to create a sound structure with considerable mass reduction. This further underlines the large potential regarding this research direction.

Regarding TO cast glass components, the main input is given by the theses which have already been developed in TU Delft recently. The majority of them have used SIMP methodology, but there is also an experiment using the Level-Set Method, which needed less post-processing than the other ones. The common characteristic was that they all have optimized according to a minimum compliance objective.

Despite the use of different methods, the main drawback in all of them was the incapacity of the commercial software to add two different constraints regarding the principal stresses during the TO process. This led to optimizing only with regard to tension – which is considered as the most critical factor – and check for compression in a later stage. This resulted in a more time-consuming procedure. Additionally, the limitation in the number of nodes which could be processed by the software using the educational license led to optimizing through a series of iterations which further increased the time and manual work needed for the simulation.

Despite the inherent limitations, all the theses resulted in well-established results since they also incorporated the respective annealing, manufacturing and transportation criteria in the process. Additionally, small prototypes were constructed in some of the projects. The final cast outcome showcased that it is actually feasible to create these complex glass forms and validated the estimation that 3d-printed sand mould is the most suitable option for this process.

Having said that, density-based methodologies and more specifically SIMP method is selected for the implementation in this project, since it is estimated as the option which is most likely to lead in a robust result. Regarding the problem formulation, it is decided to try to implement a volume-based approach in order to

achieve the most lightweight structure possible for the given constraints. However, given that compliance-based approaches have been more documented in the literature, it was decided to apply both of them and do a comparative review of the results obtained.

The structural, annealing, manufacturing and transportation criteria as discussed in chapters 3 and 4 will be applied to the algorithm through the adaptation of methods which have already been suggested by several papers.

5. Case Study Setup

In this chapter, the main strategy for the case study application will be discussed, as well as the main guidelines which are going to be taken into consideration in order to later be applied during the optimization process.

5.1 Overview

As discussed in Chapter 2, the case study example which is going to be examined for the needs of this project refers to a small interior pedestrian bridge in the Great Court connecting the Reading Room to the main volume of the British museum.

To begin with, it needs to be underlined that the optimization process is going to explore the design of the monolithic slab only in terms of its structural part. The railing, which does not contribute to the structural integrity of the component and therefore is expected to be removed by the algorithm during the optimization, is not going to be taken into account at all in the operation. It will be added in a secondary phase in the bridge and it will consist of laminated float glass sheets, similarly to the railing that exists in the current application (Figure 44). The supports of the slab are assumed as fixed on the short sides which are facing the neighboring walls. Although the type of fixed connection has not been thoroughly investigated, it is assumed that a metal bracket connection could be applied to it.

The total monolithic glass slab (4.20m*2.30m) is going to be split in two parts serving for redundancy in case of failure (Figure 45). The division of the slab is going to be applied along the transversal axis. In this regard, each part will be kept as a whole along the longitudinal axis which is the most critical in order to have sufficient performance in terms of bending moment and maintain the necessary structural integrity. The two parts are going to be connected with a hinge connection between them in order to avoid rigidity and allow for small movements but still ensure that they will operate uniformly.

On top of the two monolithic pieces, two layers of float glass (2*10mm) are going to be placed in order to serve both for redundancy issues but, most importantly, to protect the large monolithic components from local contact stresses. This derives from the fact that contact stresses have been generally proven to be more critical for cast glass components than far-field stresses since they activate different defects and deformation mechanisms which can lead ultimately to failure. In this regard, it is underlined that they should also be taken into consideration, apart from the flexural strength data, for the design of cast glass structures (Bristogianni et al., 2021).

Figure 44 Existing slab in the British Museum.
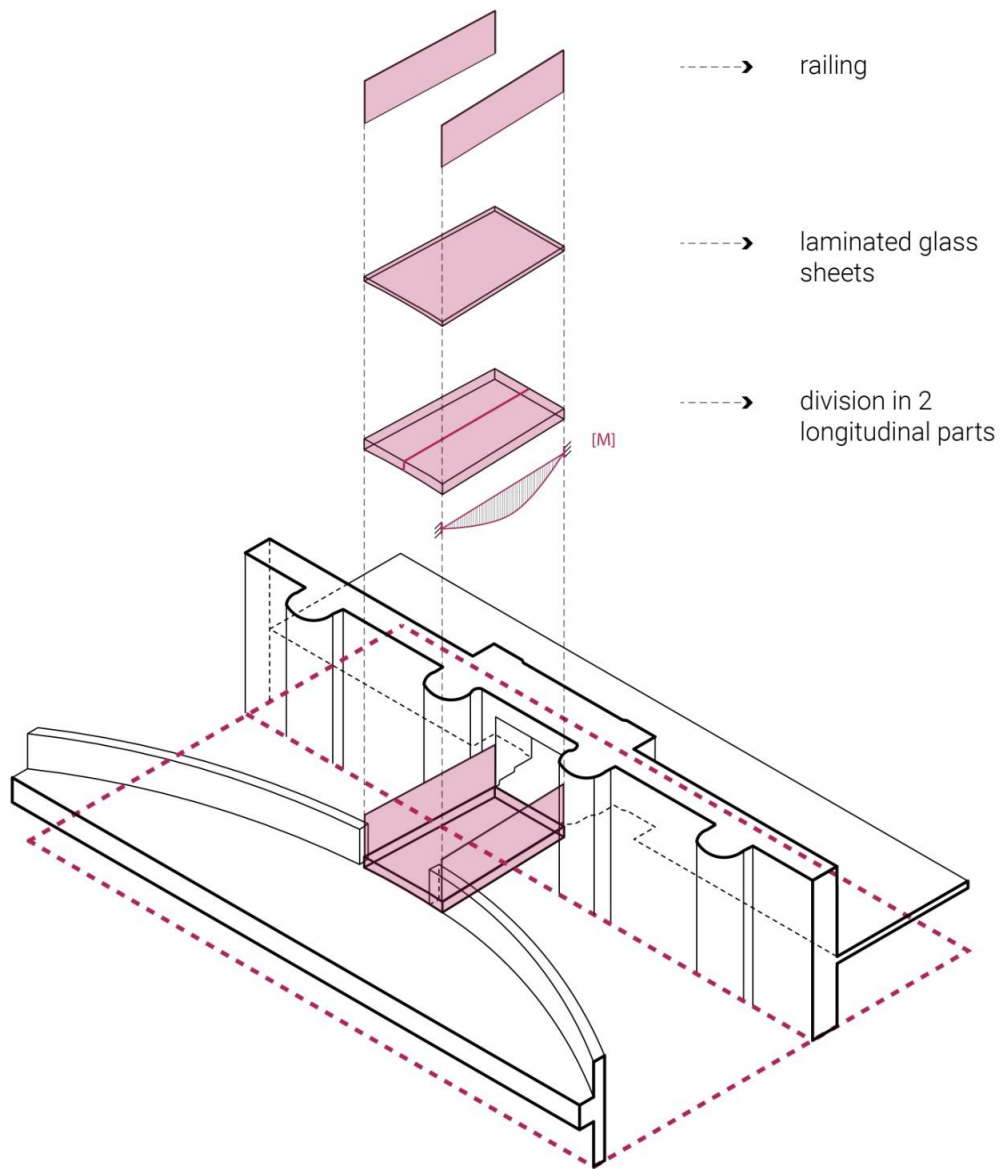
Figure 45 Axonometric diagram illustrating the design strategy.

The size of each part that derives after the division (Figure 46) complies with the limitations regarding transportation, since it is well inside the dimensions of the maximum size of the component that can be transferred inside a truck[21] However, the dimensions of each monolithic piece do not comply with the criteria regarding the maximum size of 3d-printed sand mould which is able to be manufactured. During this project it will be assumed that this problem is solved through applying the system of interlocking mould pieces made from 3d printed sand proposed by (Stefanaki, 2020)[22].

---

[21] The maximum permissible dimensions of lorry in UK are 2.9m in width and 18.65m in length (gov.uk).
[22] A frequent problem that appears when connecting different mould pieces together is the possible leakage in the seam of the two parts. In (Stefanaki, 2020), this is solved it with an interlocking connection system consisting of extensions, undercuts and frequent nodes.
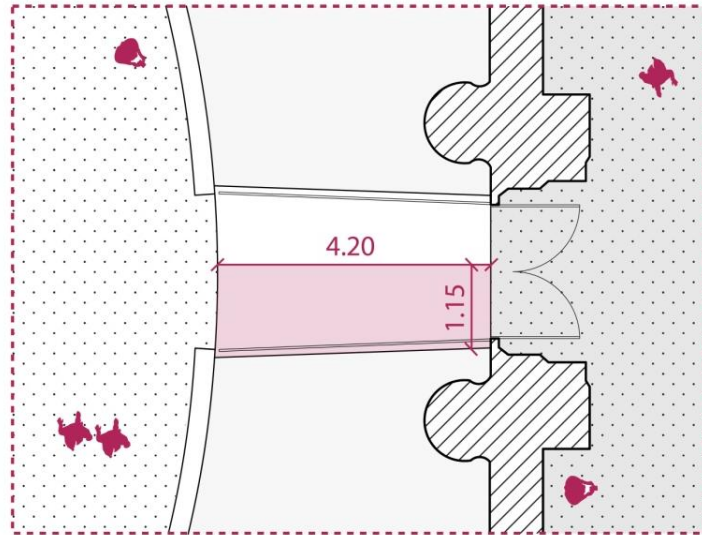
Figure 46 Overall dimensions of each monolithic part.

5.2 Design domain

Assuming that the two monolithic pieces are going to be identical, the project will emphasize on designing only one of the two parts that make up the total slab. Taking into consideration the added complexity of creating an optimization code for a 3-dimensional design, it was decided that the approach of this thesis will be to optimize the design of the characteristic 2-dimensional longitudinal section of the component. The final design will derive as an extrusion of this section along the transversal axis. This is considered as an acceptable solution since the most critical point of this optimization, in order to efficiently reduce the annealing time, is the size and shape of the element cross section.

At the same time, in order to further simplify the already anticipated complex process, the slightly curved boundary edges of the slab (Figure 46) are assumed to be straight, so that the final outline of the slab becomes a rectangle (Figure 47). At this point, it is worth mentioning that, although the shape under investigation is 2-dimensional, the input values and the structural analysis which is going to be integrated inside the optimization process are going to take into consideration the whole thickness that the component will have when extruded for the creation of the 3d structure.
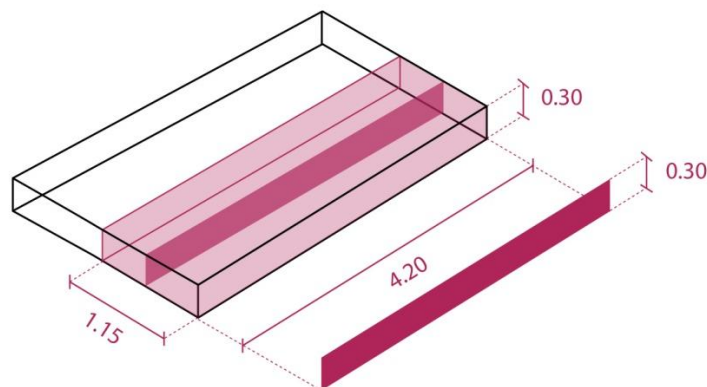
Figure 47 Axonometric diagram of the design domain.

6. Problem statement

In this chapter the problem statement, which refers to the criteria and limitations already discussed in the previous chapters, will be used in order to formulate the optimization problem in its mathematic expression with the relevant optimization objective and constraints.

6.1 Overview

As discussed in chapter 4, the algorithmic methodology which is going to be implemented is SIMP since it is well-proven to have good convergence and end in robust solutions. The numerical solution of the problem is going to be intended through the use of mathematical programming algorithms and, particularly, nonlinear programming.

As already discussed, in SIMP the main idea is that the design domain is divided into smaller elements, each of which is assigned a (pseudo)density value between 0-1[23] that reflects the material existence or not in it (Figure 48). The density values are further penalized in order to be forced to the boundaries and avoid intermediate densities that cannot be reflected in a physical state. In this project, the design domain Ω_{des}[24] is divided into quadrilateral elements that have small size (0.02*0.02m) in order to achieve as better a final mesh resolution as possible and the penalization value is set to 3.
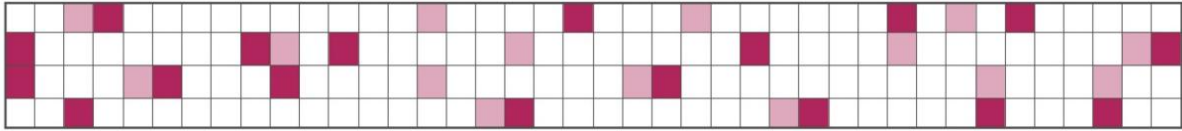
Figure 48 Assigning different pseudo-densities per element in SIMP.

Given that mathematical programming algorithms, although they can efficiently process a wide range of design variables, are only feasible to deal with a moderate number of constraints (Bendsoe & Sigmund, 2004), the optimization problem is going to be considered only in relation to the design variables. Regarding the respective structural and manufacturing constraints, they are going to be described as a function of the design variables and evaluated through a process called sensitivity analysis[25]. In this regard, the general formulation of the optimization problem is as follows:

$$\min_{x} \; f(x), \; x(e)^{p}, \qquad 0 < x_{min} \le x(e) \le 1, \qquad x_{min} = 10^{-3}, \qquad p = 3$$

$$e \in \Omega_{des} = \Omega_{mat} \setminus \Omega_{nonmat}, \; \Omega_{mat} \subseteq \Omega \subseteq R^{n}, n = 2,3$$

$$subject\ to \; g_i(x) \le 0, \qquad i = 1,2,\dots,m$$
$$h_i(x) = 0, \qquad i = 1,2,\dots,p$$

---

[23] Although in principle the range of densities is 0-1, in reality a lower bound of 1e-03 is applied in order to avoid singularities.

[24] In principle Ω_{des} is supposed to derive as the subtraction of the non-material domain (Ω_{nonmat}) from the total material domain (Ω_{mat}), such as $e \in \Omega_{des} = \Omega_{mat} \setminus \Omega_{nonmat}$. However, given that all the material domain was finally applied in the optimization and the non-material domain was not considered, it finally concluded to $\Omega_{des} = \Omega_{mat}$.

[25] Through sensitivity analysis," the displacement fields are given implicitly in terms of the design variables through the equilibrium equation" and the derivatives of the displacements according to the design variables are being used (Bendsoe & Sigmund, 2004).

6.2 Optimization scenarios

After evaluating the different ways of formulating the topology optimization problem (Chapter 4.6), it was decided that optimizing the structural weight (volume) of the component while also ensuring its structural validity and feasibility to be manufactured is the most promising approach for this project. Although compliance was the optimization objective in all the previous projects – as shown in chapter 4.8 – this time the minimization of the volume is initially selected as the objective, since it is considered as the most important aspect. This derives from the added benefits it has in reducing the annealing time, saving in terms of material use and having a more lightweight structure. Additionally, given that compliance based optimization depends a lot in the end user for the application of the volume constraint each time, it is likely that it does not result in the optimum design in terms of material usage. However, given that compliance based is more widely used and therefore there are more reference examples and benchmarks in the literature it was finally decided to add it to the exploration in order to help with the troubleshooting process and give the opportunity for a comparison between the two options at the end of the project.

The constraints which are going to be applied in the algorithm cover a wide range of critical points for the design of glass structures. They refer to both its structural performance –compliance, deflection, principal stresses, Drucker -Prager failure criterion- but also the feasibility to be manufactured –volume, annealing and manufacturing criteria.

Each objective can be combined with one or more of the constraints, building up gradually the optimization process or having iterations that take into consideration only some of the constraints at a time. In Table 11, the overview of objectives and constraints can be seen along with their possible combinations.

<div align="center">Constraints</div>

	Equilibrium*	Minimum element dimension – Filtering*	Volume	Compliance	Deflection	Principal stresses	Annealing & Manufacturing criteria (d_{max})	Drucker-Prager failure criterion
Volume	✔	✔		✔	✔	✔	✔	✔
Compliance	✔	✔	✔		✔	✔	✔	✔

Objectives (left vertical label)

Table 11 Overview of optimization problem objectives and possible constraints
(* refers to the constraints that exist always in the optimization process)

6.3 Mathematic formulation

In this chapter, the mathematic formulation of the optimization problem is described for each one of the objectives and the constraints mentioned above.

6.3.1 Objectives

As already discussed in Chapter 4.6, the objective of the optimization problem can largely affect the final outcome. Given that stress-based optimization has been proven to conclude in results with significantly deteriorated structural stiffness, it will not be taken into consideration for the development of the algorithm inside the scope of this thesis. As already mentioned, volume and compliance minimization are going to be considered and compared regarding the final results obtained from each of them.

6.3.1.1 Volume

The first objective investigated is the minimization of the volume of the structure. The structural volume is calculated as the total sum of the densities per element. The mathematic formulation is as follows:

$$\min_x V(x) = \int_{\Omega_{des}} x(e)\, d\Omega_{des}, \quad 0 < x_{min} \le x(e) \le 1, \quad e \in \Omega_{des} = \Omega_{mat} \subseteq \Omega \subseteq R^n, n = 2$$

6.3.1.2 Compliance

The second objective investigated is the minimization of the compliance of the structure. It equals the maximization of the structural stiffness of the component and it is formulated as:

$$\min_x c(x) = U^T K U = \sum_{e=1}^{N} U_e^T K_e(x_e) U_e = \sum_{e=1}^{N} U_e^T E(x_e) K_e U_e$$

$$0 < x_{min} \le x(e) \le 1, \quad e \in \Omega_{des} = \Omega_{mat} \subseteq \Omega \subseteq R^n, n = 2$$

$$E(x_e) = E_0 + x_e^p (E - E_0), \quad E_0 = 10^{-5} GPa$$

where E is the Young's modulus of the material and E_0 is a lower bound in order to avoid singularities in the elements with very low density

6.3.2 Constraints

They refer to the limitations that are applied to the optimization problem and, as shown in Chapter 4.6, they also affect largely the final shape. The number of constraints applied each time as well as the process followed in order to obtain their values has a serious impact both on the computational time needed for each operation but also on the amount of iterations needed in order to converge.

6.3.2.1 Equilibrium

It is an indispensable constraint of the optimization problem and is fulfilled at all iterations in order for an evaluation to be considered valid. It takes as input the stiffness matrix and the forces which are applied to the structure and calculates the displacements. By using as input the stiffness matrices per element and the nodal equivalents of the forces, the nodal displacements can be obtained. These are later used in order to calculate the rest of the structural sizes, such as compliance, deflection or principal stresses. The general formulation is:

$$KU = F$$

After replacing with the nodal equivalents, it becomes:

$$\sum_{e=1}^{N} K_e(x_e)U_e = \sum_{e=1}^{N} f_e \implies \sum_{e=1}^{N} E(x_e)\, K_e\, U_e = \sum_{e=1}^{N} f_e$$

6.3.2.2 Minimum element dimension – Filtering

This constraint addresses two distinct issues. Firstly, it serves to ensure that all the parts of the structure will have the minimum dimension of cross section needed in order for the glass structure to be able to be manufactured. Smaller cross sections may cool very fast and, therefore, create high local residual stresses during the annealing process resulting to failure. The second issue refers to checker boarding[26], which is an inherent problem of the SIMP approach and results in structures with checkerboard patches that appear to perform better in stiffness but cannot be manufactured in reality.

The formulation of the constraint follows the length-scale approach proposed by (Guest et al., 2004). In this regard, the density values are filtered in every iteration so that each element is assigned a density that results as the weighted average of the densities that lie inside a circular dimension with radius r_{min}. Particularly, it is formulated as:

$$x_e = \frac{\sum_{j \in S_e} x_j\, w_j\, v_j}{\sum_{j \in S_e} w_j\, v_j}, \quad j \in S_e \ if \ r_j \le r_{min}, \quad r_j = \left\| x_j - \overline{x}^e \right\|, \quad r_{min} = \frac{d_{min}}{2}$$

where S_e is the set of the nodes inside the circular region.

The weighted factors that are assigned to each element of the circular region are inversely proportional to the distance from the central element and they are calculated as:

$$w_j = \begin{cases} \dfrac{r_{min} - r_j}{r_{min}}, & if \ j \in \Omega_s \\[2em] 0 \end{cases}, \quad j \in \Omega_s \ if \ r_j = dist(e,j) \le r_{min}$$

Minimum element dimension constraint is an indispensable constraint in the optimization problem, given that it also addresses the checkerboard problem which is inherent in the SIMP formulation. Consequently, it is applied, along with the equilibrium constraint, in all the different constraint combinations.

6.3.2.3 Compliance

The constraint referring to the compliance of the structure is calculated in the same way as the compliance objective, deriving as a function of the stiffness matrices per element and the nodal displacements. The mathematic formulation is based on the approach proposed by (Bruggi & Duysinx, 2012). Particularly:

$$\frac{c(x)}{c_L} \le 1, \quad c(x) = \sum_{e=1}^{N} U_e^T E(x_e) K_e U_e, \quad c_L = a_c c_0$$

---

[26] Described in chapter 4.3.1.1.B

where c_0 is the compliance evaluated for the full domain and α_c is the percentage that defines the allowable limit.

In (Bruggi & Duysinx, 2012), it is shown that a lower value of α_c improves the performance of the algorithm especially in the first iterations gathering faster the material around the optimal layout. On the other hand, a very strict compliance limit may ultimately act as a threshold for the optimization, limiting significantly the feasible area of the solutions and, therefore, converging into local minima.

6.3.2.4 Volume

Contrary to the volume objective, which derives as a sum of the element density variables, the volume constraint is formulated in reference to the volume fraction[27]. This allows for easier modification of the allowable limit of the volume every time. Therefore, the volume constraint becomes:

$$\frac{V(x)}{V} \leq f$$

where f is the allowable material fraction, $V(x)$ is the total volume in each operation and V is the total volume of the virgin material.

6.3.2.5 Deflection

It refers to the maximum value of total deflection that is permissible for glass structures. The deflection of the total structure is evaluated through assessing the vertical displacements (v) of each element node (k). They are going to be extracted through applying the Finite Element Method equations and the mathematic formulation of the constraint is:

$$v_k^e < \frac{1}{500} l, \qquad k = 1,2,3,4, \qquad e \in \Omega_{des} = \Omega_{mat} \subseteq \Omega \subseteq R^n, n = 2$$

6.3.2.6 Principal stresses

As already discussed in Chapter 3, glass is a brittle material and, therefore, has considerably unequal properties regarding tension and compression. In this regard, both of the allowable limits should be checked during the optimization process in order to ensure that the algorithm will converge in a feasible structure. In this project, plane stress conditions are assumed and the principal stress values are calculated by applying the Finite Element Method equations for the case of 4-node quadrilateral elements. Regarding the numerical issues that arise from the application of the stress constraint, and particularly the 'singularity' problem as described in Chapter 4.6.2, the qp approach proposed by (Bruggi, 2008) will be implemented. Specifically, in this thesis the alteration of the method as applied in (Bruggi & Duysinx, 2012) will be adopted and, thus, the principal stress constraints are formulated as:

$$x_e^{(p-q)} \left(\frac{\sigma_{comp,e}}{\sigma_{comp,lm}} \right) \leq 1, \qquad e = 1,2,\dots,N$$

---

[27] The volume fraction is the ratio of the total volume of the structure in each operation to the total volume of the virgin material.

$$x_e^{(p-q)} \left(\frac{\sigma_{ten,e}}{\sigma_{ten,lm}} \right) \leq 1, \qquad e = 1,2,\dots,N$$

where p is the penalization value applied from the SIMP approach, q is the exponent related to the stress relaxation introduced by the qp approach, $\sigma_{comp,e}$ & $\sigma_{ten,e}$ are the compressive and tensile stresses extracted per element and $\sigma_{comp,lm}$ & $\sigma_{ten,lm}$ are their respective limits related to glass material.

It is important to highlight that, in this regard, the relaxation parameter affects only the stress constraints in the elements with low densities, whereas the constraints in the high density elements remain almost unaffected.

6.3.2.7 Annealing & Manufacturing criteria

This criterion aspires to combine the annealing and manufacturing constraints of glass structures in one uniform constraint referring to the maximum dimension of cross section that each part of the structure can have. The first aspect which is taken into consideration is the maximum annealing time. As mentioned in Chapter 3.4, the annealing time derives as a function of the maximum dimension of the cross section related to each part of the structure. It is calculated from the formula[28]:

$$T_{ann}(d) = \frac{\Delta T}{\frac{\sigma_{res}}{\frac{E \times \alpha_{ex}}{1-\mu} \times \frac{\rho \times c_p}{\lambda} \times d^2 \times b}}$$

The cross section dimension that corresponds to the maximum annealing time is calculated and, afterwards, compared with the respective maximum dimension related to the glass manufacturing constraints. Particularly, it is necessary that the cross sections of each part in the structure lie inside a specific range in order to ensure a homogeneous shrinkage[29]. Otherwise, as discussed in Chapter 3.4, the large difference between the cross section dimensions will be reflected in significantly different cooling times that can cause large stress concentrations and even lead to fracture. The maximum allowable limit d_{max} derives from the comparison of these two values as:

$$d_{max} = \begin{cases} 2 \times d_{min}, & if\ T_{ann}(2 \times d_{min}) \leq T_{annmax} \\ \sqrt{\frac{T_{annmax} \times \sigma_{res}}{\Delta T \times \frac{E \times \alpha_{ex}}{1-\mu} \times \frac{\rho \times c_p}{\lambda} \times b}}, & if\ T_{ann}(2 \times d_{min}) > T_{annmax} \end{cases}$$

The d_{max} limit is then used to form the optimization constraint following an approach similar to the maximum length scale constraint described by (Guest, 2009). Particularly, a circular region Ω_r is introduced with diameter respective to d_{max}. The total volume inside this region is calculated and checked with the allowable limit using the formula as followed:

---

[28] You can find a detailed description of the formula in Chapter 3.4.
[29] Inhomogeneous shrinkage may also happen because of the existence of sharp edges in the structure. However, because this cannot be directly assessed during the optimization, it will be evaluated in a secondary phase after the boundary is created from the range of the densities.

$$\int_{\Omega_{r(e)}} x_j d\Omega \, < \, V_{max} \quad \forall \, e \, \in \Omega_{des}, \qquad j \, \in \, \Omega_r^e \quad if \quad r_j = dist(e,j) \leq \frac{d_{max}}{2}$$

$$V_{max} = \, v_{lim} \times v_e \times \int_{\Omega_{r(e)}} x_{full} d\Omega$$

where v_{lim} is the allowable limit referring to the ratio of empty to full inside the circular region, v_e is the volume of each element and x_{full} are the density variables in the virgin material state (x=1).

6.3.2.8 Drucker - Prager failure criterion

The main advantage of using a material failure criterion instead of evaluating individually the principal stresses in each element is the ability to combine both of the principal stress constraints into one combined factor per element. This allows for reducing significantly the number of constraints posed in the optimization.

Although stress constrained topology optimization usually takes into consideration the Von Mises criterion, this can only serve the case of ductile materials and is considered inadequate in the case of materials that have unequal properties in tension and compression. In the latter case, failure criteria such as the Drucker - Prager failure criterion which is used in the case of brittle materials, such as concrete of rocks should be applied (Duysinx et al., 2008). Given that glass is a brittle material with considerably different properties regarding its tensile and compressive allowable limits - as already stated in Chapter 3 - Drucker-Prager is considered as the most adequate criterion to use for the evaluation of its strength.

Following the formulation presented in (Bruggi & Duysinx, 2012), the equivalent stress which is going to be evaluated is calculated as:

$$\sigma^{eq} = \frac{s+1}{2s}\sqrt{3J_{2D}} + \frac{s-1}{2s}I_1$$

where s is the asymmetry ratio of the compressive to tensile allowable strength limits such as that $s = \frac{\sigma_{comp,lm}}{\sigma_{ten,lm}}$ and I_1, J_2 are the first stress invariant and the second deviatoric stress invariant respectively. The stress invariants are defined based on the stress tensors which are calculated per element during each iteration. For plane stress conditions, the respective formulas are:

$$I_1 = \, \sigma_{11} + \, \sigma_{22}$$

$$3J_{2D} = \, \sigma_{11}^2 + \, \sigma_{22}^2 - \, \sigma_{11}\sigma_{22} + \, 3\sigma_{12}^2$$

The equivalent stress should be lower than the allowable limit for tension in each element. Additionally, in order to address the singularity phenomenon as already posed in the principal stresses constraint, the mathematical perturbation following the qp approach described by (Bruggi,2008) will be applied. In this regard, the constraint is defines as:

$$x_e^{(p-q)} \frac{\sigma^{eq}}{\sigma_{ten,lm}} \leq 1$$

The difference in the range of admissible solutions between the case of principal stresses and the case of the Drucker - Prager criterion for an asymmetry ratio $s = \frac{\sigma_{comp,lm}}{\sigma_{ten,lm}} > 1$ is shown qualitatively in Figure 49[30].
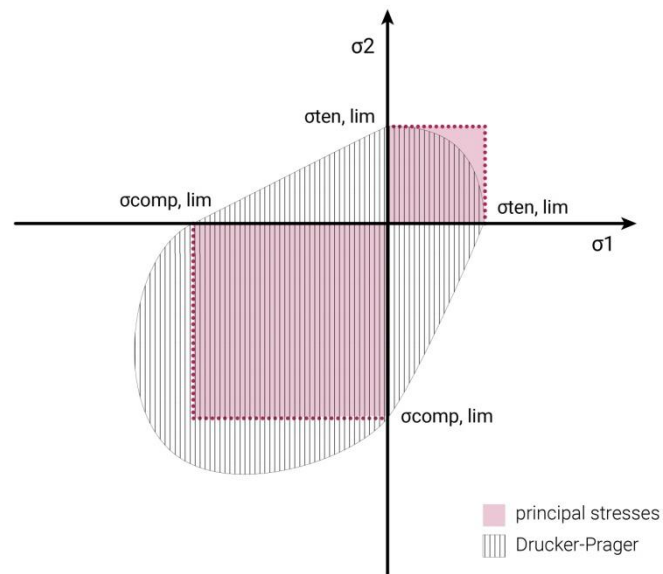
Figure 49 Qualitative diagram of admissible range of solutions between principal stresses & Drucker – Prager criterion.

---

[30] The diagram is based on data from (Bruggi & Duysinx, 2012).

7. Algorithm Development

In this chapter, the main logic of the code is going to be described and the individual functions are going to be explained. Additionally, the first results that serve to check the performance of the algorithm are going to be demonstrated and discussed.

The structural analysis with FEM and the first optimization experiments were held using a Dell laptop with an Intel(R) Core(TM) i7-4510U CPU @ 2.00GHz processor and 8 GB installed RAM. However, because of the limited computational capacity, the last optimization simulations were held using a desktop computer with 2 Intel(R) Xeon(R) CPU E5-2640 v4 @ 2.40GHz processors and 64 GB installed RAM.

The algorithmic implementation of the problem is divided into two parts. Firstly, the structural model is created by applying the Finite Element Method equations through programming in Matlab. The results are validated through comparison with results obtained through other commercial software (ANSYS). Secondly, the optimization setup is created and the problem is solved using the fmincon solver provided by the Matlab Optimization toolbox.

7.1 Overview

Overall, the code is separated into different parts which serve distinct roles in the operation (Figure 50). The most characteristic parts are defined into separate functions in order to be easier to organize the algorithm and facilitate, firstly, the troubleshooting process and, secondly, the application of modifications in the code when needed.

The first part refers to setting the input values and the hard criteria related to the glass material as defined in Table 8 & 9 (Chapter 3.7), the loads applied in the structure, the penalization values related to the SIMP method as well as the dimensions of the design domain and the size of the mesh refinement. Based on that, the design variables for the optimization along with their initial values as well as their upper and low boundaries are going to be defined.

Afterwards, the neighbors for the minimum (filtering) and the maximum element dimension are going to be defined. It is important to highlight that these operations are happening outside the optimization part and, therefore, save a lot in the computational time needed. The indexes of the neighbors per element in each of the two cases (minimum & maximum element dimension) are stored in arrays which are recalled in the optimization when needed.

All the aforementioned values are used as input for the optimization operation. This consists of three main parts; the optimization solver which runs the consecutive iterations in order to find the optimum value, the objective function which sets the minimization goal and the non-linear constraint function which includes all the equality and inequality constraints that will be posed as criteria for the optimization. In the beginning of both the objective and the non-linear constraint function, the design variables which are tested from the solver each time are filtered according to the minimum element dimension/filtering constraint.

The design variables are plotted after every iteration in order to be able to check visually the convergence trajectory and to be able to identify at an early stage possible bugs in the algorithm. At the same time, the density variables are also stored in an Excel file in order to be able to import them in Grasshopper and extract the final result.

Afterwards, the most characteristic parts of the algorithm are going to be analyzed and the differences between the benchmark and the case study application are going to be highlighted.
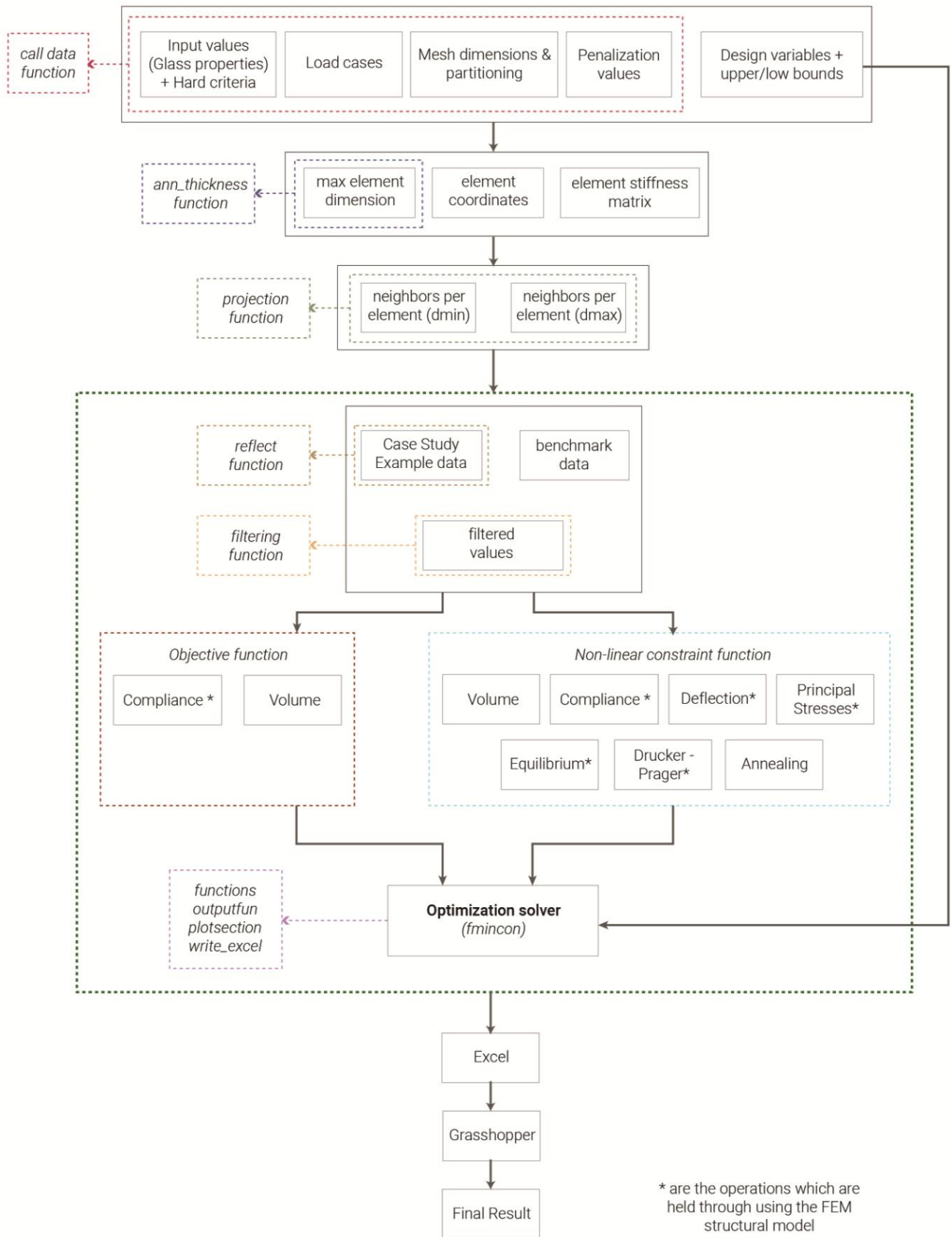
Figure 50 Diagram describing the logic for the development of the algorithm (green outline is the operations that happen iteratively inside the optimization sequence).

7.2 Initial Setup

7.2.1 Mesh partitioning

As already mentioned, one of the first parts of the optimization process refers to partitioning the continuous domain into discrete elements in order to use them for the application of the Finite Element Method equations as well as for the SIMP approach during the optimization. During this project, the initial mesh was divided into 4-node quadrilateral elements of relatively small size (0.02cm*0.02cm) in order to achieve a good balance between the resolution of the final outcome and the added computational cost in the analysis.

During both the structural analysis and the optimization, 2 different setups are tested (Figure 51). The first one refers to the classical problem of the MBB beam (benchmark problem) and serves to validate the results extracted with this algorithm through comparing them with the results presented in the literature. In this project, the optimization results which are going to be taken as reference for the benchmark problem are the ones presented in (Liu & Tovar, 2014)[31]. The second setup refers to the 2-dimensional section of the case study slab as it is presented in Chapter 5. The algorithm will be applied to it in a secondary phase after it has been proven to give reliable results through the first check runs.
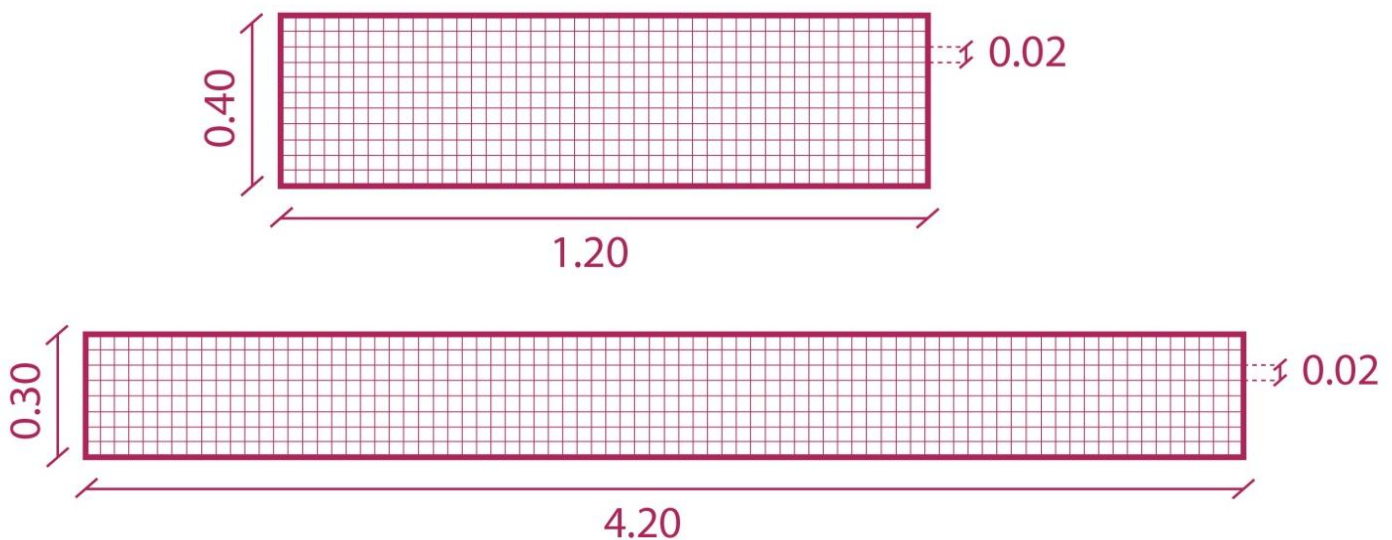
Figure 51 Mesh partitioning & general dimensions (top) MBB beam (benchmark problem), (bottom) Case Study example.

7.2.2 Design variables

The mesh refinement defines drastically the way of distributing the design variables in the design domain. In general, each element of the mesh is assigned a density variable which is later also used in the Finite Element Analysis in order to reflect if the same element corresponds to a full or void in the structure.

The two aforementioned setups follow a slightly different approach in the defining these variables which are later going to used as the input for the optimization (Figure 52). Particularly, although the benchmark problem

---

[31] The paper solves the MBB problem in 3 dimensions. Given that the cross section shape do not change drastically along the z axis, the equivalent 2 dimensional shape of the section is going to be assumed as reference for this project.

follows the classical approach of assigning densities in all the elements, in the case study example half of the elements are assigned a density and the final range of densities for the whole beam derives as a symmetric reflection along the vertical axis. This is based on the fact that, since the beam has similar geometric characteristics along its length and the boundary conditions in the section are also identical in the two sides, the final outcome is already anticipated to be symmetric. This modification reduces considerably the computational time needed for the operation. The 'reflection' of the densities is realized in the algorithm through the reflect function in the beginning of both the objective and the constraint function before the filtering (Figure 50).
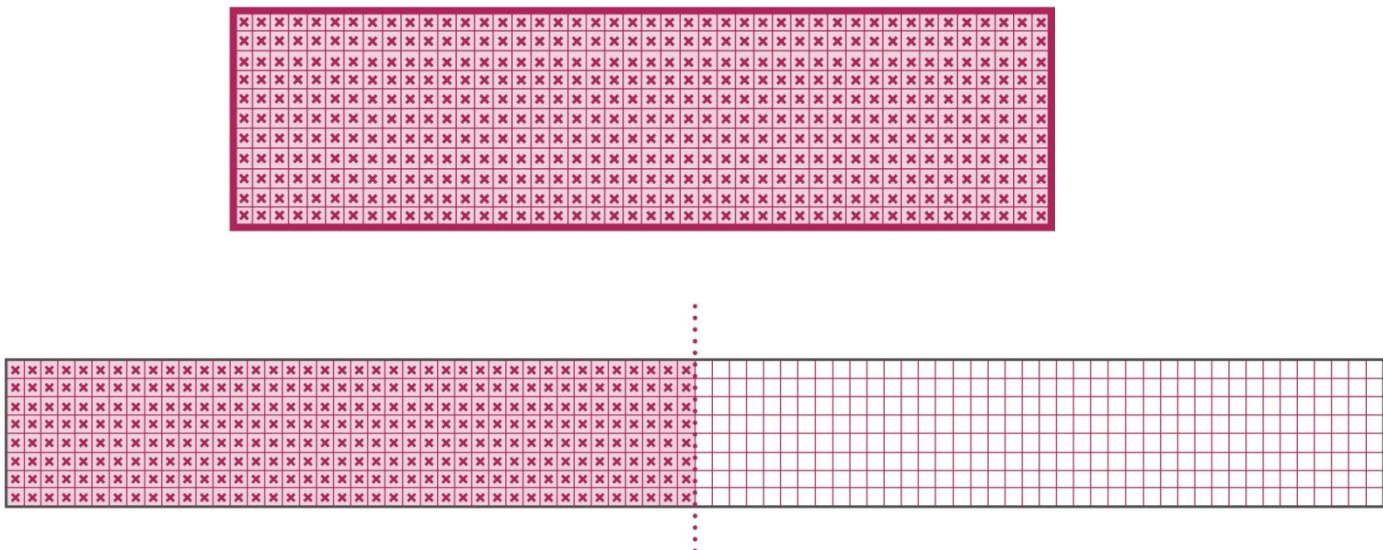
Figure 52 Design variables (element densities) in (top) Benchmark problem (bottom) Case Study example.

7.2.3 Filtering

As already mentioned, the filtering is supposed to serve two different roles in the algorithm. Firstly, it serves to ensure that the each element has the minimum dimension needed by the constraints and, secondly, it prevents the appearance of checkerboard pattern in the structure. The whole process is divided into two parts inside the algorithm; the projection function, which serves to map in an array the indexes of the elements that are inside a circular region with centre the centroid of each element and radius d_{min}, and the filtering which recalls the indexes and calculates the weighted average of the element densities every time (Figure 53). The calculated value is applied afterwards as the filtered density in the central element of the circle. The projection function happens before the optimization starts, whereas the filtering happens during the optimization sequence at the beginning of both the objective and the constraint functions.
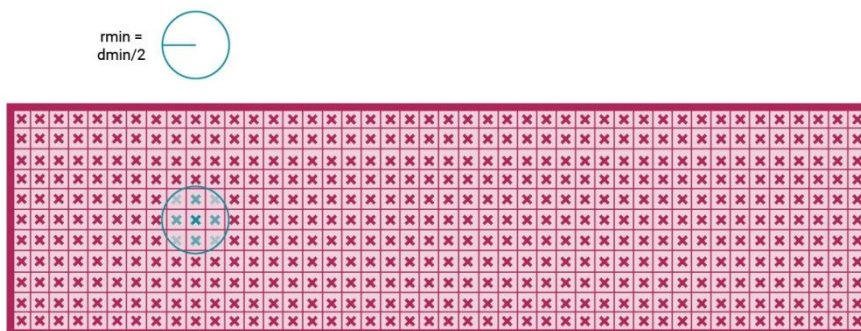
Figure 53 Diagram describing the filtering function (Benchmark problem setup).

7.2.4 Input values

The algorithm takes into account the input values for the material properties and the hard criteria (allowable limits) referring to glass as demonstrated in Chapter 3.7. Regarding the loads that are applied in the structure, they are defined based on the Eurocode 1, Chapter 6 as described in (Vitalis, 2017). At this point, it is important to highlight that, because of the case study example being placed in an interior space, only the vertical loads are going to be taken into account in this project – self weight and short time loads – and not the lateral ones, such as wind load. The final load case is defined taking into consideration both the permanent and short loads and the respective safety factors related to glass material as described in (Oikonomopoulou, 2022).

	Symbol	Units	Value
Permanent load - Self weight (slab) (uniform / should be applied in all the nodes but now only in the top part)	f_{sw}	kN/m2	9,8
Permanent load – float glass sheets[32] (uniform / on the nodes of the top surface)	f_{fl}	kN/m	1,2
Short-term load – people (uniform / on the nodes of the top surface)	$f_{s,p}$	kN/m2	5
Short-term load – maintenance (uniform / on the nodes of the top surface)	$f_{s,o}$	kN/m2	0,4
Safety factor (permanent loads)	s_p	-	1,2
Safety factor (short-term loads)	s_s	-	1,5
<u>Load case 1</u>	f_{tot}	kN/m2	$1,2*(f_{sw} + f_r) + 1,5*(f_{s,p} + f_{s,o})$

Table 12 Load values referring to the case study example.

7.3 Structural Model

7.3.1 Introduction

As already mentioned, the structural model is created based on the equations of the Finite Element Method which allows for approximating the response of structures under the application of specific forces by discretizing their continuous domain into a finite number of elements (Andriotis, 2021). In general, this renders the problem feasible to be solved by computers and, therefore, is considered as the adequate solution for applying in this Topology Optimization algorithm

---

[32] Only the load of the float glass sheets (2*10mm) applied on top of the monolithic parts is going to be taken into consideration. The load of the railing is not going to be considered at this phase.

The algorithm uses as input for the method the boundary conditions of the structure –dimensions, supports and loads- and the stiffness of the material applied in order to extract the displacements per node (Figure 54). In this project, these values are going to be used later in order to extract other structural sizes, such as the compliance and the maximum & minimum principal stresses. Separate functions which interfere in the algorithm can serve to crosscheck the application of loads and supports in the design domain (checkwhere function) or plot the diagrams of the resulting values (plotprincipal function).
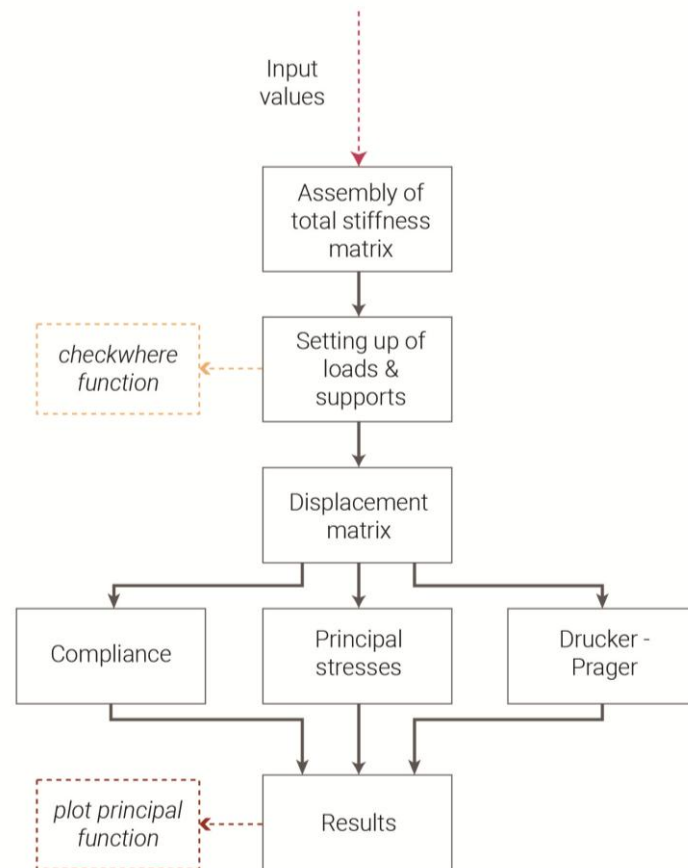
Figure 54 Diagram describing the logic for the development of the FEM Structural model.

7.3.2 Boundary Conditions

The boundary conditions are different for each setup (Figure 55). Regarding the MBB beam, it is defined as a cantilever beam fixed on one of the short sides. Regarding the Case study slab, given that it is attached on the two sides in concrete floor, it is going to be considered as fixed on both sides. The physical interpretation of this connection could be a metal bracket fixed with bolts to the neighboring walls but it is not going to be investigated further at this point during this project.

85
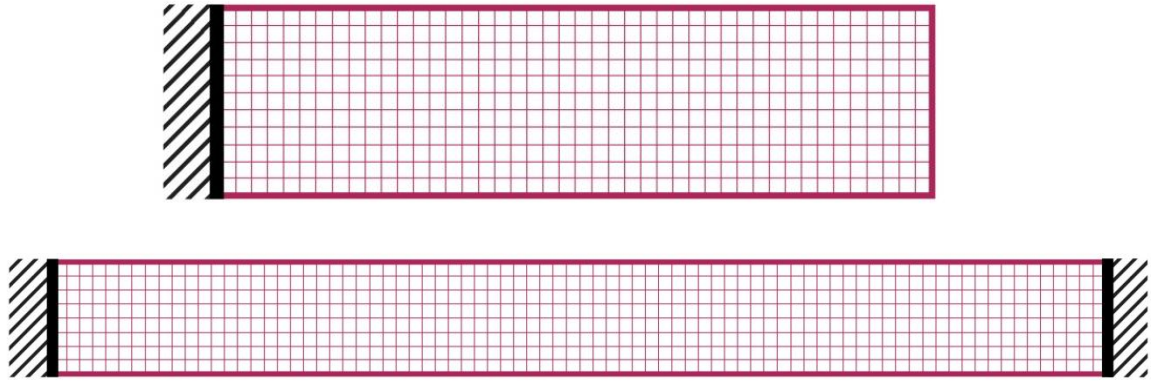
Figure 55 Boundary conditions (top) Benchmark problem, (bottom) Case Study example.

7.3.3 Loads

In FEM, the forces are applied on the structures through their nodal equivalents. In the case of the benchmark problem, the total load value is applied as a point force on the bottom element in the free side of the cantilever[33]. In the Case study slab, a uniform load is assumed so the total force is divided equally to the nodes of the upper part[34] (Figure 56).
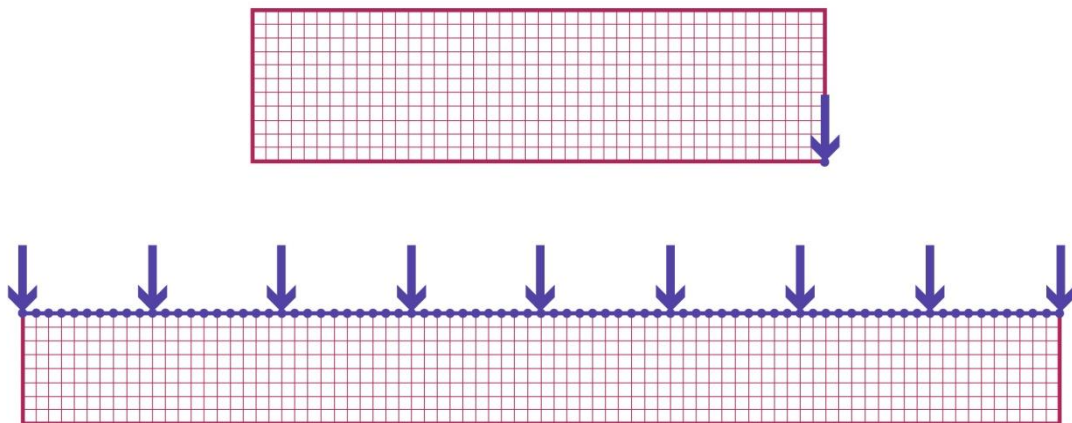
Figure 56 Load application (top) Benchmark problem, (bottom) Case Study example.

---

[33] For the sake of simplicity, the absolute value of this load is going to be the same as the total value calculated for load case 1 (case study example).
[34] Given that we are performing a 2D analysis, each node has 2 degrees of freedom (dof). The nodal loads are applied to the dofs which are related to the vertical displacements.

7.3.4 FEM Analysis[35]

As already mentioned, the FEM analysis is based on two-dimensional quadrilateral plane stress elements. The first part refers to the creation of the assembly matrix from the matrices of each element. For the special case of square finite elements as applied in this project, the element stiffness matrix is an 8x8 symmetric square matrix[36]. The total stiffness matrix of the structure is assembled through placing the separate element matrices in the positions respective to the indices of their nodes. Afterwards, the nodal displacements derive from the total stiffness matrix and the nodal forces according to equilibrium equation ($F = KU$).

Using the nodal displacements acquired on the previous step, the principal stresses can be derived. Unlike the displacements which refer to each node and degree of freedom, the principal stresses are properties of each finite element. However, given that the mesh is divided into quadrilateral elements, the values of the principal stresses vary throughout their surface[37]. In order to calculate the values at each point, the shape functions and the strain-displacement matrix $[B]$ that derives from them are used. Particularly, the strain-displacement matrix serves to obtain the strains ε per element from the displacements of its nodes, according to the formula:

$$\varepsilon = [B]U_{el,n}$$

The stress matrix derives from the material stiffness matrix $[E]$ and the strain matrix ε according to the formula:

$$\sigma = [E]\varepsilon$$

Based on the stress matrix, the stress tensor (2x2) is obtained. The principal stresses derive ultimately as the eigenvalues of the stress tensor. Regarding the Drucker - Prager criterion, the equivalent stress is calculated from the stress matrix by using the first stress invariant and the second deviatoric stress invariant as described in Chapter 6.3.2.8.

7.3.5 Verification of results

In order to validate the structural model, the results obtained from the Matlab simulation were compared with the results derived from commercial software (ANSYS) for components of the same dimensions and boundary conditions under the application of the same loads[38]. In general, there was a small divergence ($\pm\,10\,\%$) in the values obtained (Tables 13 & 14) but the diagrams showed that the behavior of the components in the two simulations (ANSYS & Matlab) was identical (See Appendix A.1.1 & A.1.2).

---

[35] The main literature sources for the development of the Finite Element code in this project are (Papadrakakis, 2001) and (Andriotis, 2021).
[36] Every element consists of 4 nodes x 2 degrees of freedom = 8 degrees of freedom in total.
[37] Given that the peak values regarding the principal stresses are expected to be found in the corners of the square, the algorithm evaluates the principal stresses in each of the element nodes and keeps the maximum & minimum values found as the tensile and compressive stress of the element respectively.
[38] Special attention was given in order to simulate the exact same conditions in ANSYS. In this regard, a 2D analysis was selected with linear quadrilateral elements of the same size. The loads were applied per node in the same positions.

	Displacement (m)	Maximum principal stress (kN/m2)	Minimum principal stress (kN/m2)
ANSYS[39]	-0,0000416	3,38e+03	-1,41e+03
Matlab code	-0,0000441	3,09e+03	-1,88e+03

Table 13 Displacement & Principal stresses results for the MBB beam.

	Displacement (m)	Maximum principal stress (kN/m2)	Minimum principal stress (kN/m2)
ANSYS	-0,0000987	2,18e+03	-2,16e+03
Matlab code	-0,0000977	2,25e+03	-2,22e+03

Table 14 Displacement & Principal stresses results for the Case study slab.

7.4 Optimization

The optimization was held in Matlab v.2021b using the Optimization Toolbox, the Symbolic Math Toolbox and the Statistics and Machine Learning Toolbox. Given that the constraints applied were nonlinear, *fmincon* programming solver was applied to the optimization. From the algorithms offered through *fmincon*, 'interior-point' was selected, since it has been proven to be robust in solving large scale problems, it always satisfies the bound values posed and it can recover from Nan or Inf results. In contrast, 'sqp', 'sqp-legacy' and 'active-set' are not large scale algorithms and therefore were not favored for this optimization, since a large number of constraints are expected to be posed. Lastly, 'trust-region-reflective' algorithm was not selected since it requires providing the gradients which was beyond the scope of this thesis[40]. Additionally, it is worth mentioning that the feasibility mode was enabled in order to ensure that the constraints are going to be respected at all times. A detailed table of the optimization options and tolerances can be found in Appendix A.2.1[41].

During the trajectory of this thesis a lot of troubleshooting had to be done in order to result to a final code that produces reasonable results which are comparable to the ones already presented in the literature studies. As it was already mentioned, the code exploration began with the option to apply volume as the optimization objective along with the respective constraints. However, since only a few literature studies have been investigating this option till now and there were not sufficient results for comparison, compliance objective it was decided to start testing the application of constraints on this framework and later passing it on the volume objective operation.

---

[39] The results originally obtained in ANSYS – and therefore illustrated in the diagrams – are measured in Pa = 10^3 kN/m^2.
[40] The information is extracted from Matlab documentation.
[41] The optimization tolerances were set in stricter limits and the number of iterations and function evaluations were defined much higher than the default values in order to allow the algorithm to converge sufficiently. However, it should be mentioned that in some of the results demonstrated in this project, the operation was terminated prematurely by the user if it was considered needed taking into consideration the convergence plot.

Afterwards, a comparative review of the results obtained from both cases is going to be presented. The optimization scenarios follow the problem formulation as described in Chapter 6 and more specifically in Table 11. In the first phase, each of the constraints is tested individually with each of the objectives in the benchmark problem in order to ensure that everything is working properly. In the second phase, a combination of constraints is applied with each objective in the case study example.

7.4.1 Objectives

Unlike the design variables and the nonlinear constraints which may refer to multiple values, the objective of the optimization has to be always the minimization of one single factor. In this regard, the volume objective is defined as the sum of all the design variables in the structure, whereas, in the case of the compliance objective, the value of the compliance for the whole structure is used[42].

7.4.2 Constraints

As already mentioned, similarly to the objectives, the constraints have to also be structured as a function in order to be connected in the optimization solver. The constraints can be one or multiple as long as they are organized as one array. However, attention must be paid on the number of constraints posed since it can significantly affect the convergence of the algorithm and the computational time needed.

In the case of fmincon, the nonlinear constraint function can contain both equality (c_{eq}) and inequality (c) constraints at the same time, such as that:
$$c \leq 0$$
$$c_{eq} = 0$$

However, in this project only inequality constraints are going to be considered. The comparative review of the results for each constraint in the case of the benchmark problem is going to follow. It needs to be underlined that equilibrium and filtering (minimum element dimension) constraints are an indispensable part of all the optimization iterations and therefore they are not going to be discussed separately. Details regarding the convergence and the computational time needed for each result can be found in Appendix A.2.1.

7.4.2.1 Volume

The first constraint which is going to be discussed is the volume constraint. It is evident that this constraint is going to be considered only in combination with minimum compliance as the optimization objective. The volume fraction limit used was 30% of the initial material. The results were compared with the ones obtained from (Liu & Tovar, 2014) for the same problem formulation in the case of a 3D mesh.

The resulting outcome from the custom Matlab code (Figure 57) is considered successful since only minor deviation from the result of (Liu & Tovar, 2014) is observed[43].However, it showcase that although the filtering scheme applied serves perfectly to avoid the checkerboard pattern in the structure, it does not ensure that the

---

[42] It is important to mention that even in the case study example, where half of the densities are considered as design variables, the objective values take into consideration the structure as a whole and not only the half of it.
[43] The deviations in the outcome may also be connected with the inherent differences between a 2-dimensional and a 3-dimensional code.

minimum element dimension is going to be respected at all cases. Therefore, elements with thinner cross section than the minimum dimension are observed[44].
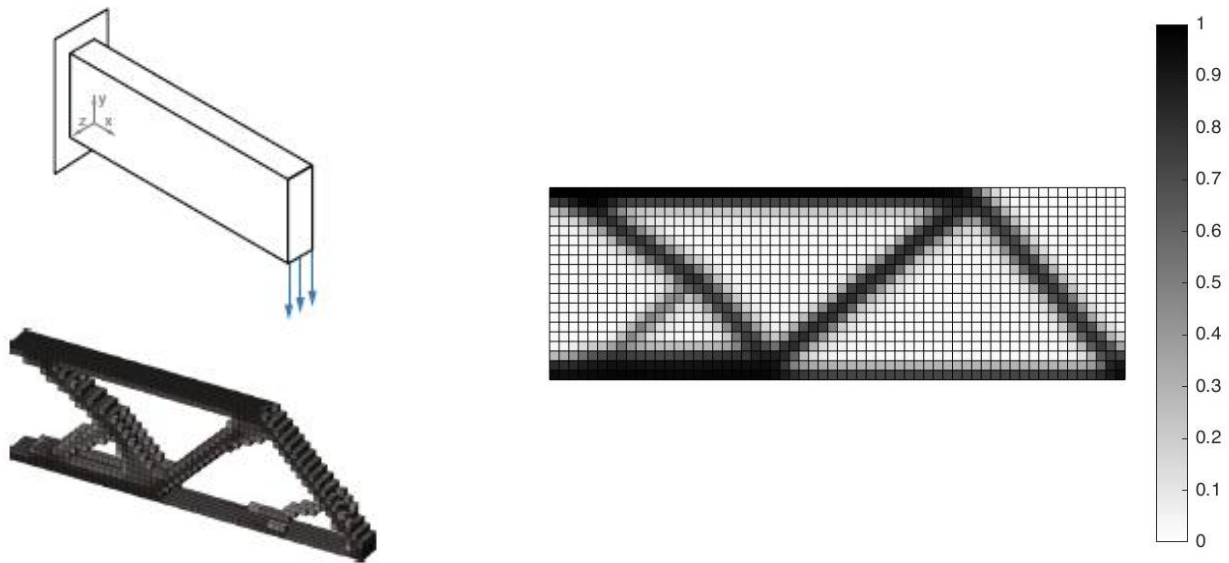
Figure 57 Results for Compliance Objective / Volume Constraint from (left) (Liu & Tovar, 2014) (right) own Matlab code.

7.4.2.2 Compliance

Compliance constraint is only tested in combination with the volume objective. As already discussed in Chapter 6.3.2.3, it is defined in its mathematic formulation as:

$$\frac{c(x)}{c_L} \leq 1, \qquad c_L = a_c c_0$$

where c_0 is the compliance of the virgin material and is calculated in a separate function prior to the optimization using the FEM structural model which has already been created and a_c is the allowable compliance percentage. Similarly to the volume fraction percentage described in Chapter 7.2.5.1, a_c depends a lot in the experience of the end user. As it can be seen in Figure 58, different values regarding a_c can result in significantly different results. This is because the algorithm tends to quickly concentrate material over an optimal layout during the first iterations in order to reach a feasible point[45] and then only accepts modifications of the design variables that result in an outcome which lies inside the feasibility area. As a result, when stricter a_c value is posed, there is not a lot of margin for alterations and the algorithm results in local minima and overall heavier structures.

---

[44] The minimum element dimension set in the algorithm was 0.06m, whereas in the resulting outcome there were elements with thinner dimension (0.04m).
[45] Feasible is considered the point that refers to design variables which fulfill sufficiently the constraints posed in the algorithm.
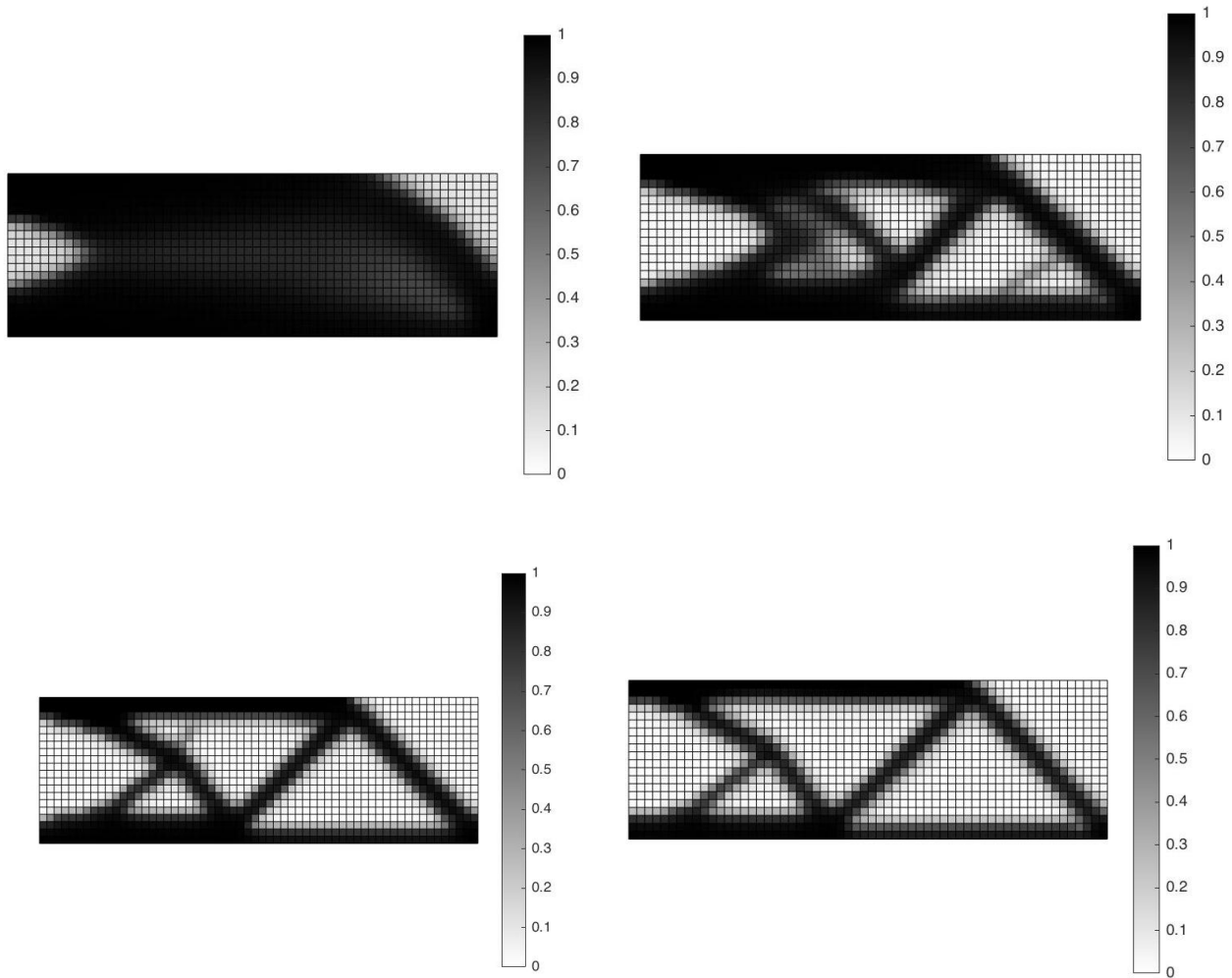
Figure 58 Results for Volume Objective / Compliance Constraint for (top left) $\alpha_c = 1,1$, (top right) $\alpha_c = 1,5$,, (bottom left) $\alpha_c = 2$, (bottom right) $\alpha_c = 2,5$.

7.4.2.3 Deflection

To begin with, it is important to highlight that the deflection constraint is not calculated per element, but it refers to the vertical displacements of the nodes of the structure. Additionally, given that, independently of the final design, the displacement is always anticipated to be higher in a specific critical point in the structure, this constraint is not applied locally in every node but only to the critical one reducing, therefore, the overall computational time needed. The critiacal node can be found intuitively and/or by applying the structural analysis using the FEM model (Appendix A.1.1). In the case of the benchmark problem, the critical node is the bottom left node of the lower element in the free side of the cantilever (Figure 59).
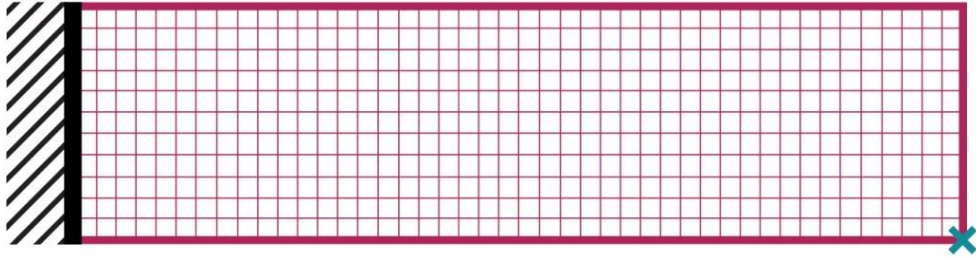
Figure 59 Critical node checked for displacement in the case of the benchmark problem.

The results obtained are different than before (Figure 60). When combined with the volume objective, the resulting shape is a very lightweight structure with a clean boundary that follows the overall outline of the results shown in the previous examples. In the case of combining it with the compliance constraint, it is seen that the algorithm tends to add material to the whole structure[46]. The only part where no extra material is added is the top right corner, which is considered justifiable since it probably did not led to any further improvement in the minimization of the compliance of the structure and the density variables were maintained with the initial point assigned to them.
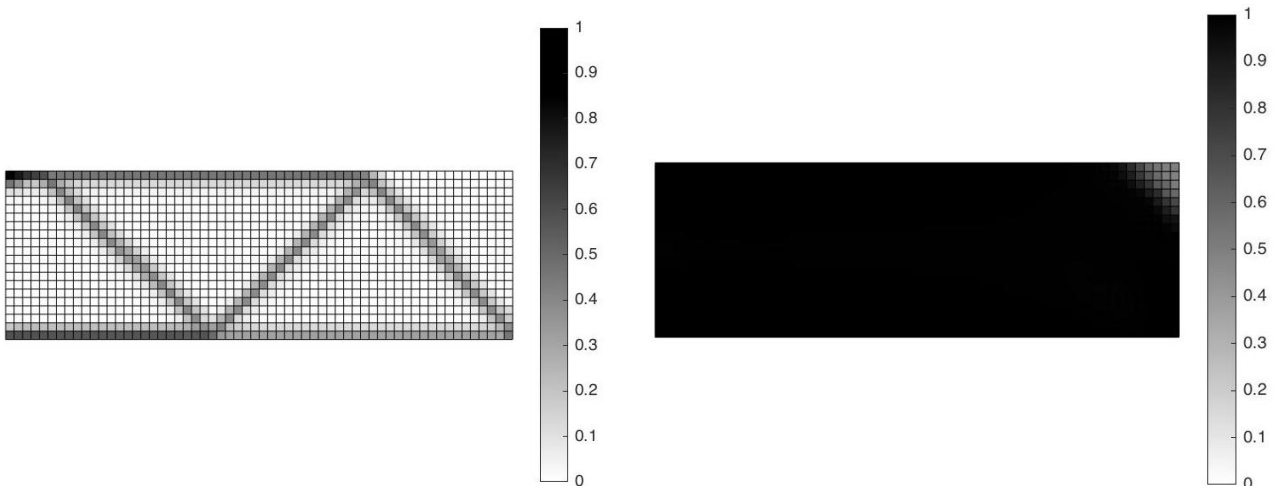
Figure 60 Results for Deflection Constraint with (left) Volume Objective (right) Compliance Objective.

7.4.2.4 Principal stresses

The principal stresses are evaluated individually in the optimization. Particularly, each element is evaluated locally for its performance both in tension and compression in reference to the admissible limits every time. The results shown in Figure 61 showcase that the stress limits, when considered without additional constraints related to stiffness, cannot ensure a reasonable result. In the case of volume minimization, the algorithm quickly removes all the material, since the no-material state complies with the stress constraints, whereas in the case of the compliance objective the algorithm leans towards a full structure similar to that of the deflection constraint. In this regard, it is evident that stress constraints cannot serve to guide the optimization process, but they only serve to ensure the feasibility of the structure that is evaluated in every iteration.

---

[46] The initial point of the optimization is $x_i = 0,3$ for the design variables in all the elements of the structure.
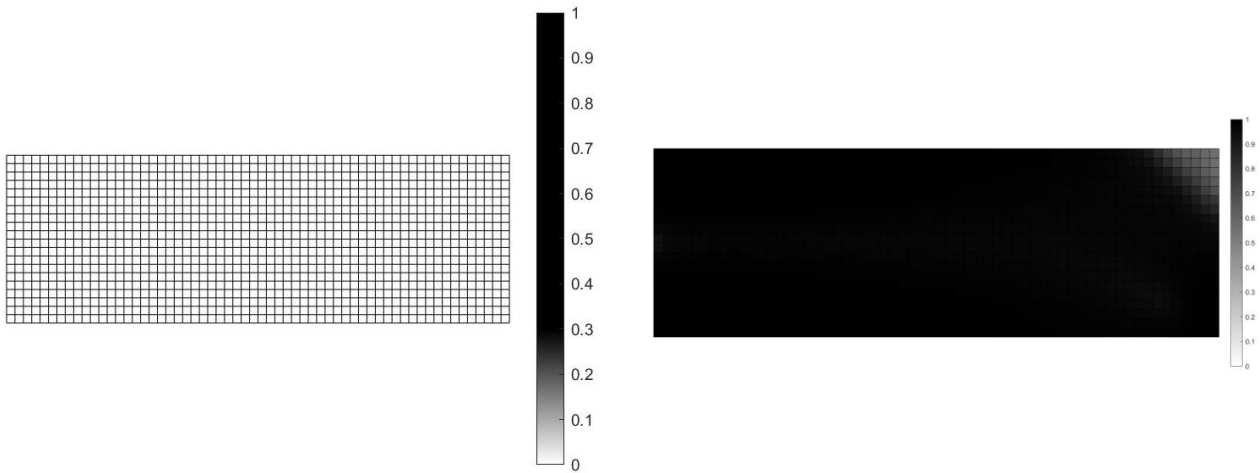
Figure 61 Results for Principal Stress Constraint with (left) Volume Objective (right) Compliance Objective.

7.4.2.5 Annealing & Manufacturing criteria (d_{max})

The annealing constraint (maximum element constraint) is formulated in the algorithm following a similar approach to the filtering constraint. Firstly, the maximum dimension (d_{max}) is defined taking into consideration the maximum annealing time (ann_thickness function) and the allowable ratio of maximum to minimum cross section. Afterwards, the indexes of the elements that lie inside the circular regions with radius $r_{max} = d_{max}/2$ are mapped before the optimization and recalled at every iteration. They are used to evaluate the full volume in each circle, which shall not surpass a specific percentage. This constraint is evaluated locally in elements that have a specific distance between them in order to reduce the overall computational time needed for it.

Similarly to the principal stresses, in the case of the volume objective the algorithm does not keep any material but quickly removes all the material from the structure since it complies with the constraint given (Figure 62). When compliance objective is set, the structure is heavier but the algorithm tries to compartmentalize it in order to create smaller elements that comply with the maximum element dimension. However, no clear boundary could be extracted after this operation.
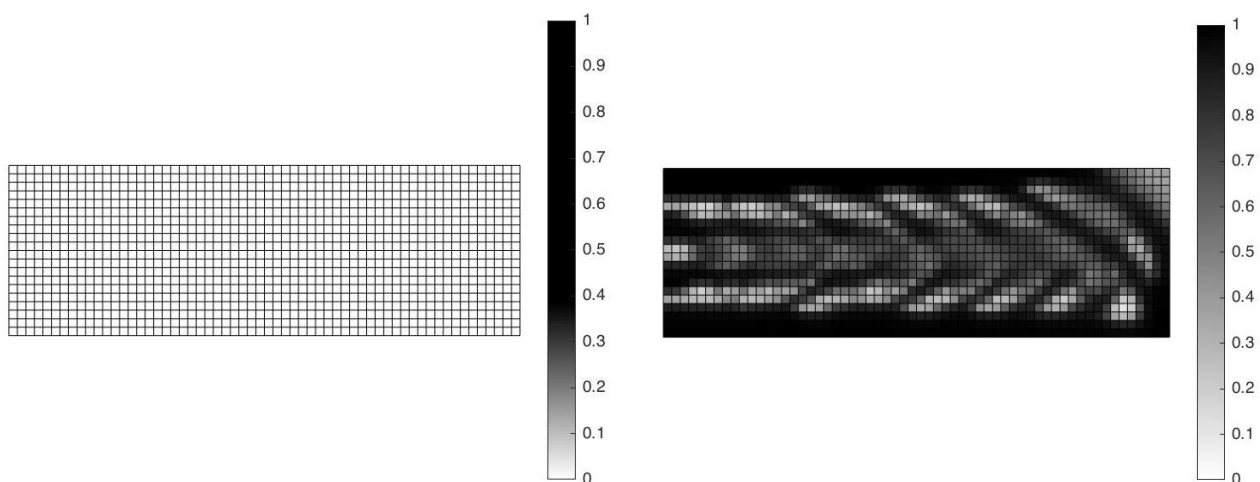
Figure 62 Results for Annealing & Manufacturing Constraint with (left) Volume Objective (right) Compliance Objective.

7.2.5.6 Drucker - Prager Material failure criterion

The last constraint tested is the one related to the Drucker – Prager material failure criterion. Similarly to the principal stresses, it is evaluated locally in every element in order to be able to efficiently identify local peak stresses in the structure. However, the main difference is that this time both tension and compression are simultaneously checked in one combined factor that takes into consideration the unequal properties of the material. The results obtained from the algorithm show that the Drucker – Prager criterion has a similar behavior with the principal stresses constraint (Figure 63).
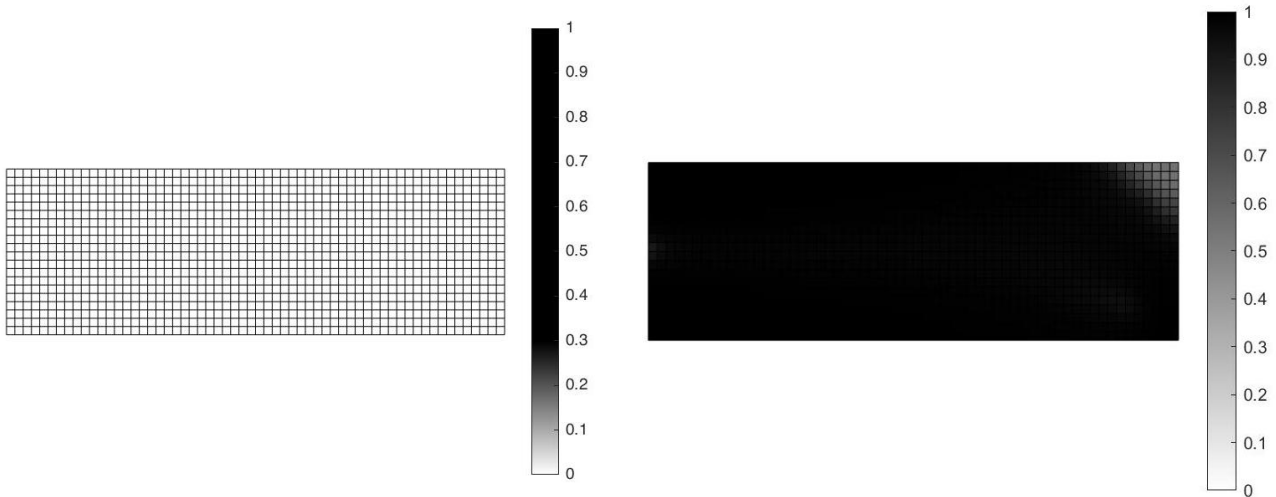
Figure 63 Results for Drucker & Prager Constraint with (left) Volume Objective (right) Compliance Objective.

7.4.3 Discussion

The results from the benchmark problem showcase that the main setup of the algorithm is efficient and works as anticipated. However, it further highlights the fact that, in order to be able to produce a reasonable outcome that can result in a final structure, more than one constraint should be taken into consideration in every operation. This derives from the fact that no constraint can ensure a sufficient performance of the structure in all the aspects. In this regard, the compliance constraint cannot evaluate simultaneously the feasibility of the structure regarding the high local peak stresses, whereas the stress constraints (both principal stresses and Drucker – prager criterion) cannot ensure a stiff structure. In the latter case, it is evident that stress constraints can only efficiently serve as a checking method when the optimization is guided by another constraint, such as compliance.

Overall, it is shown that experiments with volume-based optimization result in clearer boundaries, since the algorithm by definition tends to push the density variables to the extremes and, particularly in the case of the void material, it tends to approximate the values towards the lower boundary of the optimization. This can be very beneficial for the optimization, since it further reduces the appearance of grey – intermediate - areas in the design.

8. Case Study Design

In this chapter, the strategy regarding the algorithm implementation is applied on the case study example. A combination of constraints is intended along with each of the two objectives. The two resulting shapes are critically compared between them and the final shape of the slab is extracted.

8.1 Overview

The algorithmic implementation in the case study example follows the same strategy as in the benchmark problem. However, there are some differences that serve to further reduce the computational time and power needed. As already mentioned in Chapter 7.2.2, this time only half of the density variables are considered as input for the optimization problem. The rest of the section derives as a symmetric reflection of the densities along the vertical axis.

Additionally, the symmetry in the design is also taken into consideration when setting the points for evaluation of the constraints. Since a similar behavior is expected in the two parts, only half of the elements are evaluated for their performance in the case of the local constraints, such as annealing, principal stresses and Drucker – Prager constraint. Regarding the deformation constraint, this is calculated, similarly to the benchmark problem, only in the critical point of the structure, which in this case refers to the upper middle node (Figure 64).

The first part of the exploration refers to applying the two different problem formulations in the setup which has already been described (fixed edge supports & borosilicate glass) so that the two results have exactly the same boundary conditions and, therefore, can be directly comparable. In the second part of the exploration, the best performing formulation will be used in order to see how the final outcome can be affected by changes in the glass category, the boundary conditions and the dimensions of the design domain.
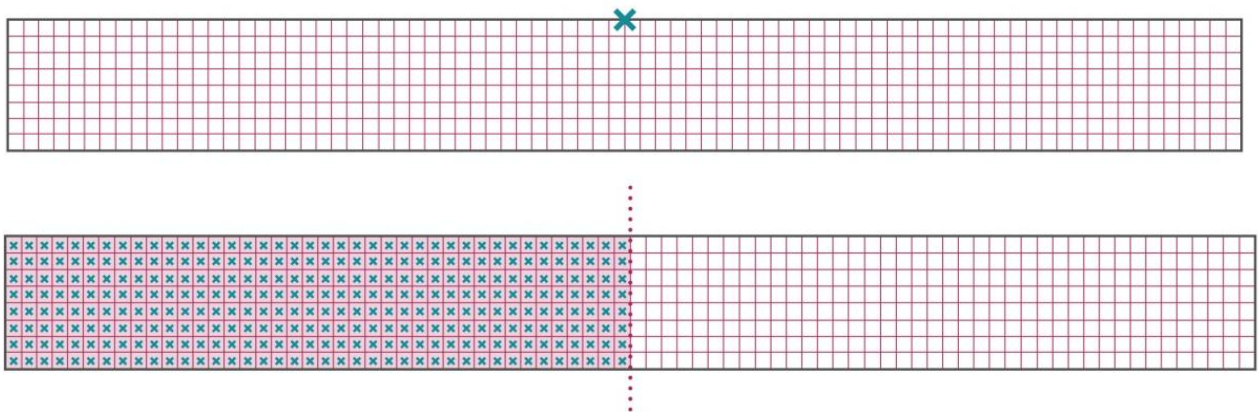
Figure 64 Elements for evaluation of (top) Deflection and (bottom) Annealing / Principal Stresses / Drucker – Prager criterion in the Case Study Example.

8.2 Results

8.2.1 Problem formulations comparison

8.2.1.1 Compliance Objective

The first experiment refers to the compliance-based optimization. Besides the equilibrium and filtering constraint, which are always integrated in the algorithm, the whole range of constraints formulated in Chapter 6, such as the volume, displacement and annealing constraint, were also evaluated during the operation. Regarding the stresses, in this operation the principal stresses constraint was applied instead of the Drucker – Prager criterion.

The final result (Figure 65) is successful in the sense that it demonstrates a reasonable structure with a clear boundary that complies with all the constraints set by the algorithm. However, there are still grey areas in the design, particularly on the sides towards the fixed edges which will be difficult to be interpreted in one sharp outline and manipulations from the part of the designer will be needed. After the optimization is finished, the final result is undergone another structural analysis in order to validate that the stresses in the cross section comply with the allowable limits (Appendix A.2.2.1). It is shown that both values are inside the allowable limits. Particularly in the case of compression, the stresses indicated in the structure are considerably lower than the respective allowable limit (Table 15).
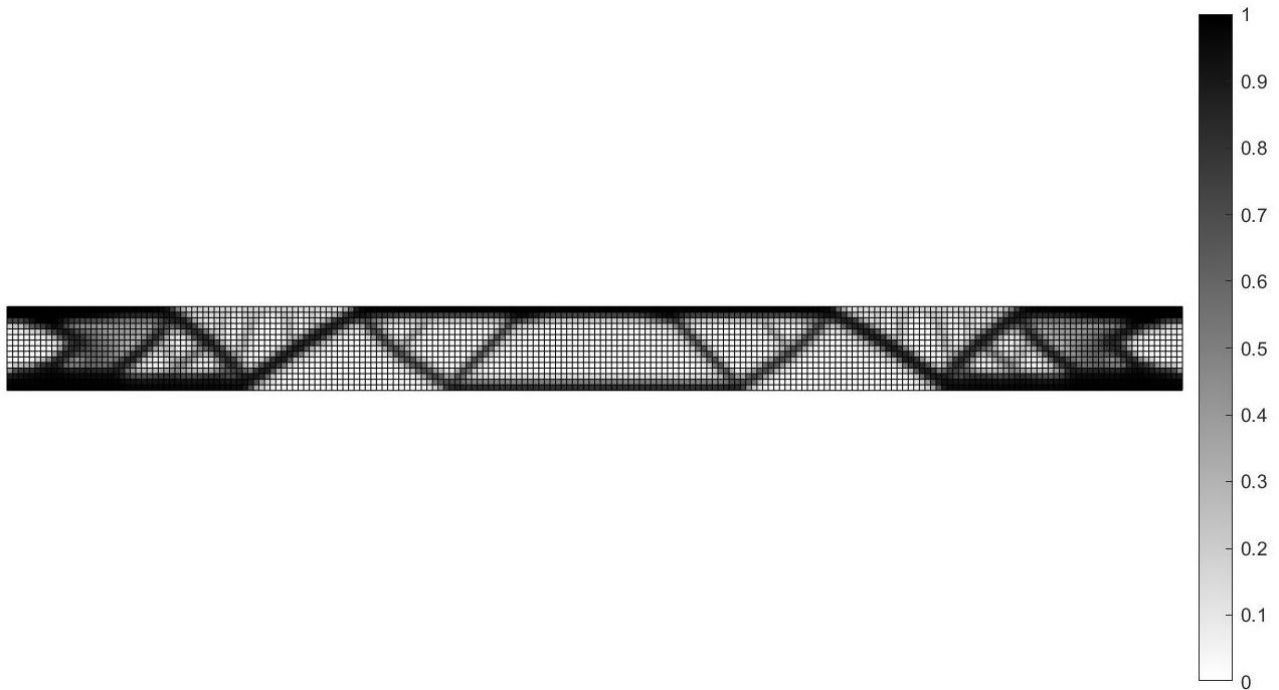
Figure 65 Resulting shape for Compliance Objective & Volume, Deflection, Annealing & Principal Stresses Constraint.

Properties	Units	Values
Deformation (at critical point)	mm	0,26
Maximum principal stress	kN/m2	4,50e+03
Minimum principal stress	kN/m2	4,49e+03

Table 15 Resulting values after the structural analysis for the Compliance Objective result.

8.2.1.2 Volume Objective

The second experiment refers to the volume –based optimization. This time, apart from the equilibrium and filtering constraint, compliance[47], deflection and annealing constraint are integrated in the algorithm. Regarding the stresses, this time the Drucker – Prager criterion was tested in order to compare the result regarding the efficiency and the computational time needed.

The final result is also considered successful since it complies with all the constraints posed in the algorithm (feasibility: 0). The resulting shape has a similar structure to the one obtained with the compliance-based formulation, but this time the boundary is a lot clearer and there are no grey zones in the structure. This is strongly related to the objective set this time, since the algorithm tends to minimize the densities as much as possible in the areas where they do not add to the stiffness of the structure. Additionally, it needs to be highlighted that, although the overall computational time devoted to the operation was hardly the same as the first experiment[48], the number of function evaluations operated this time is 1.5 times larger than the number of function evaluations in the first case. It is considered that this fact is related to the implementation of the Drucker - Prager criterion, which reduces at half the number of constraints posed since only one factor is evaluated at each element instead of the two factors evaluated in the case of the individual principal stresses.

The final result was evaluated structurally in order to check the performance of the principal stresses at this operation (Appendix A.2.3). In general, the values are higher than the ones observed in the first experiment, but they still lie inside the allowable limits.
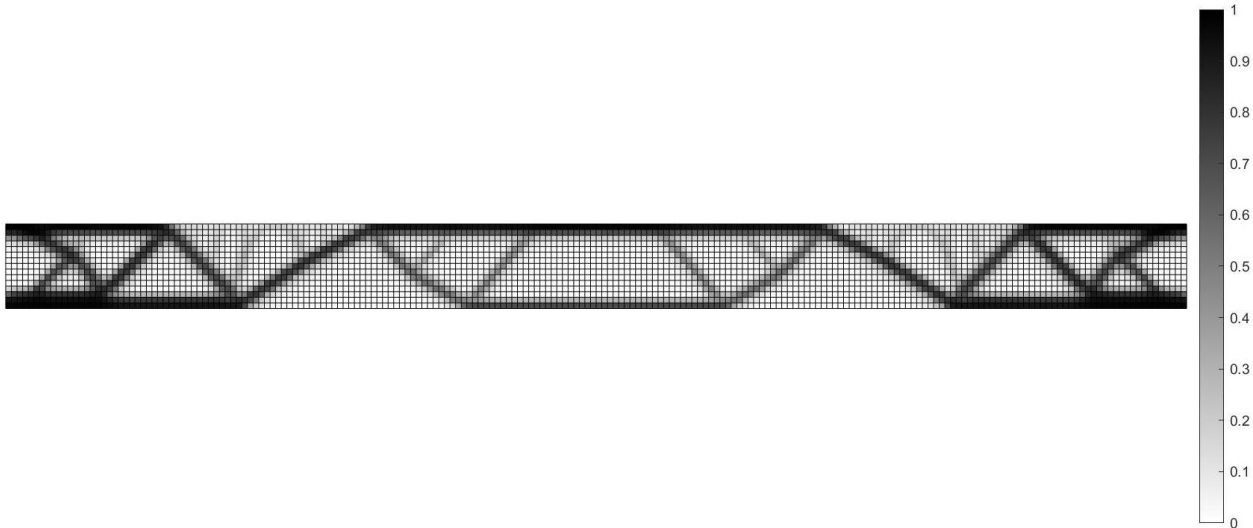
Figure 66 Resulting shape for Volume Objective & Compliance, Deflection, Annealing & Drucker - Prager Constraint.

---

[47] After experimenting with different values of the α_c factor for the compliance constraint, it was decided that it will be set as $\alpha_c = 4$.

[48] The operations were not ended due to convergence, but they were ended from the user when it was considered that not a lot of improvement is happening in the structure. This is related, firstly, to the strict tolerances that were imposed on the algorithm which were difficult to reach and, secondly, to the considerable time limitation for the handing of this report.

Properties	Units	Values
Deformation (at critical point)	mm	0,42
Maximum principal stress (tension)	kN/m2	6,19e+03
Minimum principal stress (compression)	kN/m2	-6.09e+03

Table 16 Resulting values after the structural analysis for the Volume Objective result.

8.2.1.3 Comparison of formulations

The results of both experiments have the same overall structure, which shows that the final result is independent of the objectives and constraints imposed in the algorithm. Particularly, the structure which is created can be analyzed into 3 main parts (Figure 67); 2 cantilevers with fixed supports on the sides and one beam in the middle part which is supported mainly through the points of connection with the cantilevers. In this case, the structure performs as if the middle part imposes two point loads on the bottom part of the free sides of the cantilevers[49].

Figure 67 Diagrammatic Analysis of final shape.

Although, the overall outline of the result in both experiments has a lot of similarities, it needs to be highlighted that the boundary in the case of the volume-based operation is much easier to define since there are not grey – intermediate – areas in the structure. This can be related both to the nature of the volume objective, which tends to make as clean as possible the areas that do not contribute to the structure, or to the application of the Drucker – Prager criterion which allows for more iterations and function evaluations at the same time. Overall, computational time was a significant limiting factor that may have influenced the convergence, since both of the operations had to be ended by the user before they reach the respective tolerances. However, it needs to be underlined that the algorithm had already reached an optimal point and no significant modifications were happening when stopped.

To sum up, volume-based formulation, firstly, leads to robust solutions with clearer boundaries and more lightweight shapes while, secondly, is related more to the ultimate aim of the optimization which is minimization of the mass. For these reasons, it is finally selected as the tool to be used for further experimentation.

---

[49] Especially in the volume-based result, the two side cantilevers have the exact same shape as the benchmark problem examined in Chapter 7 which has the same boundary conditions.

8.2.2 Design exploration

After calibrating the tools and defining the final problem formulation, the code is used as an exploration tool in order to showcase the design potential of structural optimization and, particularly, how different design guidelines can affect the final outcome. In this regard different setups are tested. They refer to different glass types (i.e. borosilicate glass & soda lime glass), different fabrication methods (i.e. casting & stacking layers of float glass sheets together), different type of edge supports (i.e. fixed edge & fixed point supports) and different design domain (i.e. shorter height of cross section)

8.2.2.1 Cast glass – Soda lime

The first setup tested has the same boundary conditions (fixed edge supports) and refers to the same fabrication method (casting) but differentiates from the initial run in terms of the glass type which is used. Particularly, the data referring to soda-lime glass are used this time. Although the structural and mechanical properties are similar to borosilicate glass and therefore the same values are used in the algorithm[50], the two glass types differ significantly regarding their thermal properties and specifically their thermal expansion coefficients (Table 17). This affects the total cooling time needed since the annealing process for the same cross section is lengthier in this case. Therefore, a smaller value regarding the maximum cross section size is expected to be posed by the algorithm.

	Symbol	Units	Input values (Soda lime glass)	Input values (Borosilicate glass)
Young's modulus	E	GPa	70	70
Poisson's ratio	v	-	0.2	0.2
Density	ρ	Kg/m^3	2500	2500
Initial cooling range (annealing process)	ΔT	^{o}C	553-485 (=68)	530-460 (=70)
Thermal expansion coefficient	α$_T$	1/K	8.5×10^{-6}	3.25×10^{-6}
Thermal conductivity	k	W/(m*K)	1.06	1.15
Specific heat capacity	c$_p$	J/(kg*K)	870	800

Table 17 Input values for the algorithm (Soda lime & Borosilicate glass).

---

[50] In reality the material properties, such as the Young's modulus and the Poisson ratio are also slightly different in the case of soda lime glass.

Despite of the different glass types, the final outcome of the optimization (Figure 68) is identical to the one obtained in the first case (Figure 66). The overall outcome is slightly heavier than the borosilicate one (Appendix A.2.4.1) while the compressive stress indicated in the structure is slightly smaller in this iteration.
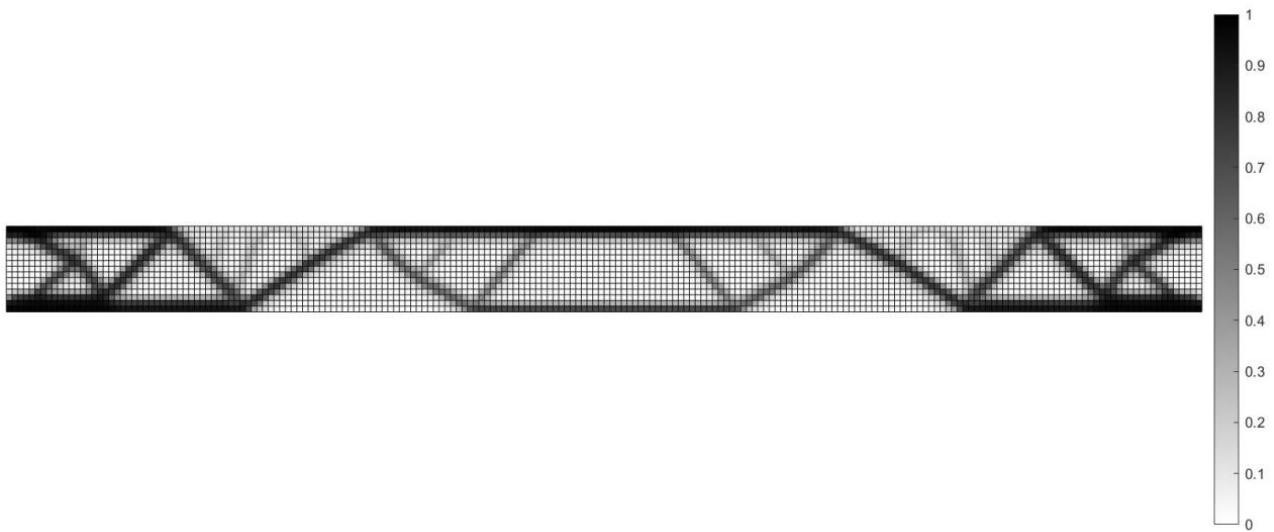
Figure 68 Resulting shape for Volume Objective & Compliance, Deflection, Annealing & Drucker - Prager Constraint (Soda lime glass).

Properties	Units	Values
Deformation (at critical point)	mm	0,43
Maximum principal stress (tension)	kN/m2	6,19e+03
Minimum principal stress (compression)	kN/m2	-5.94e+03

Table 18 Resulting values after the structural analysis for the Cast glass – Soda lime case outcome.

8.2.2.2 Float glass – Borosilicate

The difference in this iteration lies on the use of a different fabrication method for the creation of the total shape. Instead of casting, consecutive float glass sheets from borosilicate glass are assumed to form the monolithic component.
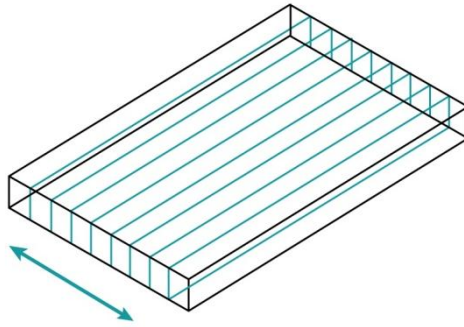
Figure 69 Direction of stacking the consecutive float glass sheets.

This affects firstly the annealing constraint, since it no longer has to be posed in the algorithm[51]. Additionally, the tensile strength in this case is higher since there is no need to compromise its value because of the risk of casting defects that could accelerate the activation of the fracture mechanisms. Following the same process as described in Chapter 3.2, the new design tensile strength is:

$$R_{d\,float} = \frac{k_{mod} * k_c * f_t}{\gamma_m} = \frac{0,4 \times 1 \times 45}{1,8} = 10\ MPa$$

Fabrication method	Units	Tensile strength	Design tensile strength
Casting	MPa	29	6,4
Consecutive float glass sheets	MPa	45	10

Table 18 Design tensile limits for casting & consecutive float glass sheets.

The result is more lightweight than in the previous cases, which is probably related to the possibility of having higher tensile stresses. Therefore, some elements of smaller dimensions are likely to be created. However, in the end the overall structural performance of the two shapes remains hardly the same and the general layout of the cross section is identical.

---

[51] Through water-jet cutting, float glass can be cut in almost any dimension, so there is no need to apply a maximum cross size dimension constraint.
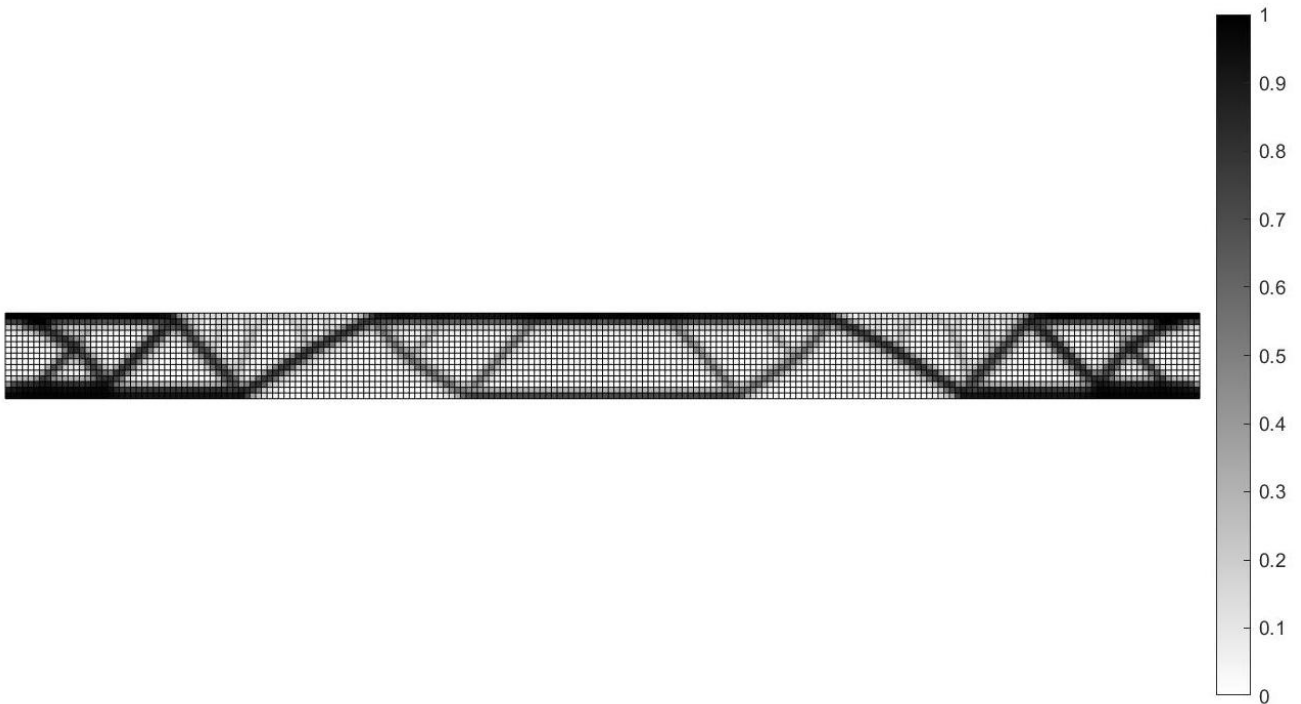
Figure 70 Resulting shape for Volume Objective & Compliance, Deflection & Principal Stresses Constraint (Float glass).

Properties	Units	Values
Deformation (at critical point)	mm	0,43
Maximum principal stress (tension)	kN/m2	6,19e+03
Minimum principal stress (compression)	kN/m2	-5.94+03

Table 19 Resulting values after the structural analysis for the Float glass - Borosilicate result.

8.2.2.3 Fixed point supports – Borosilicate

In this optimization run, the boundary conditions which are applied in the cross section are changed. Particularly, the supports are no longer fixed along the whole edges but they are only fixed on the bottom edge points, as if the component was based onto something. Similarly to the initial case, the glass type assumed in this optimization run is borosilicate glass.
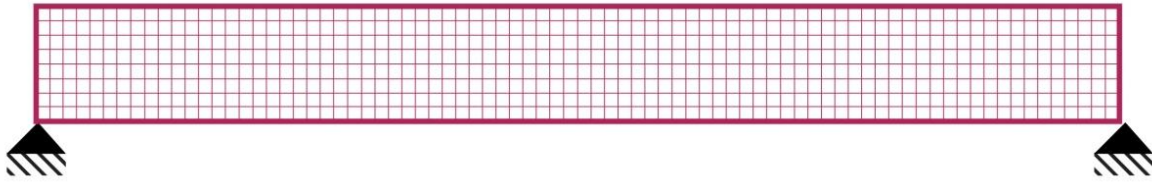
Figure 71 Placement of fixed point (node) supports.
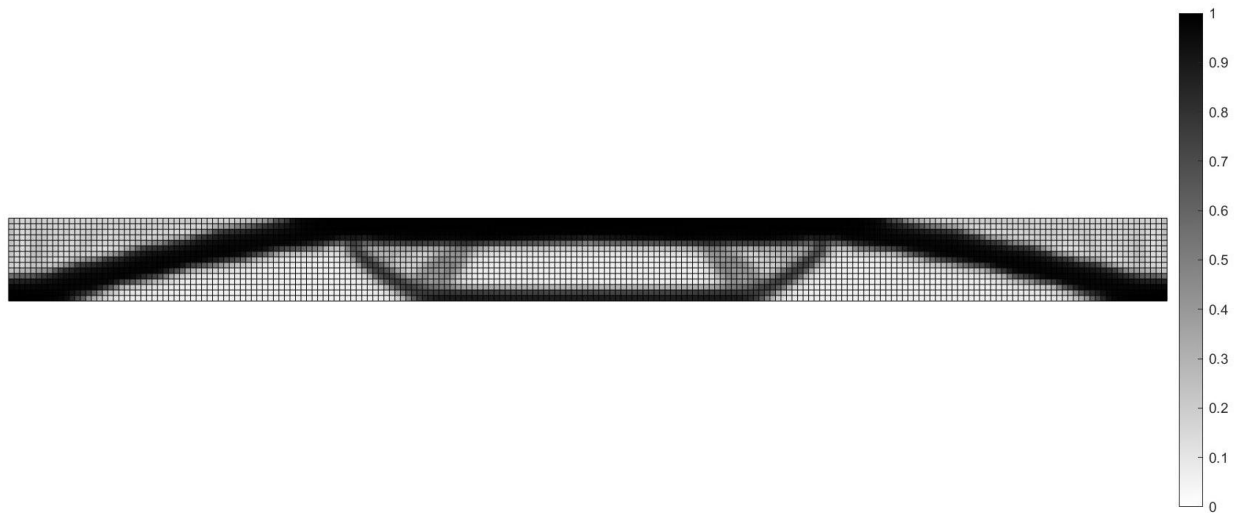
Figure 72 Resulting shape for Volume Objective & Compliance, Deflection, Annealing & Principal Stresses Constraint (Cast borosilicate glass & point supports).

It is evident that this iteration results in a considerably different outcome. This time the component resembles a whole arch which is based on the two edge points, while a netting structure in the middle adds to the overall stiffness of the structure. Moreover, it is important to highlight that the main element in this outcome has considerably larger cross section than the previous ones, which were composed overall from thin elements, and the component in general is quite heavier. Regarding the structural performance, it is important that, this time, the component behaves quite differently in terms of principal stresses, meaning that the values indicated in the final shape regarding tension and compression are quite different (Table 20). Particularly, it needs to be mentioned that the tensile stress now is well inside the allowable limit posed in the algorithm and the deformation is also smaller than before.

Properties	Units	Values
Deformation (at critical point)	mm	0,34
Maximum principal stress (tension)	kN/m2	2e+03
Minimum principal stress (compression)	kN/m2	-6,8e+03

Table 20 Resulting values after the structural analysis for the Point Supports & Borosilicate case.

8.2.2.4 Fixed point supports – Soda lime

Given that the main characteristic of the previous result was the large element dimension, it was considered as an interesting experiment to check what would be the result in the case that soda lime glass was applied. Since it has a larger thermal expansion coefficient and, therefore, cools slower, it was anticipated that the annealing constraint would not allow for such a large element cross section this time.
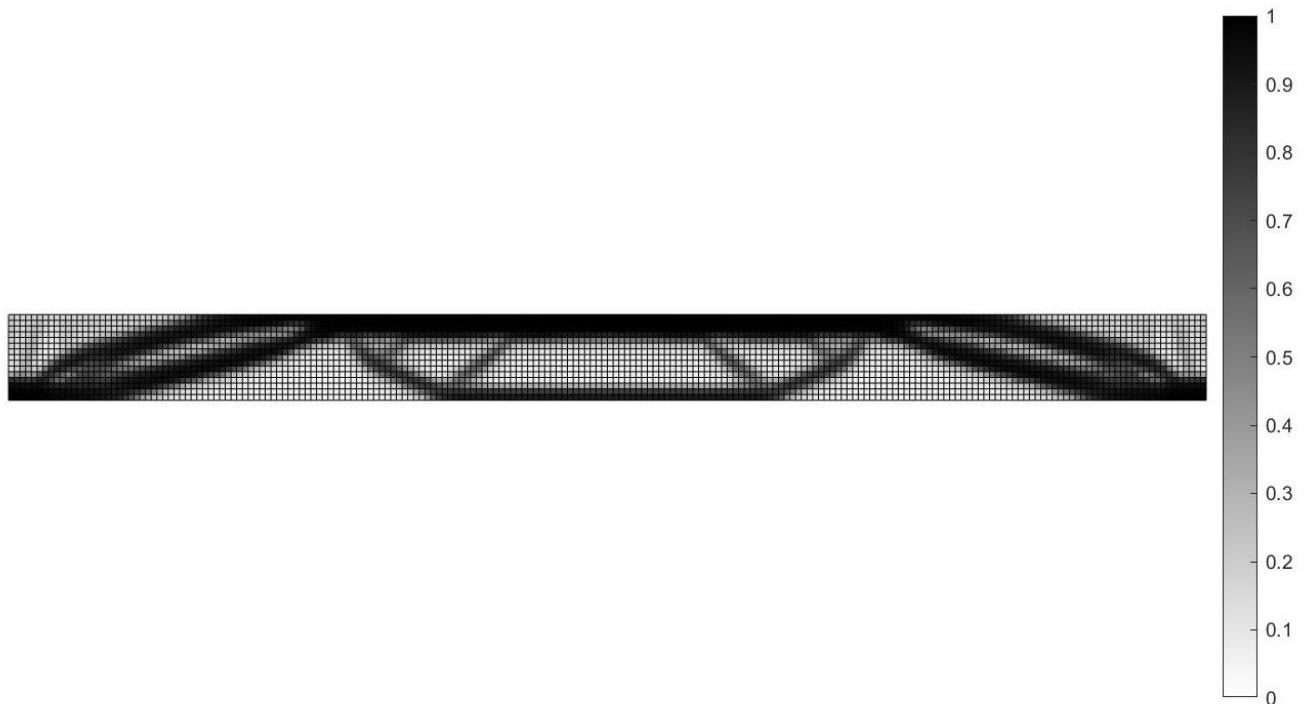
Figure 73 Resulting shape for Volume Objective & Compliance, Deflection, Annealing & Principal Stresses Constraint
(Cast soda lime glass & point supports).

The result validated the initial estimation and the larger cross sections were analyzed in smaller parts leading overall to a comparatively heavier design than the borosilicate one. Structurally, the performance is similar to before but the stress values are slightly increased.

Properties	Units	Values
Deformation (at critical point)	mm	0,34
Maximum principal stress (tension)	kN/m2	2,42e+03
Minimum principal stress (compression)	kN/m2	-7,58e+03

Table 20 Resulting values after the structural analysis for the Point Supports & Soda lime case.

8.2.2.4 Different design domain (cross section height: 20 cm)

This optimization run aims to investigate if applying a different design domain can also result in a sufficient outcome and what would be the benefit in terms of material usage in this case. Particularly, given that the overall dimensions of the case study – length & width – cannot be changed, a shorter height (20cm) was attempted. The glass type which is applied this time is borosilicate glass.
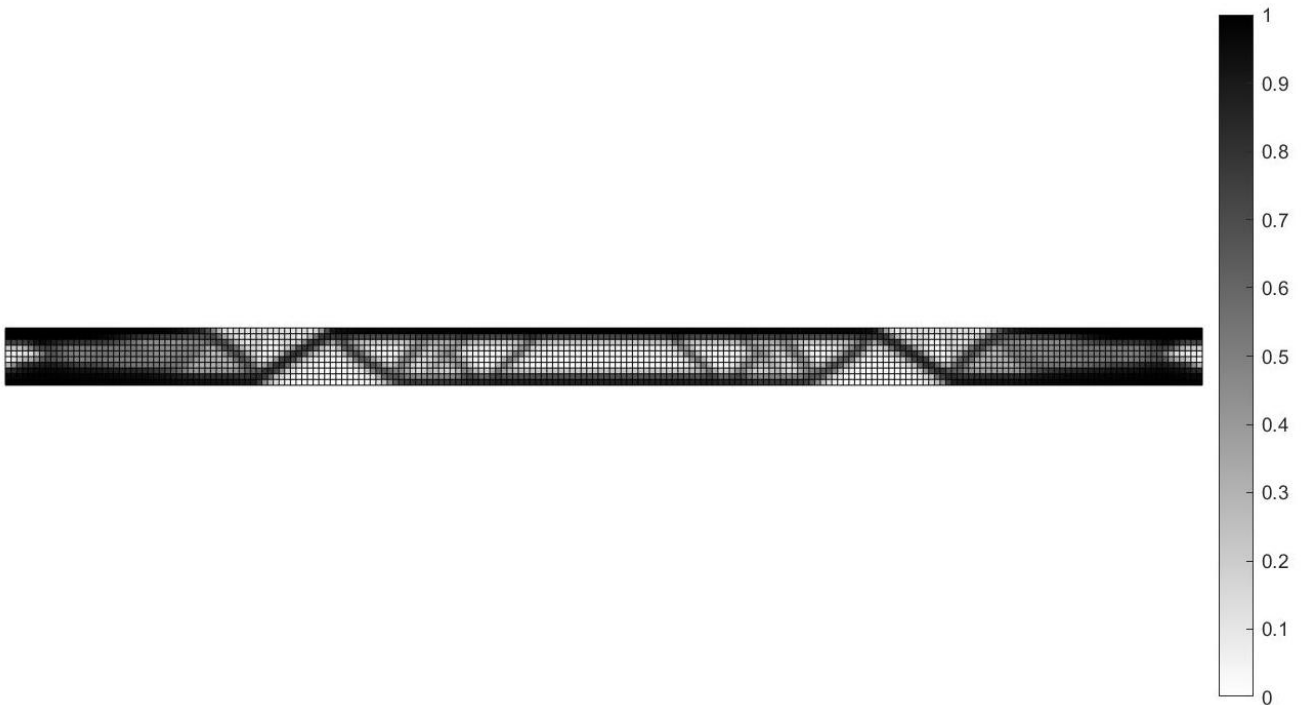
Figure 74 Resulting shape for Volume Objective & Compliance, Deflection, Annealing & Principal Stresses Constraint (Cast borosilicate glass & cross section of 20 cm height).

Overall, the shape is composed by 2 cantilevers and a netting in the middle following the same logic as described in Chapter 8.2.1.3. Although the shape is more lightweight in total, the final outcome consists of many intermediate 'grey' areas which will not be easy to be interpreted physically since a sharp boundary cannot be extracted. The structural performance indicators lie inside the respective limits but it needs to be highlighted that the deformation this time is slightly larger showing that the shape was not as stiff as before.

Properties	Units	Values
Deformation (at critical point)	mm	0,5
Maximum principal stress (tension)	kN/m2	5,56e+03
Minimum principal stress (compression)	kN/m2	-5,70+03

Table 21 Resulting values after the structural analysis for the case with the shorter cross section height (20cm).

8.2.2.5 Discussion

In order to result to the final shape of the slab, a comparison of all the different outcomes was held. Since all the results were inside the allowable limits regarding the structural performance and the annealing time, the evaluation was held mainly according to the total volume of the component (Table 22).

In this regard, the outcomes of the fixed point optimization runs, although they are performing better in terms of tension, they were directly eliminated as considerably heavier than the first results. Moreover, the result with the shorter cross section was rejected since, despite the smaller design domain, it has larger volume while, additionally, it cannot easily lead to a sharp boundary shape because of the large 'grey' areas in the outcome.

Given that the remaining cases have overall identical forms, it can be considered that the final design which will be derived could potentially be manufactured with any of the glass types and fabrication methods examined. In this project, we are going to assume that the slab will ultimately be created with borosilicate glass since a considerably lower annealing time can be achieved for the same cross size. Moreover, casting is going to be investigated as the applied fabrication method in order to discuss the potential in terms of fabrication in this case as well as other criteria that may derive from it.

Variations		Result	Volume
Casting Edge Supports Borosilicate			935.8
Casting Edge Supports Soda Lime			937.3
Stacking Edge Supports Borosilicate			914.7
Casting Point Supports Borosilicate			1500.2
Casting Point Supports Soda lime			1604.5
Stacking Point Supports Borosilicate			1381.3
Casting Edge Supports Borosilicate (20cm)			1066.1
Total volume (cross section 30cm)			3150

Table 22 Volume[52] comparison of the different optimization results.

---

[52] It needs to be underlined that these values do not correspond to the actual volume of the components in m^3. The numbers derive as the sum of densities of all the elements to which the mesh is divided each time. This was mainly related to the function of the algorithm and, particularly, served to scale up the optimization problem.

8.3 Final Design

8.3.1 Design post-processing

After concluding to the final form, the outcome from the SIMP formulation was post processed in order to create the final design of the slab. Particularly, the densities were stored through Matlab in an Excel file and, afterwards, they were imported into Grasshopper through a script that made use of the Excel Reader component from Lunchbox.

In the script, the densities, and therefore the quadrilateral elements that compose the cross section densities, were divided into 3 main categories; full material (>0.6), intermediate densities, which correspond to half of the extrusion (0.2 < densities < 0.6) and no material at all (<0.2). The edges created are filleted between them in order to avoid the creation of sharp edges, which may lead to high residual stresses and cracks as discussed in Chapter 3. The result (Figure 68) is a complete compact shape that has some smaller additions with nerves in half of the length. Besides adding to the stiffness of the slab, these nerves can also serve to support the laminated float glass sheets in order not to deform.
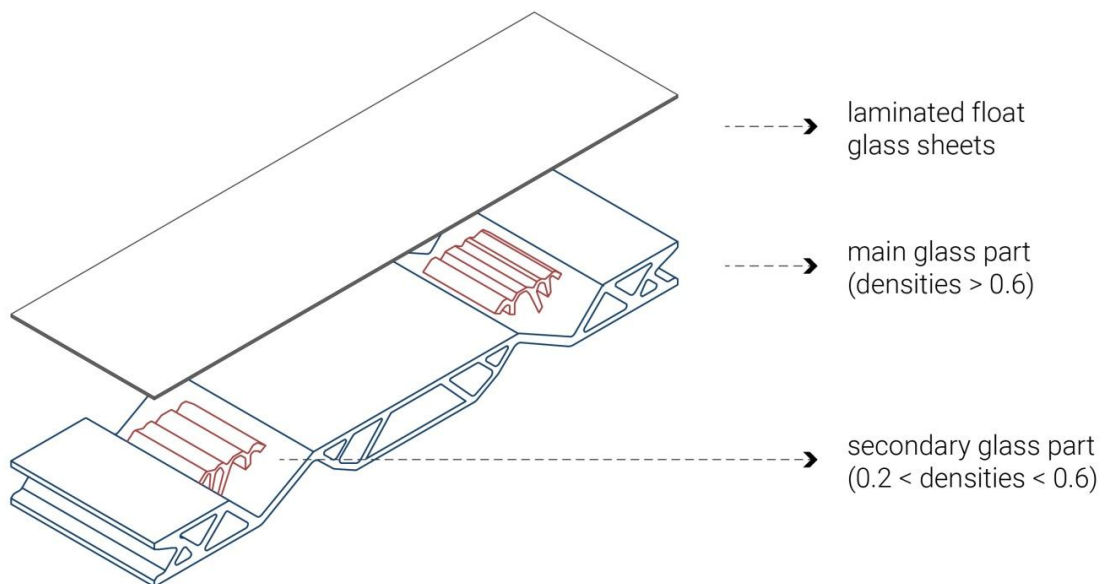
Figure 75 Diagram of the strategy followed for the extrusion.

8.3.2 Structural Verification

The final shape in 3-dimensions was verified structurally in ANSYS. The results (Appendix A.2.4.1) showcase that the principal stresses and deformation values lay inside the constraints imposed on the algorithm in the first place[53]. At the same time, it highlights the importance of taking also into consideration the deformation of the float glass sheets on top, since the maximum values for deflection are observed there. That could place an additional constraint on the maximum size of void allowed. Alternatively, a non-design domain could be considered in the upper part in order to form a solid base for the glass sheets.

---

[53] Deviations in the numbers may relate to inherent differences between a 2-dimensional and a 3-dimensional analysis.

Properties	Units	Values
Deformation (at critical point)	mm	0,12
Maximum principal stress (tension)	MPa	2,96
Minimum principal stress (compression)	MPa	-5,56

Table 23 Structural performance results after verification with ANSYS.

8.3.3 Result

The final design[54] was made into a physical model in a scale 1:10 in order to showcase the potential of the forms that can be created.

---
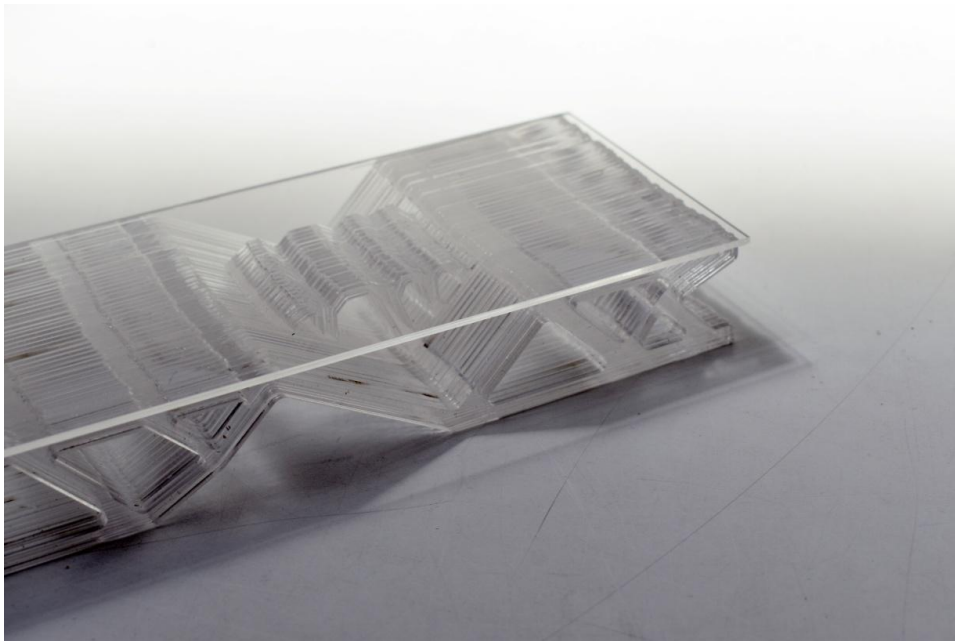
[54] The model refers to only one of the two monolithic parts that compose the total slab.
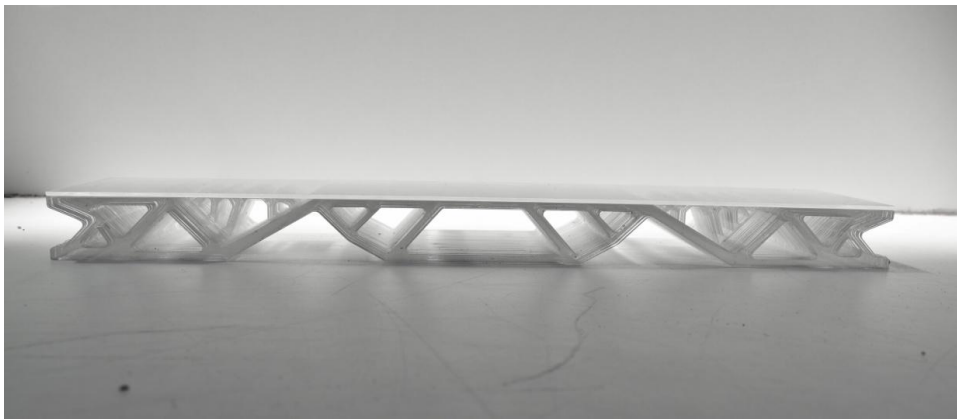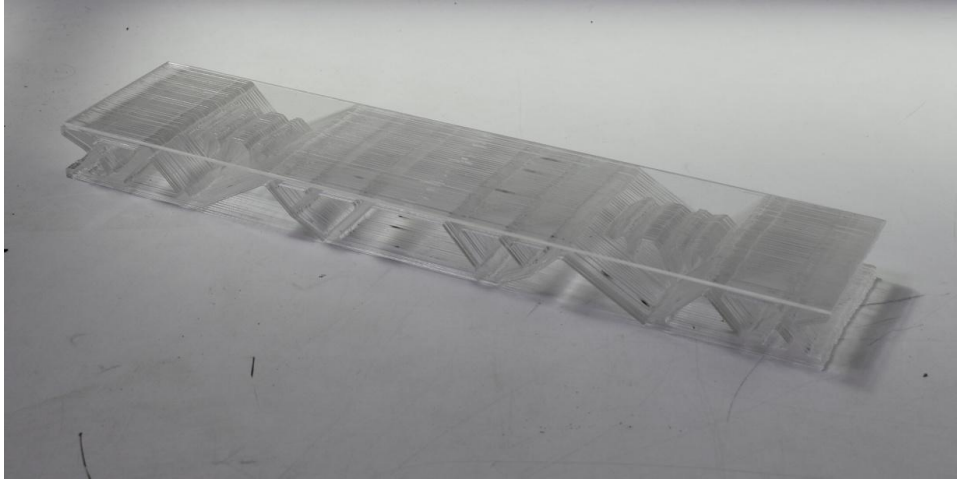
Figure 76 Photos of the physical model in scale 1:10 made from consecutive acrylic sheets.

9. Case Study Application

In this chapter, the strategy regarding the fabrication of the slab, as well as the installation on site is going to be discussed and the final form of the glass bridge is going to be presented.

9.1 Overview

As already discussed, the method which is going to be assumed for the fabrication of the glass slab is casting. Following the design guidelines defined in Chapter 5, the slab is going to be divided into two large longitudinal parts in order to serve for redundancy while, additionally, float glass sheets are going to be laminated on top of them for safety reasons. Given that the overall stiffness of each monolithic part is very high (the critical deformation in the middle is smaller than 1mm), it is considered that the two parts only need to be attached to the neighboring walls and not additionally attached together. The attachment of the glass slab to the wall is going to be facilitated with the placement of metal frames that will act as a clamp in the two short edges.

Regarding the railing, given that it was not taken into consideration during the optimization process[55], it is concluded that it should not be connected directly in the glass slab. In contrast, it is placed in a distance from the slab vertically and is supported from the two neighboring walls as a beam fixed in its two edges.

9.2 Slab Fabrication

Below the strategy for fabricating each of the two large monolithic glass parts is going to be outlined. Overall the fabrication process can be divided into two phases; the fabrication of the moulds with 3d printing and the fabrication of the glass components with casting.

9.2.1 Moulds

As already discussed in (Bhatia, 2019), the most adequate mould type for these applications is 3d printed sand mould, since it combines low manufacturing cost, easiness of fabrication and very high accuracy even in the case of complex forms. On the contrary, this may have to be compromised in the case that the conventional mould fabrication technique is applied, since it affects the shape precision and is likely to result in flaws.

In general, it was concluded that, given the overall form of the slab, the best way to cast the glass components would be with a rotation of 90 degrees. In this regard, the flow of the glass melt is aligned to the main extrusion direction and, thus, the elimination of inclusions such as bubbles and cords which may occur during the casting process is facilitated.
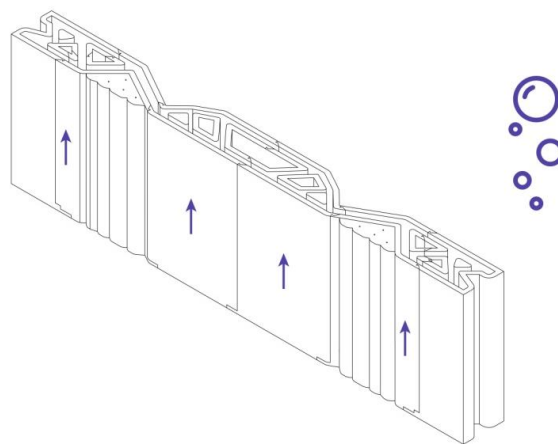
Figure 77 Vertical placement in order to eliminate the elimination of the inclusions.

---

[55] The load of the railing is applied eccentrically in the transversal axis and, therefore, it was difficult to be interpreted in a 2-dimensional optimization.

In order to reduce the material usage as well as the total time needed for the 3d printing process, the inner voids of the slab are not going to be 3d printed as a whole but only the boundary shape will be created every time. The thickness of the mould sides is defined based on the hydrostatic force that will be applied in the most critical area of the shape during the casting process.
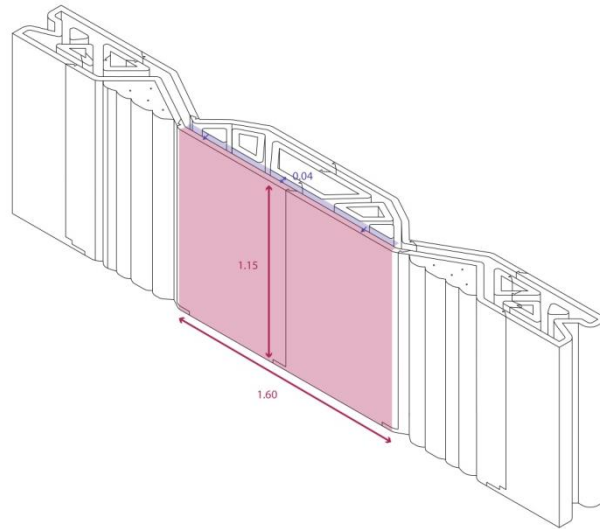
Figure 78 Dimensions of critical area for calculation of mould thickness.

Following the respective equations described in (Stefanaki, 2020), it was estimated roughly that the minimum allowable thickness of the mould should be 2,4cm (Appendix A.2.5). This was later increased to 4cm to accommodate any deviations between the calculations and the physical conditions. On the bottom surface the thickness of the mould is 5cm in order to create a stronger base. Additionally, the total height of the mould is increased by 2cm in the vertical direction in order to prevent any glass overflow.
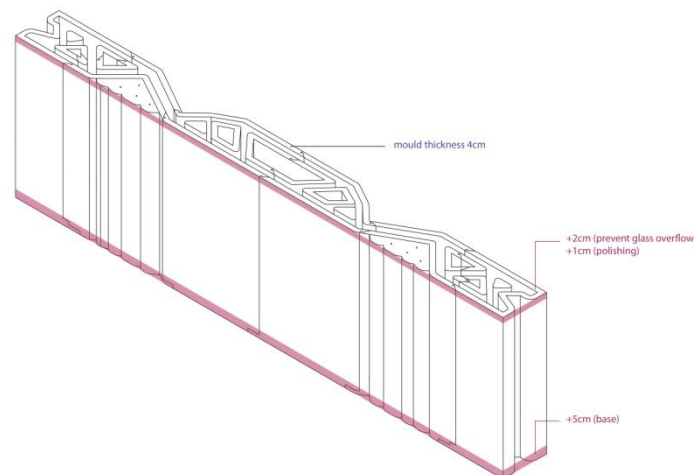
Figure 79 Mould thickness and alterations in the size.

In this regard, two different approaches were investigated. The first one referred to casting of the glass component as a whole. In this case, because of the fact that the secondary parts would be completely enclosed, there is large likelihood that inclusions and other flaws will be concentrated in these areas. Additionally, the material usage will be increased since supports should be created below these secondary areas in order to be

able to withstand both the weight of the mould but also of the glass melt which is going to be poured inside. The second option referred to casting the primary and secondary pieces individually and then fusing them together. In order to achieve it, the glass should undergo again the annealing process resulting therefore in larger energy use while, additionally, the fabrication of more moulds would be needed in this case[56].

Although fusing can be a potential good solution for the fabrication of the monolithic parts, in this project the casting in one phase is selected in order to, firstly, save in terms of the number of moulds needed and, secondly, not increase a lot the total time needed for the annealing of the structure. Regarding the 3d printing of the moulds, it was decided that the parts of the structure that correspond to the upper and lower areas of the secondary glass elements will be hollow in order to save both material but also time needed for printing. However, in the bottom part there are inner supports integrated in order to withstand the total load, whereas on the top part small paths serve to facilitate the rising of the inclusions to the surface (Figure 80).
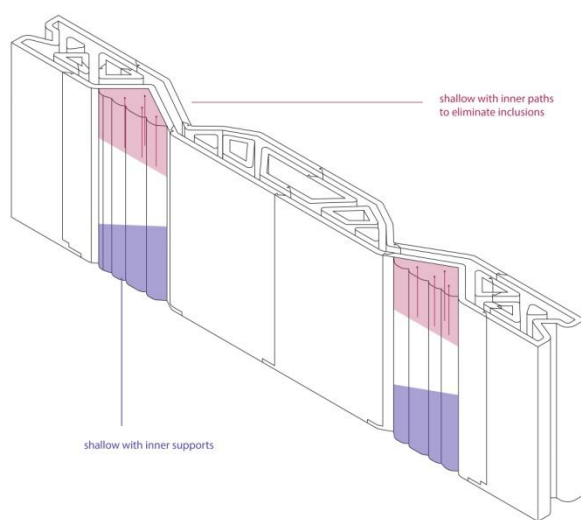
Figure 80 Alterations in the mould of the smaller parts.

Taking the aforementioned into consideration, the total dimensions of the mould is 4.28m*1,23m*0,38m. However, as it has been mentioned in Chapter 3.5, the maximum dimension of mould that can be 3d printed with sand is 4m*2m*1m. Therefore, the total mould volume needs to be separated into smaller pieces that will be combined in the end in order to compose the total shape.

The strategy for separating the moulds follows the guidelines defined by (Stefanaki, 2020). Therefore, the size and shape of the mould parts is defined taking into consideration the need to, firstly, reduce as much as possible the number of connection joints and, secondly, avoid the mould separation in areas where the shape is more complex and the elements are considered as more fragile. Additionally, the total weight of each 3d printed part is considered so that they can easily be transported by a small crane. Thus, the total weight of each part should not exceed 200-300 kg[57].

---

[56] When the pieces enter again inside the oven in order to fuse together, they need to be supported by moulds in order to be able to retain their shape during the process (Eskes,2018).
[57] The total weight of each 3d printed part is calculated using the density of the 3d printed sand mould (1,4kg/L) as defined in (Stefanaki, 2020).
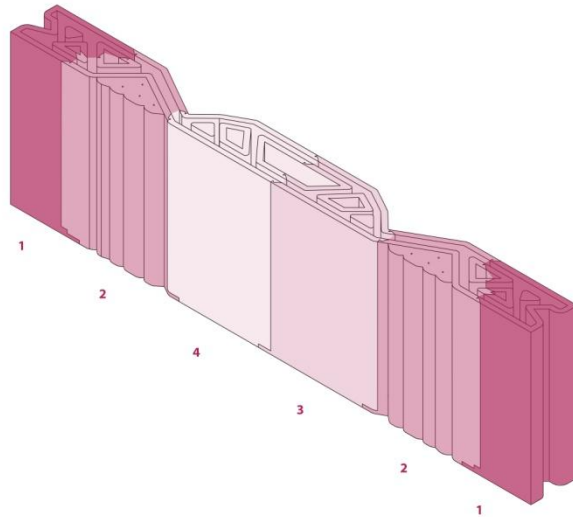
Figure 81 Distribution of total mould volume into smaller pieces & placement order.

As a result, the volume of the mould for the main part is going to be divided into four individual parts. The main problem that arises in this regard is the potential leakage in the points of connection between the different parts. In order to address this problem a system of extensions and interlocks is developed on the connection sides aiming to eliminate at maximum the leakage. The connections are designed in a way so that the interlocking of the components happens with sliding from the top in order to facilitate the fabrication sequence (Figure 82).

After the completion of the 3d printing process, the remaining sand is removed from the mould cavities. The mould sides are then cleaned and covered with a coating that will serve to create elements with smoother surfaces during casting (Bhatia, 2019).
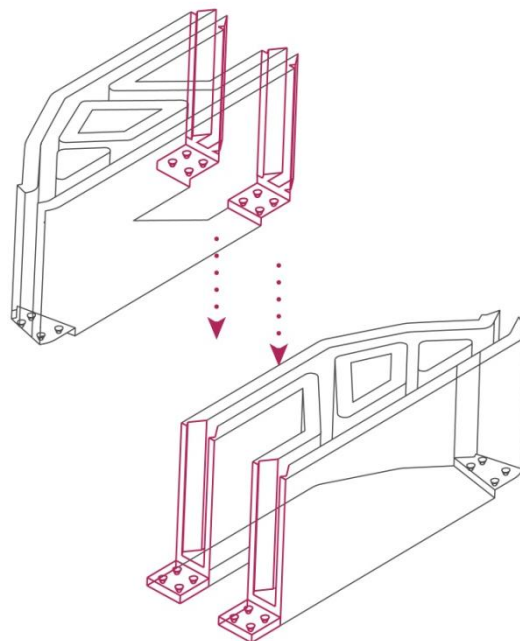
Figure 82 Interlocking system between the different mould parts.

9.2.2 Fabrication sequence

After 3d printing the mould parts, the process of fabricating the glass component is taking place. This includes the following steps:

A. Setting up the mould bases
An empty concrete container is created as the mould base for each of the different parts – main and secondary. The inner surfaces are covered with glass wool in order to balance the different material thermal expansion behaviors.

B. Placing the 3d printed sand pieces
In this phase, the 3dprinted parts are placed in their respective positions inside the concrete bases. In the case of the mould for the main part, the two side parts are placed first, whereas the middle left and middle right parts are placed consecutively afterwards in order to interlock between them.

C. Filling the voids
Although the mould thickness is calculated so as to be able to withstand the hydrostatic pressure that will be created through casting, it is also considered important to fill the inner voids in order to ensure that the structure in total will have the necessary stiffness. Based on the investigation which was held from (Stefanaki, 2020), it is decided that the infill should consist of the remaining sand which was removed from the mould cavities after the 3dprinting process of the sand moulds was finished[58].

D. Casting
As already discussed, the secondary casting process (kiln-casting) is selected as the most suitable for the fabrication of these components, since it allows for more accurate estimation of the volume of the glass melt which is going to be poured in the mould. Particularly, kiln casting entails the placement of small pre-formed glass pieces inside the mould which are going to melt together when placed in the oven. The glass melt is then going to be formed according to the mould shape. Afterwards, the cooling process will take place till the point that the glass structure reaches the sufficient temperature in order to be removed from the oven.

E. Removing the moulds
In this phase the glass forms are going to be removed from the moulds. This is anticipated to be a relatively easy process since the sand moulds are water dissolvable (Bhatia, 2019) and no severe damage in the glass form is expected. The sand can then be reused for 3d printing the moulds of the second monolithic part.

F. Post-processing
Although demoulding is expected to be a mild process for the glass components, the surfaces will still need to be cleaned and post-processed afterwards. Particularly, given that the glass surfaces are expected to be translucent and rough, grinding and polishing will need to be done manually in order to address these problems and at the same point eliminate as much as possible any surface defects that happened during casting. The surface abnormalities are expected to more intense in the part of the structure which was in direct contact with the outer conditions during the casting process (top surface) and, therefore, it is anticipated that more post-processing will be needed in this area. However, the extra thickness of 1cm which has been taken into account in the glass volume is expected to accommodate sufficiently these irregularities.

---

[58] In (Stefanaki, 2020), a comparison of different infill strategies, such as loose sand, honeycomb structure, grid infill structure and buttresses was held. Given that the mould was already sufficiently strong and there was no need for extra support, it was decided that adding the remaining loose sand in the infill was the most adequate option. This was mainly based on the fact that it is the fastest option, while it also has less added complexity and comparatively low manufacturing costs.

A

B

C

D

E
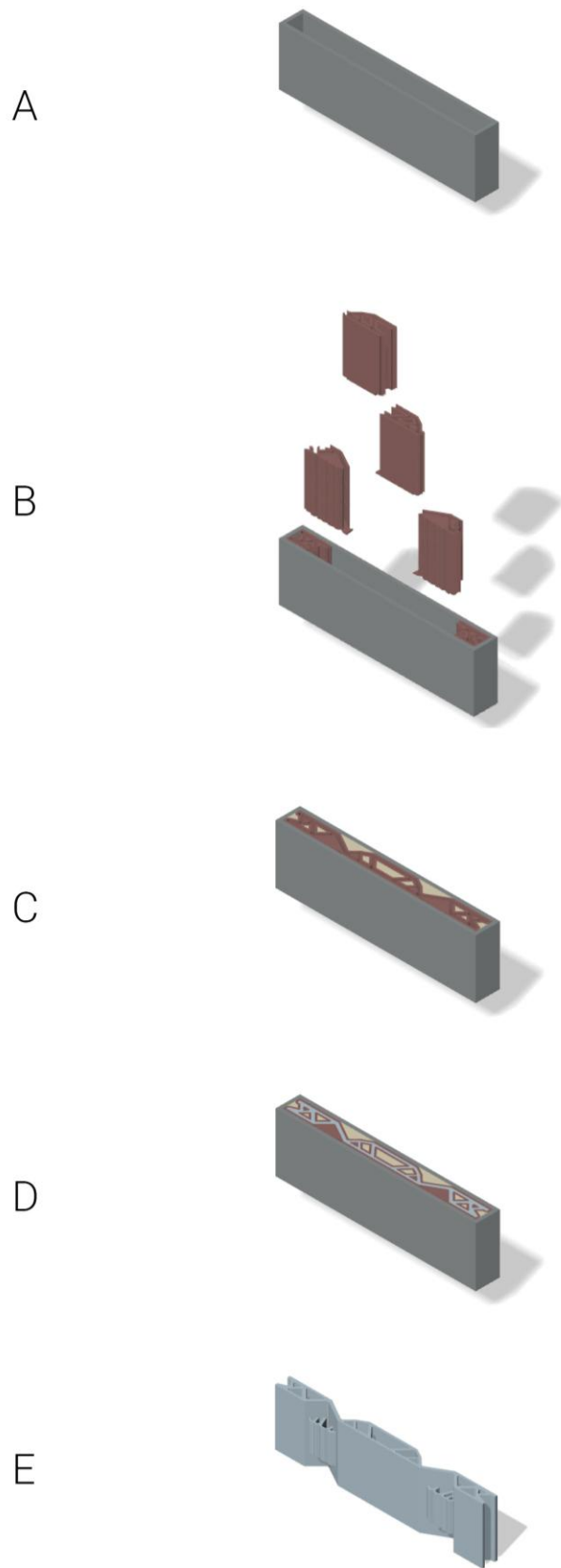
Figure 83 Axonometric illustrations of fabrication sequence.

9.3 Building Integration

9.3.1 Transport

After the two monolithic glass parts are formed, they will be transported with a truck[59] in the British Museum in order to compose the total slab. They will be headed inside the Great Court through the main entrance hall of the museum and they will be lifted up and placed in the final position with the use of a crane[60].
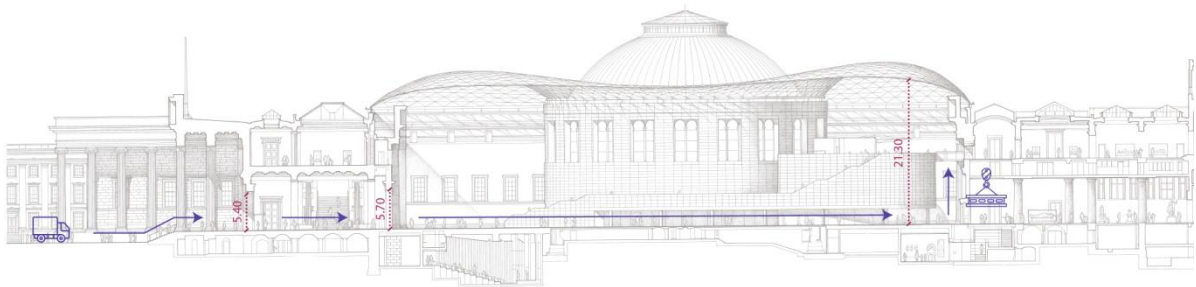
Figure 84 Transportation path inside the British Museum.

9.3.2 Installation

The installation process is analyzed in the following steps.

A. Placing the metal frames/conductors on the edges
Two frames from stainless steel are placed along the edges on the walls and are secured with bolts. They will serve as conductors for the placement of the slab components afterwards.

B. Placing the monolithic slab parts
Each of the monolithic parts of the slab is lifted up with a crane and placed on the correct position. The metal flange adapter is also placed and secured with bolts so that the whole structure functions as a clamp.

C. Placing the float glass sheets
The laminated glass sheets on the upper parts are attached to the monolithic parts with an adhesive. A potential good solution is the crystal clear spacers which are applied with the use of a primer substrate.

D. Placing the railing
The last part refers to the installation of the railing. It consists of two uniform laminated glass sheets which, similarly to before, are lifted up by a crane and are attached with metal frames to the neighboring walls.

---

[59] The two monolithic parts can be transported by a truck since they lie well inside the maximum permissible dimensions of lorry in UK which are 2.9m in width and 18.65m in length (gov.uk).
[60] The free height inside the Great Court is approximately 26 m so it allows for the use of a crane that will lift up the parts in their final position (11m height).

steel bolts 7mm
steel frame 10mm

steel bolts
10mm

crystal clear spacer 10mm*12,5mm
neoprene rubber sheet 5mm
metal flange adapter with holes to
accommodate tolerances
steel bolt 10mm
structural steel frame 10mm

0   30cm
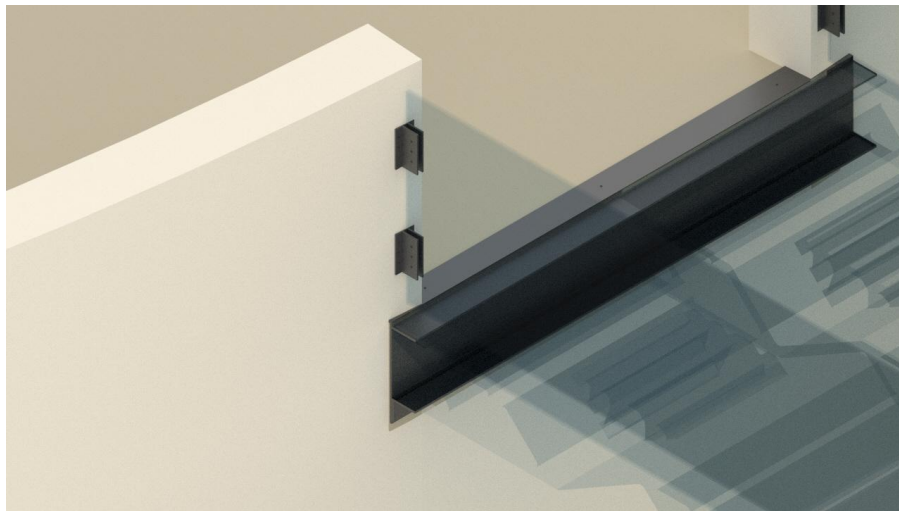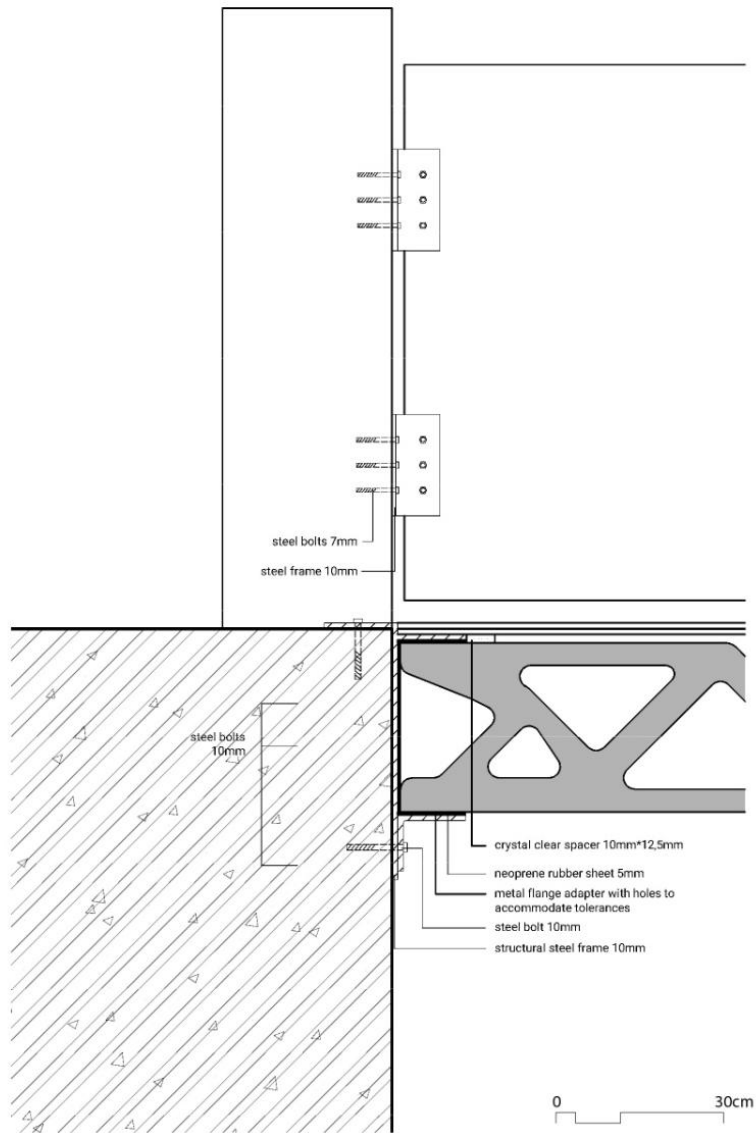
Figure 85 Detail of the connection to the wall & railing.

119

9.4 Final Result
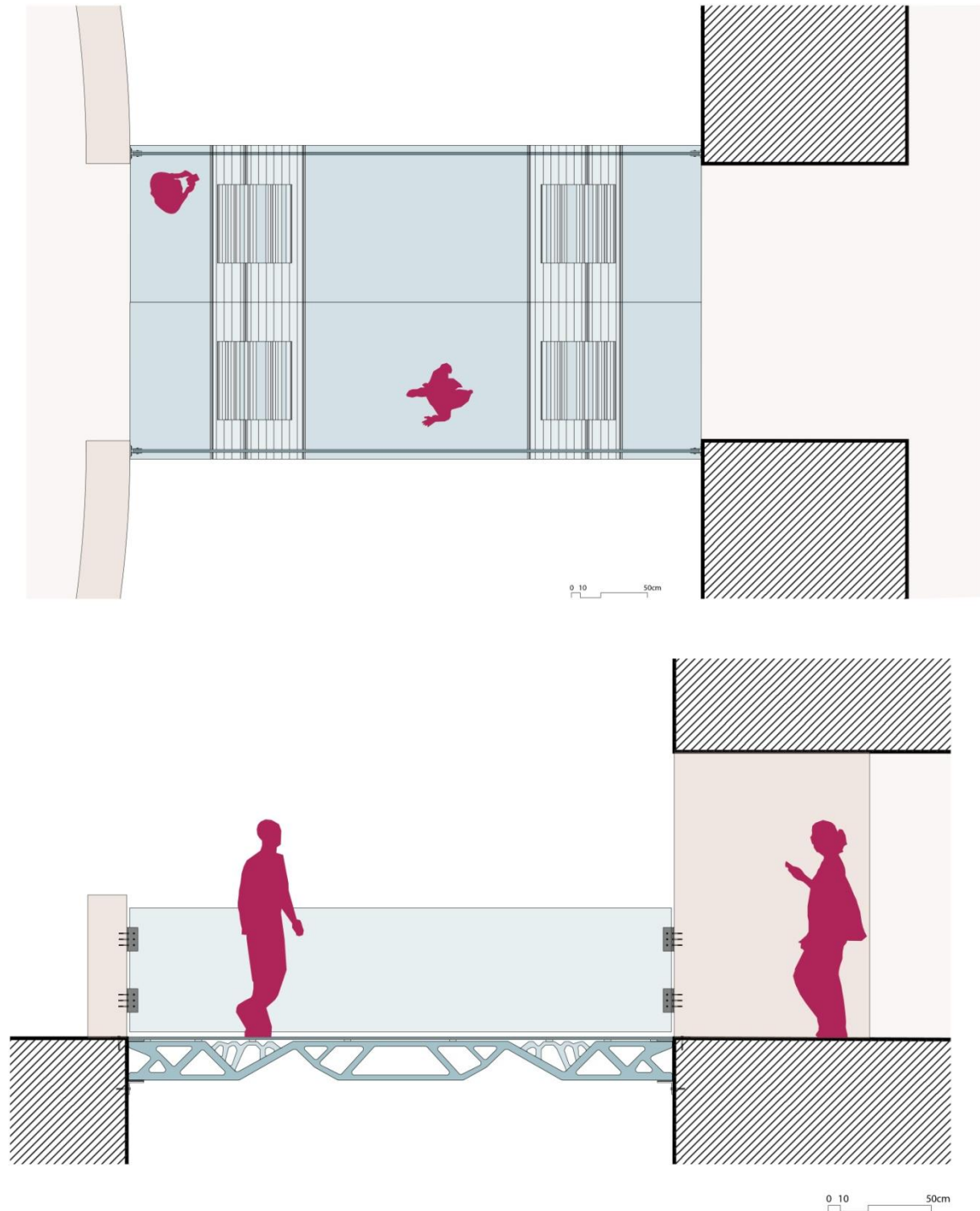
Figure 86 Plan & Section of the final design.
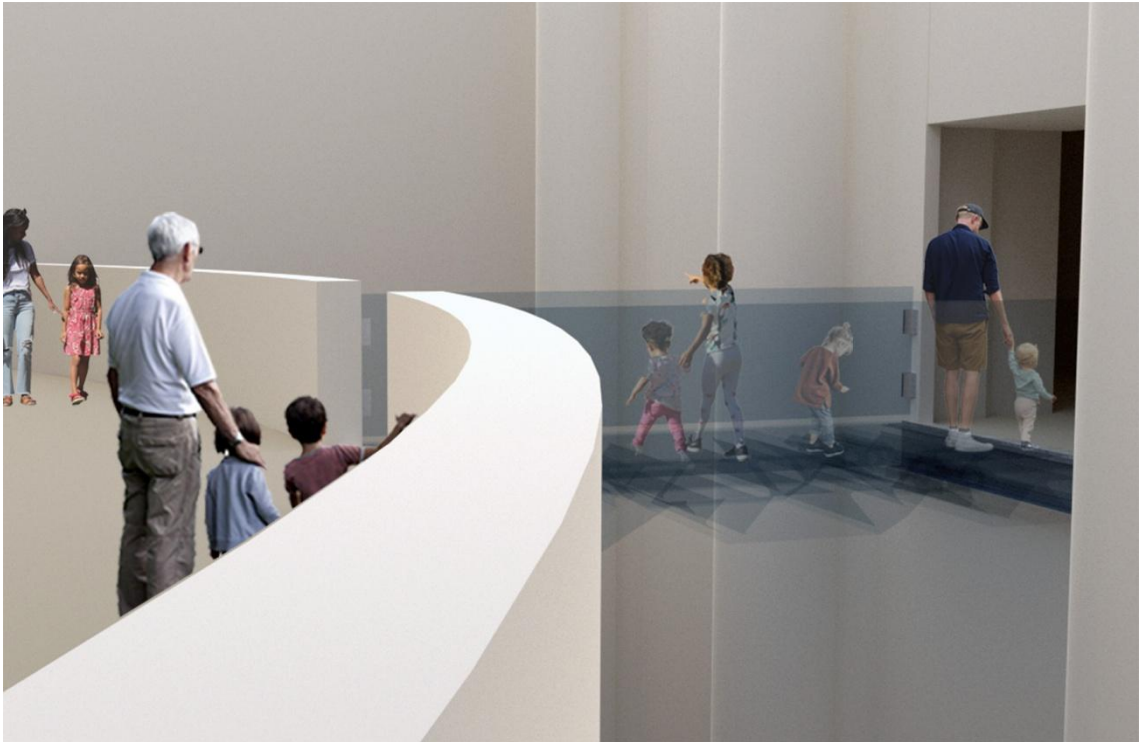
Figure 87 Final Visualization.

10. Conclusion

This thesis is a continuation of the work which has already been done in TU Delft during the previous years in the direction of using Topology Optimization techniques for the design of cast glass structures which are feasible to be manufactured. In order to achieve that, the previous theses have defined criteria related to different aspects, such as the structural performance or the manufacturing of the components. The most important constraints are, firstly, the annealing time needed for the fabrication of the elements, which may render the whole process prohibitively expensive in terms of both cost and energy needed and, secondly, the need to differentiate between the performance regarding tension and compression during the optimization process. The contribution of this work is to try to address the problems highlighted until now regarding the limitations that derive from the use of commercial software for running the optimization analysis. These have to do with the degree of mesh refinement that can be examined, the way of applying the manufacturing criteria but, most importantly, with the possibility to evaluate both principal stresses during the optimization process. This has an effect both on the overall efficiency of the structure, since glass has a very high compressive strength, but its resistance under tension is considerably limited, but also on the time needed in order to extract the design since, till now, a secondary evaluation of the stresses should occur in order to alleviate any peak stresses that may occur locally in the structure. In this regard, the main research question is defined as:

What are the main aspects and inherent limitations of composing a Topology Optimization algorithm for the design of massive cast glass structures which are time and cost efficient?

The answer to the main research question is sought through answering the following sub-questions:

Which are the structural, annealing and manufacturing criteria for the design of glass structures that will be taken into consideration for the algorithm?

Regarding the structural performance of the element, the most critical factor that should be taken into account is the significant differentiation between the allowable limits of tension and compression, whose values differ by at least one order of magnitude. In this regard, it goes without saying that a surpass of the limit, particularly the tensile one, could directly lead to brittle failure. Additionally, since glass is a brittle material and cannot absorb deformation with a plastic behavior, it is important that the maximum deflection of the component is also considered. Regarding the annealing and manufacturing process, the algorithm should take into account the maximum time that can be devoted in that part since it is the most critical factor that renders the structure able to be manufactured or not. The annealing time constraint is interpreted as a maximum cross section constraint, given that this is the aspect that defines to a large extent the overall time needed. Other aspects that can affect the total annealing time, such as the glass composition, will not be directly linked as an algorithm constraint, but they can serve as input for different iterations. The maximum cross section constraint is finally defined taking into consideration the need for homogeneous mass distribution in the glass structure as well as the constraint for the minimum element dimension. Other aspects, such as the avoidance of sharp edges which are susceptible to cracking due to their thin cross section, are taken into account in a secondary post-processing phase.

Which are the main design principles that will be taken into account for the design of the slab?

The design principles integrated in the process are directly related to the case study example selected. Particularly, the design was divided into two parts in order to serve for redundancy in case of failure. Additionally, safety was ensured with the addition of two additional layers of float glass on top of the monolithic parts. They also serve to protect the monoliths from contact stresses and accidental impact, while they allow having voids in the structure since they ensure that a flat glass surface to walk on will always exist. The railing is

not considered in the process and is added separately from the main slab. Similarly to the existing structure, it consists from layers of float glass.

Which algorithmic methodology or combination of algorithmic methodologies will be used during the Topology Optimization process?

After a thorough evaluation of the existing Topology Optimization algorithmic methodologies, it was concluded that SIMP method is going to be selected for the needs of this project. It is well-proven in the literature to provide fast and robust solutions, while it also has a simple formulation which is easier to comprehend and apply in the algorithmic process. At the same time, the mesh discretization for SIMP can be directly used as the mesh for the Finite Element analysis which further contributes to the simplicity of the process. In contrast Level-Set methods, where the overall boundary results as a contour of a Level-Set function, although they can provide a smoother final boundary, they are more complex in their application and they require additional perturbations for the creation of the FE mesh, such as the xFEM method. Additionally, they depend a lot on the initial design, fact which may lead to local minima. These factors acted as thresholds and, thus, Level-Set methods – although appealing – were not selected for application in this thesis.

Which are the objectives and constraints which are going to be posed and how the optimization problem will be formulated?

Two problem formulations were investigated and their results were critically evaluated. The first refers to maximizing the overall stiffness of the structure through the minimization of its compliance, whereas the second one aims to minimize its volume. The goal was to see which of the two can provide a more reliable result and, particularly, to evaluate if minimizing the volume can be a robust alternative to maximizing the structural stiffness. A successful experiment in this direction could prevent from trying to guess the optimum volume fraction needed to be retained in the structure each time and could possibly to even more efficient and lightweight structures. The constraints posed were directly related to the criteria related to the design of glass structures as defined before. Additionally, compliance and volume were imposed as a constraint when not placed as an objective in the algorithm in order to ensure that the optimization will be guided towards a stiffer and a more lightweight structure respectively.

Which will be the approximated annealing time for the construction of the slab?

As already mentioned, the critical factor that defines the annealing time of the component is its maximum element cross section. In the result obtained the maximum size of cross section indicated is ~ 0.1m. By applying the annealing formula used for the problem formulation, it is concluded that ~29 hours will be needed in order to anneal which further validates the feasibility of the outcome. However, it needs to be underlined that this time refers only to one of the phases of the cooling process. Nevertheless, given that this phase is the most time-consuming and therefore the most critical one, the other phases are not going to be considered now for the calculation of the time needed.

How the structural and design properties as well as the time and cost efficiency of the outcome are comparable to similar experiments using TO commercial software?

The project takes into consideration all the criteria related to the design of the glass structures and the needs in terms of structural performance which were set from the previous theses that solved the problem using TO commercial software. The main benefit this time is the ability to successfully manipulate the stresses through the optimization, ensuring that the final outcome will be feasible to be manufactured and preventing from the secondary post-processing in order to alleviate peak stresses. Additionally, it allows directly setting the maximum annealing time allowed and adapting the structure according to it. Overall, customization according

to the glass properties enables to have more specific and efficient outcome, whereas adapting the formulation to volume-based, instead of compliance as applied previously, allows for clearer boundaries and more lightweight structures. However, it needs to be underlined that this does not mean that no post-processing would be needed. The algorithm exports the final result as a range of densities which have to later be imported in Grasshopper and manipulated manually in order to result in a smooth and not jagged boundary which is not feasible to be fabricated.

How can the customized tool be used from a designer and which is the reflection on the final shape architecturally?

As it was already demonstrated through the design exploration with different design domain, boundary conditions and glass type, the developed tool can be used in combination with a wide range of different inputs and can result to significantly different outcomes every time. Each time it provides a solution which can become the base for further design development according to the needs and architectural vision, taking always into consideration that the new alterations should not become an impediment for the structural integrity or other constraints posed in the problem.

The advantage in this case is that the solutions which can be derived through the code can be non-intuitive and, therefore, they can enrich the architectural vocabulary with new forms in the early-design phase. Additionally, the designer has the possibility to change the boundary conditions or apply design guidelines in order to ensure as much as possible that the final outcome will be tailored to the needs every time. Particularly, in the case that a 3-dimensional code is implemented in the future, it could result to even more complex forms and intriguing outcomes. However, as it is usually stated regarding the computational design in general, it should always be underlined that these tools only serve to become an assistant to the designer who is responsible to make the final design decisions.

11. Limitations

During the trajectory of this thesis there were a lot of limitations that needed to be overcome. The first and most significant challenge was the lack of knowledge from the side of the student in the aspects of Topology Optimization, Finite Element method and, to some extent, mathematics and programming. This led to spending a lot of time in investigating and trying to understand the logic behind the things which, if already obtained, it could have sped up the process in the beginning.

Subsequently, the most significant limiting factor for this project was the available time. This could have been invested to both experimenting more with the algorithm and trying to interpret the result in a three-dimensional code but also to a thorough investigation of all the aspects that could be considered in terms of glass. This could be realized with prototypes in the lab, which, besides the practical contribution of evaluating what other critical factors derive related to the material and how all the process combines together, could be also very fascinating and inspiring.

Another important limitation was the computational power needed for the execution of the optimization operations. It needs to be underlined that all this investigation could not be done by using only a laptop with limited computational capacity. This, firstly, rendered non-feasible to run operations that required a large array size, which was the case in the principal stresses and the Drucker – Prager constraint, because the RAM size (8GB) was not sufficient. Additionally, even in the cases when it was possible to operate the code in the laptop, the computational time needed was significantly higher. For this reason, the contribution of VR Lab with offering a desktop computer with improved properties was significant for the development of the thesis.

12. Discussion & Recommendations

Overall, this thesis led to the creation of a working code which proved that a customized tool can be very beneficial for the design of cast glass structures and it can result to a reliable structure. At the same time, the investigation for the objective of the optimization showed that, although the classical compliance-based formulation can lead to a successful result, the volume-based approach can be a robust alternative to it. In the latter case, the result is clearer and the structure is in principle more lightweight while at the same time it complies with all the constraints imposed on the algorithm.

Nevertheless, it is important to underline that this thesis is just a basis in the direction of developing an algorithm for the design of glass structure and, therefore, can be extended and developed towards many directions. Firstly, different design variations can be explored with the application of different boundary conditions in the code. For example, eccentric loads and point forces can be experimented or the supports can be modified from fixed edge supports to fixed point supports in the bottom nodes. Moreover, the design can be manipulated with the integration of a non-design domain, e.g. the float glass sheets on top of the monolithic parts, to the operation. These slight modifications are anticipated to have a significant effect on the final design that will be obtained.

Regarding the mesh partitioning, it can be explored if a smaller mesh resolution, e.g. 0.01, will influence the design and if it can provide a more discrete boundary than the one currently extracted. However, it is anticipated that this modification will increase largely the computational time needed for the optimization to converge. Other alteration in this direction could be to change the shape of the Finite Elements from quadrilateral to triangular and check if that can give a better approximation.

In terms of algorithm implementation, it needs to be further explored how it will be ensured that all the element parts comply with the minimum cross section dimension. However, it needs to be mentioned that this is considered difficult since an approach similar to the one already applied for the maximum cross section cannot be implemented this time. This derives from the fact that a limit regarding the amount of void elements in every circular region cannot be imposed, given that there are regions in the structure which inevitably will be completely empty.

Additionally, although the algorithm covers a wide range of criteria regarding the structural performance of the structure and its feasibility to be manufactured, there are also other constraints that could be applied to it in order to specify even more the solution. Firstly, the deformation of the float glass sheets which are applied on top of the monolithic parts and the stresses which arise in them can be considered in the optimization process. Moreover, a criterion regarding the minimum void size could be applied. This refers to the constraint regarding the minimum sufficient thickness of the mould in order to be able to withstand the hydrostatic pressure when pouring the glass melt inside. Additionally, regarding the design's voids, it is important to assure that there is connectivity between them so that the mould can be removed in the end of the fabrication. This can be evaluated through applying the Virtual Temperature Method; converting the connectivity problem to a temperature problem and performing a heat flow analysis as described by (Liu et al., 2015).

Regarding the overall method applied, possible additions could be to experiment with the use of different algorithms provided by the Optimization Toolboxes, such as the genetic ones, or try to create the functions and provide the Hessians for the sensitivity analysis to the solver in order to see how this may affect its overall efficiency. Lastly, another alternative could be to use the final density range obtained from the SIMP method as the initial guess design for a Level-Set Optimization. In this regard, a more discrete boundary will be obtained in the end and, additionally, the shape optimization is less likely to fall into local minima since it will take into account the layout which is considered optimal.

The last recommendation refers to extending the code in order to create a shape in three dimensions. This will enrich considerably the potential for the final design and different resulting shapes are likely to be obtained. However, it needs to be underlined that this entails a lot of additional challenges regarding the setup of the initial mesh, the objectives and constraints but also regarding the setup of the structural model with the use of the Finite Element equations.

References

- Allaire, G., Cavallina, L., Nobuhito, M., Tomoyuki, O., & Toshiaki, Y. (2019). *The homogenization method for topology optimization of structures: old and new*. Cornell University

-Allaire, G. (2005). Topology Optimization with the homogenization and the Level-Set Methods. In Ponte Castañeda, P., Telega, J.J., & Gambin, B. (Eds.), *Nonlinear Homogenization and its Applications to Composite, Polycrystals and Smart Materials.* Kluwer Academic Publishers.

- Aghaei-Meibodi, M, Mathias Bernhard, A, Jipa, & Dillenburger, B. (2017). *The Smart Takes from the Strong.* In Sheil, B., Menges, A., Ruairi, G. & Skavara M. (Eds.), *Fabricate.* London: UCL Press. https://doi.org/10.14324/111. 9781787350014

- Andreasen, C.S., Elingaard, M.O., & Aage, N. (2020). Level set topology and shape optimization by density methods using cut elements with length scale control. *Structural and Multidisciplinary Optimization, 62.* https://doi.org/10.1007/s00158-020-02527-1.

- Andriotis, C. (2021). *Fundamentals of Finite Elements. Note series for AR3B011:* Earthy. TU Delft

- Bendsoe, M.P., & Kikuchi, N. (1988). Generating optimal topologies in structural design using a homogenization method. *Computer methods in applied mechanics and engineering, 71*

- Bendsoe, M.P., & Sigmund O. (2004). *Topology Optimisation. Theory, Methods and Applications.* Springer-Verlag Berlin Heidelberg.

- Bhatia, I. (2019). *Shaping transparent sand in sand: Fabricating topologically optimised cast glass column using sand moulds.* [Master's Thesis, Delft University of Technology]. https://repository.tudelft.nl/islandora/object/uuid%3Acaabb4cd-1bf4-48bc-b04d-e5ff8a1d1580

- Bristogianni, T., Oikonomopoulou, F., Yu, R., Veer, F.A. & Nijsse, R. (2021). Exploratory Study on the Fracture Resistance of Cast Glass. *International Journal of Structural Glass and Advanced Materials Research*, 5.

- Bristogianni, T., Oikonomopoulou, F., Yu, R., Veer, F.A. & Nijsse, R. (2020). Investigating the flexural strength of recycled cast glass. *Glass Structures & Engineering*, 5(3).

- Bruggi, M. (2008). On an alternative approach to stress constraints relaxation in topology optimization. *Structural and Multidisciplinary Optimization, 36.* https://doi.org/ 10.1007/s00158-007-0203-6.

- Bruggi, M., & Duysinx, P. (2012). Topology optimization for minimum weight with compliance and stress constraints. *Structural and Multidisciplinary Optimization, 46.* https://doi.org/ 10.1007/s00158-012-0759-7.

- Boyd, S., & Vandenberghe, L. (2004). Convex Optimization Problems. In *Convex Optimization*.(p.127-213). Cambridge University Press.

- Cheng, G.D., & Guo, X. (1997). ε-relaxed approach in structural topology optimization. *Structural Optimization, 13.*

- Collet, M., Bruggi, M., & Duysinx, P. (2017). Topology optimization for minimum weight with compliance and simplified nominal stress constraints for fatigue resistance. *Structural and Multidisciplinary Optimization, 55.* https://doi.org/ 10.1007/s00158-016-1510-6

- Damen, W. (2019). *Topologically Optimised Cast Glass Grid Shell Nodes.* [Master's Thesis, Delft University of Technology]. https://repository.tudelft.nl/islandora/object/uuid%3A2afbfe96-c9bf-44d7-bfaa-d8a710fa1ce2

- de Ruiter, M.J., van Keulen, F. (2004). Topology optimization using a topology description function. *Structural and Multidisciplinary Optimization, 26.* https://doi.org/ *10.1007/s00158-003-0375-7*

- Duysinx, P., Van Miegroet, L., Lemaire, E., Brüls, O., & Bruyneel, M. (2008). Topology and generalized shape optimization: Why stress constraints are so important?. *International Journal for Simulation and Multidisciplinary Design Optimization*, 2(4). https://doi.org/ 10.1051/ijsmdo/2008034

- Eschenauer, H., Kobelev, B., & Schumacher, A. (1994). Bubble method for topology and shape optimization of Structures. *Structural Optimization, 8*

- Eskes, A. (2018). *Connecting Glass to Glass.* [Master's Thesis, Delft University of Technology]. https://repository.tudelft.nl/islandora/object/uuid%3A73f48f2b-5da9-438f-86d0-2e3bcc70385?collection=education

- Guest, J.K., Prévost, J.H., & Belytschko, T. (2004). Achieving minimum length scale in topology optimization using nodal design variables and projection functions. *International Journal for numerical methods in engineering, 61*. https://doi.org/ 10.1002/nme.1064

- Guest, J.K. (2009). Imposing maximum length scale in topology optimization. *Structural and Multidisciplinary Optimization, 37(5)*. https://doi.org/ 10.1007/s00158-008-0250-7

- Hailu Shimels, G., Dereje Engida, W., & Fakhruldin Mohd, H. (2017). A comparative study on stress and compliance based structural topology optimization. *IOP Conference Series: Materials Science and Engineering, 241*.

- Hill, J.M., Angel, J.R.P., Lutz, R.D, Olbert, B.H., & Strittmatter, P.A. (1998). Casting the first 8.4 meter borosilicate honeycomb mirror for the Large Binocular Telescope. *SPIE 3352 \Advanced Technology Optical/IR Telescopes".*

- Hubert, M. (2015). *IMI-NFG Course on Processing in Glass Spring 2015.* CelSian Glass & Solar, Eindhoven.

- Jewett, J.L., & Carstensen, J.V. (2019). Topology-optimized design, construction and experimental evaluation of concrete beams. *Automation in Construction, 102.* https://doi.org/10.1016/j.autcon.2019.02.001.

- Jihong, Z., Han, Z., Chuang, W., Lu, Z., Shangqin, Y., & Weihong, Z. (2020). A review of topology optimization for additive manufacturing: Status and challenges. *Chinese Journal of Aeronautics, 34.* https://doi.org/ 10.1016/j.cja.2020.09.020

- Jipa, A., Bernhard, M., Meibodi, M., & Dillenburger, B. (2016). 3D-Printed Stay-in-Place Formwork for Topologically Optimized Concrete Slabs. *TxA Emerging Design and Technology.*

- Koopman, D. (2021). *The Topology Optimised Glass Bridge.* [Master's Thesis, Delft University of Technology]. https://repository.tudelft.nl/islandora/object/uuid%3Acc8454d4-2cae-42b7-bc9c-7514fc187c2f

- Kumar, P. (2016). *Synthesis of Large Deformable Contact-Aided Compliant Mechanisms using Hexagonal cells and*

Negative Circular Masks [Phd Dissertation, Indian Institute of Technology KANPUR].

- Le, C., Norato, J., Bruns, T, Ha, C., & Tortorelli, D. (2010). Stress-based topology optimization for continua. *Structural and Multidisciplinary Optimization, 41.* https://doi.org/ 10.1007/s00158-009-0440-y

- Lee, E., James, K.A., & Martins, J.R.R.A. (2012). Stress-constrained topology optimization with design-dependent loading. *Structural and Multidisciplinary Optimization, 46.* https://doi.org/ 10.1007/s00158-012-0780-x.

- Liew, A., López López, D., Van Mele, T. & Block, P. (2017). Design, fabrication and testing of a prototype, thin-vaulted, unreinforced concrete floor. *Engineering Structures, 117.* https://doi.org/10.1016/j.engstruct.2017.01.075

- Liu, S., Li, Q., Chen, W., Tong, L., & Cheng, G. (2015). An identification method for enclosed voids restriction in manufacturability design for additive manufacturing structures. *Frontiers of Mechanical Engineering, 10.* https://doi.org/s11465-015-0340-3

- Liu, K. & Tovar, A. (2014). An efficient 3D topology optimization code written in Matlab. *Structural and Multidisciplinary Optimization, 50.* https://doi.org/ 10.1007/s00158-014-1107-x.

- Martlew, D. (2005). Viscosity of molten glasses. In Pye, D., Joseph, I. & Montenero, A. (Eds.), *Properties of Glass-Forming melts.* CRC Press.

- Nathan, P., Palar, S., & Zuhal, S. (2020). SIMP versus level set function as an implicit representation model for structural topology optimization. *AIP Conference Proceedings, 2226.* https://doi.org/10.1063/5.0005031

-Naous, D. (2020). *Topologically Optimised Cast Glass Shell: Topological optimisation and new fabrication methods for compressive free-form glass structures.* [Master's Thesis, Delft University of Technology]. https://repository.tudelft.nl/islandora/object/uuid%3Aaff7d67c-27f6-40bd-ac2c-4e518006684f

- Oikonomopoulou, F., Bhatia, I.S., van der Weijst, F., Damen, W., Bristogianni, T. (2020). Rethinking the Cast Glass Mould. An Exploration on Novel Techniques for GeneratingComplex and Customized Geometries. *Challenging Glass 7, Conference on Architectural and Structural Applications of Glass.* https://doi.org/10.7480/cgc.7.4662

- Oikonomopoulou F., van der Broek, E.A.M., Bristogianni, T.,Veer, F.A., & Nijsse, R. (2017). Design and experimental testing of the bundled glass column. *Glass Structures & Engineering (2).* https://doi.org/ 10.1007/s40940-017-0041-x

- Oikonomopoulou, F. (2022). Technoledge Structural Design AR0133. Guidelines for engineering & calculating a glass structure. TU Delft.

- Oikonomopoulou, F. (2019). *Unveiling the third dimension of glass. Solid cast glass components and assemblies for structural applications.* [Phd Dissertation, Delft University of Technology] https://journals.open.tudelft.nl/abe/article/view/4088/4015

- O'Regan, C. (2014). *Structural use of glass in buildings (2nd edition).* The Institution of Structural Engineers.

- Papadrakakis, M. (2001). *Analysis of structures with the Finite Element Method (in greek).* Papasotiriou publications.

- Poulsen, T. A. (2002). A simple scheme to prevent checkerboard patterns and one-node connected hinges in topology optimization. *Structural and Multidisciplinary Optimization, 24(5).* https://doi.org/ 10.1007/s00158-002-0251-x

- Querin, O.M., Steven, G.P. (1998). Evolutionary structural optimisation (ESO) using a bidirectional algorithm. *Engineering Computations, 15(8).* https://doi.org/10.1108/02644409810244129

- Querin, O.M., Victoria, M., Alonso, C., Ansola, R., & Martí, P. (2017). *Topology Design Methods for Structural Optimization.* Elsevier Ltd

- Saxena, A. (2008). A Material-Mask Overlay Strategy for Continuum Topology Optimization of Compliant Mechanisms Using Honeycomb Discretization. *Journal of Mechanical Design, 130(8).* https://doi.org/10.1115/1.2936891

- Shand, E.B.,& Armistead, W.H. (1958). *Glass Engineering Handbook.* New York, McGraw-Hill.

- Shelby, J.E. (2005). *Introduction to Glass Science and Technology (2nd edition).* The Royal Society of Chemistry.

- Sigmund, O., & Maute, K. (2013). Topology optimization approaches. A comparative review. *Structural and Multidisciplinary Optimization, 48.*

- Sigmund, O. (2001). A 99 line topology optimization code written in Matlab. *Structural and Multidisciplinary Optimization, 21.*

- Stefanaki, M.I. (2020). *Glass Giants. Mass-optimized massive cast glass slab.* [Master's Thesis, Delft University of Technology]. https://repository.tudelft.nl/islandora/object/uuid%3Ac1a296b1-d31a-4f7b-8888-9d3bfda10ada

- van der Weijst, F.(2019). Glass Vaults. Introducing an Adjustable Mould for Casting Glass Voussoirs for Transparent Shell Structures. [Master's Thesis, Delft University of Technology]. https://repository.tudelft.nl/islandora/object/uuid%3A37a693fc-4835-4d46-a4e1-086e96c2ef1a

- van Dijk, N.P., Maute, K., Langelaar, M., & Van Keulen, F. (2013). Level-set methods for structural topology optimization: a review. *Structural and Multidisciplinary Optimization, 48.* https://doi.org/ 10.1007/s00158-013-0912-y

- Vantyghem, G., De Corte, W., Shakour, E., & Amir, O. (2020). 3D printing of a post-tensioned concrete girder designed by topology optimization. *Automation in Construction, 112.* https://doi.org/10.1016/j.autcon.2020.103084.

- Vitalis, D. (2017). *Glass Sandwich Panel: Exploring the potential of glass sandwich structures for relatively lightweight planar elements with high stiffness and controlled transparency.* [Master's Thesis, Delft University of Technology]. https://repository.tudelft.nl/islandora/object/uuid%3A8414bc7f-6dcc-49ad-b16b-2bc92a29fee6?collection=education

- Xia, L., Xia, Q., Huang, X., & Xie, Y.M. (2016). Bi-directional Evolutionary Structural Optimization on Advanced Structures and Materials: A Comprehensive Review. *Archives of Computational Methods in Engineering, 25.* https://doi.org/10.1007/s11831-016-9203-2

- Xie, Y.M., & Steven, G.P. (1992). A simple evolutionary procedure for structural optimization. *Computers & Structures, 49*

- Xie, Y.M., & Steven, G.P. (1997). *Evolutionary Structural Optimization.* Springer-Verlag London.

- Yang, R.J., & Chen, C.J. (1996). Stress-based topology optimization. *Structural Optimization, 12.*

- Yin, L., & Ananthasuresh, G. (2003). Design of Distributed Compliant Mechanisms. *Mechanics Based Design of Structures and Machines, 31.* https://doi.org/ 10.1081/SME-120020289

- Young, V., Querin, O.M., Steven, G.P., & Xie, Y.M. (1999). 3D and multiple load case bi-directional evolutionary optimization (BESO). *Structural Optimization, 18*

Image Sources

-**Figure 1**: Experiments with cast glass and kiln-casting technique (a)Glass sculpture. From https://www.pollittstudio.com/classic-moves (n.d.). (b) Interlocking glass components. From (Oikonomopoulou, 2019) (c) Glass components with customized shape. From (Bhatia, 2019) and (Damen, 2019).

-**Figure 2**: Glass brick structures with metal substructure at (top) Optical House, from https://www.dezeen.com/2013/01/27/optical-glass-house-by-hiroshi-nakamura-nap/amp (n.d.), or adhesively bonded at (bottom left) Atocha Memorial, from https://www.bellapart.com/project/monumento-11m (n.d.) and (bottom right) Crystal Houses Façade, from (Oikonomopoulou, 2019).

-**Figure 3**: Size and annealing time for glass bricks of different glass compositions. From (Oikonomopoulou et al., 2020).

-**Figure 4**: 'Opposites of white' by Roni Horn displayed in Kroller Moller museum. From https://krollermuller.nl/en/roni-horn-opposites-of-white (n.d.)

-**Figure 5**: Size and annealing time for different telescope lens. From (Oikonomopoulou et al., 2020).

-**Figure 6**: Diagram of the research methodology as followed in the project. (Own editing).

-**Figure 7**: Axonometric of the intervention & location of glass slab. From https://arquitecturaviva.com/works/renovacion-del-british-museum-2 & own editing

-**Figure 8**: Drawings & photos of the existing glass slab (Own editing & own photo archive)

-**Figure 9**: Properties based on the different glass composition. From (Oikonomopoulou, 2019), based on data from (Shand & Armistead, 1958) and (Martlew, 2005).

-**Figure 10**: Casting defects as seen through the microscope. (a) Inclusions, (b) Edge Crack. Photos by Telesilla Bristogianni

-**Figure 11**: Diagram illustrating how the crack propagates under tension but closes/remains unaffected during compression. From (Damen, 2019).

-**Figure 12**: (a) Primary and (b) secondary casting glass process. From (Oikonomopoulou, 2019)

-**Figure 13**: Diagram of viscosity as a function of temperature for a soda-lime melt. From (Shelby,2005).

-**Figure 14**: Typical annealing scheme for soda-lime glass. From (Oikonomopoulou, 2019)

-**Figure 15**: Different scenarios that can help in avoiding cracking because of thermal shock (from top to bottom: weight reduction, sharp edges, unequal mass distribution). From (Damen, 2019)

- **Figure 16**: 3d-printed sand moulds used for the casting of (top left & middle) concrete slab, from https://dbt.arch.ethz.ch/project/smart-slab and (Aghaei-Meibodi et.al., 2017)), (top right) steel node, from Arup/Davidfotografie , (bottom left & middle) cast glass node (Damen, 2019) and (bottom right) cast glass prototype (Bhatia, 2019)

-**Figure 17**: Diagrams for (left) Size, (middle)Shape and (right)Topology Optimization problems. From (Allaire et al, 2019).

-**Figure 18**: Inner structures in Homogenization method & SIMP approach. From (Kumar, 2016).

-**Figure 19**: Mesh dependence in optimization of MBB-beam example with SIMP approach. Solution for discretization with a) 2700, b) 4800 and c) 17200 elements. From (Bendsoe & Sigmund, 2004).

-**Figure 20**: Geometric singularities. (a) Checkerboard pattern (b) Point Flexures (c) Layering & Islanding. Adapted from (Kumar, 2016) &(Bendsoe & Sigmund, 2004) & (Yin & Ananthasuresh, 2003) & (Saxena, 2011).

-**Figure 21**: Jagged boundary after the optimization of a loaded knee-structure. From (Bendsoe & Sigmund, 2004).

-**Figure 22**: Process followed in the bubble method approach. From (Eschenauer et al., 1994).

Appendix

A.1 Structural Validation

A.1.1 MBB Beam

Vertical deformation obtained from (a) ANSYS (b) Matlab code.

Maximum principal stress obtained from (a) ANSYS (b) Matlab code.

Minimum principal stress obtained from (a) ANSYS (b) Matlab code.

A.1.2 Case Study Slab

Vertical deformation obtained from (a) ANSYS (b) Matlab code.

Maximum principal stress obtained from (a) ANSYS (b) Matlab code.

Minimum principal stress obtained from (a) ANSYS (b) Matlab code.

A.2 Optimization

A. 2.1 Optimization Options & Tolerances

Algorithm	interior-point
Barrier Parameter Update	predictor-connector
Display	iterative
Enable Feasibility Mode	true
Hessian Approximation	lbfgs
Max Function Evaluations	700000
Max Iterations	700000
Optimality Tolerance	1e-10
Step Tolerance	1e-09
Sub Problem Algorithm	cg
Constraint Tolerance	1e-06

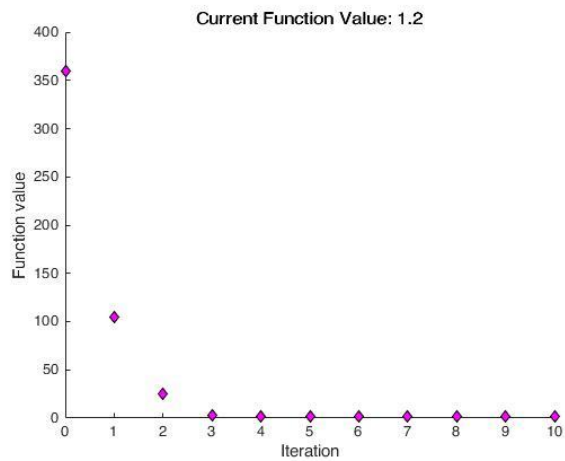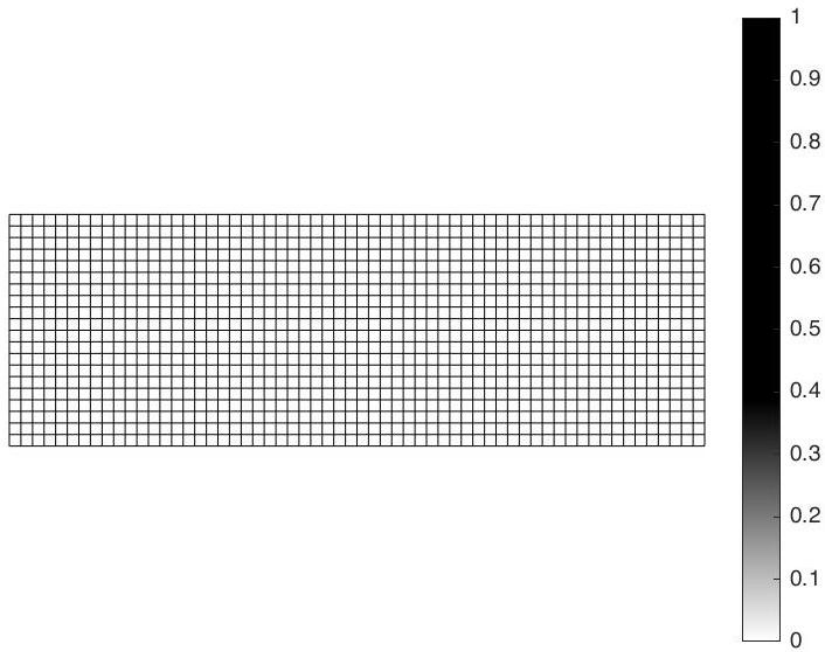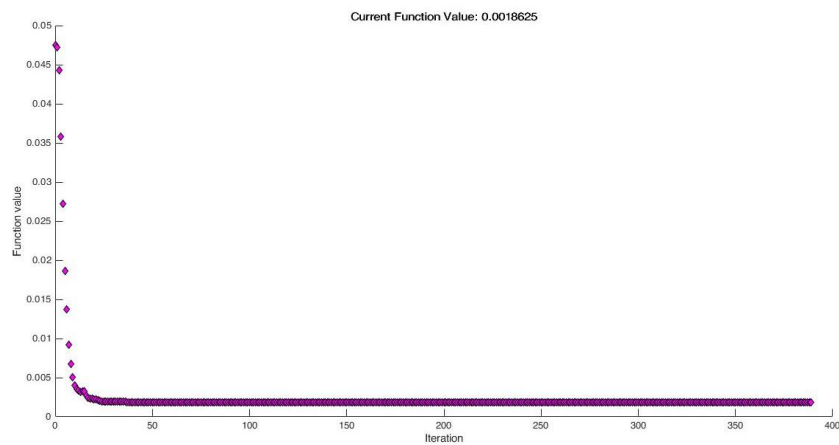## A.2.2 MBB Beam results[61]

A.2.2.1 Volume Constraint (30%)
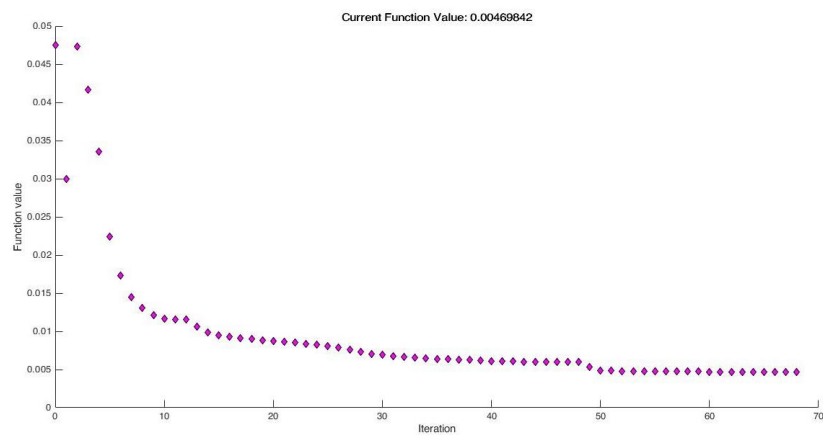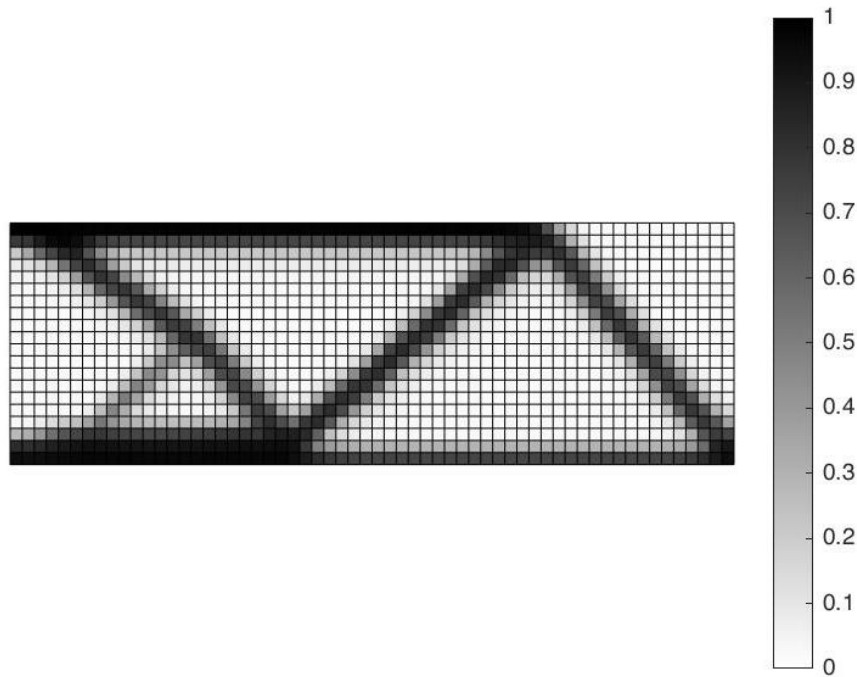
Optimization result & Plot of function values per iteration: Compliance Objective / Volume Constraint

Final function value	Iterations	Function evaluations	Feasibility	First-order Optimality	Time (hours : minutes)
0.00469	68	82869	0	9,85e-07	01:51

---

[61] In every result the final outcome along with plot of the function values are going to be demonstrated in order to show the convergence trajectory. In the respective tables, the degree of zero approximation regarding feasibility and first-order optimality numbers shows if the result from the iteration is feasible – respecting the constraints posed – and how close it is to an optimum solution respectively.

A.2.2.2 Compliance Constraint

a. $\alpha_c = 1,1$
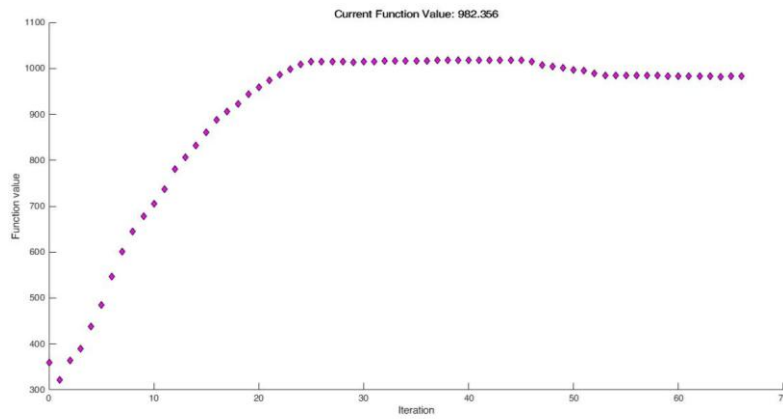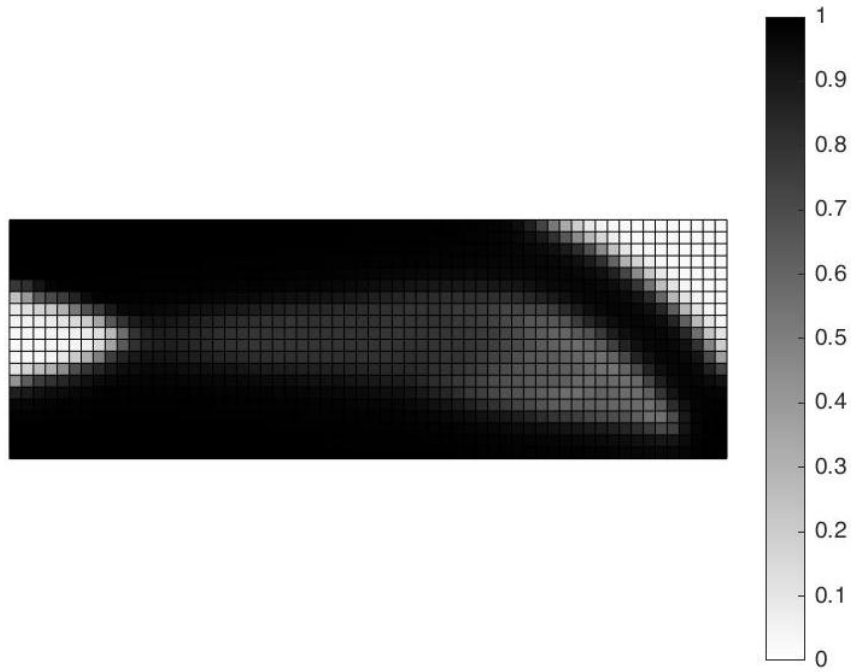
Current Function Value: 982.356

Optimization result & Plot of function values per iteration: Volume Objective / Compliance Constraint (α_c=1,1).

Final function value	Iterations	Function evaluations	Feasibility	First-order Optimality	Time (hours : minutes)
982.36	66	80467	0	1,9e-01	01:51

b. $\alpha_c = 1,5$
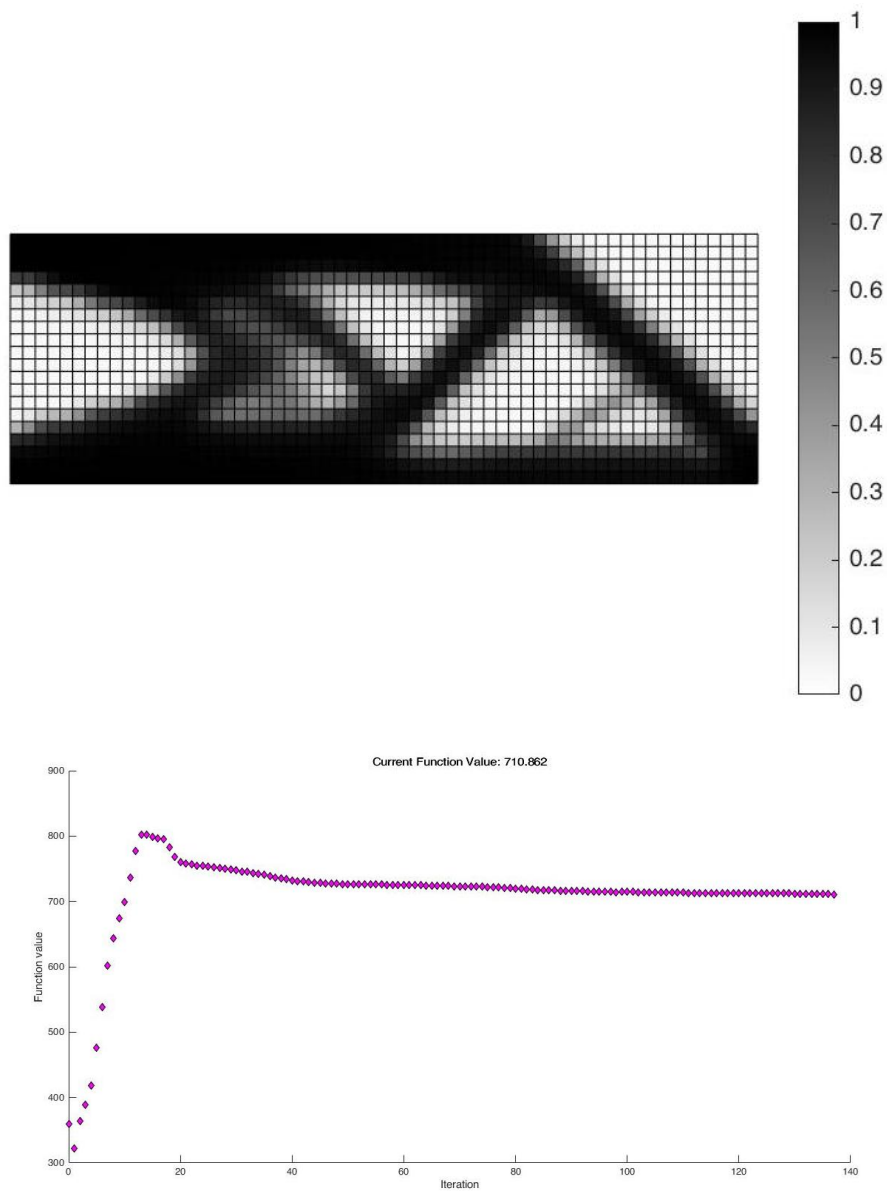
Optimization result & Plot of function values per iteration: Volume Objective / Compliance Constraint (α_c=1,5).

Final function value	Iterations	Function evaluations	Feasibility	First-order Optimality	Time (hours : minutes)
710.86	137	165738	0	1,7e-01	03:44

c. $\alpha_c = 2$
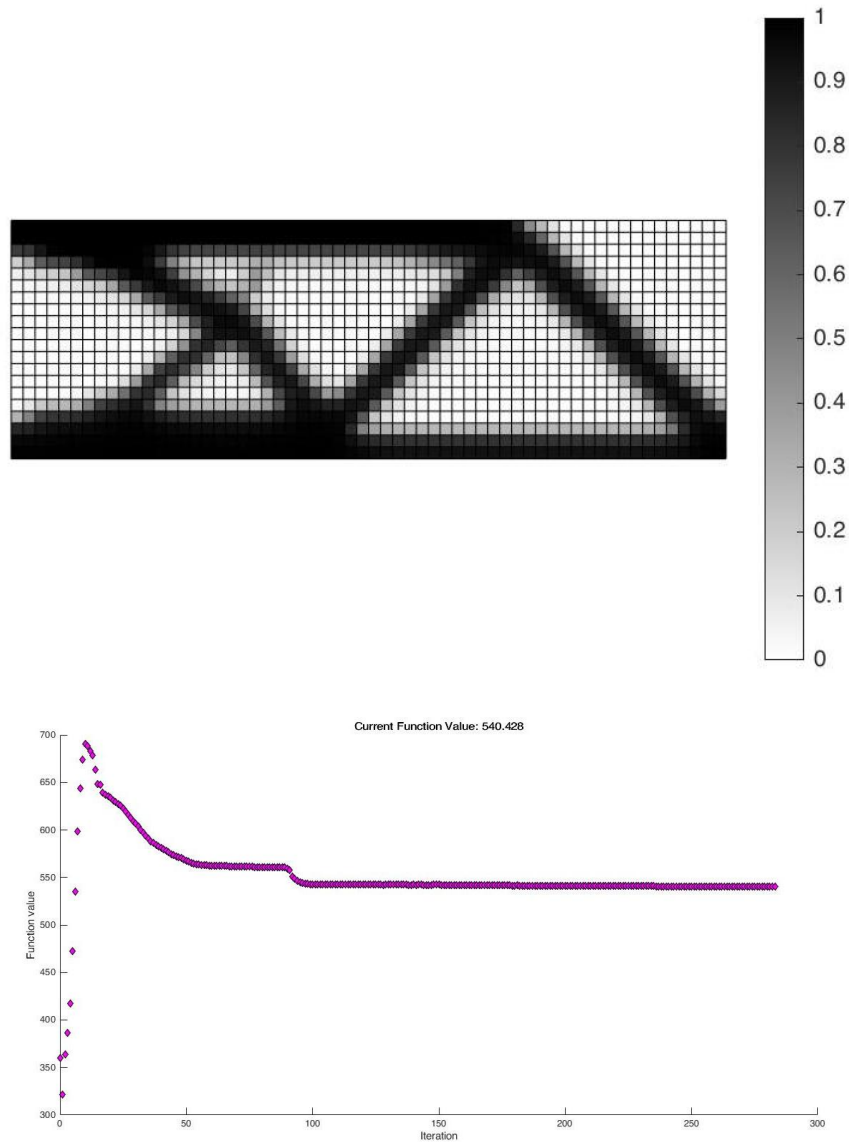
Optimization result & Plot of function values per iteration: Volume Objective / Compliance Constraint (α_c=2).

Final function value	Iterations	Function evaluations	Feasibility	First-order Optimality	Time (hours : minutes)
540.43	283	341100	0	7,05e-02	07:51

d. $\alpha_c = 2{,}5$
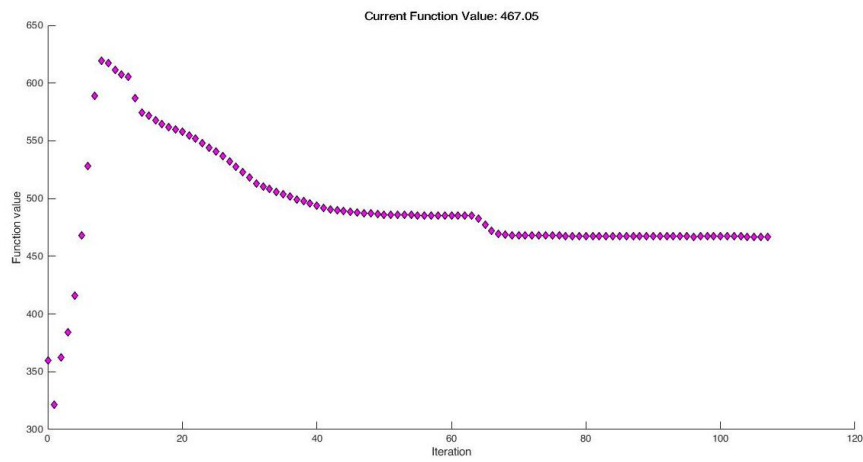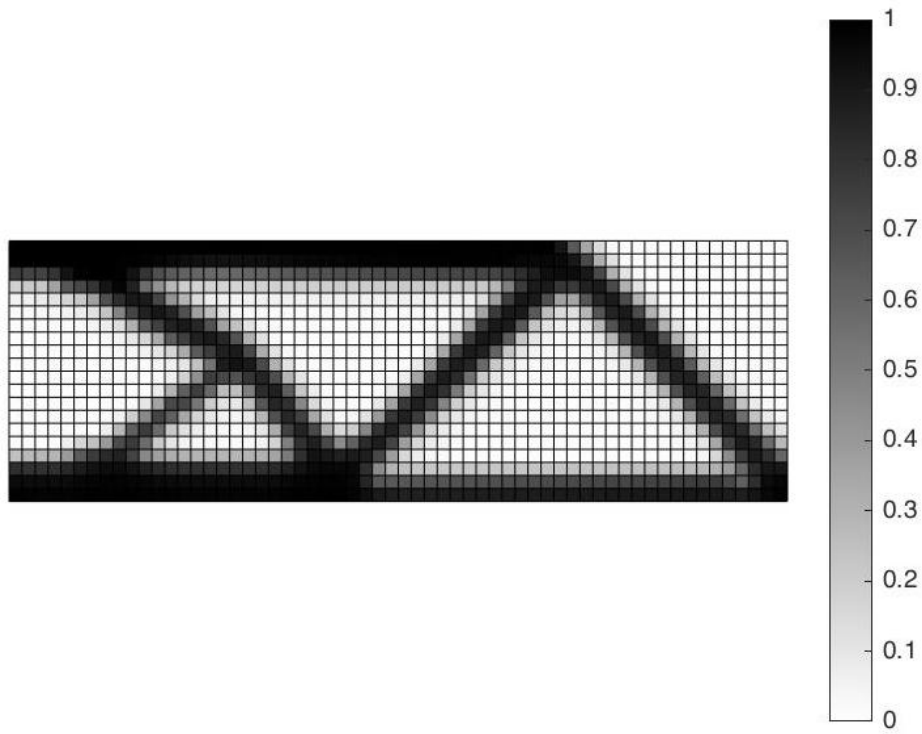
Optimization result & Plot of function values per iteration: Volume Objective / Compliance Constraint (α_c=2,5).

Final function value	Iterations	Function evaluations	Feasibility	First-order Optimality	Time (hours : minutes)
467.05	107	129708	0	2,40e-02	02:50

A.2.2.2 Deflection Constraint

a. Volume Objective
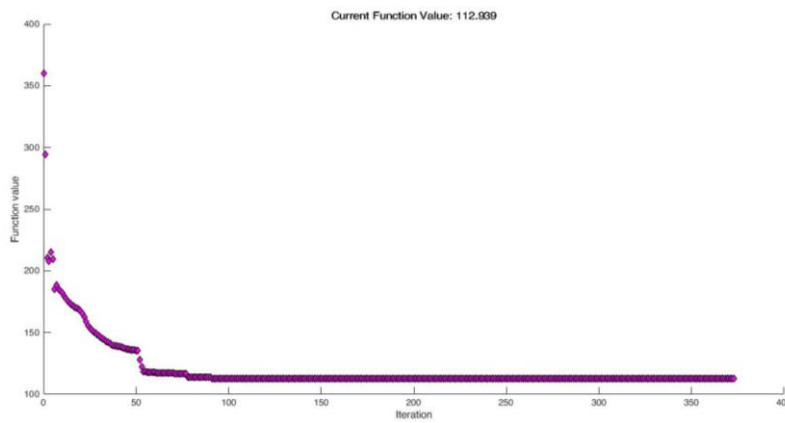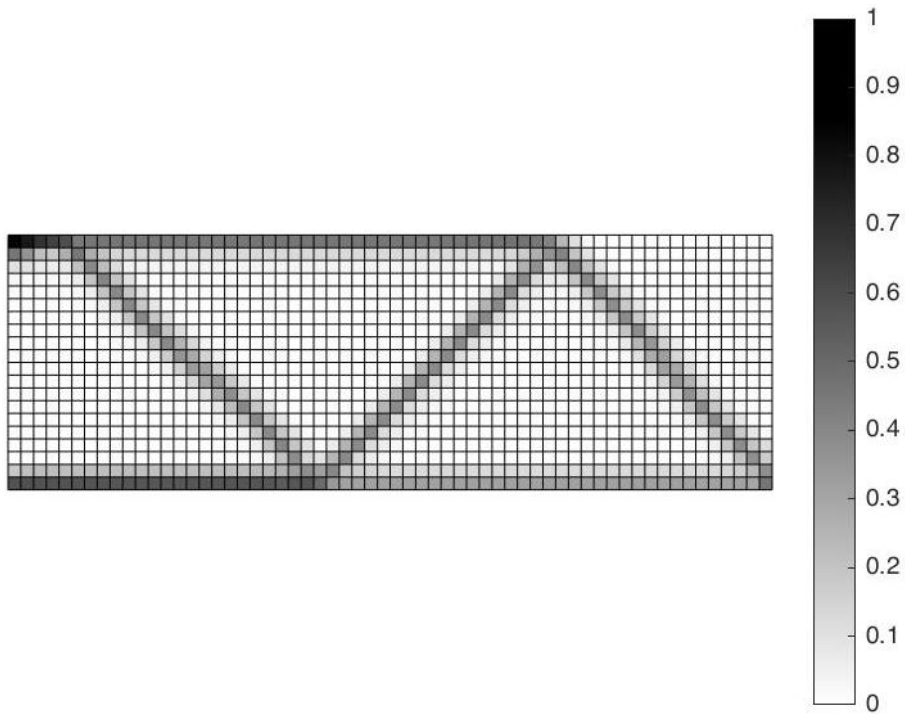
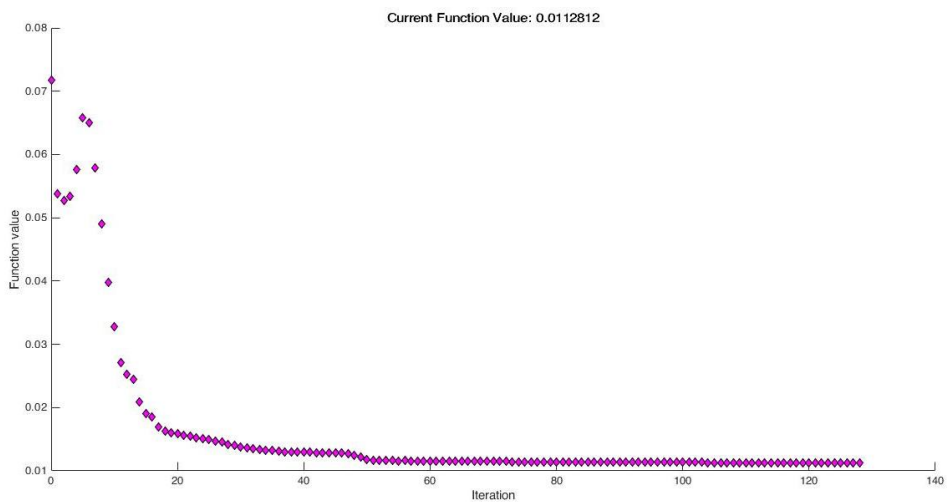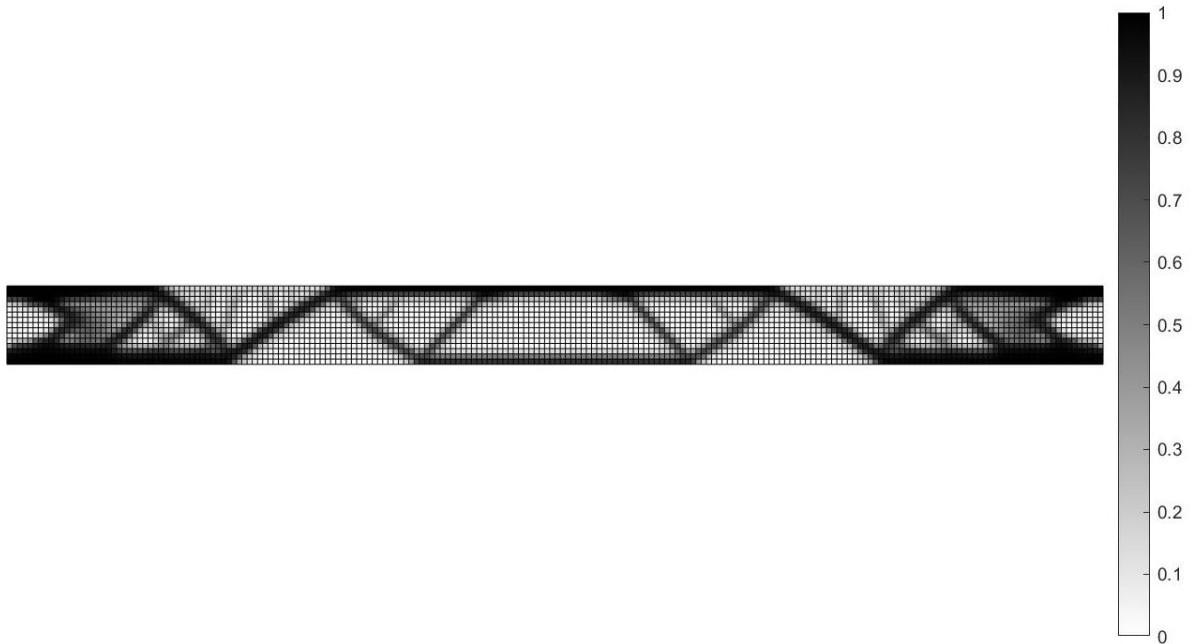*Optimization result & Plot of function values per iteration: Volume Objective / Deflection Constraint.*

Final function value	Iterations	Function evaluations	Feasibility	First-order Optimality	Time (hours : minutes)
112.94	373	449375	0	1,3e-03	14:43

A.2.2.2 Deflection Constraint

b. Compliance Objective
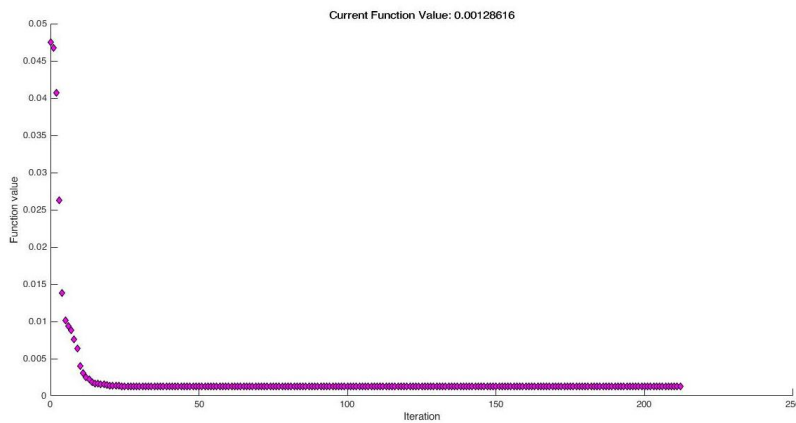
Optimization result & Plot of function values per iteration: Compliance Objective / Deflection Constraint.

Final function value	Iterations	Function evaluations	Feasibility	First-order Optimality	Time (hours : minutes)
0.00129	212	255987	0	3,79e-08	11:31

A.2.2.2 Principal Stresses Constraint

a. Volume Objective
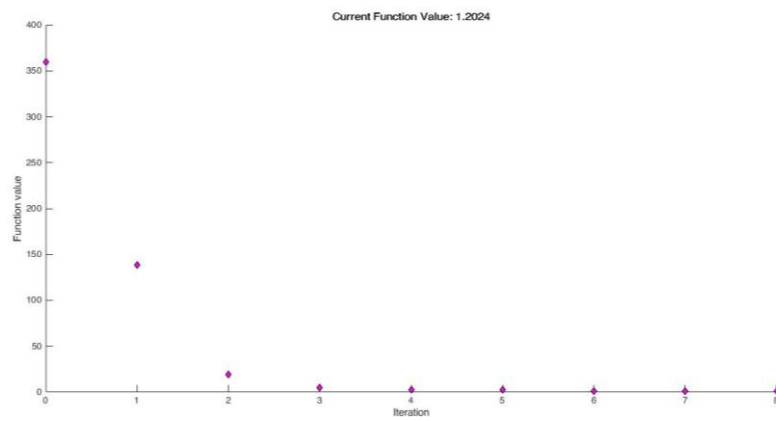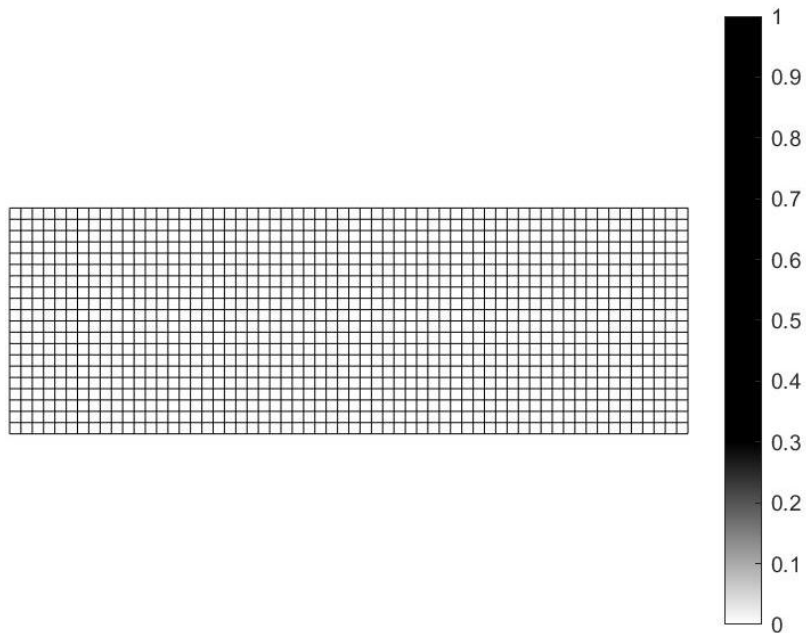
Optimization result & Plot of function values per iteration: Volume Objective / Principal Stresses Constraint.

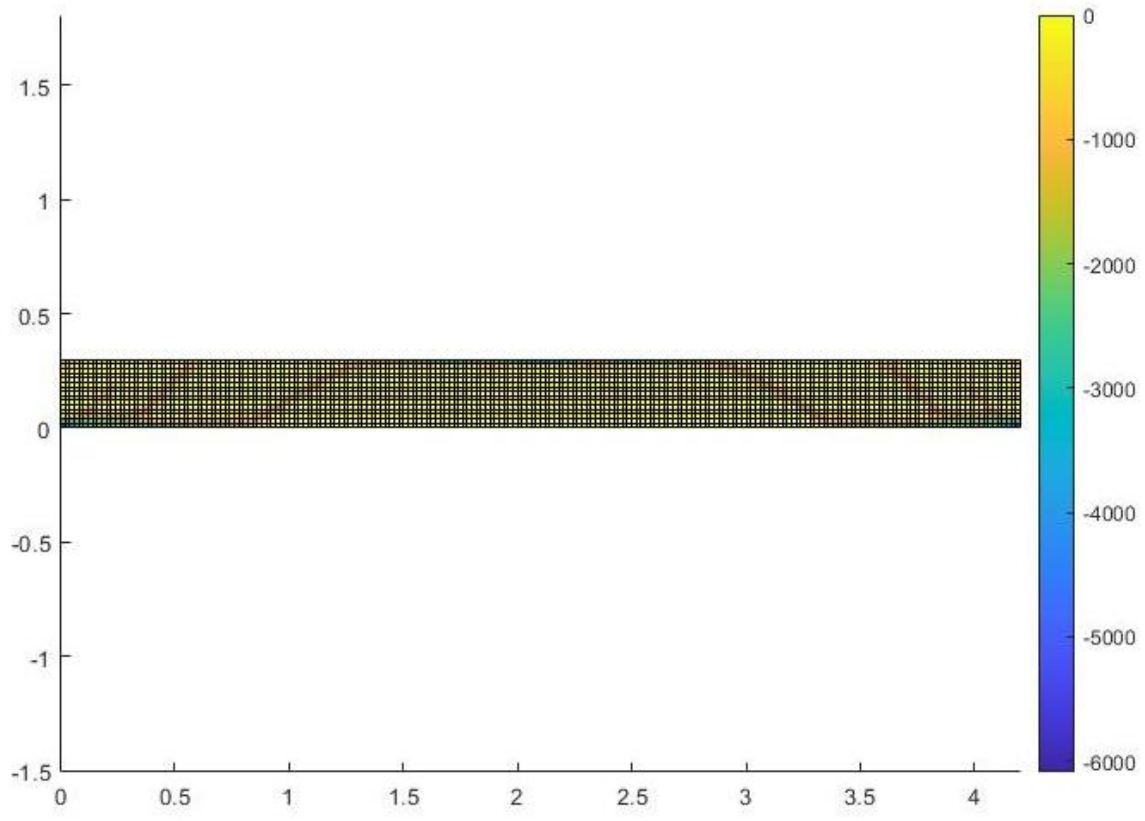| Final function value	Iterations	Function evaluations	Feasibility	First-order Optimality	Time (hours : minutes)
1.2	8	10809	0	2,30e-06	00:17

A.2.2.2 Principal Stresses Constraint

b. Compliance Objective
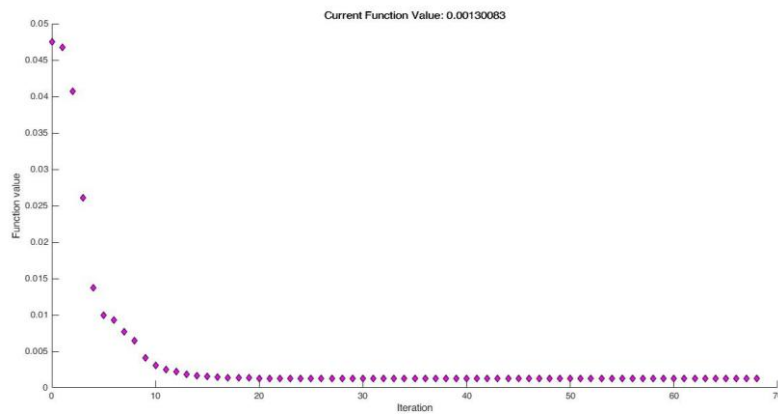
Optimization result & Plot of function values per iteration: Compliance Objective / Principal Stresses Constraint.

Final function value	Iterations	Function evaluations	Feasibility	First-order Optimality	Time (hours : minutes)
0.0013	66	80532	0	6,50e-08	04:00

A.2.2.3 Annealing & Manufacturing Constraint (d_{max})

a. Volume Objective

Optimization result & Plot of function values per iteration: Volume Objective / Annealing & Manufacturing Constraint.

Final function value	Iterations	Function evaluations	Feasibility	First-order Optimality	Time (hours : minutes)
1.2	10	13211	0	6,07e-11	00:09

A.2.2.3 Annealing & Manufacturing Constraint (d_{max})

b.   Compliance Objective
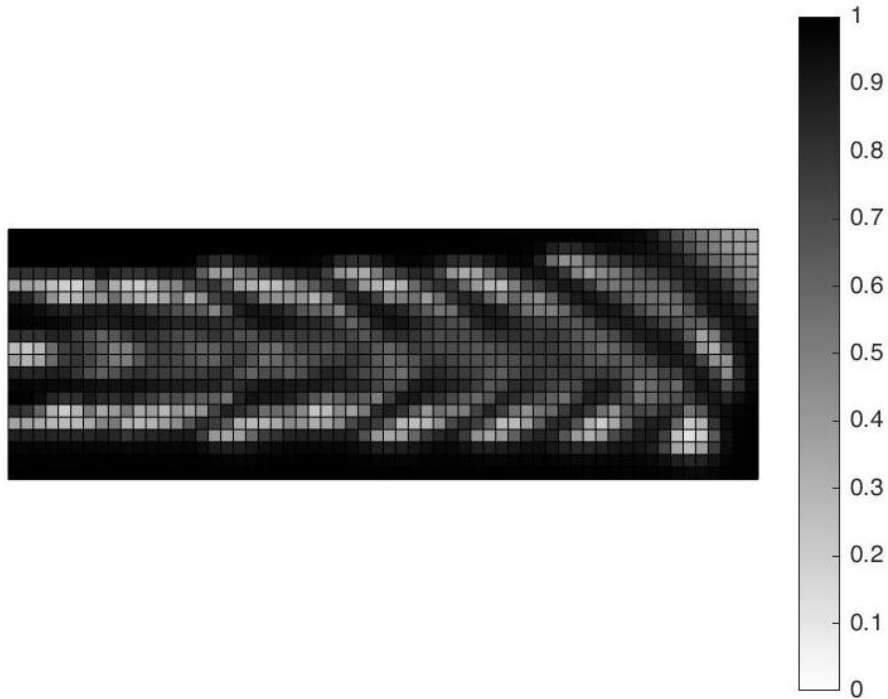
Optimization result & Plot of function values per iteration: Compliance Objective / Annealing & Manufacturing Constraint.

Final function value	Iterations	Function evaluations	Feasibility	First-order Optimality	Time (hours : minutes)
0.00186	390	415078	0	3,54e-05	15:25

A.2.2.4 Drucker - Prager Material Failure criterion

a. Volume Objective
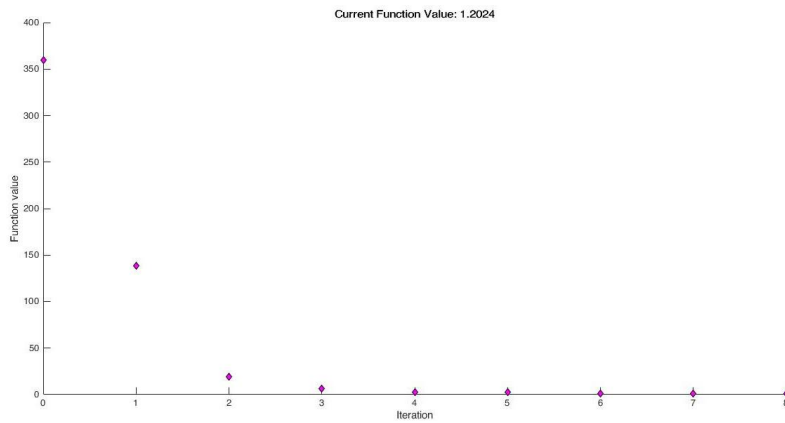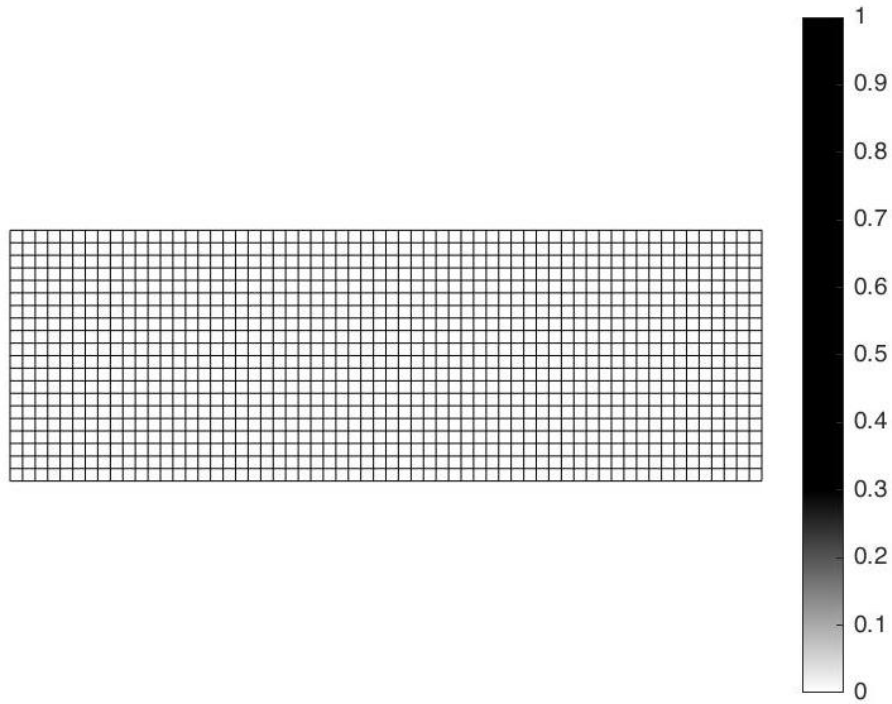
Optimization result & Plot of function values per iteration: Volume Objective / Drucker - Prager Failure Criterion Constraint.

Final function value	Iterations	Function evaluations	Feasibility	First-order Optimality	Time (hours : minutes)
1.2024	8	10809	0	2,28e-06	00:20

A.2.2.4 Drucker - Prager Material Failure criterion

b. Compliance Objective
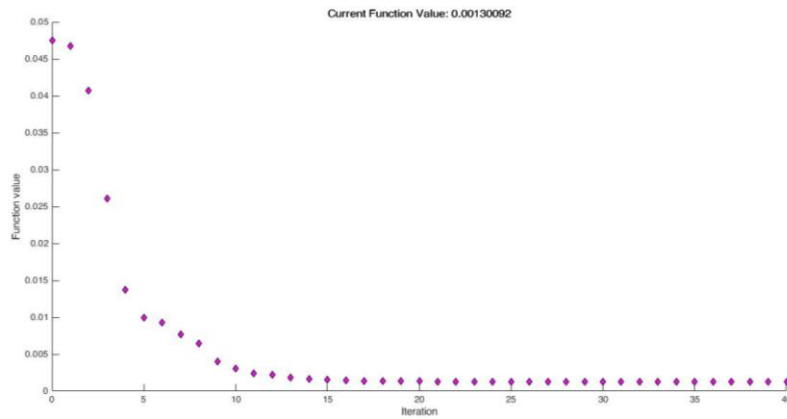
Optimization result & Plot of function values per iteration: Compliance Objective / Drucker - Prager Failure Criterion Constraint.

Final function value	Iterations	Function evaluations	Feasibility	First-order Optimality	Time (hours : minutes)
0.0013	40	49278	0	5.80e-08	03:30

A.2.3 Case Study results

A.2.3.1 Compliance Objective

Optimization result & Plot of function values per iteration: Compliance Objective / Volume, Displacement, Principal Stress and Annealing & Manufacturing Constraint.

Final function value	Iterations	Function evaluations	Feasibility	First-order Optimality	Time (hours : minutes)
0.01128	128	203562	0	4.24e-06	45:52
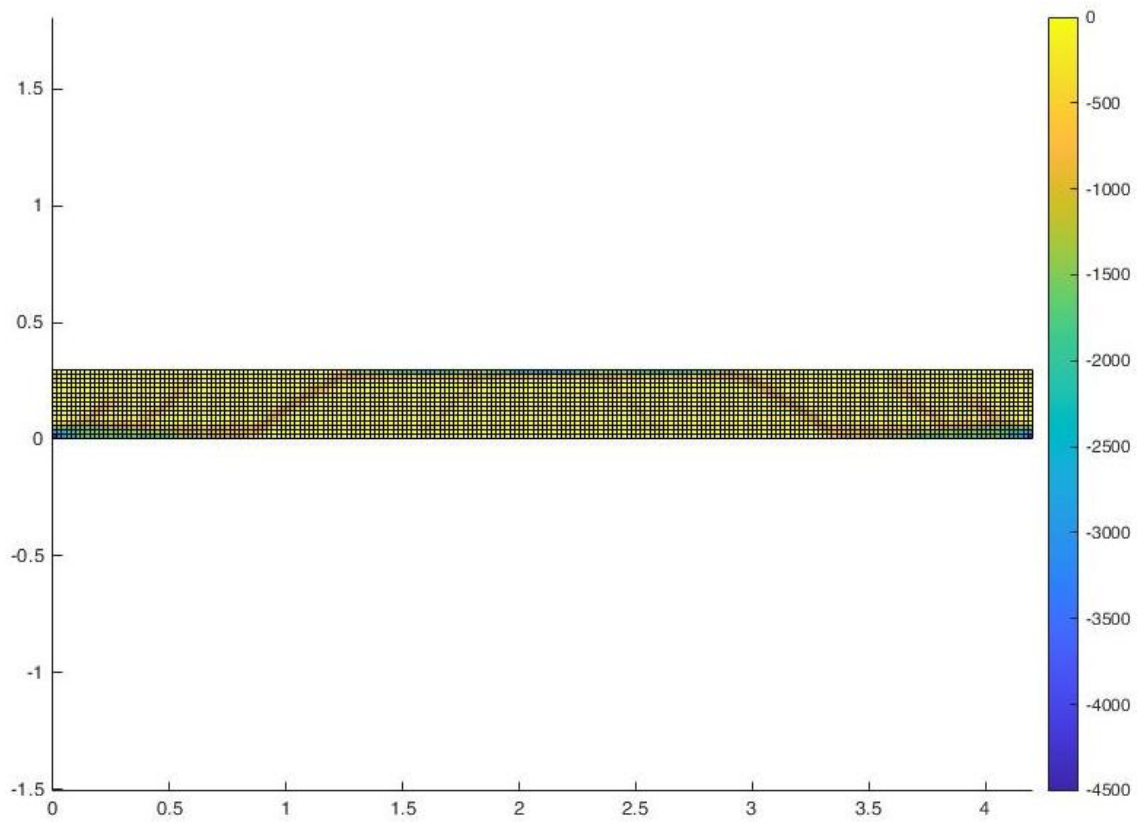
Minimum principal stress (Compression).
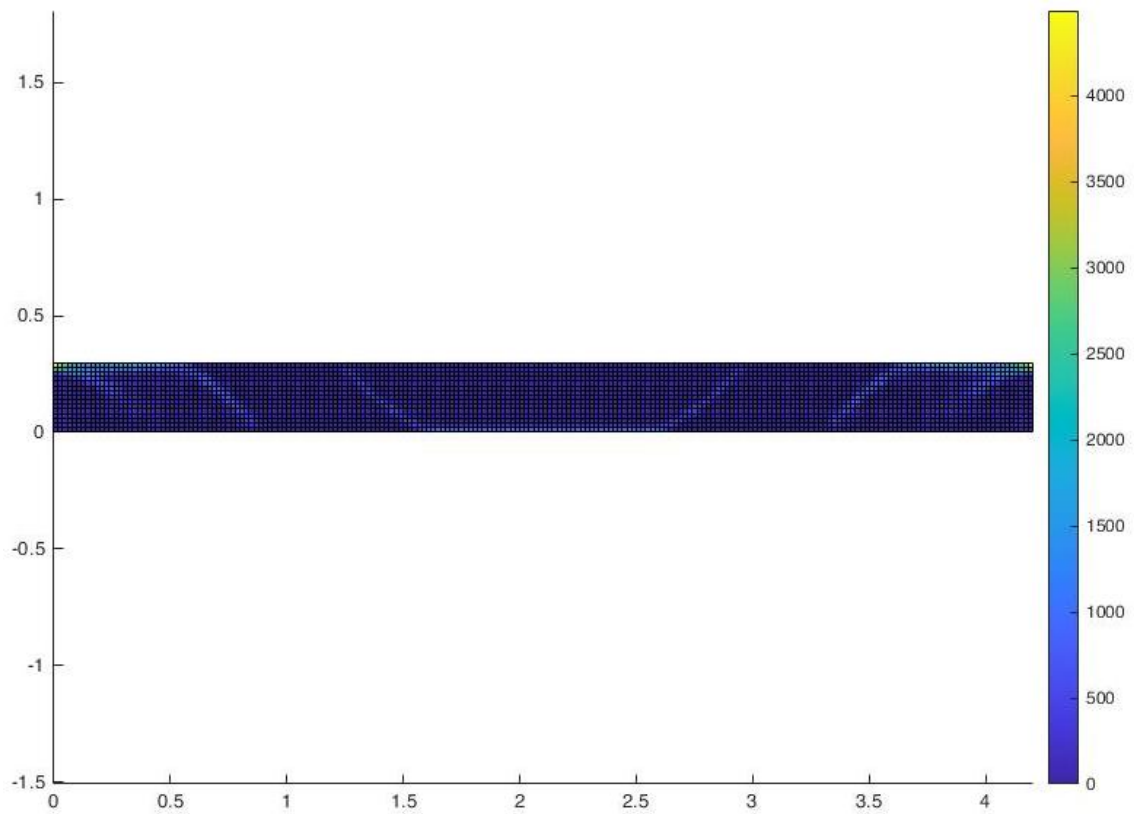
Maximum Principal Stress (Tension).

A.2.3.2 Volume Objective
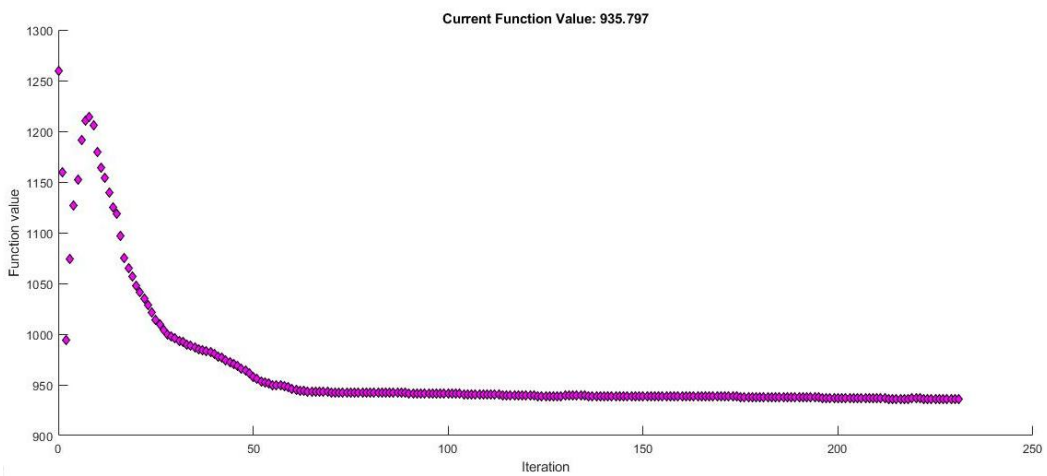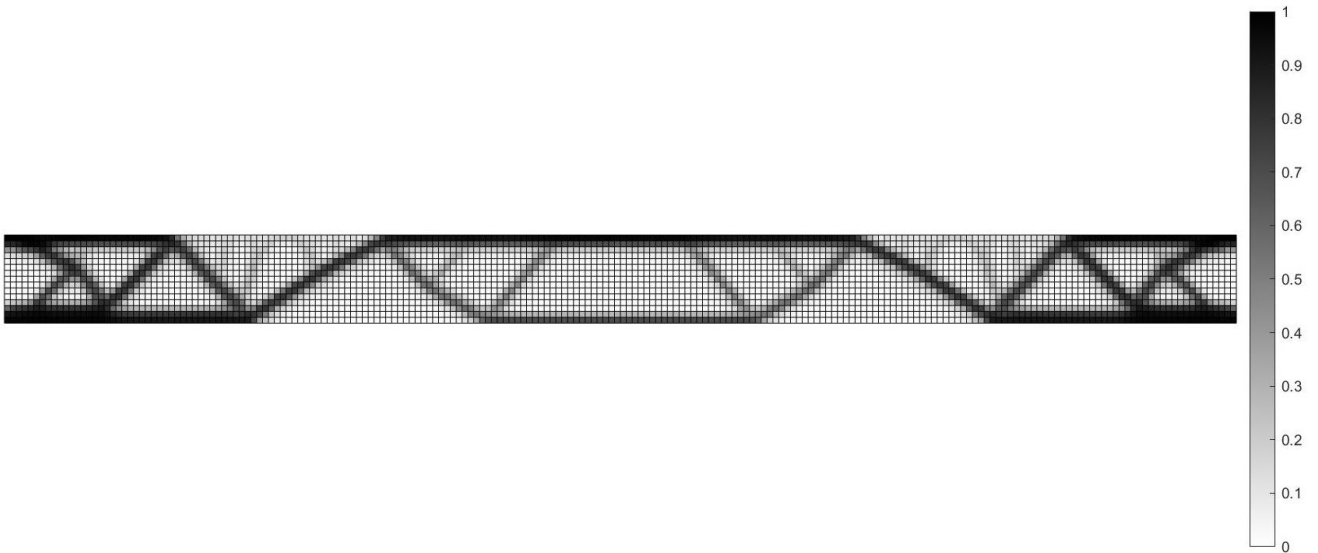
Optimization result & Plot of function values per iteration: Volume Objective / Compliance, Displacement, Drucker - Prager and Annealing & Manufacturing Constraint.

Final function value	Iterations	Function evaluations	Feasibility	First-order Optimality	Time (hours : minutes)
935.8	231	365727	0	1.61e-01	46:32

Minimum principal stress (Compression).
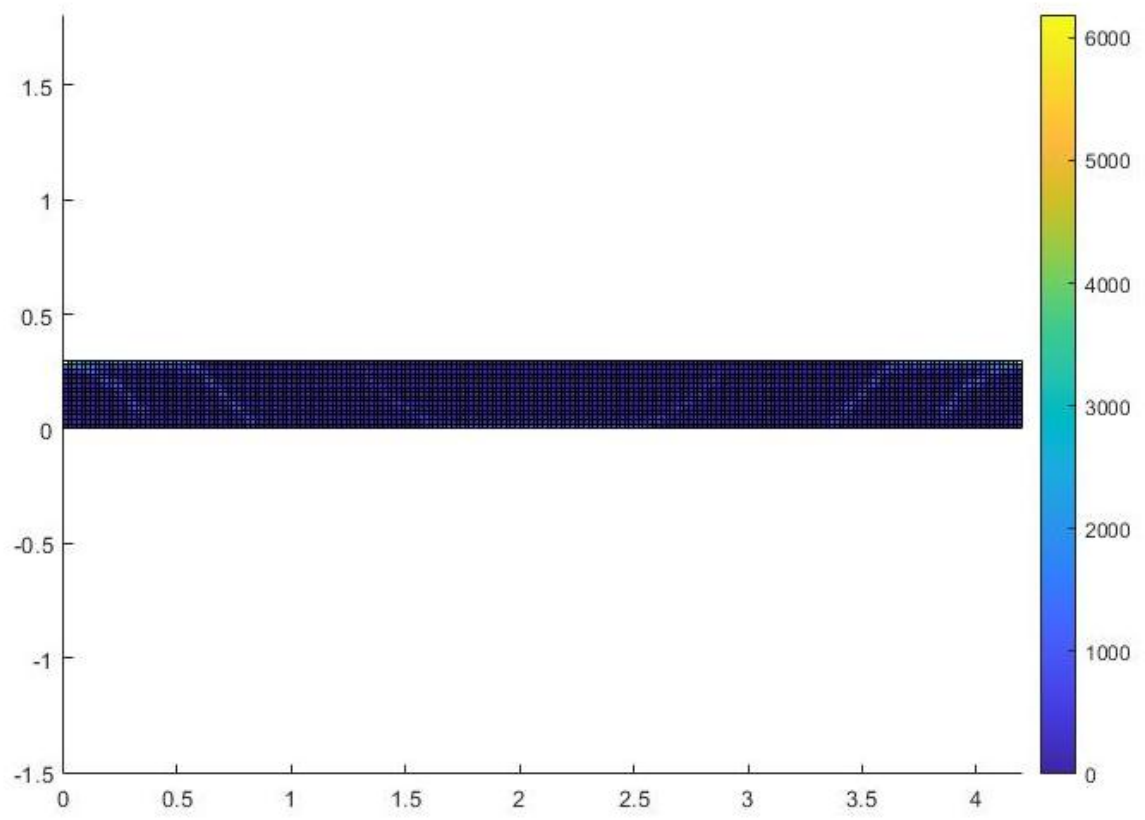
Maximum Principal Stress (Tension).

A.2.4 Design exploration

A.2.4.1 Cast glass – Soda lime
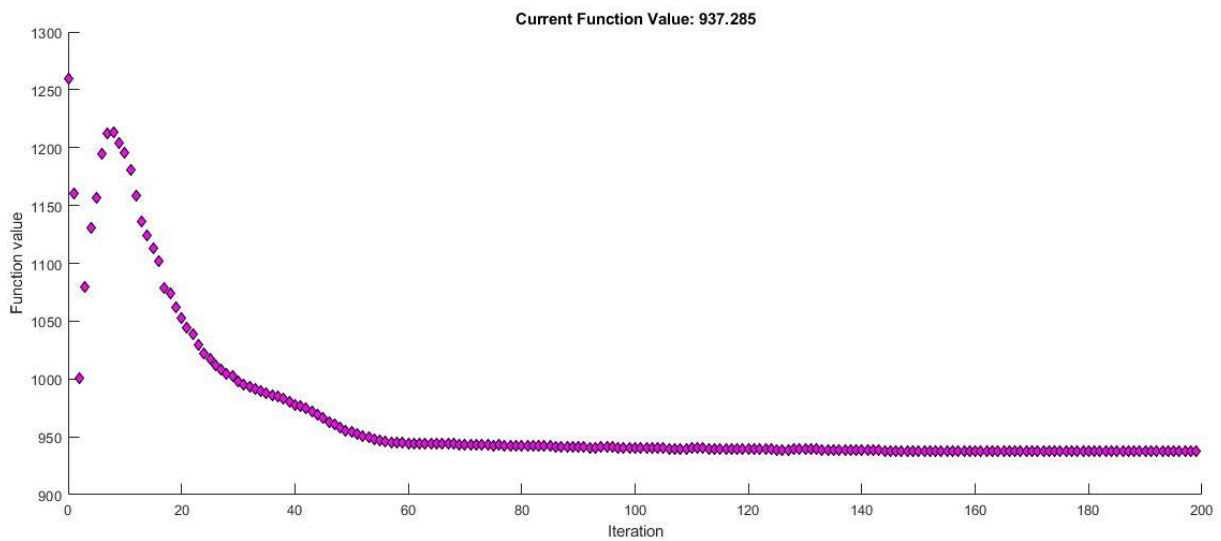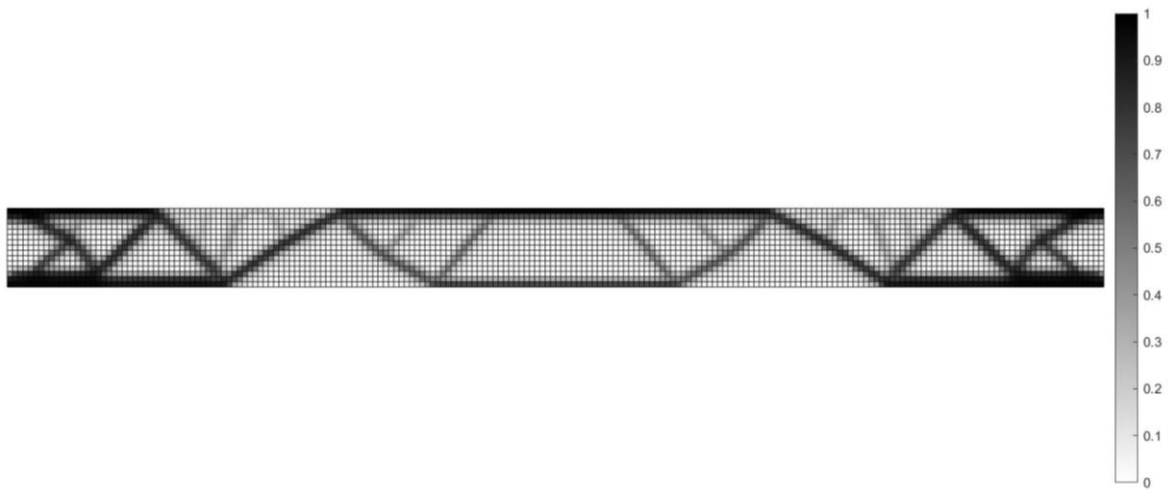
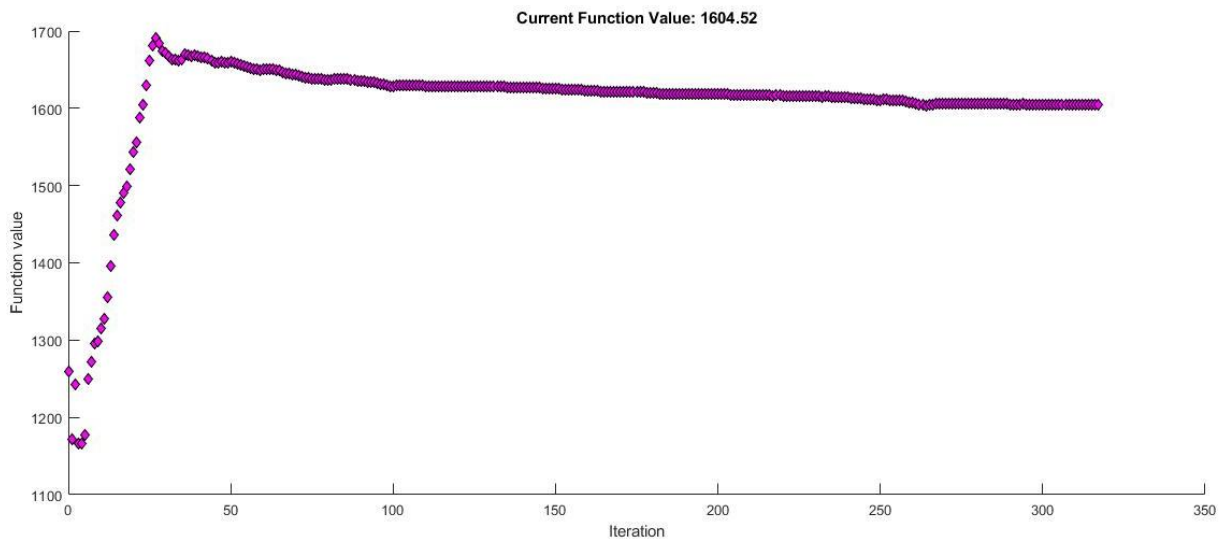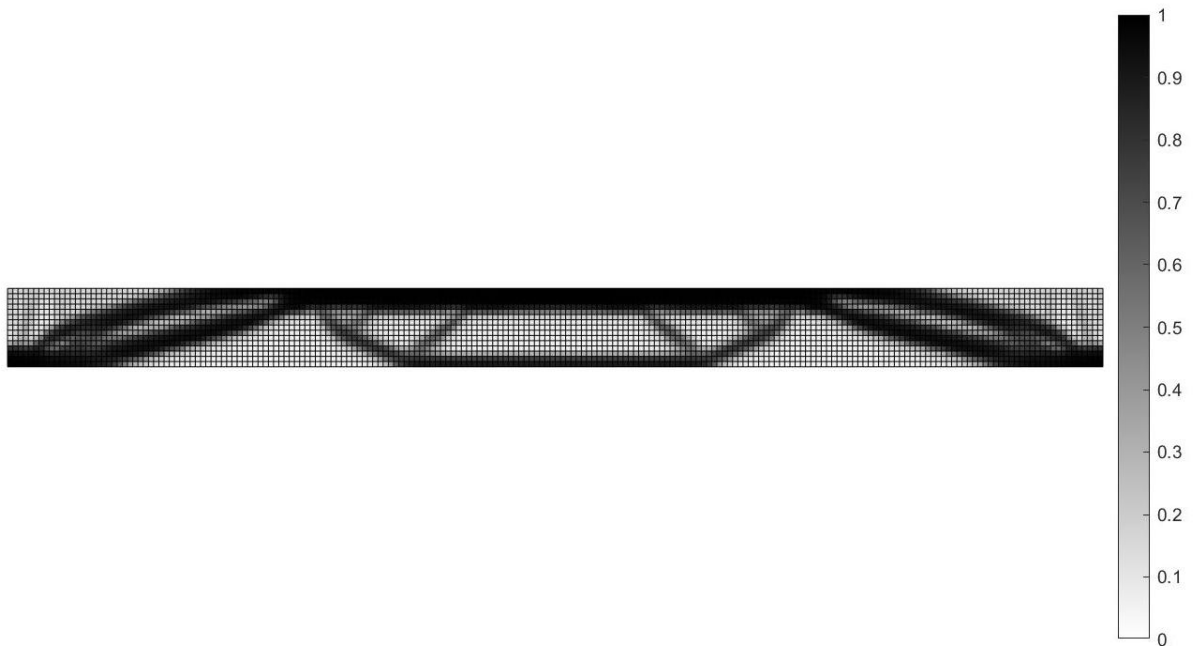*Optimization result & Plot of function values per iteration: Volume Objective & Compliance, Deflection & Principal Stresses Constraint (Soda lime glass).*

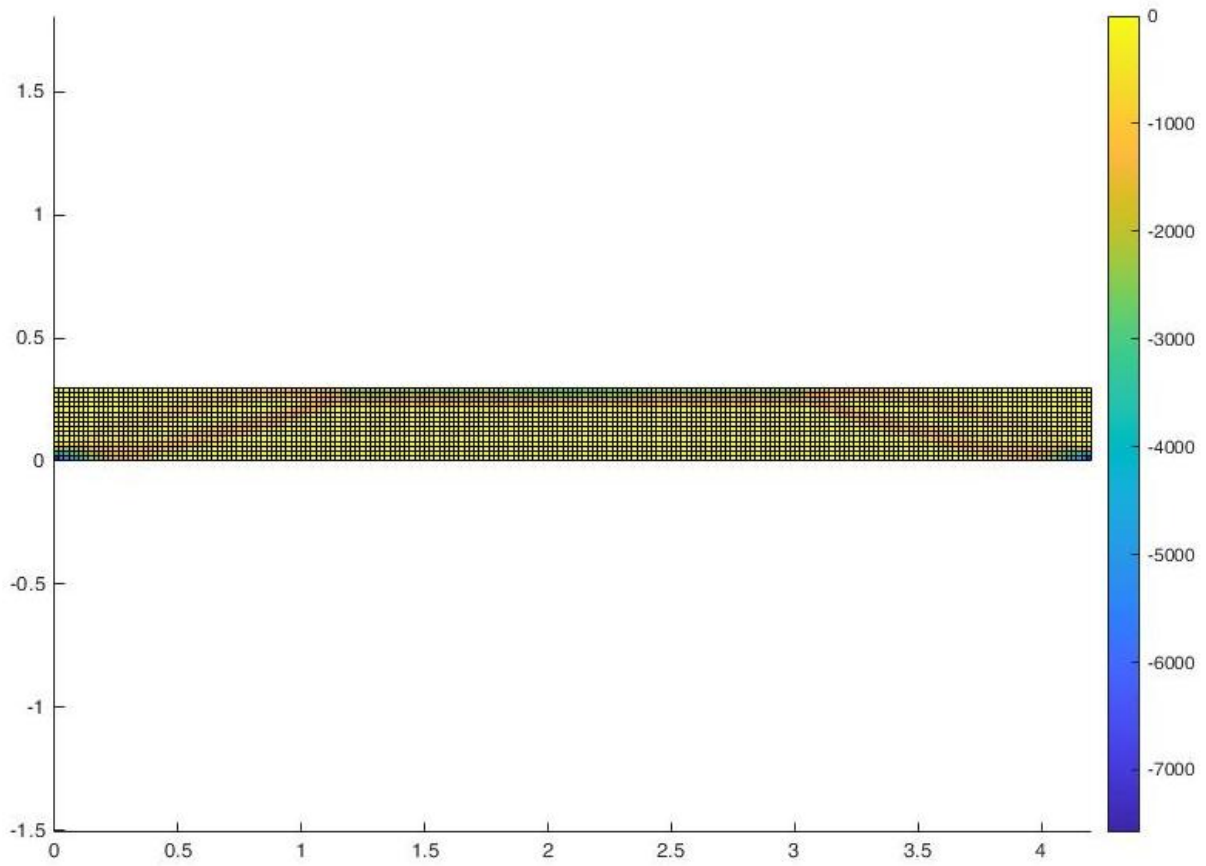| Final function value	Iterations	Function evaluations	Feasibility	First-order Optimality	Time (hours : minutes)
937.3	199	315285	0	1.43e-01	39:25

A.2.4.2 Float glass – Borosilicate
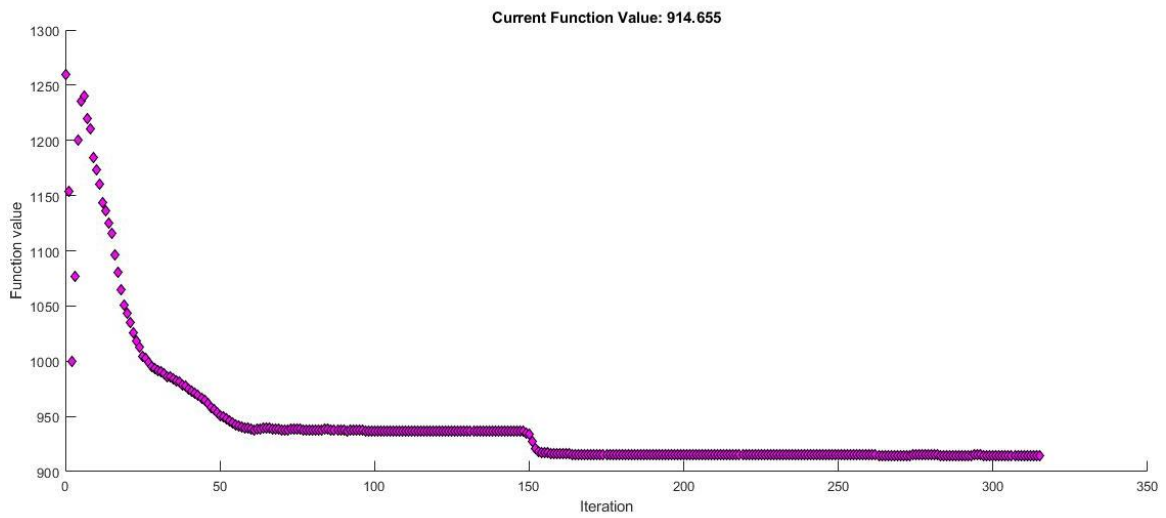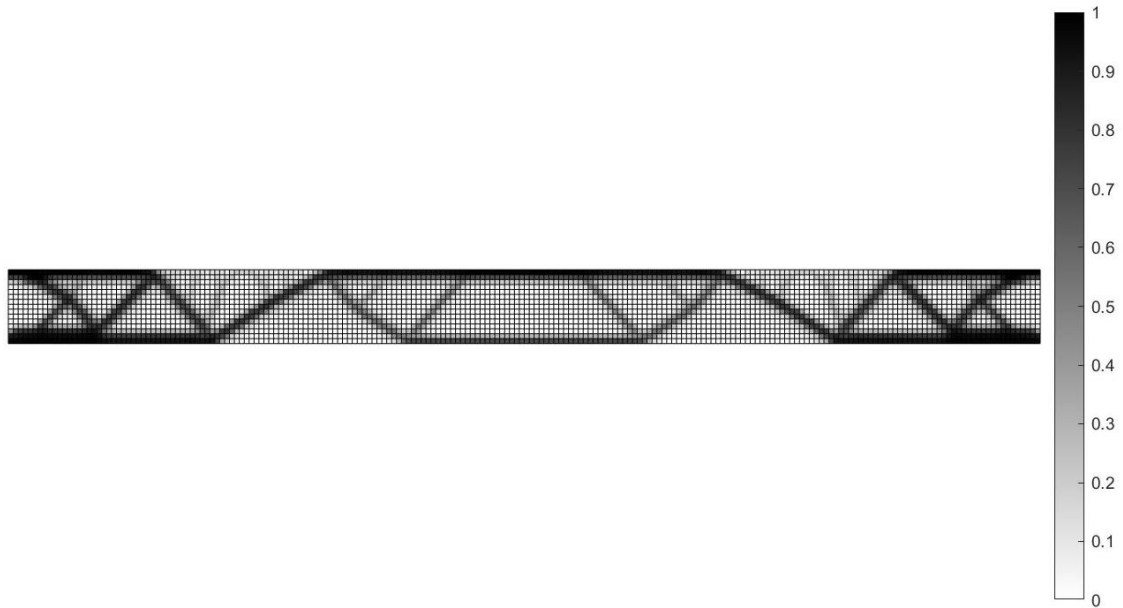
Optimization result & Plot of function values per iteration: Volume Objective & Compliance, Deflection & Principal Stresses Constraint (Float glass).

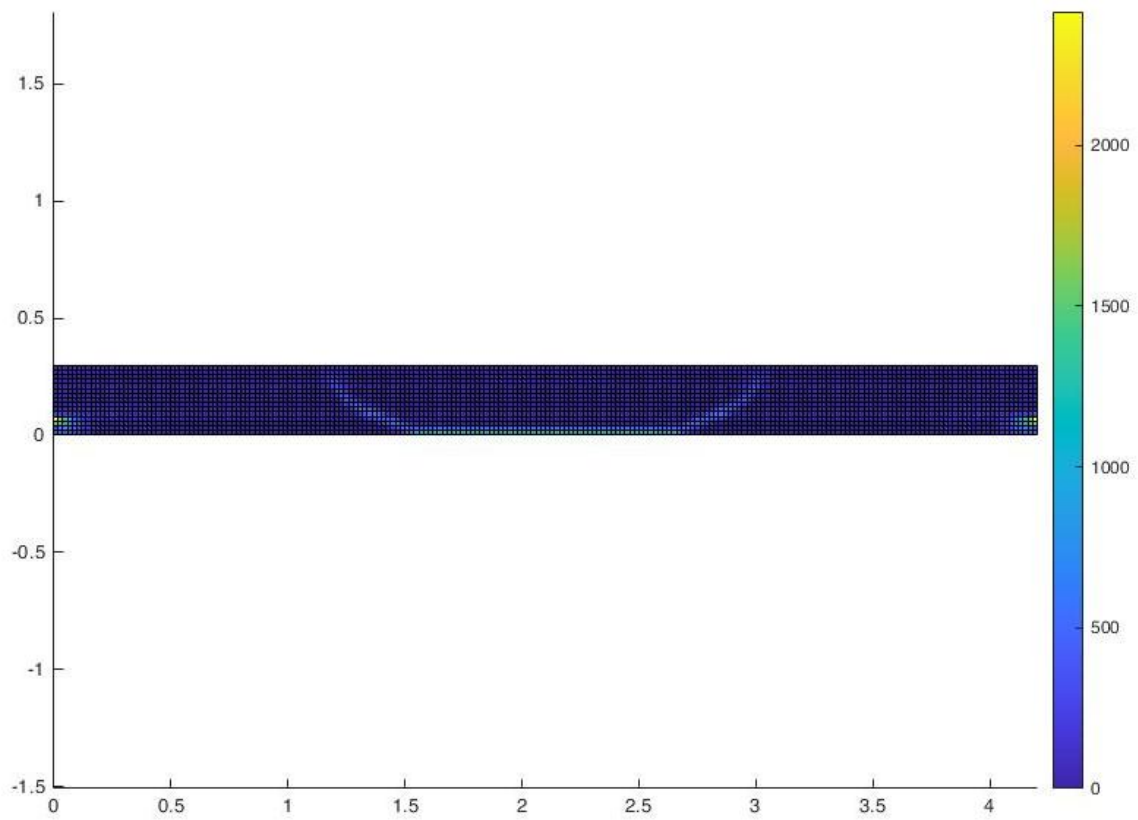| Final function value	Iterations	Function evaluations	Feasibility	First-order Optimality	Time (hours : minutes)
914.7	315	498070	0	1.46e-01	72:44

A.2.4.2 Point Supports – Borosilicate
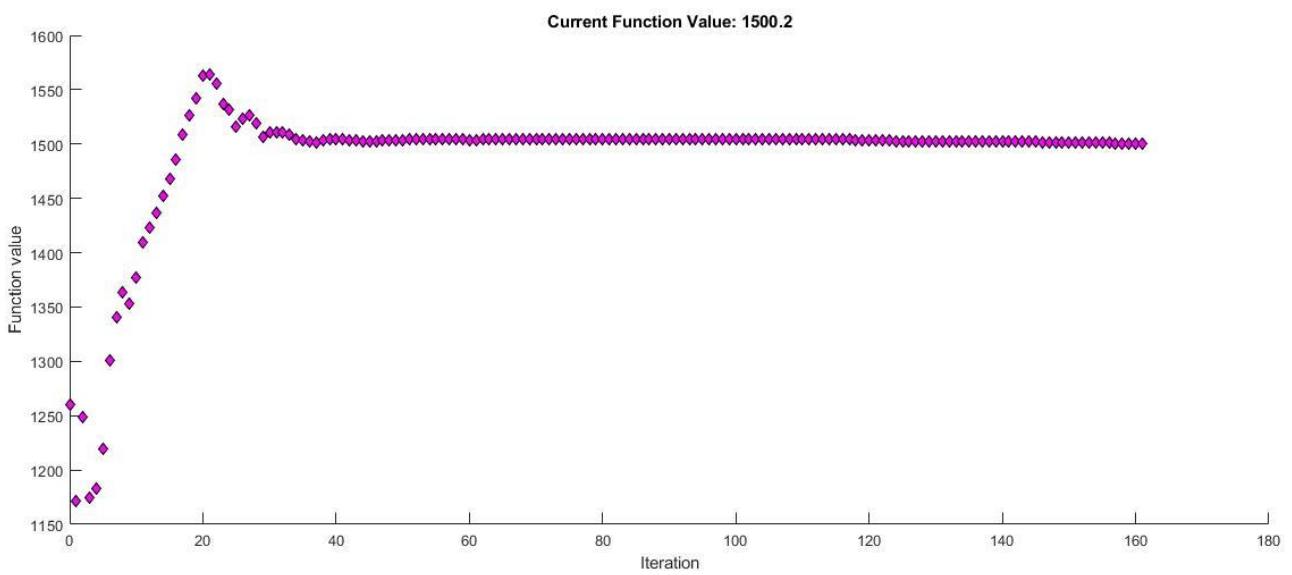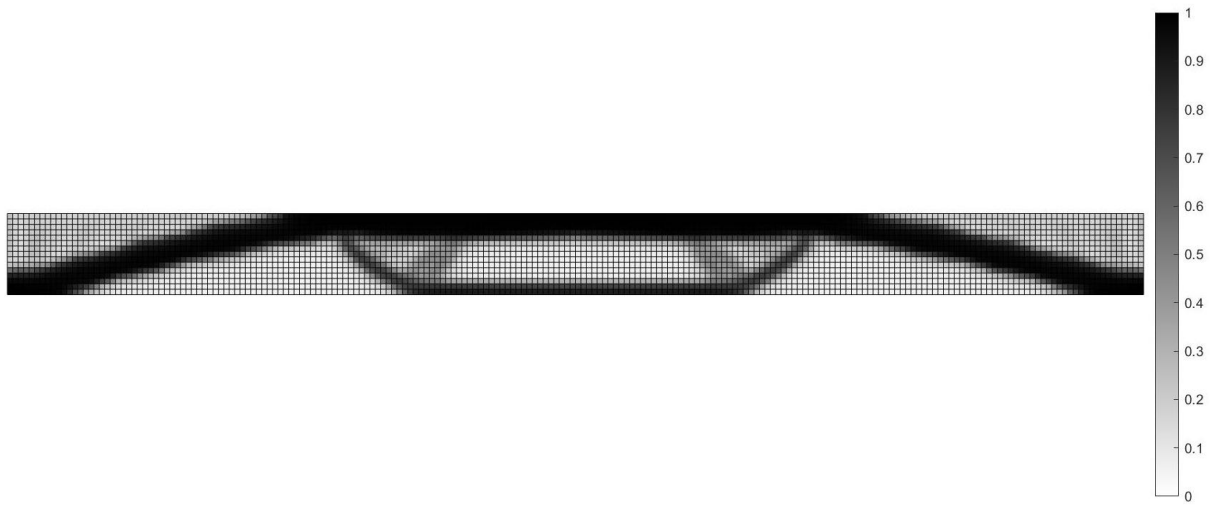
Optimization result & Plot of function values per iteration: Volume Objective & Compliance, Deflection, Annealing & Principal Stresses Constraint (Cast borosilicate glass & point supports).

Final function value	Iterations	Function evaluations	Feasibility	First-order Optimality	Time (hours : minutes)
1500.2	161	255442	0	9.5e-01	31:10

Minimum principal stress (Compression)

Maximum Principal Stress (Tension)

A.2.4.2 Point Supports – Soda lime

Optimization result & Plot of function values per iteration: Volume Objective & Compliance, Deflection, Annealing & Principal Stresses Constraint (Cast soda lime glass & point supports).

Final function value	Iterations	Function evaluations	Feasibility	First-order Optimality	Time (hours : minutes)
1604.5	317	501383	0	8.57e-01	72:53

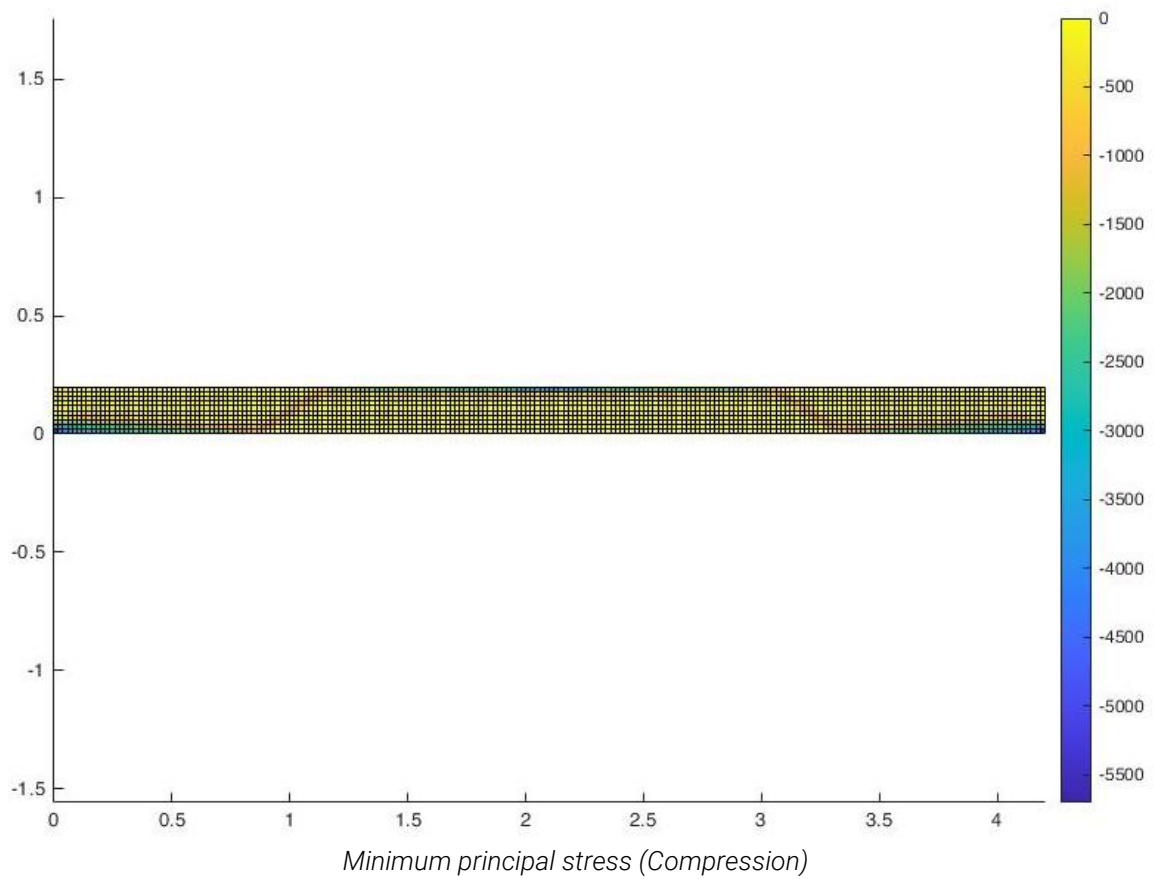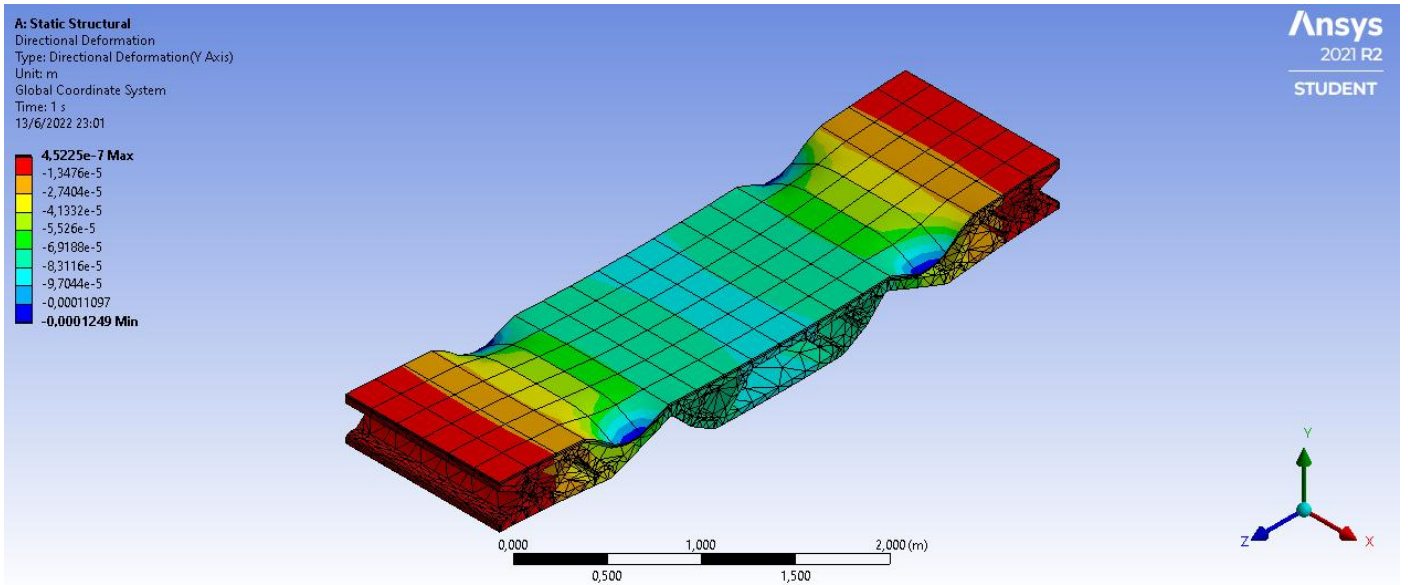*Minimum principal stress (Compression)*

Maximum Principal Stress (Tension)

A.2.4.2 Cross section height: 20 cm – Borosilicate
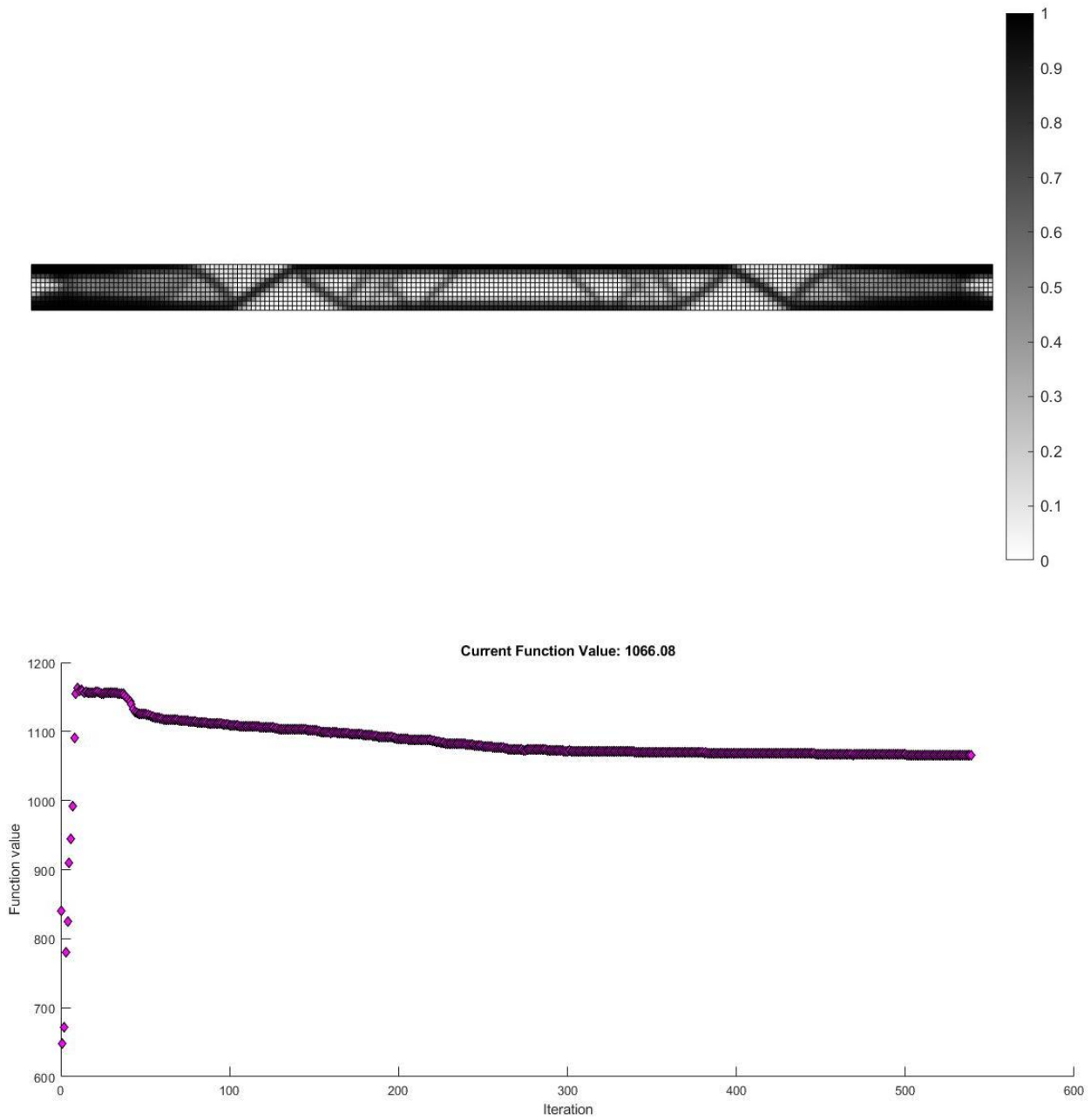
Optimization result & Plot of function values per iteration: Volume Objective & Compliance, Deflection, Annealing & Principal Stresses Constraint (Cast borosilicate lime glass &cross section total height: 20 cm).

Final function value	Iterations	Function evaluations	Feasibility	First-order Optimality	Time (hours : minutes)
1066.1	539	567789	0	4.9e-01	45:19

Minimum principal stress (Compression)

Maximum Principal Stress (Tension)
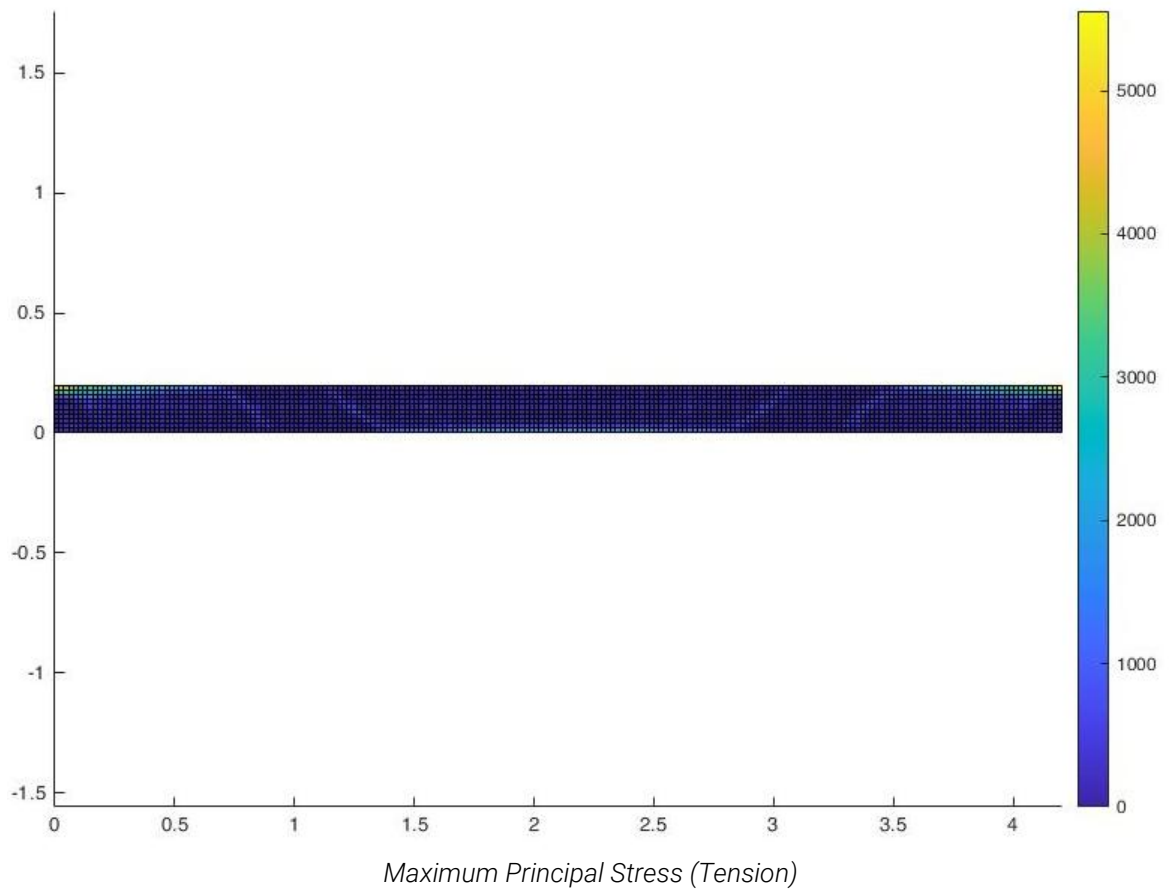
A.2.5 Final Result

A.2.4.1 Structural Verification

Deformation
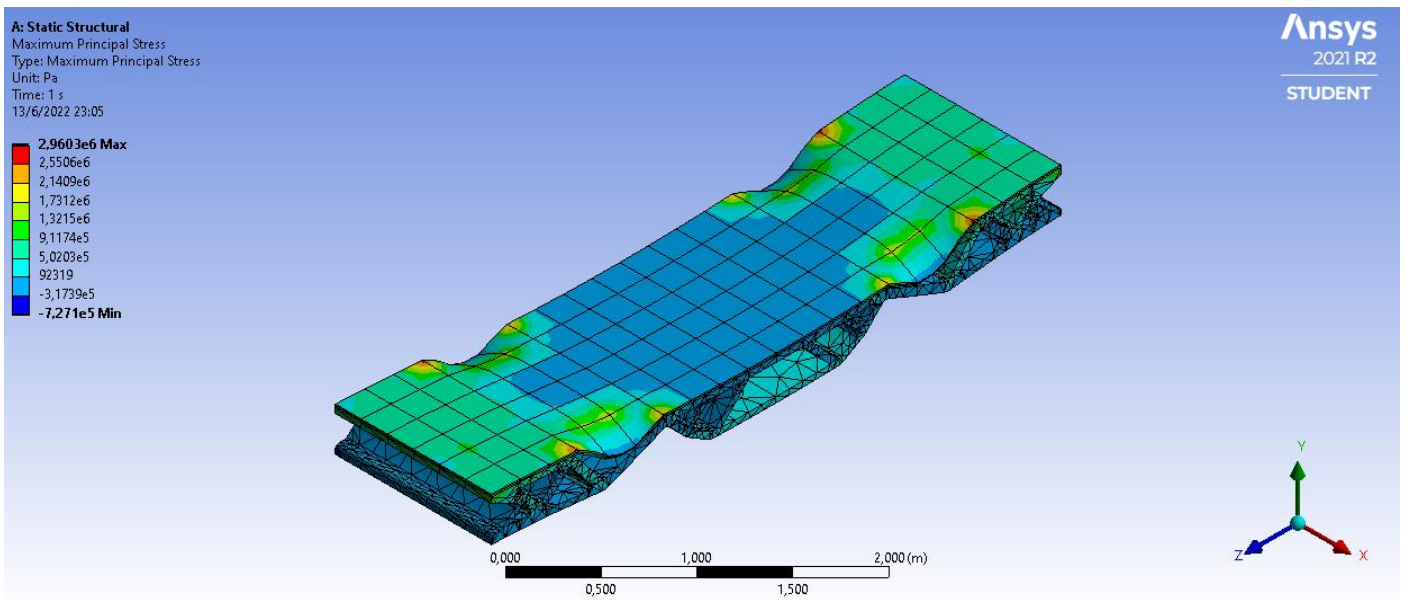
Maximum principal stress.
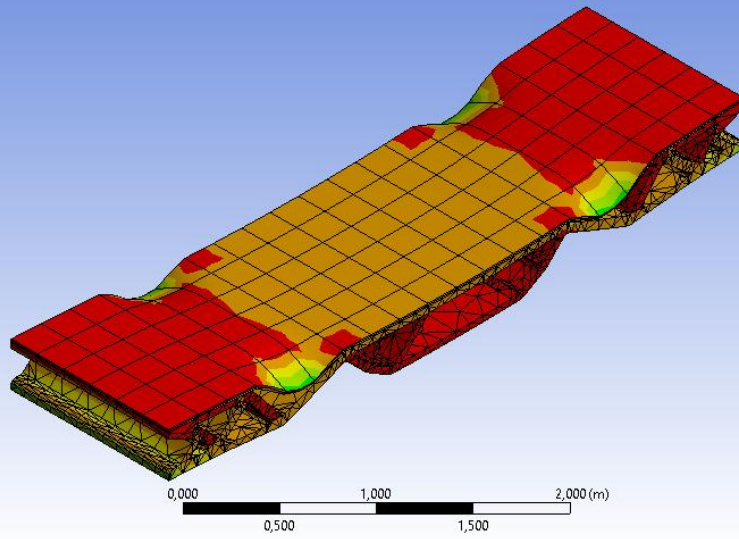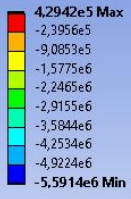
Minimum principal stress.

A.2.5 Calculations for defining the mould thickness

The thrust force which acts on the vertical side of the mould is calculated as:

$$F_A = p_A A = ((p_t + p_b)/2)A = (\rho g \frac{(h_t + h_b)}{2})A$$

where: F_A is the average thrust force, p_A is the average pressure on the vertical surface, A is the area of the bottom surface and p_t, h_t, p_b, h_b are the pressure and height on the top and bottom surface respectively. Based on that, the thrust force is:

$$F_A = (2500 \frac{kg}{m^3} \times 9,81 \frac{m}{s^2} \times \frac{(1,15m + 0m)}{2} \times (1,6m * 0,04m) = 902,52\ N$$

Considering that the hydrostatic force is applied on the 1/3 of the distance from the bottom, the bending moment applied on the mould side can be calculated as:

$$M_{max} = F_A a = 902,52 \times \left(\frac{1,15}{3}\right) = 345,96\ Nm$$

This will be used in order to define finally the thickness of the mould. In order to do that, the allowable limit of bending strength for the 3d printing sand mould is also taken into account. According to (Stefanaki, 2020), Voxeljet company has defined the bending strength range (σ_{bend}) to 220-300 N/cm^2. In this regard, the minimum thickness of the mould is calculated as:

$$\sigma_{bend} = \frac{My}{I} = \frac{\frac{Md}{2}}{\frac{1}{12}bd^3} \Rightarrow d = \sqrt{\frac{6 \times M}{\sigma_{bend} b}} = \sqrt{\frac{6 \times 345,96 Nm}{220 \times 10^4 \frac{N}{m^2} \times 1,6\ m}} = 2,4cm$$